UNIVERSITEIT VAN PRETORIA
UNIVERSITY OF PRETORIA
YUNIBESITHI YA PRETORIA

Piggybacking Fischer carbene complexes

by

Nora-ann Harris

Submitted in partial fulfilment of the degree

Magister Scientiae

In the Faculty of Natural and Agricultural Sciences

University of Pretoria

Pretoria

Supervisor: Professor S. Lotz

July 2013

© University of Pretoria

Declaration

I declare that the dissertation, which I hereby submit for the degree Magister Scientiae at the University of Pretoria, is my own work and has not previously been submitted by me for a degree at this or any other tertiary institution.

Crystal structure determinations (data collection and structure refinements) were performed by Mr. D.C. Liles at the University of Pretoria.

Signature: 

Date: 2013/07/05

© University of Pretoria

Acknowledgements

I would like to express my sincere gratitude to the following people and institutions that individually played an important role in the completion of this study:

My supervisor, Prof Simon Lotz for support, motivation and guidance during the study.

Mr Eric Palmer for NMR data collection of samples and specialist advice on obtaining useable data on air sensitive samples.

My friends and colleagues for their constant support and interest.

The financial assistance of the National Research Foundation (NRF) towards this research is hereby acknowledged. Opinions that are expressed and conclusions arrived at are those of the author and not necessarily to be attributed to the NRF.

© University of Pretoria

Table of Contents

© University of Pretoria

© University of Pretoria

© University of Pretoria

© University of Pretoria

Summary

Piggybacking Fischer carbene complexes

by

Nora-ann Harris

Supervisor: Prof S. Lotz

Submitted in partial fulfilment of the requirements for the degree Magister Scientiae, Department of Chemistry, University of Pretoria, South Africa

The study involved two separate sections. In the first part of the study single and multiple chromium and tungsten Fischer carbene complexes were synthesised on tri(2-furyl)phosphine, tris(4-bromophenyl)amine and N,N-dimethylaniline(arene)-tricarbonylchromium. The reaction of tri(2-furyl)phosphine (PFu_3, Fu = C_4H_3O) with excess *n*BuLi, metallation and alkylation with Et_3OBF_4 yielded the monocarbene, [{$M(CO)_5C(OEt)Fu'$}PFu_2] (M = Cr(**1a**)/ W(**1b**), Fu' = C_4H_2O), biscarbene [{$M(CO)_5C(OEt)Fu'$}$_2$PFu] (M = Cr(**4a**)/ W(**4b**)) and triscarbene complexes, [{$M(CO)_5C(OEt)Fu'$}$_3$P] (M = Cr(**6a**)/ W(**6b**)). In addition the formation of the known monocarbene, [$M(CO)_5${$C(OEt)Fu$}] (M = Cr(**2a**) /W(**2b**)), and biscarbene complexes, [$M(CO)_5${$C(OEt)Fu'C(OEt)$}$M(CO)_5$] (M = Cr(**5a**) /W(**5b**)) were also observed while the formation of the butylphosphine-furylcarbene complex, [$M(CO)_5$ {$C(OEt)Fu'P(nBu)Fu$}] (M = Cr(**3a**), W(**3b**)) was unexpected. By contrast stepwise lithiation and reaction with $M(CO)_6$ (M = Cr/ W) of tris(4-bromophenyl)amine gave mono-, bis- and trismetalacylates and after subsequent alkylation with Et3OBF4 afforded only the monocarbene, [{$M(CO)_5C(OEt)C_6H_4$}NPh_2] (M = Cr(**7a**)/ W(**7b**)), biscarbene, [{$M(CO)_5C(OEt)C_6H_4$}$_2$NPh] (M = Cr(**8a**)/ W(**8b**)), and triscarbene complexes [{$M(CO)_5C(OEt)C_6H_4$}$_3$N] (M = Cr(**9a**)/ W(**9b**)). The lithiation, metallation with $M(CO)_6$ (M = Cr/ W) and sequential alkylation with Et_3OBF_4 of N,N-

© University of Pretoria

dimethylaniline(arene)-tricarbonylchromium yielded three monocarbene products: *o*-(**10**), *m*- (**11**) and *p*-[η^6-$(CH_3)_2N(C_6H_5)OCH_2CH_3$}$Cr(CO)_3$] (**12**) (M = Cr(**a**) or W(**b**)).

The solid state crystal structures of **10b**, **11b** and **12b** revealed almost planar geometry around the nitrogen atom; however no π-conjugation was used for stabilisation of the carbene complex. While the geometry around the nitrogen atom in the solid state of **7a** is planar the geometry of **1b** around the phosphorous atom is trigonal pyramidal, indicating less involvement of the phosphorous lone pair in π-conjugation compared with the nitrogen atom in **7a**, making **1b** an excellent potential ligand.

The second part of the study involved coordination of **1a** and **1b** via the P-atom to a range of transition metals. **1a** was successfully coordinated to group 5 transition metals: $W(CO)_6$ (**13**) and $Cr(CO)_6$ (**14**), while **1b** was coordinated to group 6 transition metal complexes $Re_2(CO)_9(NCMe)$ (**15**) and $Mn_2(CO)_{10}(NCMe)$ (**16**). Other complexes in which **1b** was coordinated included $PtCl_2(COD)$ (**17**) and $PdCl_2$ (**18**) to form *trans*(**a**)- and *cis*(**b**)-phosphine coordinated complexes; as well as $Ni(COD)_2$ to form [$Ni(COD)_2$(**1b**)] (**19a**) and [Ni(COD)(**1b**)$_2$] (**19b**) complexes. **1b** was lastly coordinated to group 11 transition metals forming products [AuCl(**1b**)] (**20a**), [CuBr(**1b**)$_n$] (**22a**) and [CuCl(**1b**)$_n$] (**22b**) where n = 1-3. In the coordination reaction of **1b** to AgBr a carbene transfer reaction was observed, forming [{AgBrC(OEt)Fu'}PFu_2] (**21a**), after the carbene transfer reaction occurred, the 21a coordinated to the unreacted remaining AgBr to form complexes [AgBr(**21a**)$_n$] where n = 1 (**21b**), 2 (**21c**) and 3 (**21d**). During the coordination reactions of **1b** to $PdCl_2$ and AuCl, the carbene centre in **1b** underwent catalytic and metathesis transformations to form ester compounds (**18c**, **20b**) and E (**18d**, **20d**)/ Z (**18e**, **20e**) olefins. An aldehyde product (**20c**) was also observed in the coordination reaction of **1b** to AuCl.

© University of Pretoria

List of complexes

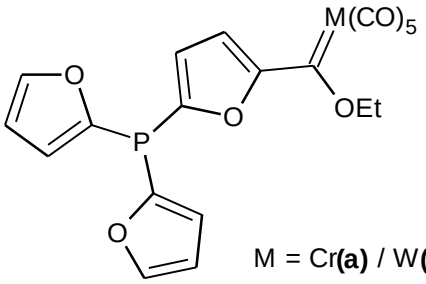

M = Cr**(a)** / W**(b)**

1

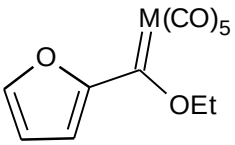

M = Cr**(a)** / W**(b)**

2

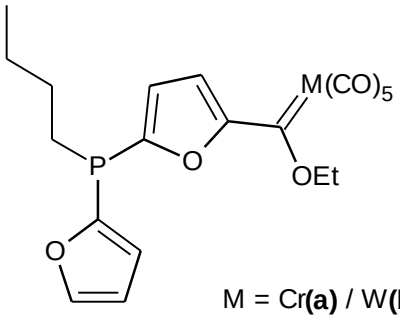

M = Cr**(a)** / W**(b)**

3

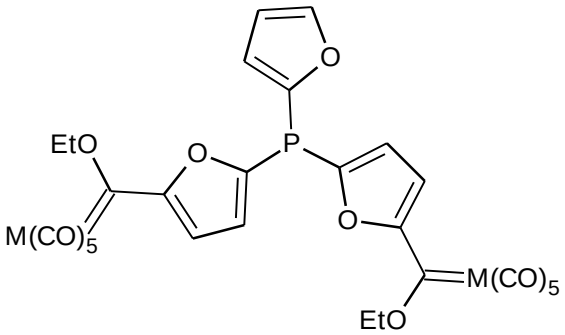

M = Cr**(a)** / W**(b)**

4

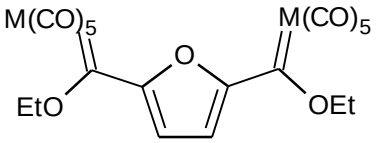

M = Cr**(a)** / W**(b)**

5

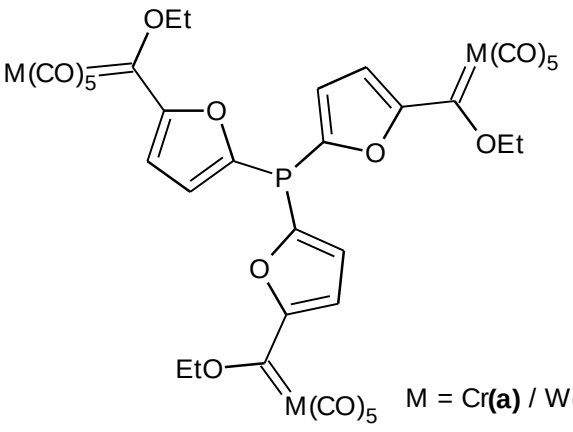

M = Cr**(a)** / W**(b)**

6

© University of Pretoria

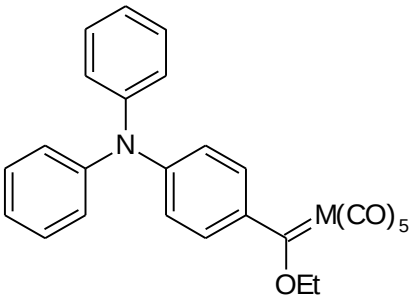

M = Cr**(a)** / W**(b)**

7

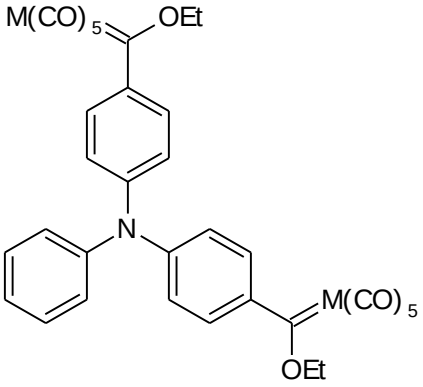

M = Cr**(a)** / W**(b)**

8

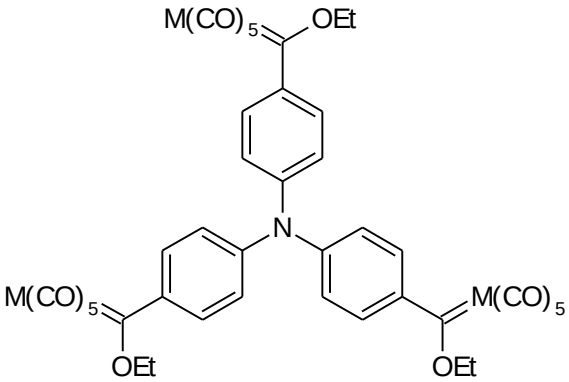

M = Cr**(a)** / W**(b)**

9

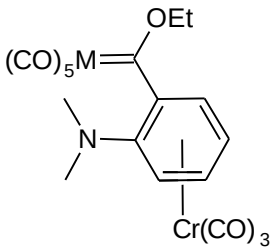

M = Cr**(a)** / W**(b)**

10

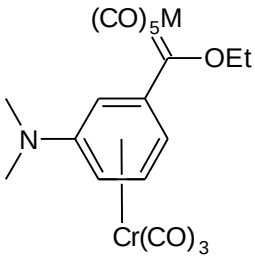

M = Cr**(a)** / W**(b)**

11

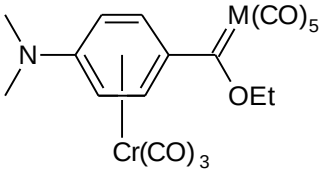

M = Cr**(a)** / W**(b)**

12

© University of Pretoria

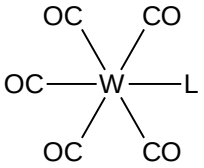

L = **1a**

13

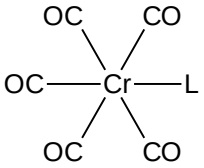

L = **1a**

14

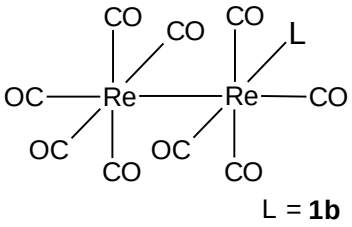

L = **1b**

15

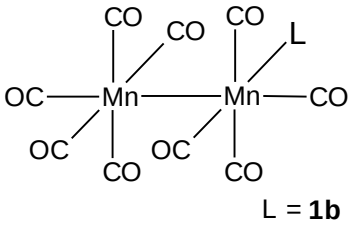

L = **1b**

16

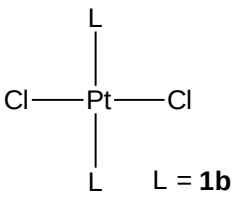

L = **1b**

17a

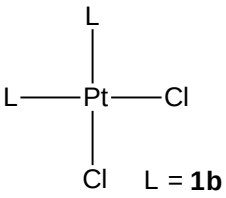

L = **1b**

17b

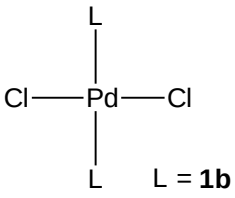

L = **1b**

18a

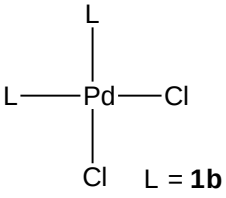

L = **1b**

18b

© University of Pretoria

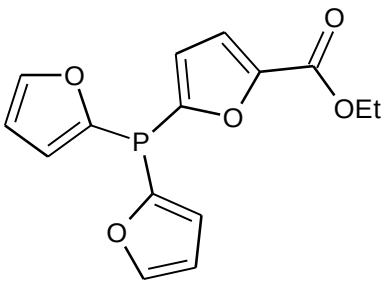

18c, 20b

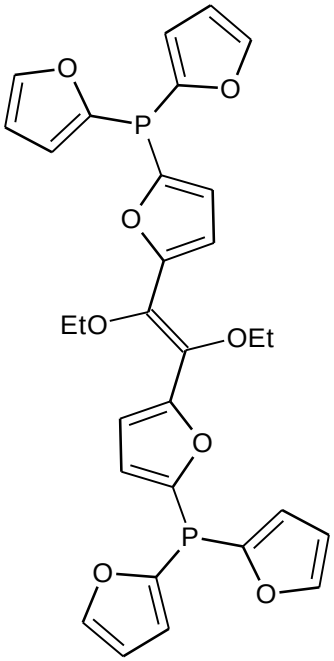

18d, 20d

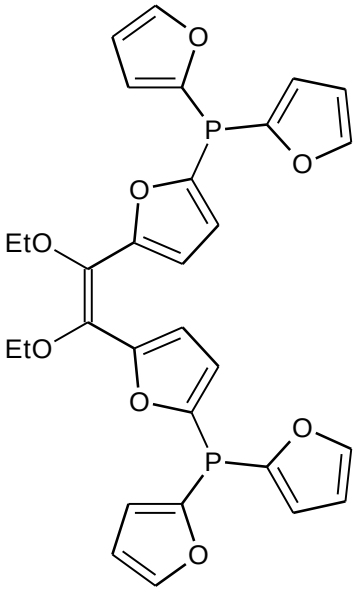

18e, 20e

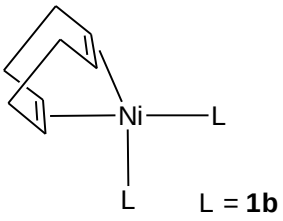

19

© University of Pretoria

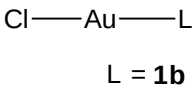

L = **1b**

20a

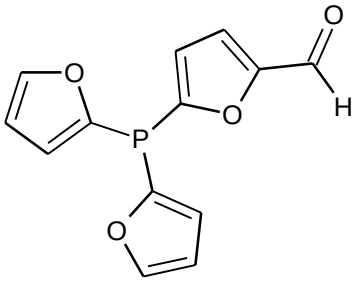

20c

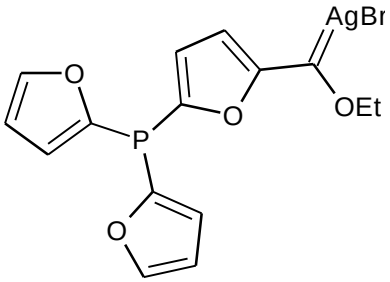

21a

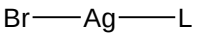

L = **21a**

21b

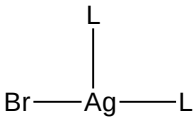

L = **21a**

21c

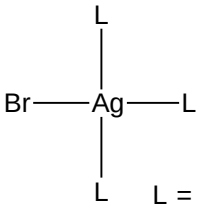

L = **21a**

21d

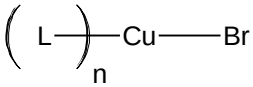

n = 1 - 3 L = **1b**

22a

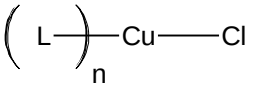

n = 1 - 3 L = **1b**

22b

© University of Pretoria

List of abbreviations

br	:	broad
d	:	doublet
DCM	:	dichloromethane
dd	:	doublet of doublets
ddd	:	doublet of doublet of doublets
Et	:	ethyl
Fu	:	2-furyl
Fu’		2,5-furylene
IR	:	infrared spectroscopy
J	:	coupling constant
m	:	multiplet
m		*meta*
Me	:	methyl
*n*BuLi		n-butyl lithium
NMR	:	nuclear magnetic resonance
n.o.	:	not observed
o		*ortho*
p		*para*
Ph	:	phenyl
R	:	alkyl group
RT	:	room temperature
s	:	singlet
THF	:	tetrahydrofuran
THT		tetrahydrothiophene
Å	:	angstrom
δ	:	chemical shift

© University of Pretoria

Chapter 1

Introduction

1.1 A short introduction to carbene chemistry

To start this introduction, it is first necessary to state the definition of a carbene. A carbene is a highly reactive neutral carbon atom of which two of its possible four bonds are utilised and has six valence electrons[1].

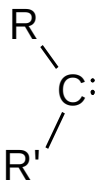

Figure 1.1 An illustration of a free carbene

A carbene complex is said to exist when a carbene and a metal fragment combine to yield an organometallic complex. The transition metal to which the carbene is coordinated is said to stabilise the carbene carbon, thus forming two different groups of carbene complexes: Fischer and Schrock type carbenes. The first carbene complex was synthesised by Fischer and Maasböl in 1964[2], naming the Fischer class of carbene complexes. These carbenes are known for their electrophilic nature while the Schrock carbene complexes, synthesised for the first time in the 1970s[3], are nucleophilic of character.

1.1.1 Schrock carbene complexes

Schrock carbene complexes are mostly recognised by an early transition metal in a high oxidation state. The high oxidation state transition metals are usually surrounded by ligands of strong σ-donor and weak π-acceptor abilities. Schrock carbene complexes can further be described as a coupling of a neutral triplet carbene ligand with a triplet transition metal fragment[4]. The π electrons are almost

© University of Pretoria

equally distributed between the carbene and the metal and a true double bond exists between the carbene carbon and the metal[1].

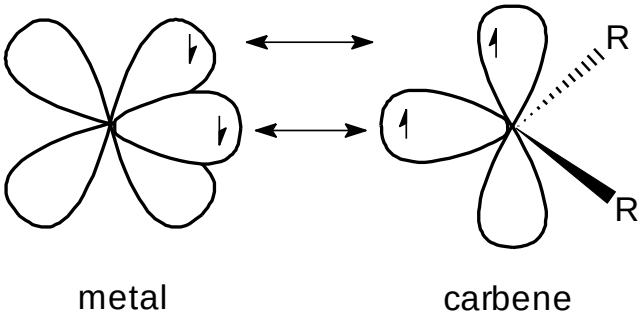

Figure 1.2 The triplet state bonding found in Schrock carbene complexes

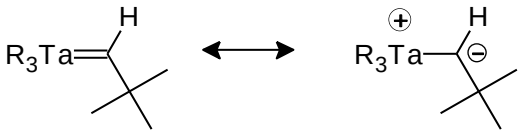

Figure 1.3 The resonance structures that exist in a Schrock carbene complex

There are many significant applications in which Schrock carbene complexes are involved. They play very prominent roles in olefin metathesis, biochemical oxidation and the Fischer-Tropsch process[5]. There are three scientists that received the Nobel Prize in chemistry in 2005 for "development of the metathesis method in organic synthesis"[6]. Schrock and his co-workers developed tungsten and molybdenum alkylidene complexes[7] while ruthenium carbene or alkylidene complexes were introduced by Grubbs[8].

1.1.2 Fischer carbene complexes

Fischer carbene complexes contain mostly middle transition metals in low oxidation state, stabilised by ligands with high electron acceptor properties like CO[9]. The carbene complex is usually stabilised by a hetero-atom or aromatic groups on the carbene carbon. They can be viewed as a singlet-type carbene that is donating electron density to the metal through its sp^2 hybridised orbital and also receives back-donated electron density from the metal into its empty p-orbital with the π-electrons that would be polarised towards the metal[4] (Figure 1.4). Represented in

© University of Pretoria

Figure 1.5 are the resonance structures that exist for the first carbene complex that was characterised by X-ray crystallography[10].

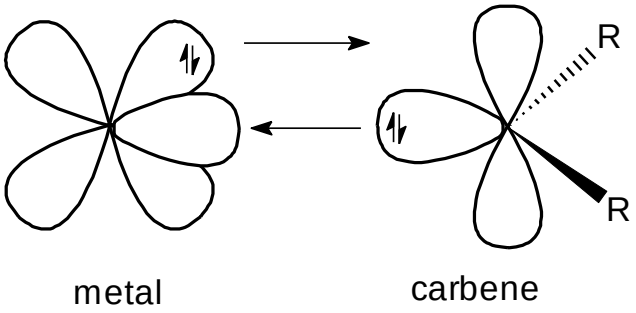

Figure 1.4 A representation of the singlet state bonding of a Fischer carbene complex

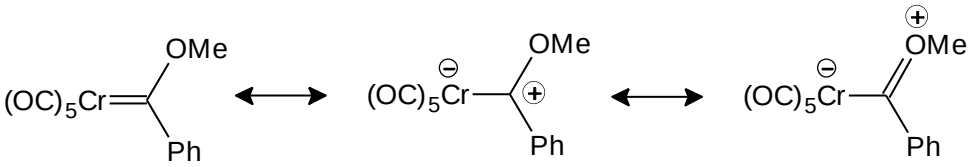

Figure 1.5 The resonance structures that exist for a Fischer carbene complex

Fischer carbene complexes show different reactivity behaviour in different environments as illustrated by Scheme 1.1[9]. The electrophilic carbene carbon is the preferred site of attack by nucleophiles (route a) while electrophiles could possibly be attacked by the heteroatom lone pair of electrons (route b). In the case of alkylcarbene complexes, the C-H bonds in the α –position of the carbene ligand are activated. In the presence of a base, the alkylcarbene complexes are deprotonated (route c). It is also possible to substitute the carbonyl or carbene ligands in the carbene complex for other ligands (route d).

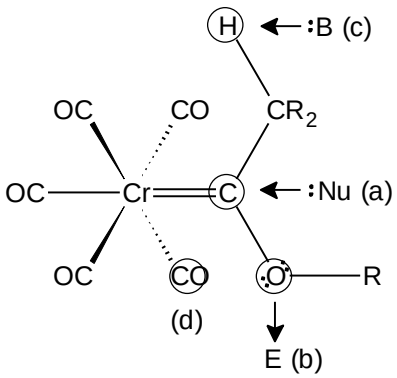

Scheme 1.1 The reactive centres found in a Fischer carbene complex

© University of Pretoria

Another type of Fischer carbene complex that has received much attention in recent years is the N-heterocyclic carbene or NHC. It was first isolated and crystallised as a free carbene in 1991 by Arduengo[11]. These carbenes compete favourably with phosphines in their σ-donor properties, thus opening a new door to reactions where phosphines showed limitations[12].

There are many different applications for Fischer carbene complexes, especially in organic synthesis reactions of which many of these appear in a review by Dötz and Stendel[13]. Some of the latest research on carbene chemistry involves carbene transfer reactions from one transition metal to another[14], the carbene acting as a ligand itself. However, a metal-carbene complex has never been synthesised as a guest on a phosphine or amine ligand.

1.2 Piggybacking Fischer carbene complexes

Even though Fischer carbene complexes will play an important role in this project, there is a larger concept that has to be revealed throughout this research.

There is a large amount of reaction-active transition metal materials that have been developed with particular functions in mind like catalysis, metathesis, luminescence, switches and many more. The ligands coordinated to these transition metals play very important roles in their specific functions.

The most widely used class of ligands in catalysis are phosphines which can be tuned with respect to their electronic and steric factors by varying their substituents. The σ-bonding properties of these ligands can be altered by adding electron withdrawing or electron donating substituents while their steric properties can be altered by increasing or decreasing the size of the substituents. The steric factor is defined by the cone angle concept[15] (Figure 1.6). Another important property of phosphines is their ability to act as π-acceptors by accepting electron density into the empty d-orbitals of the phosphorous atom.

© University of Pretoria

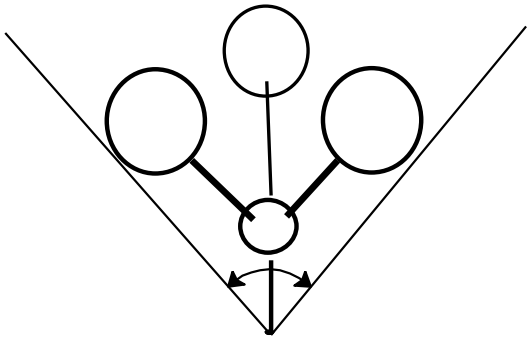

Figure 1.6 The cone angle of phosphine ligands where the circle represents any alkyl/aryl group.

Equally important in coordination chemistry are amine ligands. They are also strong σ-donor ligands but lack π-acceptor properties.

Throughout this project, a question is asked: will it be possible to combine two different functions in a single molecule? By incorporating a chemically active species, like a Fischer carbene complex, onto a potential ligand and coordinating this ligand to a catalytically active transition metal, could potentially open a new field of research.

1.3 Aim of the study

Since the isolation of the first Fischer carbene complex, all the possible aspects of these complexes have been tirelessly explored and are still being explored. In this project, the Fischer carbene complex will not be explored in itself, but rather act as a tool to investigate and alter the properties of phosphine and amine ligands.

The aim of this project can be divided into two separate segments. The first part will be to synthesise a phosphine and amine ligand containing one or multiple Fischer carbene complexes as substituents. The second part of the project will be devoted to “piggybacking” the carbene complexes via the ligand, specifically the P-atom, into the coordination sphere of middle and late transition metals. The ligand acts as a host for a guest substituent which is a metal carbene fragment.

© University of Pretoria

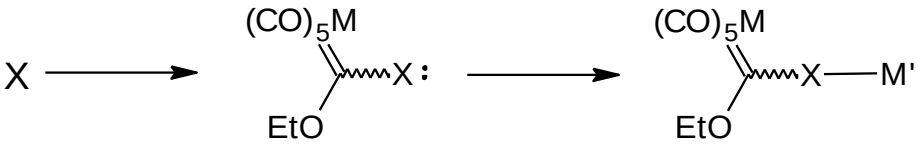

Scheme 1.2 The piggybacking concept of a Fischer carbene complex

On synthesising the carbene containing ligands, there are factors that have to be addressed and investigated before coordination of these novel ligands can occur. These factors will be addressed in a series of questions:

i. Will it be possible to introduce more than a single Fischer carbene substituent onto a particular ligand?
ii. How will the carbene substituent present on the ligand influence the ability of the particular ligand to coordinate to other metals?
iii. Will the carbene substituent be able to survive the environment required for ligand coordination onto transition metals?
iv. Will the metal to which the ligand has to be coordinated have an effect on, or react with the carbene substituent on the ligand?

On successful coordination of these ligands to transition metals, new possible electronic alteration of the carbene has to be considered as well as any possible additional interactions either intermolecular or intramolecular. These include the stability of the carbene fragment on coordination of the ligand, possible catalytic or metathesis reactions that occurred during the coordination of the ligand and even effects that the coordination of the compound will have on the transition metal centre. It is important to realise that, since this is only the very beginning of the "piggybacking" concept, there are still many questions that have to be answered as well as many different concepts that can be considered inside and outside the field of Fischer carbene complexes.

The chapters will be discussed in the order of the prepared ligands and their properties and the transition metals to which the ligands were coordinated with characteristic effects observed after coordination of the ligands. Finally the experimental procedures are reported with additional mass spectral data of selected compounds.

© University of Pretoria

1.4 References

1. P. de Frémont, N. Marion and S. P. Nolan. Carbenes: Synthesis, properties, and organometallic chemistry. *Coord. Chem. Rev.* (2009) **253,** 862–892.

2. E. O. Fischer and A. Maasböl. On the Existence of a Tungsten Carbonyl Carbene Complex. *Angew. Chem. Int. Ed.* (1964) **3,** 580–581.

3. R. R. Schrock. Alkylidene complexes of niobium and tantalum. *Acc. Chem. Res.* (1979) **12,** 98–104.

4. T. E. Taylor and M. B. Hall. Theoretical comparison between nucleophilic and electrophilic transition metal carbenes using generalized molecular orbital and configuration interaction methods. *J. Am. Chem. Soc.* (1984) **106,** 1576–1584.

5. T. R. Cundari and M. S. Gordon. Principal resonance contributors to high-valent, transition-metal alkylidene complexes. *J. Am. Chem. Soc.* (1991) **113,** 5231–5243.

6. R. H. Grubbs. Olefin-Metathesis Catalysts for the Preparation of Molecules and Materials (Nobel Lecture). *Angew. Chem. Int. Ed.* (2006) **45,** 3760–3765.

7. R. R. Schrock, J. S. Murdzek, G. C. Bazan, J. Robbins, M. DiMare and M. O'Regan. Synthesis of molybdenum imido alkylidene complexes and some reactions involving acyclic olefins. *J. Am. Chem. Soc.* (1990) **112,** 3875–3886.

8. R. H. Grubbs. Olefin metathesis. *Tetrahedron* (2004) **60,** 7117–7140.

9. K. H. Dötz. Carbene Complexes in Organic Synthesis [New Synthetic Methods (47)]. *Angew. Chem. Int. Ed.* (1984) **23,** 587–608.

10. O. S. Mills and A. D. Redhouse. Carbon compounds of the transition metals. Part XII. Crystal and molecular structure of phenylmethoxycarbenepentacarbonylchromium. *J. Chem. Soc. A* (1968) 642–647.

11. A. J. Arduengo, R. L. Harlow and M. Kline. A stable crystalline carbene. *J. Am. Chem. Soc.* (1991) **113,** 361–363.

12. S. Díez-González and S. P. Nolan. Stereoelectronic parameters associated with N-heterocyclic carbene (NHC) ligands: A quest for understanding. *Coord. Chem. Rev* (2007) **251,** 874–883.

13. K. H. Dötz and J. Stendel. Fischer carbene complexes in organic synthesis: metal-assisted and metal-templated reactions. *Chem. Rev.* (2009) **109,** 3227–74.

14. S.-T. Liu and K. R. Reddy. Carbene transfer reactions between transition-metal ions. *Chem. Soc. Rev.* (1999) **28,** 315–322.

© University of Pretoria

15. C. A. Tolman. Steric effects of phosphorus ligands in organometallic chemistry and homogeneous catalysis. *Chem. Rev.* (1977) **77,** 313–348.

© University of Pretoria

Chapter 2

Fischer Carbene Complexes on Tri(2-furyl)phosphine (PFu_3)

2.1 Background

For many years, the steric and electronic properties of tertiary phosphines have been investigated because these properties play a very important role in the chemical reactivity and catalytic activity of many metal centres. Both properties can influence the ability of a particular phosphine ligand's Lewis acidity. Farina[1] stated that ligands with poorer electron donating properties would be more effective pertaining specifically to the Stille reaction. In comparing PFu_3 with tri-phenyl phosphine (PPh_3), the furyl-containing molecule had a smaller electron donating effect than that of the phenyl-containing molecule. Thus, PFu_3 would be a better ligand suited for the purpose than PPh_3. A question can further be formulated from this particular study: What happens when PFu_3 becomes an even poorer electron donating ligand? Fischer carbenes are known to have electron-withdrawing properties[2]. In this part of the study, metal-carbene substituents are introduced onto PFu_3. The features of the products and starting materials are compared to determine the effect of the metal-carbene complex on the phosphine ligand.

2.2 PFu_3 as precursor for a novel ligand

After the discovery that PFu_3 was a much better ligand than PPh_3 for the Stille reaction, many different studies were conducted on other cross-coupling reactions[3]. The difference between PPh_3 and PFu_3 is that the furyl substituents on PFu_3 are electron excessive aromatic systems due to the presence of 6 π-electrons in a five-membered ring; however, the oxygen present in the ring was the determining factor in making it an electron-withdrawing group. The oxygen has strong negative inductive effects and positive mesomeric properties making the furyl group electron-

© University of Pretoria

withdrawing[4]. Aromatic groups are known to provide stabilisation for electrophilic Fischer carbene complexes[2] via π-electron delocalisation. This makes the conjugated electron system of the each furyl group ideal for the stabilisation of Fischer carbene substituents. The increased stabilisation occurs via the electron lone pair present on the phosphorous atom: This concept is illustrated in Figure. 2.1. For this reason, PFu_3 was chosen as the phosphine ligand on which the study was conducted.

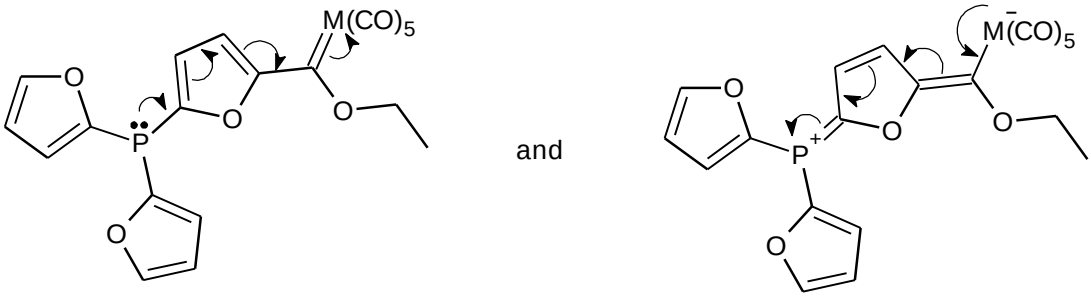

Figure 2.1: Fischer carbene substituent stabilisation via π-electron delocalisation through the conjugated π-system of PFu_3

It is important to note that through this stabilisation, significant deactivation of the carbene substituent on the furyl ring occurs, making the carbene centre less reactive than when the phosphorous atom is absent. When the ligand coordinates, the phosphorous electron lone pair is used for bonding to a transition metal and the carbene complex becomes more activated and is expected to show significantly increased fragility. This can be explained since the lone pair of electrons present on the phosphine can no longer be used throughout the conjugated system for stabilisation of the carbene substituent on the furyl ring, but is instead used for coordination to a second transition metal.

In the following section, two different procedures were used to synthesise the desired metal carbonyl phosphine complexes. Reactions were carried out with either one equivalent *n*BuLi or an excess. Initially, both chromium and tungsten carbonyls were used as the metal-carbene substituents of the phosphines. This section is divided into subsections pertaining to the two different reaction routes.

© University of Pretoria

2.2.1 Reaction of PFu_3 with one equivalent of *n*BuLi (reaction 1)

The subsequent steps of reaction of PFu_3 involved deprotonation at the 5-position of a furyl substituent with a single equivalent of *n*BuLi. A metal acylate was formed by addition of one equivalent of metal carbonyl followed by alkylation with oxonium salt. Other products observed for this reaction was a furyl-monocarbene and a phosphine compound containing two furyl groups of which the one contained a metal-carbene substituent and where the third furyl group was replaced by a butyl group. The following products were isolated from the reaction (Scheme 2.1).

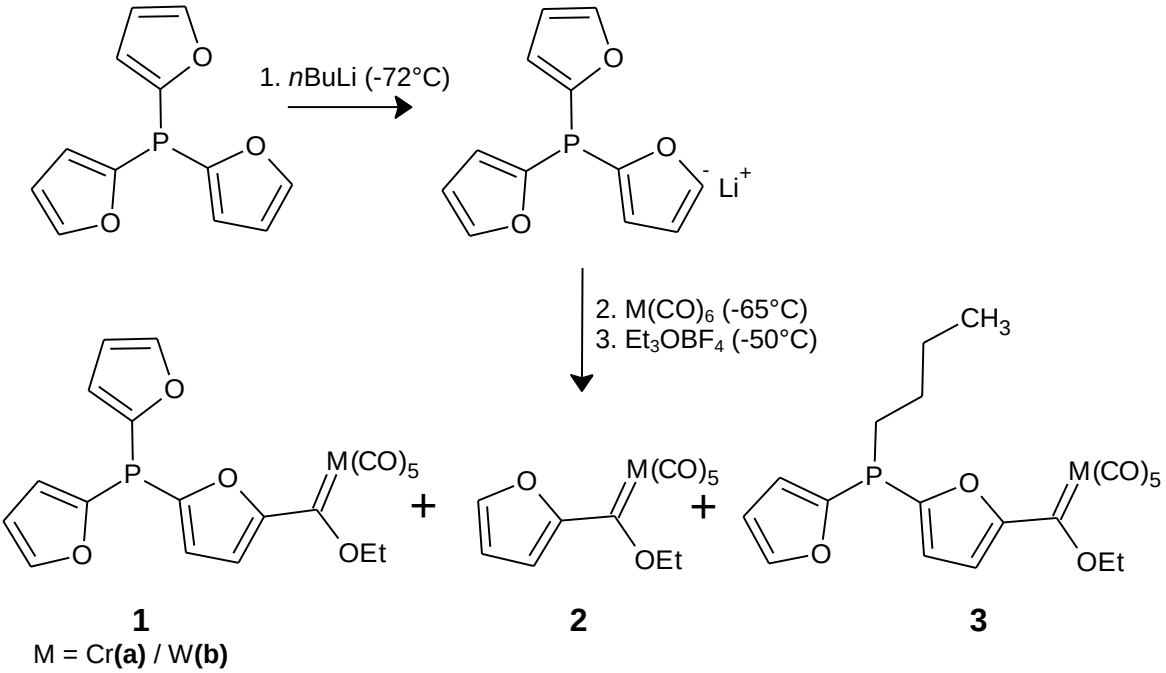

Scheme 2.1 Reaction procedure of PFu_3 with one equivalent *n*BuLi followed by metallation and alkylation

Three products were formed from this reaction of which **1** was the desired product. After isolating the products on a silica column, it was found that **1** was wine red with an oily consistency. **2** was an unexpected product which was bright orange and isolated as a solid. The formation of **2** could be explained indirectly by the presence of product **3**. It was found that **3** was a modified phosphine that contained a furyl ring, a butyl group and metal-carbene substituent on the 4-position of the other furyl ring. A completely organic, modified phosphine would be expected if nucleophilic substitution occurred at the furyl containing the metal carbene substituent, however, this was not observed. Since no organic products were isolated from the reaction,

© University of Pretoria

nucleophilic substitution on the phosphine occurred at a furyl group with no metal carbene substituents present on the ring. It was not possible to determine from these reaction conditions whether the nucleophilic substitution reaction occurred before or after metallation of the reaction mixture. The formed furyl nucleophile reacted with $M(CO)_6$ present in the reaction mixture to form furyl metal acylate. On alkylation of the reaction mixture, the products **1**, **2** and **3** were formed.

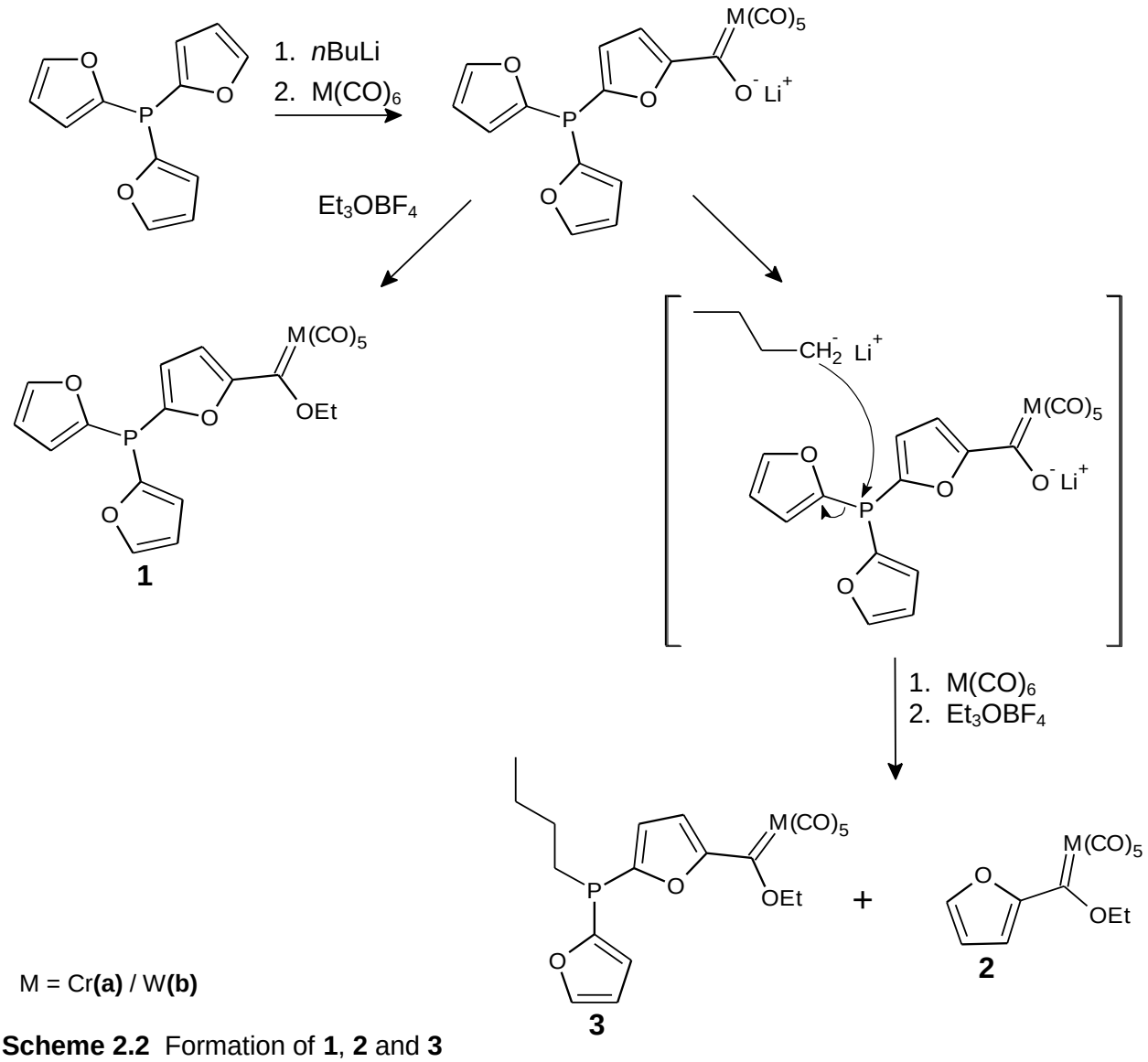

M = Cr**(a)** / W**(b)**

Scheme 2.2 Formation of **1**, **2** and **3**

On the grounds of the isolated products obtained, the nucleophilic substitution of PFu_3 was eliminated as a possible product formation reaction. The high yield of **1** compared to **2** and **3** further supported this statement. The metal acylate that formed had a strong electron withdrawing character, thus the P-furyl bond, on which

© University of Pretoria

the metal acylate was a substituent, increased in strength while the P-furyl bonds were weakened. If nucleophilic substitution occurs, it will be one of the weaker P-furyl bonds that will break.

2.2.2 Reaction of PFu_3 with excess *n*BuLi (reaction 2)

This reaction was initially used to synthesise the phosphine ligand containing multiple carbene complexes on a single phosphine. In this procedure, a stepwise addition of *n*BuLi and $M(CO)_6$ was employed. The reaction steps involved adding one equivalent of *n*BuLi for deprotonation at the active site of a furyl ring. Addition of one equivalent of the chosen metal carbonyl followed, which allowed for the formation of the metal acylate at the deprotonated site of the furyl ring. These two steps were repeated twice before the mixture of products was alkylated with three equivalents of Et_3OBF_4. Six products were isolated from the reaction.

Table 2.1: Reaction products of PFu_3 with excess *n*BuLi, metal carbonyl and oxonium salt*

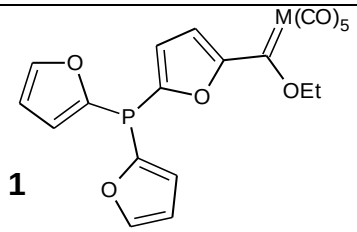 **1**	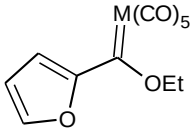 **2**	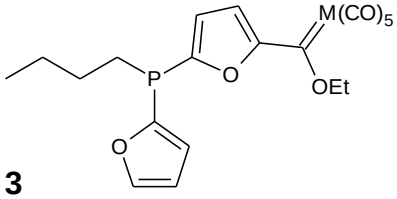 **3**
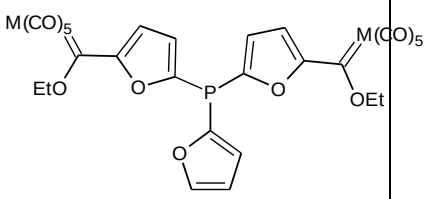 **4**	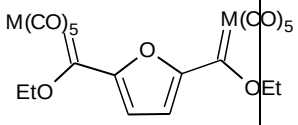 **5**	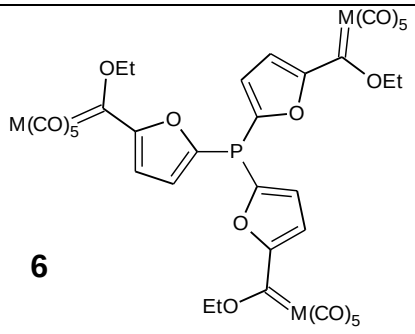 **6**

* M = Cr**(a)** / W**(b)**

Products **1**, **4** and **6** were the desired compounds. **1** contained a single metal-carbene substituent on the phosphine, **4** contained two metal-carbene substituents on two different furyl groups, while **6** contained three metal-carbene substituents on all three furyl groups present on the phosphine. All three products had an intense wine red colour and an oily consistency as pure products.

© University of Pretoria

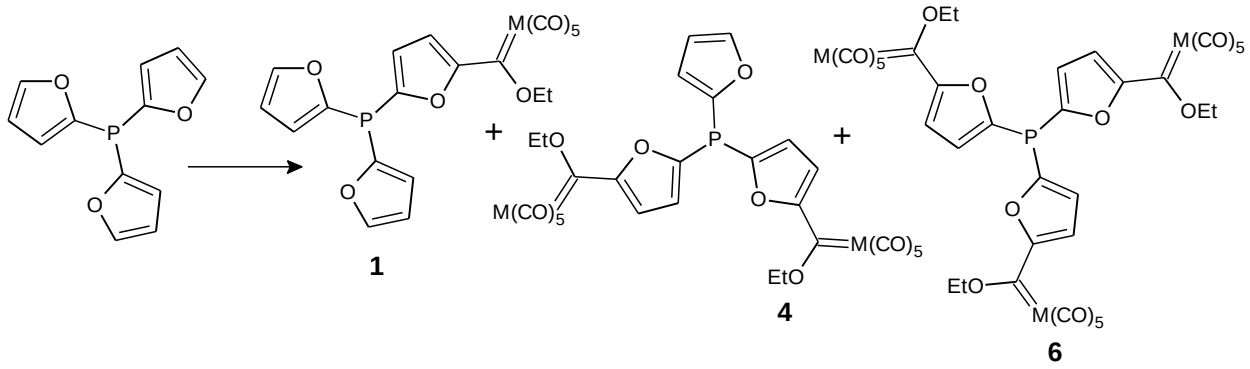

Scheme 2.3 Illustration of *mono*, *bis* and *tris* metal-carbene phoshines formed from tri(2-furyl)phosphine.

The formation of **2**, **3** and **5** could be explained, as in the previous section, by additional reactions that occurred in the presence of excess *n*BuLi (Scheme 2.2). The excess *n*BuLi acted as a nucleophile, substituting a furyl group to form product **3**, a modified phosphine. Deprotonation of a furyl acylate by a second equivalent *n*BuLi, followed by a reaction with $M(CO)_6$ and alkylation with Et_3OBF_4 afforded both products **2** and **5**. Product **5** could also have been formed after the second deprotonation step and metal-acylate formation of PFu_3. Butyl attack after the formation of the bis-metal acylate phosphine intermediate and reaction with $M(CO)_6$ afforded the elimination of a dimetal furyl acylate (Scheme 2.4). The furyl acylate substituent could represent a weaker P-furyl bond compared to a furyl substituent. This was supported by the fact that a phosphine with a butyl and two furyl-carbene substituents did not form and explained the high yields of product **5**.

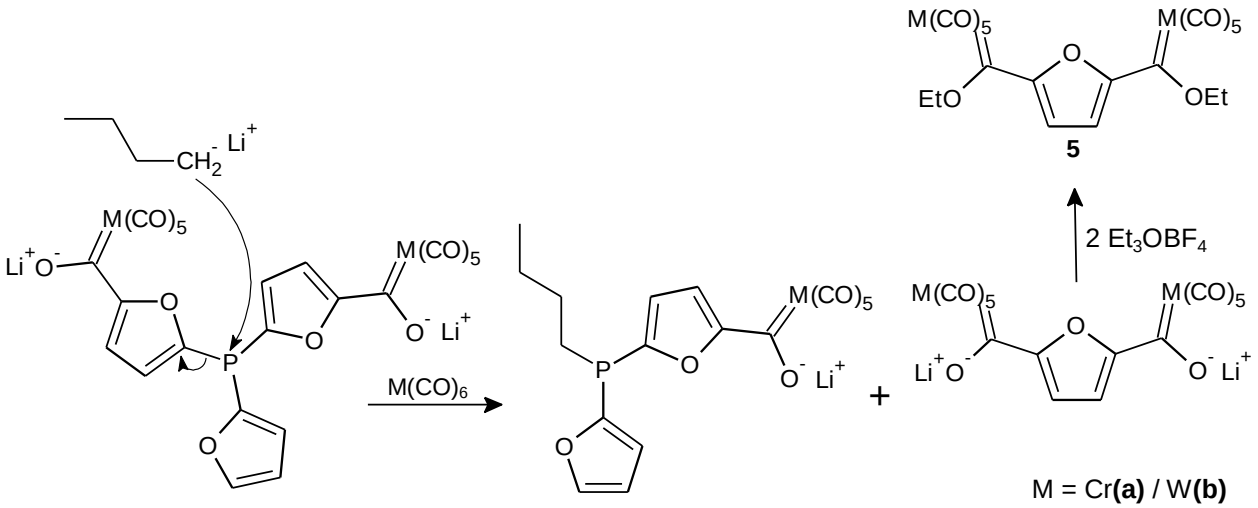

Scheme 2.4 Formation of mono and bismetal acylates and **5** after alkylation

© University of Pretoria

2.2.3 Characterisation of reaction products

In this section all products, both tungsten and chromium Fischer carbene complexes are characterised and discussed. It was found that the ^{1}H and ^{13}C NMR spectra of the phosphorous-containing compounds were extensively coupled. The phosphine atom was able to couple to both the carbon and hydrogen atoms present in the molecule. This phenomenon simplified the process of assigning the peaks in spectra, since the atoms closer to the phosphorous atom generally had a larger coupling constant than those further away[5].

The ^{1}H, ^{13}C, ^{31}P and IR data of complex **1a** and **1b** are listed in Tables 2.2 to 2.5

Compound 1 characterisation

1H, 13C and 31P NMR analysis

Table 2.2 ^{1}H NMR data ($CDCl_3$) of **1**

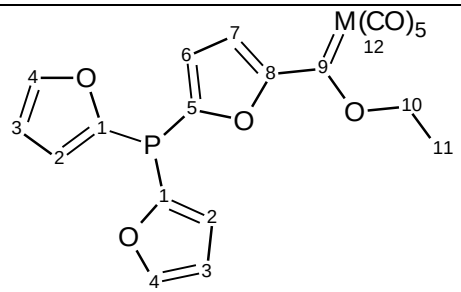

M = Cr**(a)** / W**(b)**

Proton position	**1a**			**1b**		
	δ_H/ppm	Multiplicity *J*/Hz	Integration	δ_H/ppm	Multiplicity *J*/Hz	Integration
2	6.44	ddd, 3.4, 2.0, 1.8	2H	6.46	ddd, 3.4, 2.0, 1.8	2H
3	6.95	ddd, 3.3, 1.8, 0.2	2H	6.99	ddd, 3.4, 2.4, 0.7	2H
4	7.67	ddd, 1.9, 0.7, 0.2	2H	7.70	ddd, 1.8, 0.7, 0.5	2H
6	6.85	dd, 3.6, 1.3	1H	7.06	dd, 3.7, 1.2	1H

© University of Pretoria

7	6.64	d, 3.5	1H	6.70	dd, 3.6, 0.3	1H
10	5.10	q, 7.1	2H	4.94	q, *J* = 7.1	2H
11	1.60	t, 7.1	3H	1.60	t, *J* = 7.1	3H

The proton spectra of **1a** and **1b**, revealed that the chromium carbene phosphine generally appeared slightly upfield compared to that of tungsten. The furyl rings with no metal-carbene substituent also showed proton coupling from four bonds away for both Cr and W compounds. The large downfield shift of the ethyl protons (H10 and H11) correlated with the strong electron-withdrawing character of the $M(CO)_5\{C(C_4H_2O)P\}$ fragment when compared to a value of 3.6 ppm for R-O-CH_2-R' protons. The proton shift values of the methylene protons of $–OCH_2CH_3$ groups (H11) were also metal specific, for Cr and W the values of 5.10 and 4.94 ppm respectively, indicating metal carbene complexes with greater electron density had upfield chemical shifts for the $–OCH_2R$ group.

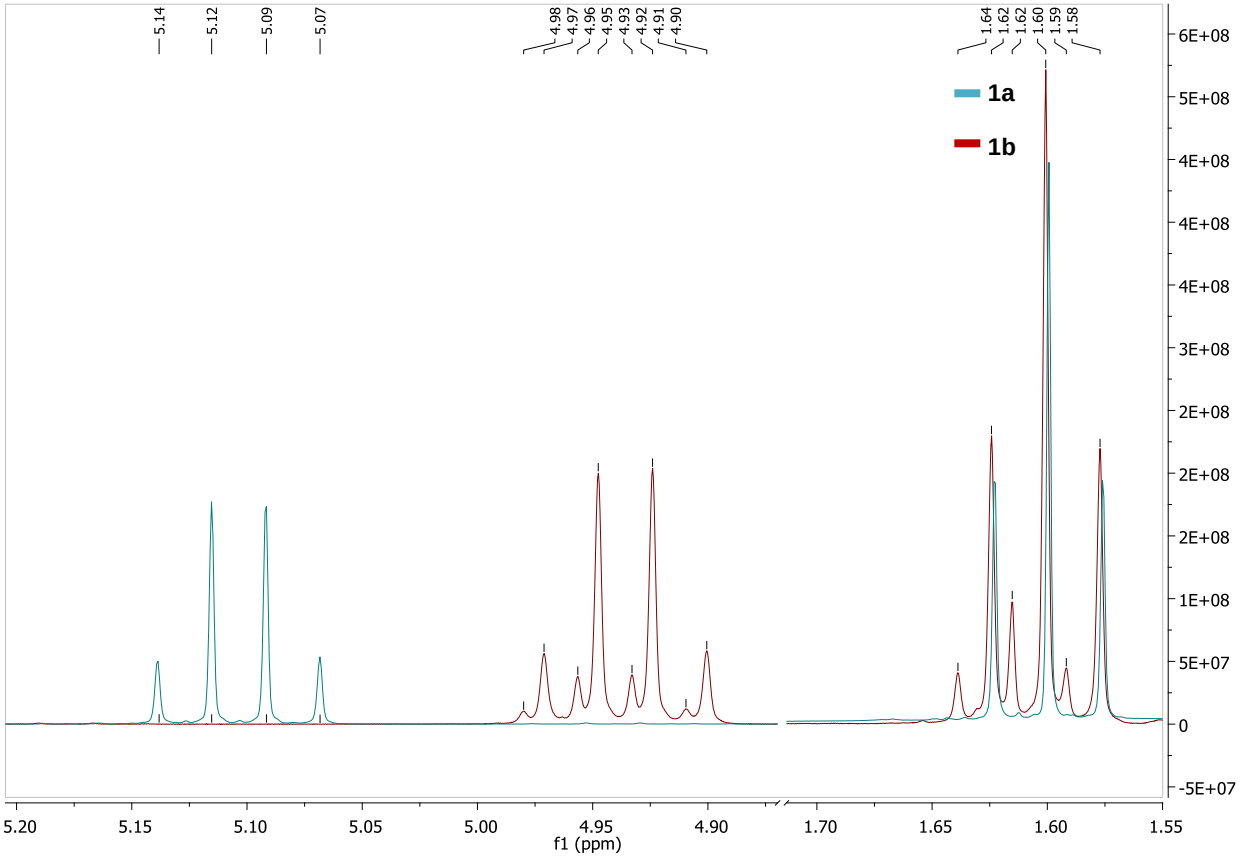

Figure 2.2 Superimposed ^{1}H spectra of **1a** and **1b** for the ethoxy substituent

© University of Pretoria

The ^{1}H NMR spectrum of **1a** and **1b** is presented in Figure 2.2 in blue and red colours respectively. This superimposed spectrum clearly gives an indication of the differences between the two modified phosphines. The most significant difference lies in the position of the –CH_2 groups. The position of the –CH_2 group is much more downfield in the case of Cr-carbene phosphine relative to the W-carbene phosphine, hence the carbene carbon of **1a** is more prone to nucleophilic attack than **1b**. It is important to note that the spectrum for **1b** in Figure 2.2 clearly shows a mixture of products. The spectrum for **1b** will be discussed later in this chapter.

Another indication that leaned towards the increased stability of the W carbene complex compared to that of the Cr-carbene complex was the ^{13}C NMR spectra of the two compounds.

Table 2.3 ^{13}C NMR data ($CDCl_3$) of **1**

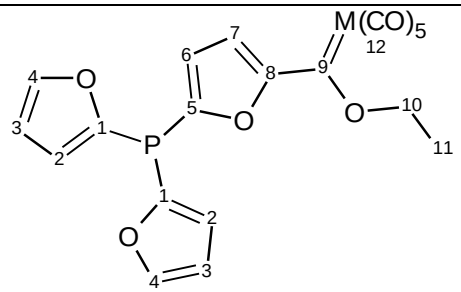

M = Cr(a) / W(b)

Carbon position	**1a**		**1b**	
	δ_c/ppm	Multiplicity J_{PC}/Hz	δ_c/ppm	Multiplicity J_{PC}/Hz
1	121.1	d, J = 25.9	123.2	d, J = 29.5
2	111.0	d, J = 7.1	110.9	d, J = 7.7
3	111.1	d, J = 1.8	120.9	d, J = 4.7
4	147.5	d, J = 2.5	148.2	d, J = 2.6
5	123.1	d, J = 29.1	125.1	d, J = 34.5
6	120.8	d, J = 13.8	113.2	d, J = 20.4
7	110.7	d, J = 6.8	121.1	d, J = 8.2
8	160.4	d, J = 4.2	160.7	d, J = 3.2
9	310.6	-	284.0	-
10	75.6	-	78.1	-
11	15.2	-	14.9	-
12	224.4(trans),	-	203.8(trans),	-

© University of Pretoria

	216.6(cis)		197.1(cis)	

The Cr and W containing phosphines had carbene chemical shifts of 310.58 and 284.04 ppm, respectively. Again, a major deshielding effect was observed in the case of the Cr-carbene containing phosphine, making this particular phosphine more fragile and prone to react at the carbene centre. Literature on the stability of W- and Cr-carbene complexes further supported this claim[6,7] as the Cr-carbene complexes decomposed at room temperature and the W-carbene complexes only started to show significant decomposition at temperatures above 50°C. In this study, the W-carbene containing phosphine (**1b**) was used for coordination to a range of transition metals due to the higher stability of the Fischer carbene substituent.

Table 2.4 ^{31}P NMR data ($CDCl_3$) of **1** (δ_p/ppm)*

1a	**1b**
-72.79	-72.80

* M = Cr**(a)** / W**(b)**

The ^{31}P NMR spectrum played a very important role, not only in this chapter, but throughout the entire project in determining the composition of a new compound. It is known throughout literature that the ^{31}P NMR chemical shifts of a phosphorous-containing compound give a direct indication of the environment in which the P-atom is found. The ^{31}P-chemical shifts were used to determine if the metal carbene phosphine acted as a ligand or was present as a free phosphine. It is important to note the ^{31}P chemical shift of **1a** and **1b** listed in Table 2.4 since these are the modified phosphines chosen to be coordinated to a range of transition metals. They were chosen because of their ease of synthesis and isolation and their stability compared to compounds **4** and **6**. A change in the ^{31}P values of the compound will indicate either coordination of the phosphine or a significant electronic change that influences the character of the phosphorous atom.

IR analysis

It is known that the vibrational frequency of a free carbonyl group is 2143 cm^{-1} and lies between 1850 and 2120 cm^{-1} for terminal carbonyl ligands[8]. The metal-carbonyl

© University of Pretoria

bond gets stronger and shorter as back-bonding from the metal to the carbonyl ligand increases. It follows that the C-O bond becomes longer and the carbonyl stretching frequency shifts to lower wavenumbers. The CO vibrations of metal-carbene carbonyls are found to occur at lower wavenumbers than the corresponding metal carbonyls because the back-bonding between the metal and carbonyl ligands increase due to the weaker π-acceptor abilities of a carbene substituent.

There are four different carbonyl vibration modes for a $LM(CO)_5$ complex. These consist of two A_1 vibrations of which $A_1^{(2)}$ is infrared active and $A_1^{(1)}$ obtains intensity because of coupling of the A_1 vibration modes. The pattern of bands of an $M(CO)_5$ fragment with C_{4V} symmetry is characteristic. According to Orgel[9] the sign of the interaction constant between the carbonyl group vibrations place the weaker $A_1^{(1)}$ band at a higher frequency than the E-band and the position of the stronger $A_1^{(2)}$ band is dependent on the unique ligand's bonding properties and could appear just before or just after the strong E band. Sometimes these bands overlap. The $A_1^{(2)}$ band obtains its greatest contribution from a vibration mode *trans* to L and mirrors the bonding properties of L in the complex. The carbonyl vibrations in the equatorial plane contributes greatly to the $A_1^{(1)}$ band while the B band is infrared inactive and detectable by Raman spectroscopy. The different vibration modes are shown in Figure 2.3.

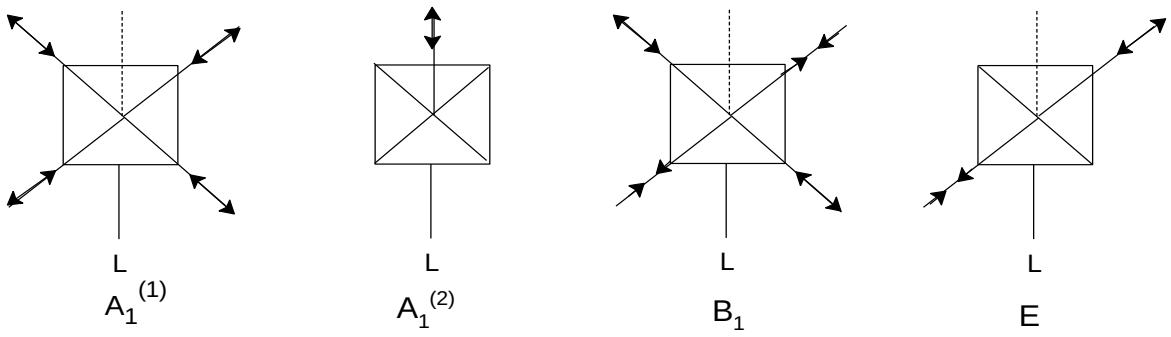

Figure 2.3 IR modes of vibration observed for a metal pentacarbonyl fragment

Table 2.5 Infrared carbonyl data (hexane) of **1**

Compound	**IR carbonyl stretching frequencies (cm^{-1})**			
	$A_1^{(1)}$	**$A_1^{(2)}$**	**B_1**	**E**
1a	2060	1944	1990	1944

© University of Pretoria

1b	2069	1957	-	1944

* M = Cr**(a)** / W**(b)**

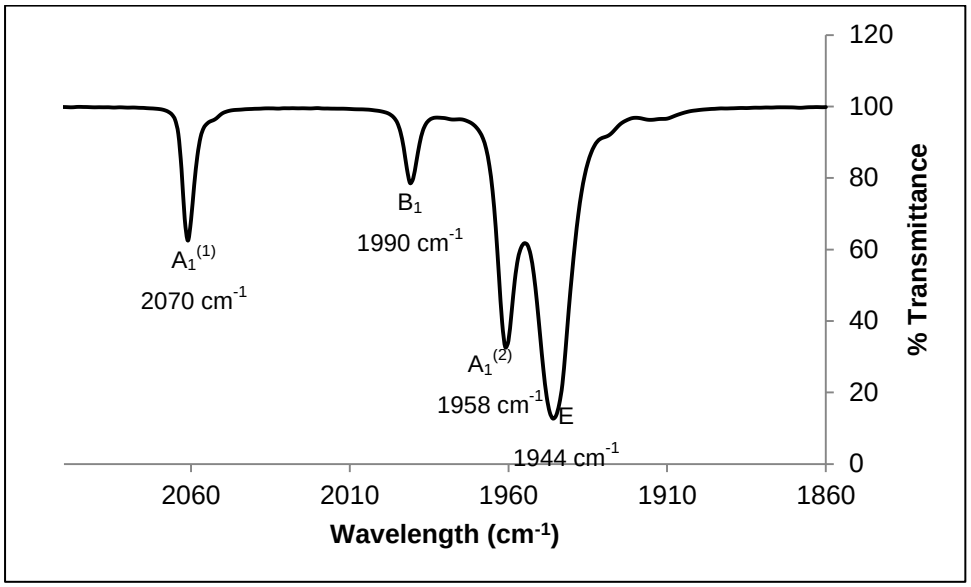

Figure 2.4 Infrared spectrum (hexane) of **1a** in the carbonyl region

The typical pattern of a pentacarbonyl fragment (C_{4V} symmetry), where each band represents a specific CO bond vibration, is shown in Figure 2.4. In some cases, it was found that an overlap occurs between the E and $A_1^{(2)}$ bands, as in the case of **1a** in Table 2.5. In other cases it may be found that the B-band gains intensity because of distortions of CO orientations in the $M(CO)_5$ fragment.

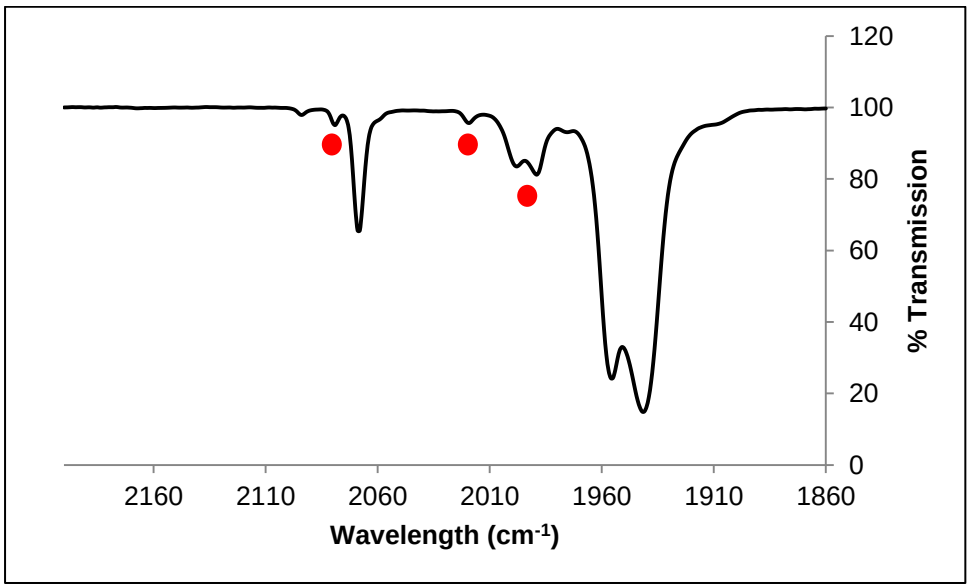

Figure 2.5 IR spectrum of **1b** in the carbonyl region

© University of Pretoria

The IR spectrum of **1b** showed an additional set of pentacarbonyl peaks marked with red dots in Figure 2.5. It was obvious from the IR data that the two pentacarbonyl groups experience very different electronic environments, hence the significant increase in wavelengths at which the minor product CO bonds are vibrating. It was further observed that the smaller $A_1^{(2)}$ and E bands at 2001 and 1996 cm^{-1} respectively, showed overlap with the B band of the main product.

The mixture of products was also observed in the NMR spectra of compound **1b**:

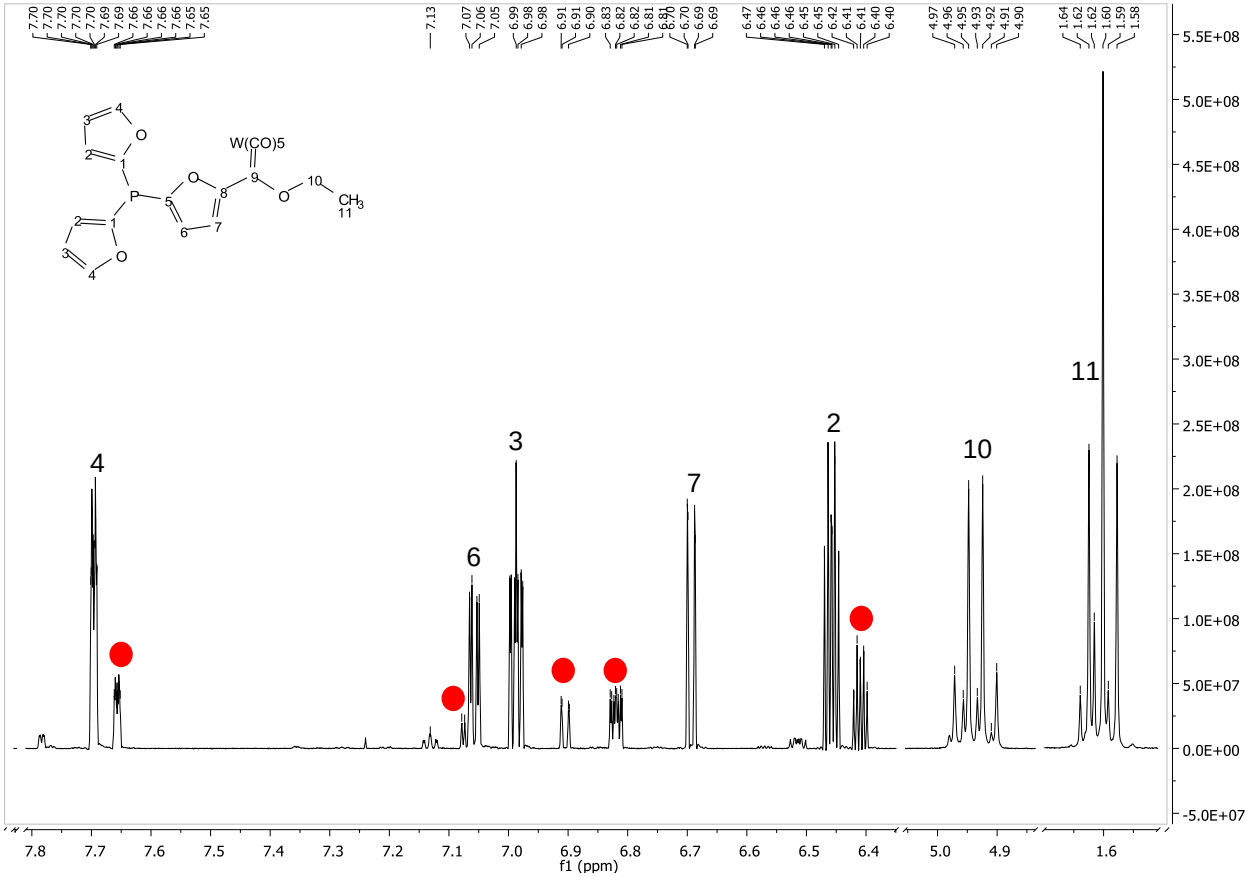

Figure 2.6 ^{1}H NMR spectrum ($CDCl_3$) of **1b**

The spectrum in Figure 2.8 showed the ^{1}H NMR resonances of the fraction containing **1b**. This NMR spectrum clearly showed a mixture of products that were not able to be separated during the isolation process. An additional set of five signals of lower intensity for the furyl rings are clearly visible. The integration of the ^{1}H NMR signals showed that the two products were present in a 1:4 ratio, indicating that one of the compounds was significantly preferred over the other. The additional

© University of Pretoria

minor product was marked with red dots on Figure 2.6. All the signals pertaining to the minor product could also be assigned to protons of a compound very similar to that of compound **1b**. The minor product signals clearly indicated $^{31}P\{^{1}H\}$ coupling. Thus, the phosphorous atom was still present in the additional product, disproving the possible formation of **2b** as a decomposition product in the mixture. The first possible explanation for this observation involved an equilibrium between compound **1b** and a product in which the synthesised phosphine acted as a ligand. Figure 2.7 illustrates this equilibrium between the uncoordinated phosphine and the coordinated ligand.

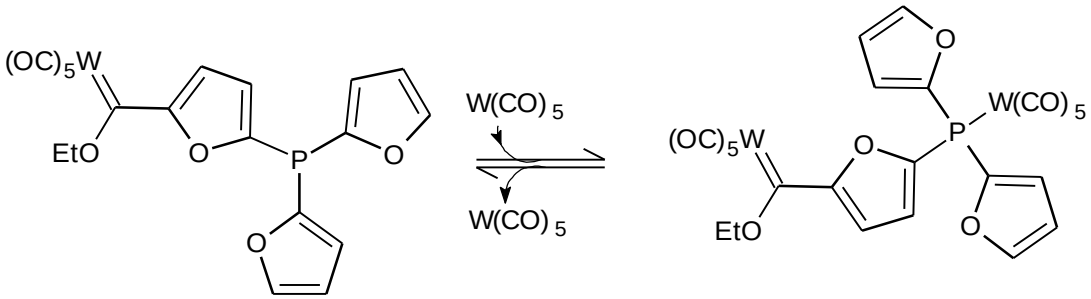

Figure 2.7 The equilibrium between **1b** and **1b** coordinated to $W(CO)_6$

A second possible explanation for this observation was the formation of isomers during the reaction. A review by M. Bigorgne[10] states that each isomer in solution exhibits its own peaks, while Fernández, et al.[11] showed with computational modelling that there are two different ways in which the alkoxy substituent on the Fischer carbene complex could orientate during synthesis of carbene complexes. Jayaprakash, *et al.*[12] explained why such a significant difference in the NMR resonances of *syn* and *anti*-conformations of ethoxy groups relative to the carbene complex could exist. It is stated that in the *anti*-conformation the ethoxy group is found in an anisotropic shielding zone of the aromatic ring, thus the protons can experience an upfield shift as high as 0.9-1.0 ppm relative to the protons of the *syn* conformation. These two conformations are represented in Figure 2.8. It was further reported that the *syn* and *anti*-conformations were convertible via the C-heteroatom bond, however, there were many effects that play a role in which isomer was the preferred one (like solvent effects and ligand donating or withdrawing groups).

© University of Pretoria

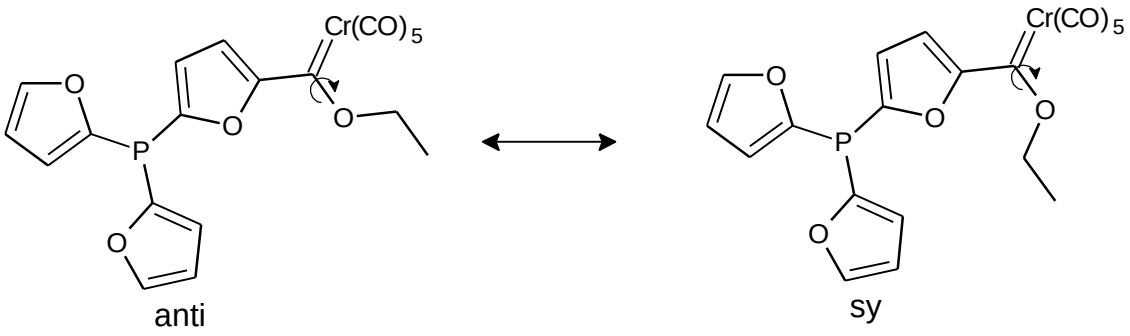

Figure 2.8 *syn* and *anti*-conformations of the ethoxy group of Fischer carbene complexes

More likely, as it represents a far greater electronic impact, is a structure where the ethoxy substituent is either on the same side as the oxygen of the furan ring (Z isomer) or on opposite sides (E isomer), represented in Figure 2.9.

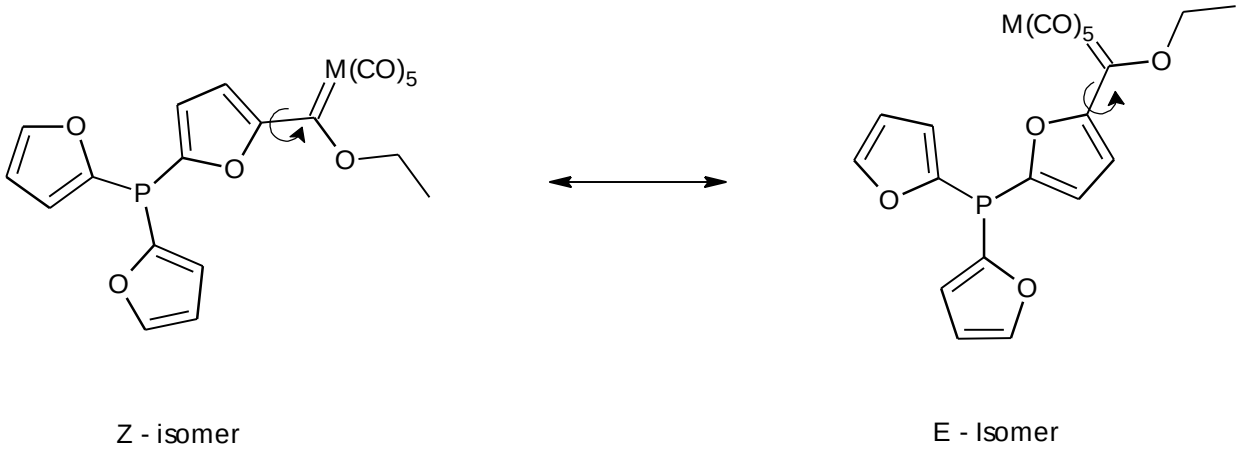

Figure 2.9 E/Z isomers formed due to restricted rotation of the furyl carbon and carbene carbon bond

The electronic difference between the isomers is greater because the effect is closer to the furan ring. Such a structure was reported by Crause[13] where both possibilities were found in the same molecule of a biscarbene complex of furan in the solid state.

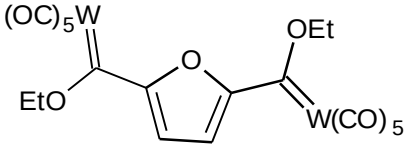

Figure 2.10 Bistungsten carbene complex of furan[13]

© University of Pretoria

Knowing that there were four possible products present in the isolated sample, the next challenge was to assign the products to their respective ^{31}P NMR spectral peaks shown in Figure 2.11.

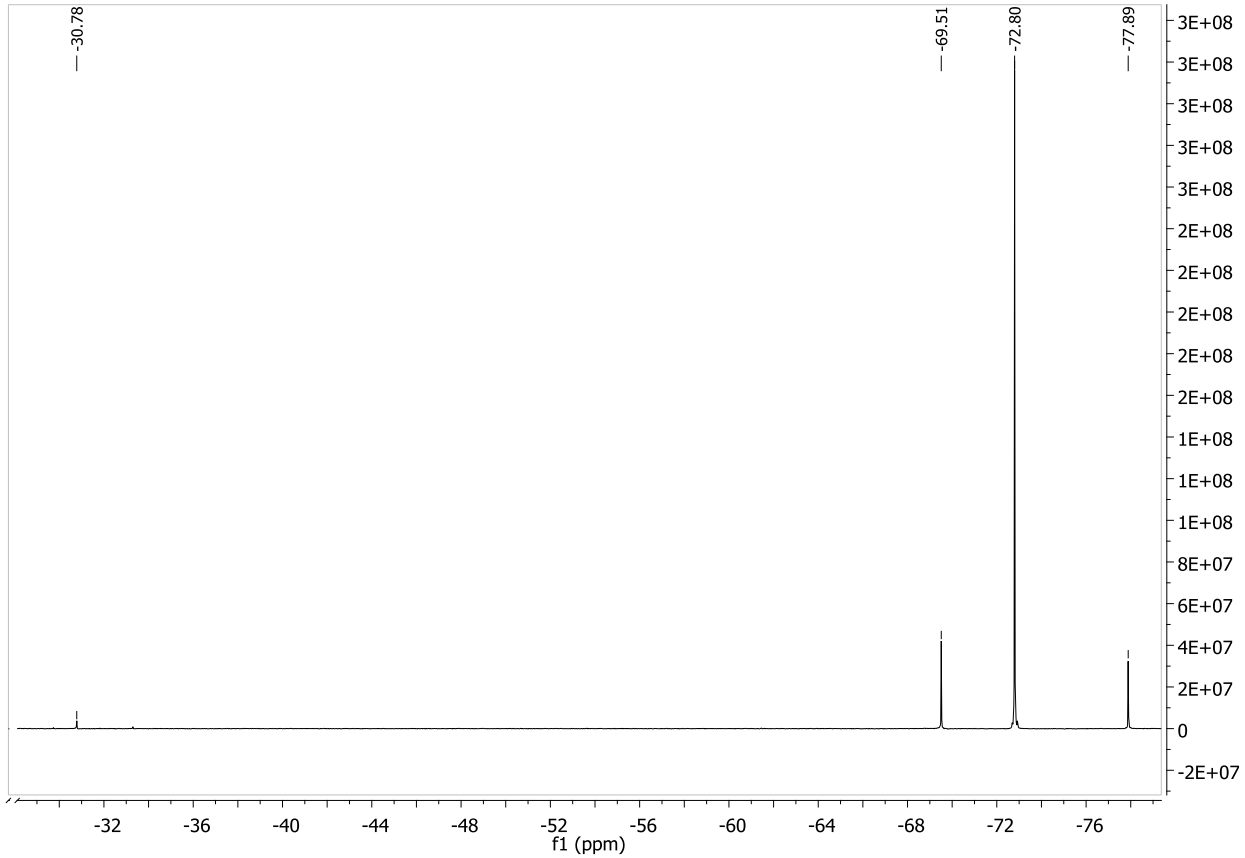

Figure 2.11 The ^{31}P NMR spectrum of compound **1b**

A phosphine coordinated to a metal has a ^{31}P NMR chemical shift value between -30 and -35 ppm while the free phosphine has a value of between -50 to -80 ppm. These values were observed on analysis of coordinated and free phosphine products throughout this project. From the spectrum in Figure 2.11, it was possible to see that the major product (**1b**) was present at a value of -72.9 ppm and that two other free phosphines were present as minor products with ^{31}P NMR values at -69.5 and -77.9 ppm. The fourth product was present in very small amounts at -30.8 ppm.

The infrared spectrum showed two pentacarbonyl moieties which were electronically very different from each other, indicating the formation of a coordinated phosphine ligand within the isolated product solution. The ^{31}P NMR signal at -30.8 ppm (Figure 2.11), and the weak duplication of IR bands definitely reveals the presence of

© University of Pretoria

coordination to a second $W(CO)_5$ fragment by the phosphorous atom. The ^{31}P NMR spectrum of compound **1b** lies more in favour of the formation of different isomers within the product solution, since the NMR spectrum showed only free phosphines present. It was still a difficult task to draw conclusions as to what the additional two minor products were.

It is important to note that the presence of additional isomeric products is observed only for **1b** and not for **1a**. This implies a steric complication and is the result of restricted rotation caused by the large $W(CO)_5$ moiety. Thus the large fragment restricts rotation around the C(furyl)-C(carbene) and C(carbene)-O bonds. By contrast, the $Cr(CO)_5$ fragment is much smaller and the complication of restricted rotation does not exist for **1a**. A crystal structure of the biscarbene complex isolated by Crause[13] (Figure 2.10) contained the two different conformations for tungsten carbene complexes on a single molecule confirms the existence of such isomeric compounds. It would be expected that there will be a difference in the electronic environments of the carbene substituents of the isomers, but not a very big difference in ^{31}P NMR chemical shift values. In taking both the NMR and IR spectra into consideration, it can be concluded that the three upfield resonances observed in the ^{31}P NMR spectra of **1b** are isomers. The duplication of the furyl signals in the ^{1}H NMR spectra can be ascribed to E/Z isomers as different orientation of the –OEt substituents should not affect the chemical shifts of the furyl units.

X-Ray crystallographic structure of 1b

The growing of crystals and the obtained molecular structure of **1b** came as a surprise since the compound was oily in consistency and spectral analysis of the compound revealed the presence of isomers. The obtained crystal was that of the E-isomer and was grown in a 1:1 mixture of DCM:Hexane at 5°C. The ligand environment around the tungsten atom is octahedral while that around the phosphorous atom is trigonal pyramidal. As a result of this the molecule looks lop-sided with a high density of atoms around the bridging furan‘s oxygen. The lone pair on the phosphorous atom points to the open side of the molecule away from the bulky $W(CO)_5$ group.

© University of Pretoria

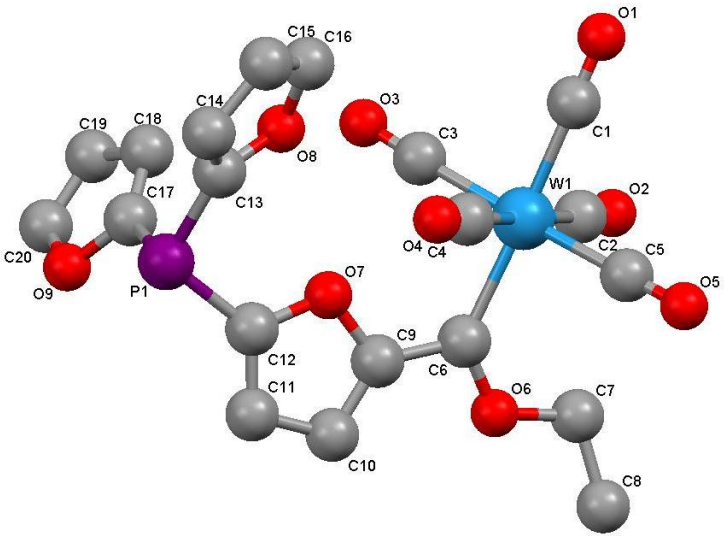

Figure 2.12 Ortep diagram of **1b**

Selected bond lengths, angles and torsion angles of **1b** are listed in Tables 2.6 and 2.7.

Table 2.6 Selected bond lengths of **1b**

Atoms	Bond length (Å)	Atoms	Bond length (Å)
W1-C1	2.031(2)	P1-C12	1.812(2)
W1-C6	2.171(2)	P1-C13	1.789(2)
C6-O6	1.327(2)	P1-C17	1.812(2)
C6-C9	1.460(2)	C13-C14	1.361(3)
O7-C9	1.376(2)	C14-C15	1.419(3)
O7-C12	1.366(2)	C15-C16	1.335(3)
O8-C13	1.376(2)	C17-C18	1.355(3)
O8-C16	1.371(3)	C18-C19	1.424(3)
O9-C17	1.379(2)	C19-C20	1.330(3)
O9-C20	1.372(3)	W1-C2	2.049(2)
C9-C10	1.366(2)	W1-C3	
C10-C11	1.412(2)	W1-C4	
C11-C12	1.366(3)	W1-C5	

© University of Pretoria

Table 2.7 Selected bond and torsion angles of **1b**

Atoms	Bond angle (°)	Atoms	Torsion angle (°)
C1-W1-C4	89.93(8)	W1-C6-C9-O7	8.4(2)
C3-W1-C4	90.52(8)	O6-C6-C9-C10	6.8(3)
C3-W1-C6	90.48(7)		
W1-C6-O6	131.5(1)		
W1-C6-C9	123.4(1)		
06-C6-C9	105.0(1)		
C12-P1-C13	103.54(8)		
C12-P1-C17	99.99(8)		
C13-P1-C17	100.68(8)		

The aromatic furyl ring is thought to contribute significantly to the stability of the compound. By investigating and comparing the bond lengths of the furyl ring containing the carbene substituent with the other furyl substituents, it was possible to determine if the lone pair of electrons present on the phosphorous atom plays a role in the stabilisation of the carbene substituent in **1b**. On comparing the three P-furyl bond distances, it was found that there was no significant difference between the bond lengths. There are more prominent differences observed when the different furyl groups in the molecule are compared. It is observed that the furyl that carries the carbene substituent has one significantly different double bond compared to the other furyl groups. The C15-C16 and C19-C20 bonds are significantly shorter than that of C9-C10 (on the carbene carrying furyl group) with values of 1.335(2) and 1.330(2) to 1.366(2) Å. The carbon-carbon single bond in the furyl groups are slightly shorter for the carbene containing furyl group and has a value of 1.412(2) Å compared to 1.419(2) Å for the other furyl groups. This indicates some delocalisation from C9 to the carbene carbon C6.

© University of Pretoria

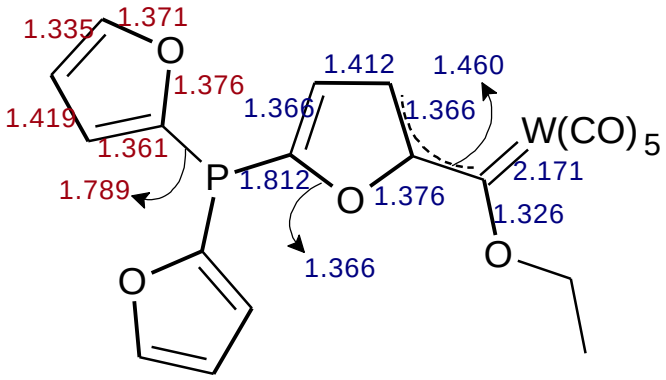

Figure 2.13 Bond distances (Å) in **1b**

The most important aspect of the structure is found in the angles of the substituents around the phosphorous atom. Angles around the phosphorous atom clearly show that the molecule has a very prominent cone angle with an average value for the C-P-C angles as 101.40(2)°. This shows that the lone pair of phosphorous is not involved in stabilizing the carbene carbon by electron delocalisation via π-conjugation in the solid state (compared to the structure of **7a** in Chapter 3). The angles around the carbene carbon: W1-C6-O6, W1-C6-C9 and O6-C6-C9 have respective values of 131.5(1), 123.4(1) and 105.0(1)°. Comparing these angles to the phenylmethoxycarbenecarbonyl complex of Mills and Redhouse[14], it was also found that the Cr-carbene-OMe angle had a large size of 134(2)°. This observation is attributed to steric constraints within the molecule.

A plane is constructed through the carbene containing furyl ring to look at the orientations of the other carbene and phosphine substituents.

© University of Pretoria

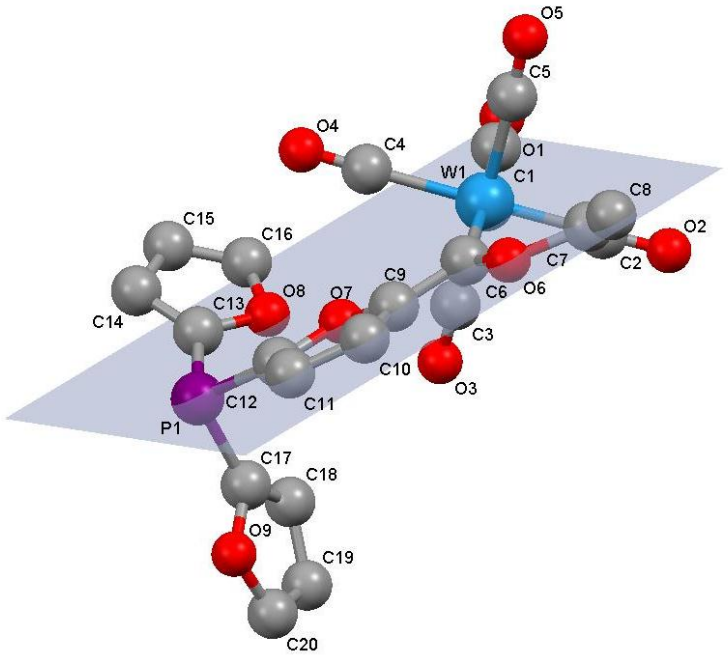

Figure 2.14 Plane through the carbene containing furyl group of **1b**

Figure 2.14 supports the observation that the $W(CO)_5$ group lies slightly above the plane and the phosphorous atom below. The torsion angle W1-C6-C9-O7 has a value of 8.4(2)°, indicating the small degree to which the $W(CO)_5$ group lies above the plane. The O6-C6-C9-C10 torsion angle has an even smaller value of 6.8(3)° showing that O6 lies slightly below the plane. The small values of these two torsion angles support the presence of a conjugated system around the carbene carbon; however, this conjugated system does not extend all the way to the phosphorous atom. The structure of **1b** revealed a tetrahedral arrangement around the phosphorous atom if the lone pair is taken into account. This supports the idea that **1b** should be a good potential ligand, using the lone pair of electrons present on the phosphorous atom.

^{1}H, ^{13}C NMR, IR and data of 2 and 5

Complex **2** and **5** were synthesised before in our laboratories as part of another project. Both classes of compounds have been published[13] and only sets of ^{1}H and ^{13}C NMR data are given here.

© University of Pretoria

(M = Cr**(a)** / W**(b)**)

2a ^{1}H NMR ($CDCl_3$): 7.82 (dd, J = 1.5, 1.0 Hz, 1H, CH), 6.98 (dd, J = 3.5, 1.0 Hz, 1H, CH), 6.57 (dd, J = 3.5, 1.5 Hz, 1H, CH), 5.15 (q, J = 7.1 Hz, 2H, CH_2), 1.64 (t, J = 7.1 Hz, 3H, CH_3). ^{13}C NMR ($CDCl_3$): 310.9, 223.9, 216.8, 164.1, 149.9, 112.9, 112.3, 75.8, 15.3. IR (hexane): 2061, 1961, 1991, 1946 cm^{-1}. MS (EI): m/z 316 [M^+].

2b ^{1}H NMR ($CDCl_3$): 7.85 (dd, J = 1.7, 0.8 Hz, 1H, CH), 7.14 (dd, J = 3.7, 0.8 Hz, 1H, CH), 6.60 (dd, J = 3.7, 1.7 Hz, 1H, CH), 4.96 (q, J = 7.1 Hz, 2H, CH_2), 1.64 (t, J = 7.1 Hz, 3H, CH_3). ^{13}C NMR ($CDCl_3$): 185.1, 203.3, 197.4, 166.3, 149.8, 114.8, 113.4, 78.4, 15.0. IR (hexane): 2070, 1958, 1990, 1944 cm^{-1}. Ms (EI): m/z 448 [M^+].

5a ^{1}H NMR ($CDCl_3$): 7.20 (s, 2H, CH), 5.20 (q, J = 7.1 Hz, 4H, CH_2), 1.71 (t, J = 7.1, 6H, CH_3). ^{13}C NMR ($CDCl_3$): 312.9, 224.0, 216.4, 161.9, 119.7, 77.2, 15.2. IR (hexane): 2054, 1964, 1955, 1949 cm^{-1}. MS (EI): m/z 564 [M^+]

5b ^{1}H NMR ($CDCl_3$): 7.28 (s, 2H, CH), 4.95 (q, J = 7.0 Hz, 4H, CH_2), 1.68 (t, J = 7.0, 6H, CH_3). ^{13}C NMR ($CDCl_3$): 285.7, 203.4, 197.7, 166.8, 121.1, 78.4, 15.3. IR (hexane): 2062, 1990, 1958, 1951 cm^{-1}. MS (EI): m/z 828 [M^+]

^{1}H, ^{13}C and ^{31}P NMR and IR data of compound 3

Table 2.8 ^{1}H, ^{13}C and ^{31}P NMR spectra of **3** ($CDCl_3$)

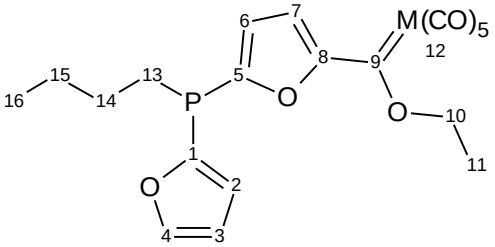

M = Cr**(a)** / W**(b)**

	3a	**3b**
^{1}H NMR		

© University of Pretoria

Proton position	δ_H/ppm	Multiplicity *J*/Hz	Integration	δ_H /ppm	Multiplicity *J*/Hz	Integration
2	6.49	m	1H	6.40	ddd, 3.4, 1.8, 0.4	1H
3	7.03	dd, 3.4, 1.6	1H	6.87	ddd, 3.2, 2.4, 0.7	1H
4	7.66 – 7.65	m	1H	7.63	dd, 1.8, 0.7	1H
6	6.89	dd, 3.7, 1.3	1H	7.00	dd,3.6, 1.3	1H
7	6.85	dd, 3.9, 0.9	1H	6.67	dd, 3.6, 0.5	1H
10	5.13	q, 7.0	2H	4.91	q, 7.1	2H
11	1.63	t, 7.1	3H	1.59	t, 7.1	3H
13	1.67 – 1.59	m	2H	2.31 – 2.10	m	4H
14	2.67 – 2.51	m	2H			
15	1.47 - 1.41	m	2H	1.44 – 1.32	m	2H
16	0.91	t, 7.1	3H	0.90 – 0.84	m	3H

^{13}C NMR				
Carbon position	δ_c/ppm	Multiplicity J_{PC}/Hz	δ_c/ppm	Multiplicity J_{PC}/Hz
1	121.1	d, 15.6	120.9	d, 17.5
2	111.3	d, 5.9	110.4	d, 6.0
3	111.0	d, 4.8	113.3	d, 2.0
4	148.2	d, 3.8	147.7	-
5	122.0	d, 17.7	122.2	d, 29.2
6	120.8	d, 14.7	120.0	d, 24.7
7	111.2	d, 4.1	110.7	d, 7.2
8	159.0	-	151.8	d, 17.5
9	312.0	-	283.8	-
10	76.0	-	78.1	-
11	15.2	-	15.0	-
12	223.8, 216.5	-	203.7, 197.3	-
13	29.1, 23.8, 25.7, 13.4	-	27.9, 23.9, 25.0, 13.7	-
14				
15				
16				

© University of Pretoria

^{31}P NMR		
	δ_p/ppm	δ_p/ppm
	-55.28	-54.97

In the case of **3a** and to a smaller extent **3b**, it was found that the ^{1}H NMR chemical shift values at positions 13 and 14 were opposite from what was expected. The proton shifts in the case of **3a** of proton 13 and 14 were 1.63 and 2.60 ppm respectively, thus the proton closer to the phosphine appeared downfield from the second proton in the butyl group. This observation gave a possible indication of the proton shielding ability of the lone pair of electrons present on the phosphorous atom.

Table 2.9 Infrared data of **3** (hexane) in the carbonyl region*

Compound	**IR carbonyl stretching frequencies (cm^{-1})**			
	$A_1^{(1)}$	**$A_1^{(2)}$**	**B_1**	**E**
3a	2069	1958	2000	1952
3b	2070	1948	1988	1948

* M = Cr**(a)** / W**(b)**

^{1}H, ^{13}C and ^{31}P NMR and IR data of compound 4 and 6

Tables 2.10 and 2.11 list the spectroscopic data of complexes **4** and **6**. Both these complexes contain multiple Fischer carbene complexes.

Table 2.10 ^{1}H, ^{13}C and ^{31}P NMR spectra($CDCl_3$) of compound **4**

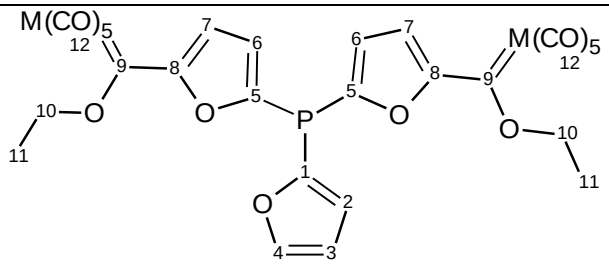

M = Cr**(a)** / W**(b)**

	4a	**4b**
^{1}H NMR		

© University of Pretoria

Proton position	δ_H/ppm	Multiplicity *J*/Hz	Integration	δ_H/ppm	Multiplicity *J*/Hz	Integration
2	6.43	ddd, 3.6, 2.0, 0.5	1H	6.41	br	1H
3	6.93	ddd, 2.5, 1.0, 0.5	1H	6.81	br	1H
4	7.66	d, 2.0	1H	7.77	br	1H
6	6.89 – 6.84	m	4H	7.05	br	2H
7				6.97	dd, 3.7, 1.2	2H
10	5.10	q, 7.0	4H	4.93	q, 7.1	4H
11	1.60	t, 7.0	6H	1.61	t, 7.1	6H

^{13}C NMR				
	δ_c/ppm	Multiplicity J_{PC}/Hz	δ_c/ppm	Multiplicity J_{PC}/Hz
1	122.8	d, 22.9	123.1	d, 18.0
2	110.7	d, 6.5	110.7	d, 6.5
3	111.2	d, 2.7	121.0	d, 5.4
4	149.1	-	148.3	d, 2.1
5	124.9	d, 33.7	125.9	d, 24.2
6	120.7	d, 13.5	113.3	d, 30.1
7	110.9	d, 7.0	121.7	d, 16.2
8	160.4	d, 4.0	160.7	d, 3.7
9	311.5	-	284.2	-
10	75.7	-	78.1	-
11	15.2	-	14.9	-
12	224.3, 216.5	-	203.7, 197.1	-

^{31}P NMR		
	δ_p/ppm	δ_p/ppm
	-69.59	-69.39

© University of Pretoria

Table 2.11 Infrared data of **4** (hexane)*

Compound	IR carbonyl stretching frequencies (cm^{-1})			
	$A_1^{(1)}$	$A_1^{(2)}$	B_1	E
4a	2061	1961	1996	1948
4b	2070	1956	1992	1942

* M = Cr**(a)** / W**(b)**

Table 2.12 ^{1}H, ^{13}C and ^{31}P NMR spectra ($CDCl_3$) of compound **6**

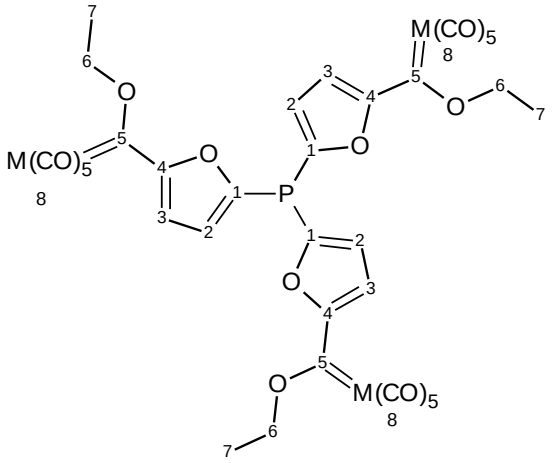

M = Cr**(a)** / W**(b)**

	6a			**6b**		
^{1}H NMR						
Proton position	δ_H/ppm	Multiplicity *J*/Hz	Integration	δ_H/ppm	Multiplicity *J*/Hz	Integration
2	6.95	dd, 3.7, 1.4	3H	7.00	m	3H
3	7.00	d, 3.7	3H	7.13	m	3H
6	5.13	q, 7.0	6H	4.91	m	6H
7	1.63	t, 7.0	9H	1.59	m	9H

^{13}C NMR				
	δ_c/ppm	Multiplicity J_{PC}/Hz	δ_c/ppm	Multiplicity J_{PC}/Hz
1	123.9	d, *J* = 18.1 Hz	125.5	-
2	154.3	d, *J* = 7.9 Hz	122.6	-
3	112.2	d, *J* = 2.4 Hz	128.4	-
4	167.4	d, *J* = 2.8 Hz	168.2	-
5	311.9	-	284.5	-

© University of Pretoria

6	76.2	-	78.5	-
7	15.2	-	14.9	-
8	224.0, 216.5	-	203.3, 197.0	-

^{31}P NMR		
	δ_p/ppm	δ_p/ppm
	-63.51	-63.18

Table 2.13 Infrared data (hexane) of **6** in the carbonyl region*

Compound	**IR carbonyl stretching frequencies (cm^{-1})**			
	$A_1^{(1)}$	**$A_1^{(2)}$**	**B_1**	**E**
6a	2061	1952	1996	1952
6b	2070	1948	1994	1948

* M = Cr**(a)** / W**(b)**

2.2.4 Compounds compared

The effect of the phosphorous atom on activation or stabilisation the carbene substituent was a very important factor that needed to be addressed. If it could be determined that the lone pair on the phosphorous atom did indeed contribute to the stability of the carbene substituents present on the molecule, the ligand coordination properties of this compound will be significantly influenced by the carbene substituent.

In the synthesis of the carbene containing phosphines, it was found that all three of the compounds, **1**, **4** and **6** were wine red. This gave the indication that each carbene substituent that was present in the compound acted as a single carbene substituent, with no electronic properties of a multiple carbene compound. A possible reason for this observation could be that the each furyl group contained enough electron density for each carbene substituent to be supported individually.

The ^{31}P NMR signals showed a slight move towards positive numbers as the amount of Fischer carbene complexes increased on the molecule. For example, values of -

© University of Pretoria

72.79, -69.59 and -63.51 ppm were observed for the **1b**, **4b** and **6b** respectively. Since the furyl groups themselves are electron-withdrawing, the carbene complex present on a furyl ring would further increase the electron-withdrawing power of the furyl group.

A final comparison that is required before any conclusions can be made is the infrared spectra of the carbonyls present in the carbene substituents of the molecules.

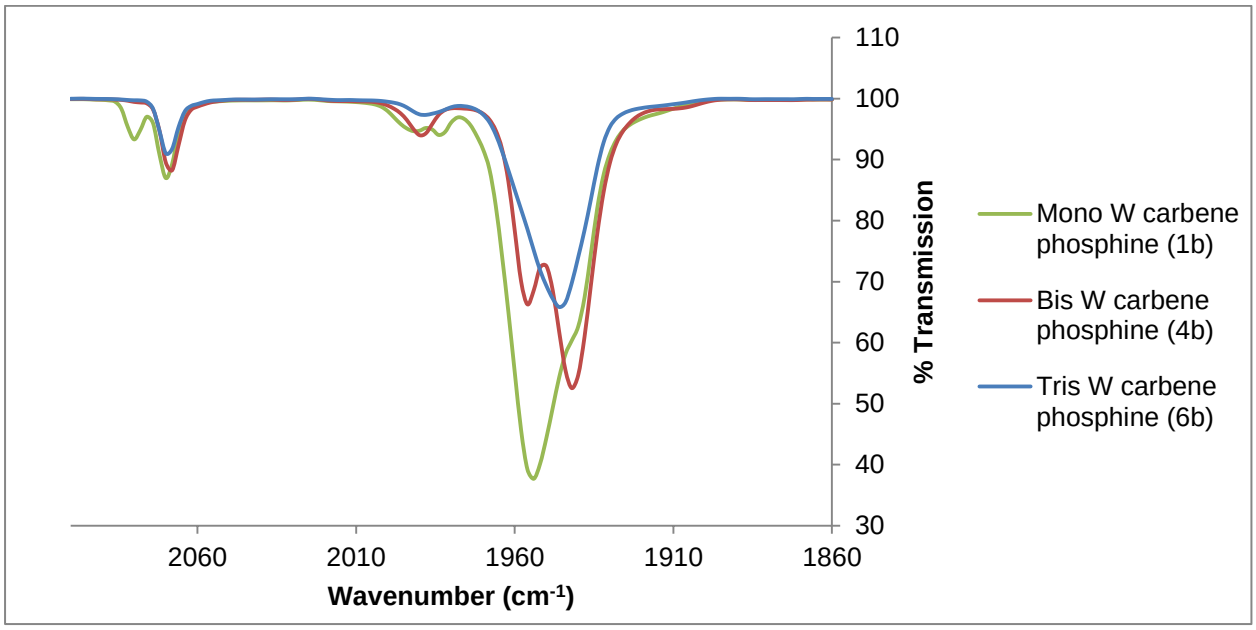

Figure 2.15 IR spectra of compounds **1b**, **2b** and **3b**

The graph above shows the differences in IR properties of **1b**, **4b** and **6b**. An important observation is that the E and $A_1^{(2)}$ bands overlap for **6b**, but in 1b the $A_1^{(2)}$ band is a shoulder of the E band. There is not any correlation between the number of carbene complexes present on the molecule and the observed wavenumber of the E band, which is the most prominent peak in the spectra.

In the overall conclusions on the multiple carbene synthesis on tri(2-furyl)phosphine it can be stated that each carbene complex present in the molecule act as an individual carbene moiety and do not influence each other electronically to any great extent. Further it was observed that the phosphine, while carrying a carbene substituent, does not lose its ligand properties and is still capable interact with transition metals.

© University of Pretoria

2.3 References

1. V. Farina. New perspectives in the cross-coupling reactions of organostannanes. *Pure Appl. Chem.* (1996) **68,** 73–78.

2. C. F. Bernasconi. Developing the physical organic chemistry of Fischer carbene complexes. *Chem. Soc. Rev.* (1997) **26,** 299–307.

3. N. G. Andersen and B. A. Keay. 2-Furyl Phosphines as Ligands for Transition-Metal-Mediated Organic Synthesis. *Chem. Rev.* (2001) **101,** 997–1030.

4. M. Ackermann, A. Pascariu, T. Höcher, H.-U. Siehl and S. Berger. Electronic Properties of Furyl Substituents at Phosphorus and Their Influence on ^{31}P NMR Chemical Shifts. *J. Am. Chem. Soc.* (2006) **128,** 8434–8440.

5. M. Hesse, H. Meier and B. Zeeh. *Spectroscopic Methods in Organic Chemistry*. (Thieme, 1997). 152 – 154.

6. E. O. Fischer, T. Selmayr and F. R. Kreißl. Übergangsmetall-Carben-Komplexe, CII. Pentacarbonyl(acyloxyorganylcarben)-Komplexe des Chroms(0) und Wolframs(0). *Chem. Ber.* (1977) **110,** 2947–2955.

7. M. Y. Darensbourg and D. J. Darensbourg. Spectroscopic studies of some carbene pentacarbonyl complexes of chromium(0) and tungsten(0). *Inorg. Chem.* (1970) **9,** 32–39.

8. P. S. Braterman. *Metal carbonyl spectra*. (Academic Press Inc., 1975).

9. L. E. Orgel. The Infrared Spectra of Substituted Metal Carbonyls. *Inorg. Chem* (1962) **1,** 25–29.

10. M. Bigorgne. Vibrational spectroscopy of metal carbonyls. *J. Organomet. Chem.* (1975) **94,** 161–180.

11. I. Fernández, F. P. Cossío, A. Arrieta, B. Lecea, M. J. Mancheño and M. A. Sierra. Structure and Conformations of Heteroatom-Substituted Free Carbenes and Their Group 6 Transition Metal Analogues. *Organomet.* (2004) **23,** 1065–1071.

12. K. N. Jayaprakash, D. Hazra, K. S. Hagen, U. Samanta, M. M. Bhadbhade, V. G. Puranik and M. Sarkar. Solution and solid state conformation of Fischer carbene complexes vis-à-vis conformation of aryl carboxamides: complexation of the aromatic ring by tricarbonylchromium makes a difference. *J. Organomet. Chem.* (2001) **617–618,** 709–722.

13. C. Crause, H. Görls and S. Lotz. Binuclear biscarbene complexes of furan. *Dalton Trans.* (2005) 1649–1657.

© University of Pretoria

14. O. S. Mills and A. D. Redhouse. Carbon compounds of the transition metals. Part XII. Crystal and molecular structure of phenylmethoxycarbene-pentacarbonylchromium. *J. Chem. Soc. A* (1968) 642–647.

© University of Pretoria

Chapter 3

Fischer Carbene Complexes of Aromatic Amine ligands

3.1 Background

Amines are ligands which are known to coordinate to a wide range of transition metals. They bind to metals in coordination complexes, enzymes and organometallic compounds. This project focuses on two specific tertiary amines and their ability to coordinate to particular transition metals. Seligson and Trogler[1] stated that amine ligand binding can be explained by using both steric and electronic parameters. In this chapter, both the steric and electronic properties of the chosen amines are altered and their ability to coordinate also brought into question. The two chosen amines are tris(4-bromophenyl)amine, $N(C_6H_4Br)_3$, and NN-dimethylaniline $(CH_3)_2NC_6H_5$. The electronic alteration of $N(C_6H_4Br)_3$ and $(CH_3)_2NC_6H_5$ involves addition of one or more Fischer carbene substituents to the phenyl rings present in each of the amines. N,N-dimethyl analine is further altered by coordination of a π-arene ring to $Cr(CO)_3$ to activate the aromatic ring for further reactions. Steric implications of the novel amines will finally determine if coordinating to a second metal is possible.

3.2 Tris(4-bromophenyl)amine as precursor for a novel ligand

Lithium-halogen exchange was first used to introduce R groups at specific positions on aromatic rings by Gilman and Jacoby[2] in 1938. The concept was developed further to include electrophilic and other functional groups which could be placed at strategic positions on aromatic molecules[3]. Most metal stabilised Fischer carbene complexes were synthesised with lithiation at an activated site of an aromatic ring. However, the activation of a specific site by bromination of an aromatic compound lead to very specific lithiation reactions[4]. Site-specific carbene formation for unreactive aromatic compounds was now able to occur.

© University of Pretoria

Fischer and Maasböl constructed one of the very first Fischer carbene complexes with a phenyl ring[5]. It was understood that the π-electron density on the ring would provide some stability to the very electrophilic carbene carbon once the substituent was synthesised. Taking this assumption into account, this part of the project involved the syntheses and analysis of more than one carbene substituent on tris(4-bromophenyl)amine and the investigation of the stability of the formed compounds.

3.2.1 The reaction of $N(C_6H_4Br)_3$ with excess *n*BuLi

As with the tri(2-furyl)phosphine in chapter 2, $N(C_6H_4Br)_3$ was capable of carrying more than one Fischer carbene substituent. The carbene substituents were introduced onto the molecule in subsequent steps as shown in Scheme 3.1.

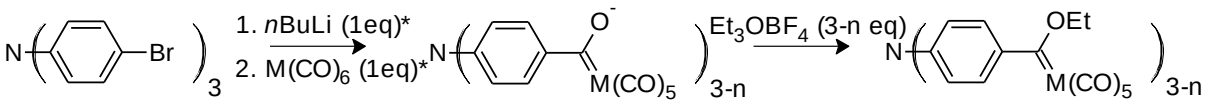

Scheme 3.1 Synthesis of multi-carbene complexes on $N(C_6H_4Br)_3$

Lithiation at the bromo-position of the phenyl ring with a single equivalent of *n*BuLi replaced the electronegative bromine atom with a Li^+ atom, making the particular carbon very electron rich. On addition of 1 equivalent metal carbonyl ($Cr(CO)_6$ or $W(CO)_6$), the lithiated carbon on the phenyl ring reacted with one of the carbonyls of the metal, forming a metal acylate. On addition of the alkylation agent, Et_3OBF_4, the carbene complex was successfully synthesised. For the synthesis of more than one carbene substituent on the amine, stepwise addition of a second and third equivalent of *n*BuLi and metal carbonyl was required before the addition of three equivalents of the alkylation agent (Table 3.1). The following products were obtained from the reaction:

© University of Pretoria

Table 3.1 Reaction products of carbene synthesis on $N(C_6H_4Br)_3$

7	8	9
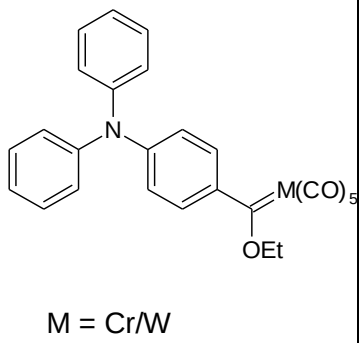 M = Cr/W	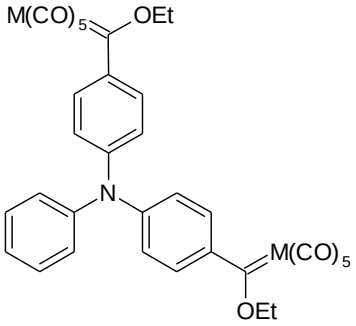	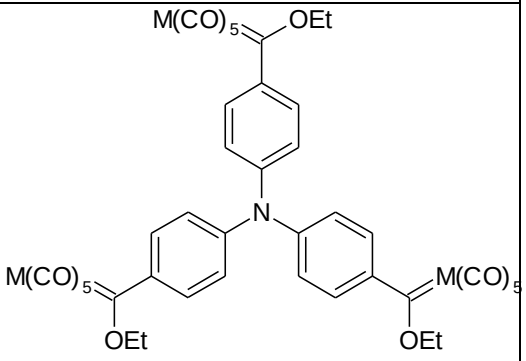

On separation of the products, all three compounds were found to have an intense orange colour, with increased colour intensity as the amount of carbene substituents on the molecule increased. In earlier work by our research group[4,6], it was found that if more than one carbene complex was present in a molecule the biscarbene compound would usually be a different colour (purple) from the monocarbene (orange) due to significant differences in the electronic properties of the molecules that were induced by the additional carbene ligands on the compound.

Comparing compounds **7**, **8** and **9** with that of the previous research' results one would think each carbene substituent present on the amine acted as a single carbene substituent. This same observation was made in the synthesis of multiple carbene substituents on PFu_3 in Section 2.2.2. The obtained results suggested that the lone pair of electrons present on the nitrogen atom was delocalised throughout the molecule, as is depicted in Figure 3.1.

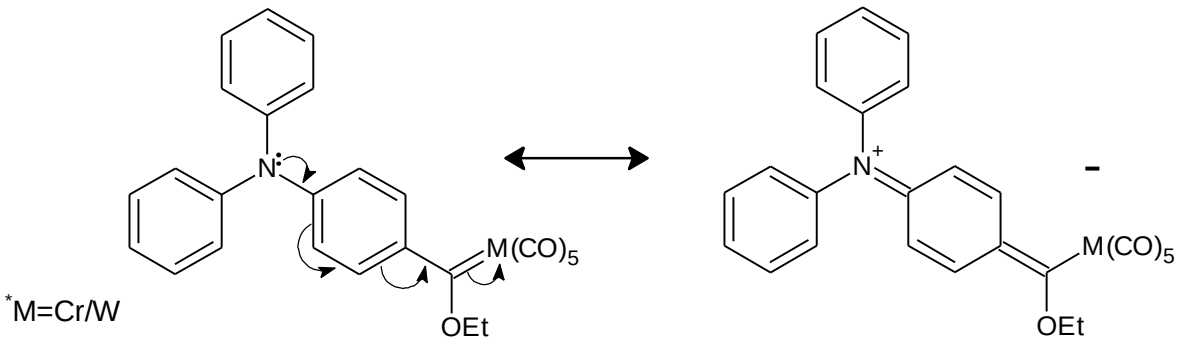

Figure 3.1 Resonance structures of carbene stabilisation in **7**.

© University of Pretoria

One of the very first observations was made after product isolation, was that the bromine atoms that were supposed to be present on the *para*-position in **7** and **8** was no longer present. There are two possible explanations for this observation. It was believed that the bromine atom could be lost during the reaction itself where it was able to obtain a proton during the alkylation step with Et_3OBF_4. Another possibility was that the bromine atom was lost during product separation on the column. It is believed that the slight acidity and aqueous environment of the column played a catalytic role in the debromination, The synthesis of 4-Nitrophenyl-bis(4'-bromophenyl) amine by Eberson[7] also involved separation of products on a silica gel column, though, the bromine substituents were still present after product isolation. This could indicate that the bromine substituents were lost during the synthesis of the compounds themselves.

3.2.2 C^{13} and H^1 NMR data analysis of reaction products

The ^{13}C and ^{1}H NMR analysis of compounds 7, 8 and 9 are listed in Tables 3.2 to 3.4 followed by the discussion of the data of all three compounds. Due to the poor resolution of the ^{1}H NMR of these compounds in $CDCl_3$, NMR spectra were also obtained in C_6D_6.

Table 3.2 H^1 and C^{13} NMR data ($CDCl_3$) of **7**

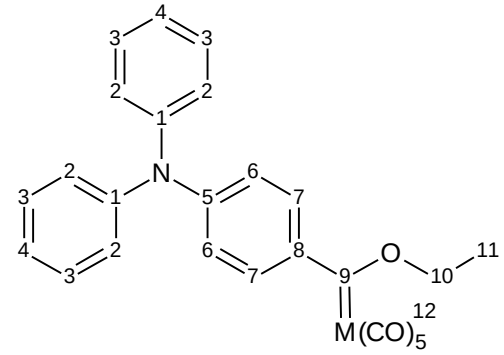

M = Cr**(a)** / W**(b)**

	7a			**7b**		
			H^1 NMR			
Proton position	δ_h/ppm	*J*/Hz	Integration	δ_h/ppm	*J*/Hz	Integration
2	7.16	br	4H	7.43	d, 8.7	4H
3	7.33	br	4H	7.16	dd, 12.1,	4H

© University of Pretoria

					7.9	
4	7.16	br	2H	7.20	br	2H
6	6.91	br	2H	7.01	d, 9.2	2H
7	7.70	br	2H	7.78	d, 9.4	2H
10	5.15	q, 7.1	2H	5.01	q, 7.1	2H
11	1.93	t, 7.1	3H	1.66	t, 7.1	3H

C^{13} NMR		
	δ_c/ppm	δ_c/ppm
1	145.4	146.5
2	129.9	129.3
3	126.5	130.9
4	118.5	126.8
5	145.0	147.3
6	125.2	121.1
7	130.4	131.6
8	152.4	150.9
9	332.2	308.5
10	76.6	79.1
11	14.7	15.0
12	224.3, 217.8	197.9, 191.1

7a H^1 NMR (C_6D_6): 7.66 (d, J = 7.9 Hz, 2H, CH), 6.98 (d, J = 6.9 Hz, 4H, CH), 6.93 (d, J = 6.6 Hz, 4H, CH), 6.87 (d, J = 6.6 Hz, 2H, CH), 6.78 (d, J = 8.1 Hz, 2H, CH), 4.71 (q, J = 6.4 Hz, 2H, CH_2), 1.04 (t, J = 6.4 Hz, 3H, CH_3).

Table 3.3 H^1 and C^{13} NMR data ($CDCl_3$) of **8**

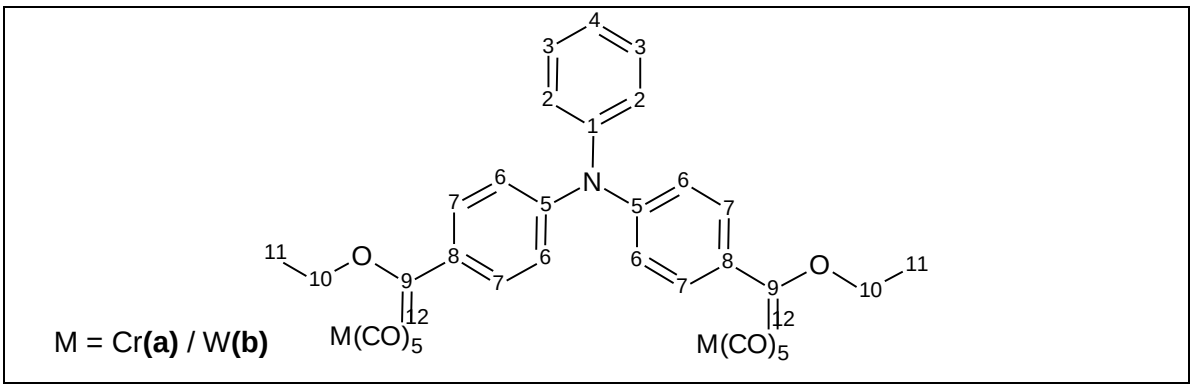

© University of Pretoria

	8a			8b		
H^1 NMR						
Proton position	δ_h/ppm	*J*/Hz	Integration	δ_h/ppm	*J*/Hz	Integration
2	7.37	br	2H	7.47	d, 8.8	2H
3	7.16	br	2H	7.17-7.14	m	2H
4	7.23	br	1H	n.o	-	-
6	7.07	br	4H	7.74	d, 8.9	4H
7	7.61	br	4H	7.06	d, 8.9	4H
10	5.15	br	4H	5.03	q, 7.1	4H
11	1.74	br	6H	1.68	t, 7.1	6H

C^{13} NMR		
	δ_c/ppm	δ_c/ppm
1	145.4	146.8
2	127.0	128.0
3	130.0	130.1
4	126.0	126.8
5	147.3	148.9
6	121.6	121.8
7	128.5	130.9
8	149.9	150.0
9	337.9	311.1
10	77.0	79.6
11	15.2	15.0
12	223.9, 216.8	203.1, 197.7

8a H^1 NMR (C_6D_6): 7.47 (d, J = 7.5 Hz, 4H, CH), 6.99 (d, J = 6.0 Hz, 1H, CH), 6.92 (d, J = 6.7 Hz, 2H, CH), 6.87 (d, J = 6.4 Hz, 2H, CH), 6.79 (d, J = 7.7 Hz, 4H, CH), 4.66 (q, J = 6.4 Hz, 4H, CH_2), 1.03 (t, J = 6.5 Hz, 6H, CH_3).

© University of Pretoria

Table 3.4 H^1 and C^{13} NMR data ($CDCl_3$) of **9**

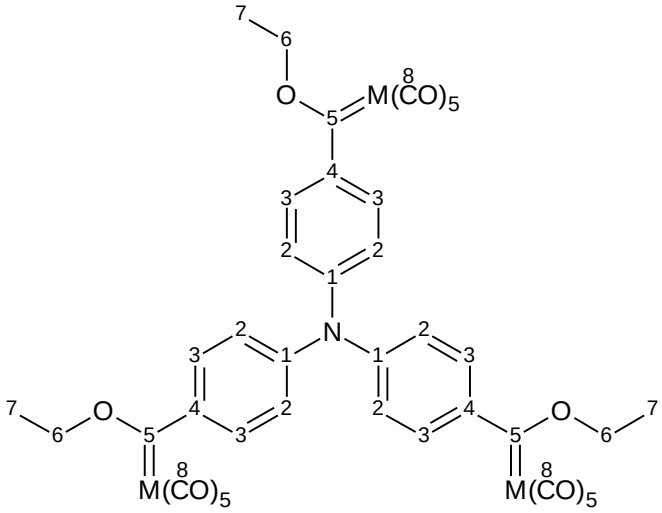

M = Cr**(a)** / W**(b)**

	9a			**9b**		
H^1 NMR						
Proton position	δ_h/ppm	*J*/Hz	Integration	δ_h/ppm	*J*/Hz	Integration
2	6.79	d, 8.7	6H	6.77	d, 8.8	6H
3	7.38	d, 8.7	6H	7.57	d, 8.8	6H
6	4.64	q, 7.0	6H	4.60	q, 7.0	6H
7	1.03	t, 7.0	9H	1.04	t, 7.1	9H

C^{13} NMR		
	δ_c/ppm	δ_c/ppm
1	148.9	149.3
2	123.5	123.3
3	127.8	130.2
4	149.3	150.1
5	340.2	312.4
6	77.4	79.8
7	14.7	14.1
8	224.1, 217.1	203.2, 197.5

Eberson, Hartshorn and Svensson[7] synthesised compounds very similar to **7**, **8** and **9** with the exception that a nitro-substituent was present at the 4-position instead of a carbene substituent. On comparison of the proton spectra of Eberson to the

© University of Pretoria

synthesised compounds, it was found that the proton spectra of the phenyl ring containing the nitro-substituent were more downfield (between 9.10 and 6.95 ppm) than that of the phenyl ring containing a carbene substituent (6.77 and 7.80). This collaborates with the fact that the nitro group is known to be one of the most chemical deactivating groups within the electron withdrawing aromatic substituent series[8].

Illustrated in the Figure 3.2 was the observed difference in the C^{13} NMR spectra of the three different compounds, where **7a**, **8a** and **9a** had carbene carbon NMR shifts of 333.00, 338.24 and 340.72 ppm respectively. Thus, as the number of carbene substituents on the molecule was increased, the carbene carbon shift appeared more downfield. Further it is observed that the chemical shift values of the *trans*-carbonyl peaks remain constant throughout the increase of the carbene substituents on the molecule at 223.8 ppm while the *cis*-carbonyl peaks appear more upfield as the number of carbene substituents is increased on the molecule.

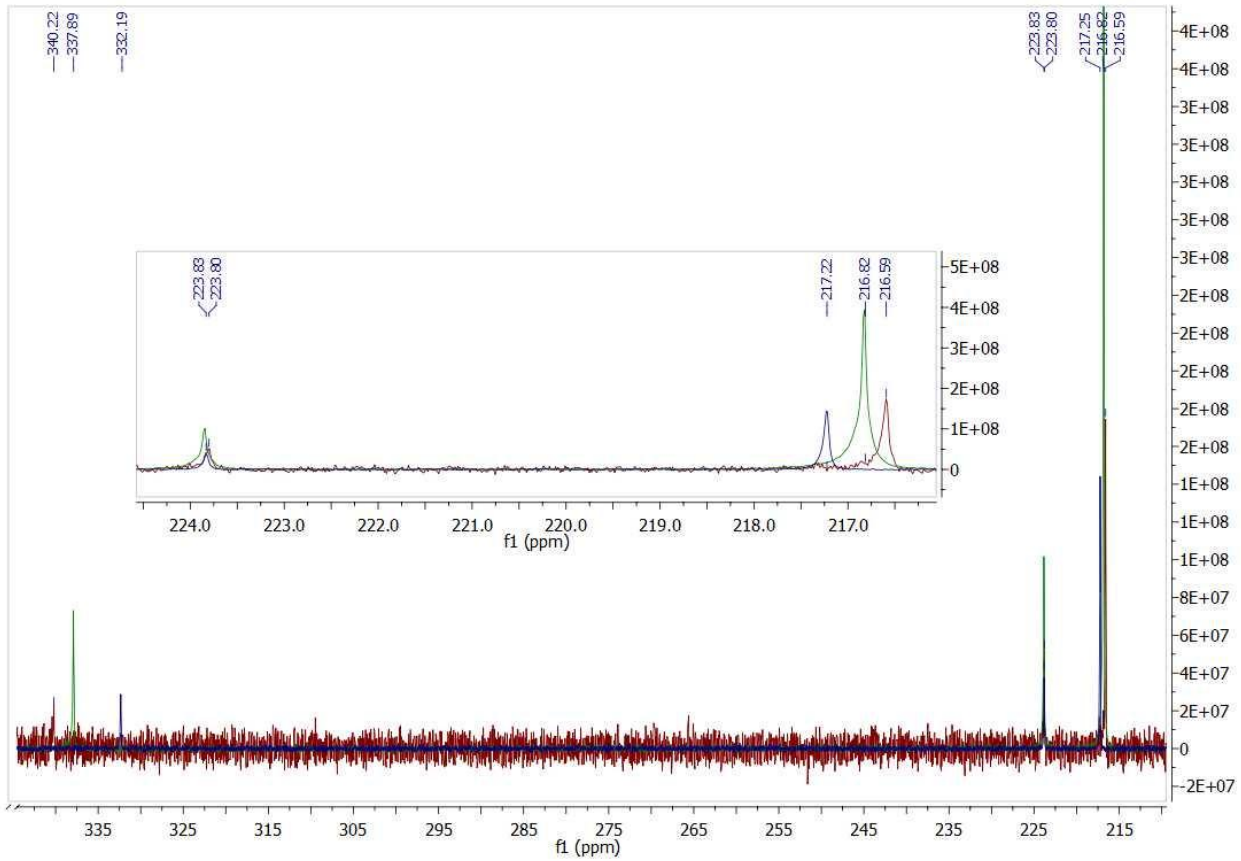

Figure 3.2 Superimposed C^{13} NMR spectra ($CDCl_3$) of carbene and carbonyl chemical shift values of **7a**, **8a** and **9a**

© University of Pretoria

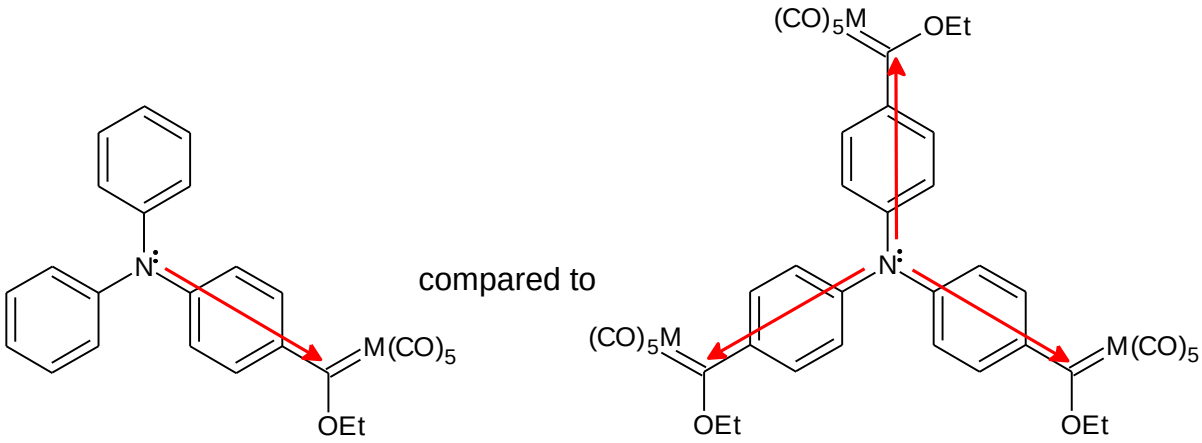

Figure 3.3 Carbene substituent stabilisation effects of the electron lone pair present on the nitrogen in **7** and **9**

Figure 3.3 illustrates the effect that additional carbene substituents have on the carbene system itself. It is known that the carbene carbon present in the complex is highly electron deficient[9], which supported the very high resonance values of carbene carbon in each particular complex. In Figure 3.2 it was noted that the more carbene substituents present on the molecule, the more deshielded the carbene carbons became. When the number of the carbene substituents were increased, the electron density present on the nitrogen was spread throughout the molecule, thus less electron density was available for the stabilisation of a single carbene substituent since the carbenes had to share the electron density.

3.2.3 IR analysis of reaction products

The only carbonyl ligands that were present, were in the carbene substituent, which contained a pentacarbonyl fragment.

Table 3.5 IR data (hexane) in the carbonyl region of **7a**, **8a** and **9a**

	IR carbonyl stretching frequencies (cm^{-1})			
	$A_1^{(1)}$	**$A_1^{(2)}$**	**B_1**	**E**
7a	2056	1950	1984	1944
8a	2057	1950	1987	1950

© University of Pretoria

9a	2057	1949	1983	1949

Table 3.6 IR data (hexane) in the carbonyl region of **7b**, **8b** and **9b**

	IR carbonyl stretching frequencies (cm^{-1})			
	$A_1^{(1)}$	**$A_1^{(2)}$**	**B_1**	**E**
7b	2064	1950	1988	1950
8b	2066	1948	1984	1948
9b	2058	1952	1988	1952

From Table 3.5 it was observed that the $A_1^{(1)}$ band remained relatively constant for all the compounds. Nevertheless, there were small changes in the wavenumbers of the $A_1^{(2)}$ and E-bands of the different compounds. Cotton and Kraihanzel[10] stated that carbonyl stretch-stretch interaction constants should increase with increasing replacement of CO with ligands with lower π-bonding ability. This meant that as the back-bonding from the metal to the carbonyl groups increased, the metal-carbene bond became weaker. The C-O bond became weaker accordingly and carbonyl stretching frequency appeared at lower wavenumbers. Carbene ligands are weaker π-acceptors than carbonyl ligands, thus back-bonding from the metal to the carbonyl ligands increased and the ν_{CO} vibrations occurred at lower wavenumbers than for the metal carbonyl complexes[11].

It was expected that the CO stretching vibrations of **7**, **8** and **9** should have increasing E-band wavenumbers since less electron density from the nitrogen is available for carbene stabilisation as the amount of carbene substituents present in the molecule increases. This observation was noted in Table 3.5 in the wavenumbers of the E stretching mode which had values of 1944 and 1949 cm^{-1} for **7a** and **9a** respectively. It was also observed that the values of the E-bands of **8a** and **9a** were very similar, thus not following the expected pattern.

© University of Pretoria

3.2.4 X-ray Crystallography

Single-crystal X-Ray diffraction analysis confirmed the structure for **7a**, but it was unfortunately not possible to obtain crystals for **8a** or **9a**. It was also found that only Cr carbene complexes formed crystals while the tungsten analogs were amorphous. The crystal structure of **7a** supported the loss of the bromine atoms during the synthesis of the compounds. The complexes were crystallised during slow vacuum removal of hexane and the obtained crystals were bright red coloured. Figure 3.4. represents the ORTEP[12] + POV-Ray[13] plot of the geometry of compounds **7a** as well as the atom numbering scheme used for further analysis of the structure. The structure display an octahedral arrangement of ligands around the chromium atom. The metal-carbene substituents and nitrogen are all in the same plane.

Selected bond lengths, angles and torsion angles are tabulated in Table 3.7.

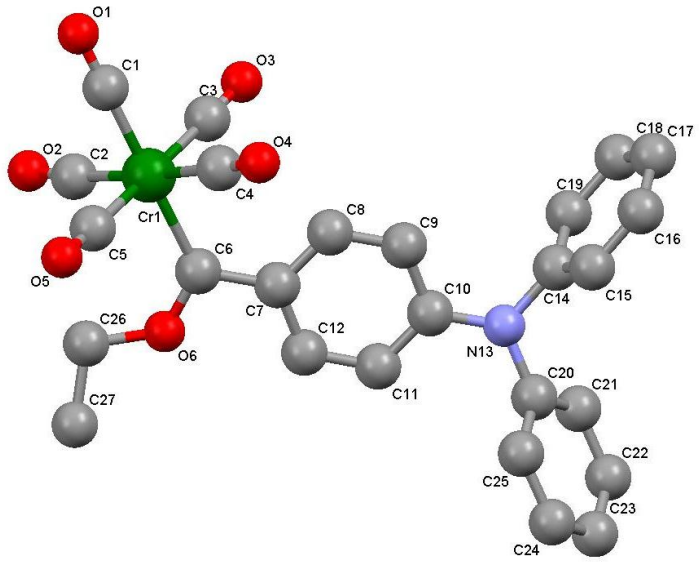

Figure 3.4 Ortep diagram of **7a**.

Table 3.7 Selected bond lengths of **7a**.

Atoms	Bond length (Å)	Atoms	Bond length (Å)
Cr1-C1	1.875(2)	Cr1-C2	1.903(2)
Cr1-C6	2.096(2)	Cr1-C3	

© University of Pretoria

C6-O6	1.328(2)	Cr1-C4	
C6-C7	1.480(3)	Cr1-C5	
C7-C8	1.402(2)	C14-C15	1.385(2)
C7-C12	1.413(3)	C14-C19	
C8-C9	1.377(3)	C15-C16	
C9-C10	1.408(3)	C16-C17	
C10-C11	1.408(2)	C17-C18	
C11-C12	1.377(3)	C18-C19	
C10-N13	1.378(3)	C20-C21	1.386(3)
N13-C14	1.446(2)	C20-C25	
N13-C20	1.434(3)	C21-C22	
		C22-C23	
		C23-C24	
		C24-C25	

Table 3.8 Selected bond and torsion angles of **7a**.

Atoms	**Bond angles (°)**	**Atoms**	**Torsion angles (°)**
C1-Cr1-C4	90.07(8)	Cr1-C6-C7-C8	0.9(2)
C2-Cr1-C5	94.36(8)	O6-C6-C7-C12	-1.9(2)
C2-Cr1-C6	93.33(7)	C6-O6-C26-C27	-163.9(2)
C3-Cr1-C4	91.92(8)	C9-C10-N13-C14	-4.4(2)
C10-N13-C14	120.5(1)	C10-N13-C14-C19	-78.1(2)
C10-N13-C20	122.6(1)	C14-N13-C20-C21	-65.2(2)
C14-N13-C20	116.3(1)		
Cr1-C6-O6	126.9(1)		
Cr1-C6-C7	127.2(1)		
O6-C6-C7	105.9(1)		

The angles involving the central nitrogen atom deviate only slightly from 120° which indicated that the nitrogen lies in a flat plane with the carbons of the bridging-phenyl ring attached to it. The bond closely resembles a sp^2-hybridised nitrogen with the lone pair in a p-orbital. The latter is favourably orientated to participate in π-interaction with the bridging 1,4-phenylene π-cloud and the empty p-orbital of the carbene carbon atom. This solid state feature supports the NMR data of extensive

© University of Pretoria

delocalisation of the N-atom lone pair towards the carbene atoms (also expected in 8 and 9). The torsion angle between C9-C10-N13-C14 is small, i.e. -4.4(2)°, further supporting the previously mentioned statement. An interesting observation lies in the fact that the torsion angle of the bond between the carbene carbon and the phenyl carbon to which it is attached, atoms Cr1-C6-C7-C8, has a value of 0.9(2)°. This observation is in contrast with the observations made by Mills and Redhouse[14] who did crystallographic studies on phenylmethoxycarbenepentacarbonylchromium (which was first synthesised by Fischer and Maasböl[15]) and found that the structure showed the phenyl plane was roughly perpendicular to the carbene plane. This implied that the π-electron system did not interact with the carbene substituent present on the ring. However, this represents the major difference between the single phenyl system when compared to the multiple phenyl system of this study. Another difference of compound **7a**, compared to Mills and Redhouses's phenyl carbene structure is the angles around the carbene. They recorded a value of 134° for the Cr-carbene-O angle, 122° for the C-carbene-O angle and 104° for the C-carbene-Cr angle. Compound **7a** revealed angles of 126(1)°, 127(1)° and 105(1)° for the respective angles. The observed difference can be attributed to steric factors.

Seeing as there was no significant cone angle between the nitrogen and phenyl ipso-carbon atoms, which further supports the fact that the electron lone pair on the N-atom is delocalised. A comparison of the bond distances in the bridging phenylene ring with the two other phenyl rings present in the molecule will give an indication as to how the electron lone pair has been delocalised.

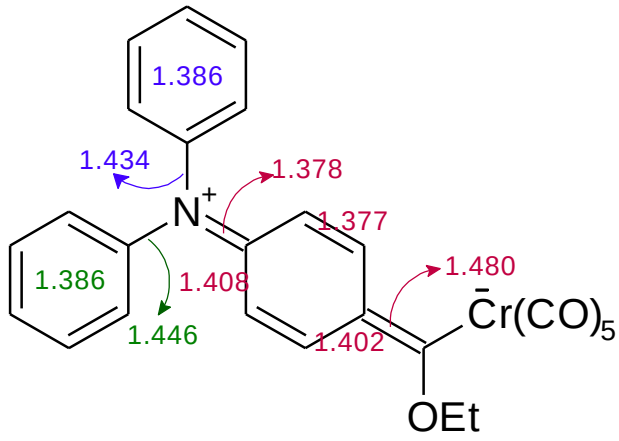

Figure 3.5 Bond lengths (Å) of the phenylene and phenyl rings of **7a**

© University of Pretoria

Figure 3.5 clearly shows the delocalisation of the nitrogen lone pair into the bridging phenylene to show diene character rather than phenyl character as in the case of the other two phenyl rings in the molecule. The bond between the nitrogen and the phenyl ring containing the carbene substituent, C10-N13, is significantly shorter when compared to the other nitrogen-phenyl bond lengths. The carbene-phenyl bond has a distance of 1.480(3) Å and is in the range of the expected value for the bonding between two sp^2 hybridised carbon atoms[16].

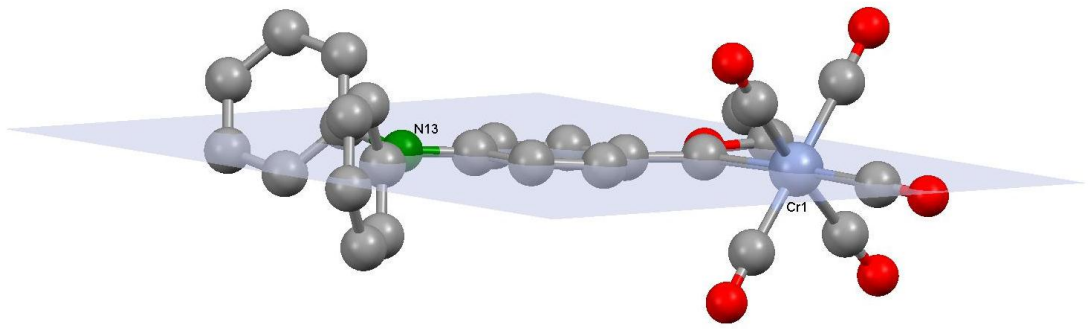

Figure 3.6 A plane through the phenyl ring and its carbene substituent of **7a**

Figure 3.6 illustrates the plane through the six carbon atoms of the phenyl ring containing the carbene substituent and the nitrogen atom. The chromium metal-centre falls in the same plane as the phenyl ring. This supported the concept that the electron lone pair present on the nitrogen is delocalised throughout the conjugated system towards the carbene carbon.

When the phenylmethoxycarbene compound of Mills and Redhouse[14] was compared to **7a**, there were similarities such as that the chromium-carbonyl bond distances were smaller than the chromium-carbene distance, with mean values of 1.903(2) and 2.096(2) Å respectively. This is because the π-acceptor ability of the CO ligand is greater than that of the carbene-carbon.

Compound **7a** belongs to the monoclinic P-1 space group. The unit cell of the **7a** is interesting as illustrated by Figure 3.7. The most prominent characteristic of the packing was the orthogonal orientation of the phenyl rings on the different molecules

© University of Pretoria

relative to each other, with the carbene substituents being on opposite sides. This indicated a clustering of phenyl rings but no obvious π-stacking.

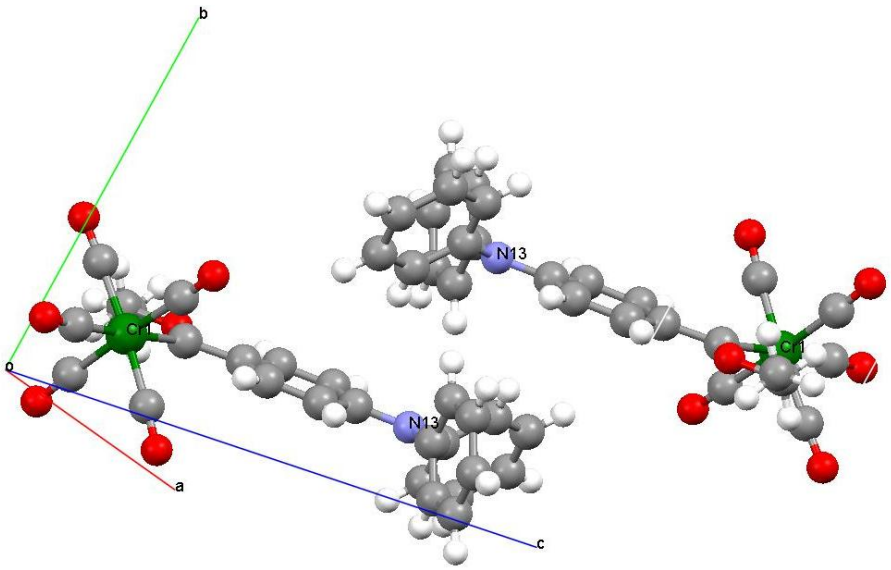

Figure 3.7 ORTEP + POV-Ray plot of the unit cell of **7a**

3.2.5 Coordination ability of compounds 7, 8 and 9

Triphenylamine was a poorer coordinating ligand compared to triphenylphosphine, triphenylarsine, triphenylantimony and even triphenylbismuth when coordinated to rhodium[17]. Taking this into account and the fact that in **7a** there was very little electron density left on the nitrogen of the synthesised amines due to the presence of the conjugated system and the electron withdrawing carbene substituent, these compounds are expected to be very poor ligands. They were not further analysed for their ability to coordinate to other transition metals in this project. Instead, attention was shifted to dimethylanaline where two phenyl substituents were replaced by two methyl substituents.

3.3 π arenechromiumcarbonyl amines as precursors for novel ligands

3.3.1 Background

© University of Pretoria

In this section, an ethoxy Fischer carbene substituent was synthesised on N,N-dimethylaniline via a lithiation synthetic route. N,N-dimethylaniline is an aromatic compound that contains a lone pair of electrons on the nitrogen which is able to interact with the π-system of the benzene ring. The presence of the conjugated system can lead to the delocalisation of the lone pair over the benzene ring (Figure 3.8) resulting in a greater electron density on the ring. Katritzky and Topsom[18] stated that the dipole moment of this molecule was directed towards the ring. The conjugated system allowed for resonance effects which lead to the stabilisation of the *ortho*- and *para*-positions on the ring as shown in Figure 3.8.

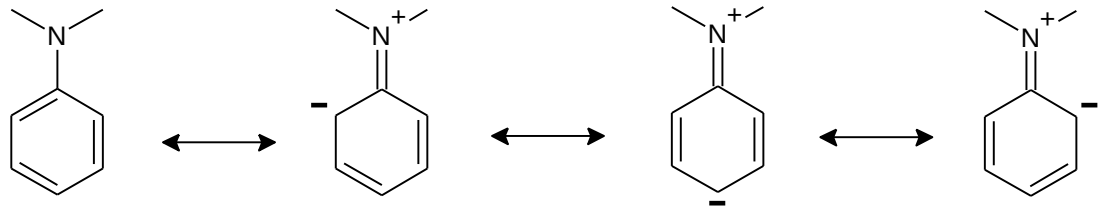

Figure 3.8 Stabilisation of phenyl ring with an electron donating substituent

Earlier studies showed that $Cr(CO)_3$ could be used to activate the aromatic ring for substitution reactions by nucleophiles and bases[19] and could easily be added and removed from the aromatic nucleus[20]. Through the complexation of the arene ring to $Cr(CO)_3$, the acidity of the C-H bonds of the arene is dramatically increased[21]. It is expected that the *ortho*- and *para*-position of the ring to be less activated than that of the *meta*-position, since electron density could be transferred to these positions through the aromatic system (Figure 3.8). Card and Trahnovsky[19] showed that lower *ortho*-lithiation selectivity was observed while greater amounts of the *meta*-product and less of the *para*-product formed when N,N-dimethylaniline was complexed to $Cr(CO)_3$. Lepley[22] showed that lithiation of uncoordinated N,N-dimethyl aniline mainly occurred at the *ortho*-position of the benzene ring.

Carroll and McGlynn[23] showed that there was a net transfer of electron density from the aromatic ring to the arene metal tricarbonyl complex, but despite this, the chromium was still positively charged. This is due to the electron-withdrawing character of the carbonyl groups since the π-back-bonding character of the CO-group was much greater than the σ-bonding character of the arene. It was, however,

© University of Pretoria

stated that the $Cr(CO)_3$ group was able to stabilise either positive or negative intermediates during product formation[19] and also had the ability to vary the extent of charge donation to an electron deficient centre[24].

3.3.2 Synthesis of Fischer carbene complex on arene metal carbonyl

Lithiation of N,N-dimethylaniline was problematic and difficult to repeat because of the many centres of reactivity towards deprotonation in the molecule. To activate the N,N-dimethylaniline ring protons to form lithiated products, the arene metal carbonyl first had to be synthesised. As mentioned earlier, the addition of the $Cr(CO)_3$ group was readily be achieved by refluxing $Cr(CO)_6$ in high boiling solvents in the presence of the benzene ring present in the molecule. The formed arene metal carbonyl product was lithiated with *n*BuLi, removing a proton. Metalation with either $Cr(CO)_6$ or $W(CO)_6$ gave the metal acylate, followed by alkylation with Et_3OBF_4 to neutralise and stabilise the synthesised carbene complex.

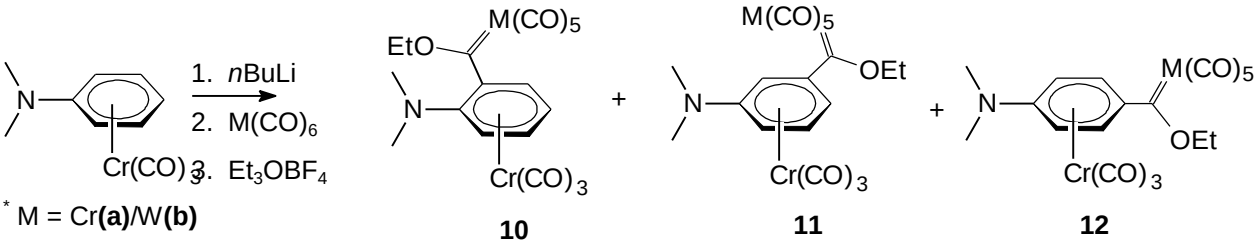

* M = Cr**(a)**/W**(b)**

Scheme 3.2 Reaction products of Fischer carbene synthesis on N,N-dimethylaniline-(arene)tricarbonylchromium

It was determined that all three of the possible diasteriomers were formed during the reaction, the *para*-product (**12**) being the major product while the *ortho*- and *meta*-products were present in smaller amounts. It was found that the complexed $Cr(CO)_3$ group activated the arene ring enough to allow all the positions to be lithiated as was found by Card and Trahanovsky[19]. Their product ratio was ortho:meta:para, 30:52:18. These values did not correlate with the ratio of the synthesised products as **10** and **11** formed in a much smaller ratio than that of **12**, with a ratio of 15:25:60 respectively. This result could give an indication of the electron-donating effect of the NMe_2 group present in the molecule, being supported by the electron withdrawing effect of the carbene substituent. A second aspect that must be

© University of Pretoria

remembered is that delocalisation of electron density from the NMe_2 substituent is hampered by the π-coordination to the $Cr(CO)_3$ fragment. This coordination can be seen as locking the benzene double bonds in set positions preventing delocalisation. These explanations partially solved the observed results. However, the *ortho*-product was still observed in a much smaller ratio than what was expected. Another aspect that had to be considered was the steric factor between the synthesised carbene substituent present at the *ortho*-position of the arene-metalcarbonyl complex.

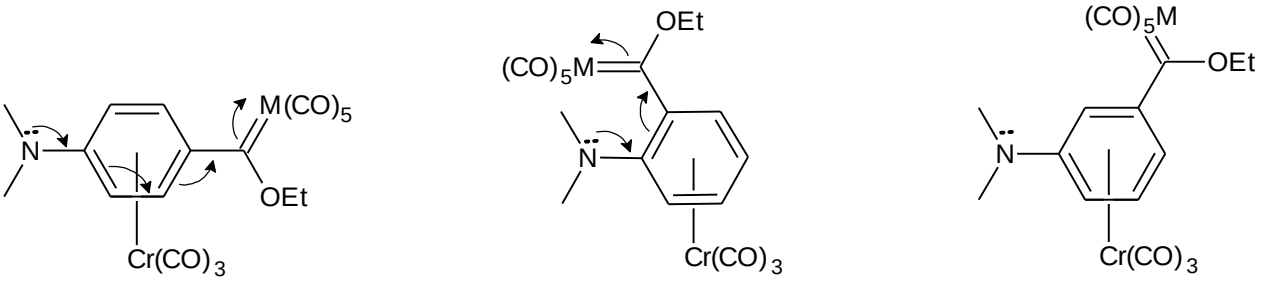

electronically and sterically favoured

electronically favoured sterically crowded

electronically not favoured sterically less crowded

Figure 3.10 Stabilisation of the *ortho* and *para*-positions on a arene ring by electron delocalisation

It is important to note the difference in stability between the tungsten and the chromium carbene substituents. It was found that significant decomposition occurred in the case of the chromium carbene complexes. It was also observed that a significant amount of the chromium tricarbonyl was no longer π-bonded to the N,N-dimethylaniline carbene complex. In contrast to these findings, the metal-arene compound with the substituted tungsten carbene substituent showed very little (if any) decomposition. It was also found that in this case it was extremely difficult to remove the Chromium tricarbonyl from the system to render the uncomplexed N,N-dimethylaniline with a W-carbene substituent for further coordination to other metals.

© University of Pretoria

3.3.3 H^1 and C^{13} NMR data analysis of reaction products

Table 3.9 H^1 and C^{13} NMR data ($CDCl_3$) of **10**

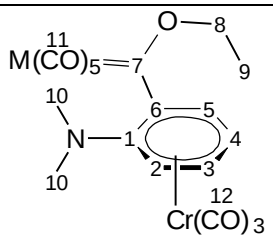

M = Cr**(a)** / W**(b)**

	10a			**10b**		
H^1 NMR						
Proton position	δ_h/ppm	*J*/Hz	Integration	δ_h/ppm	*J*/Hz	Integration
2	4.86	d, 5.3	1H	4.87	br	1H
3	5.50	d, 6.2	1H	5.28	br	1H
4	5.34	br	1H	5.06	br	1H
5	5.58	br	1H	5.51	br	1H
8	5.34	br	2H	4.93	br	2H
9	1.36	t, 7.1	3H	1.76	br	3H
10	2.93	m	6H	2.69	br	6H

C^{13} NMR		
	δ_c/ppm	δ_c/ppm
1	116.7	114.7
2	74.8	91.4
3	84.2	82.0
4	77.21	82.9
5	95.2	94.4
6	129.4	125.6
7	331.3	320.3
8	73.42	81.0
9	14.3	14.3
10	39.9	43.7
11	223.4, 216.1	203.3, 191.1
12	233.9	233.9

© University of Pretoria

The H^1 NMR spectra of **10** showed weak signals in the aromatic region indicating aniline which is no longer π-bonded to $Cr(CO)_3$.

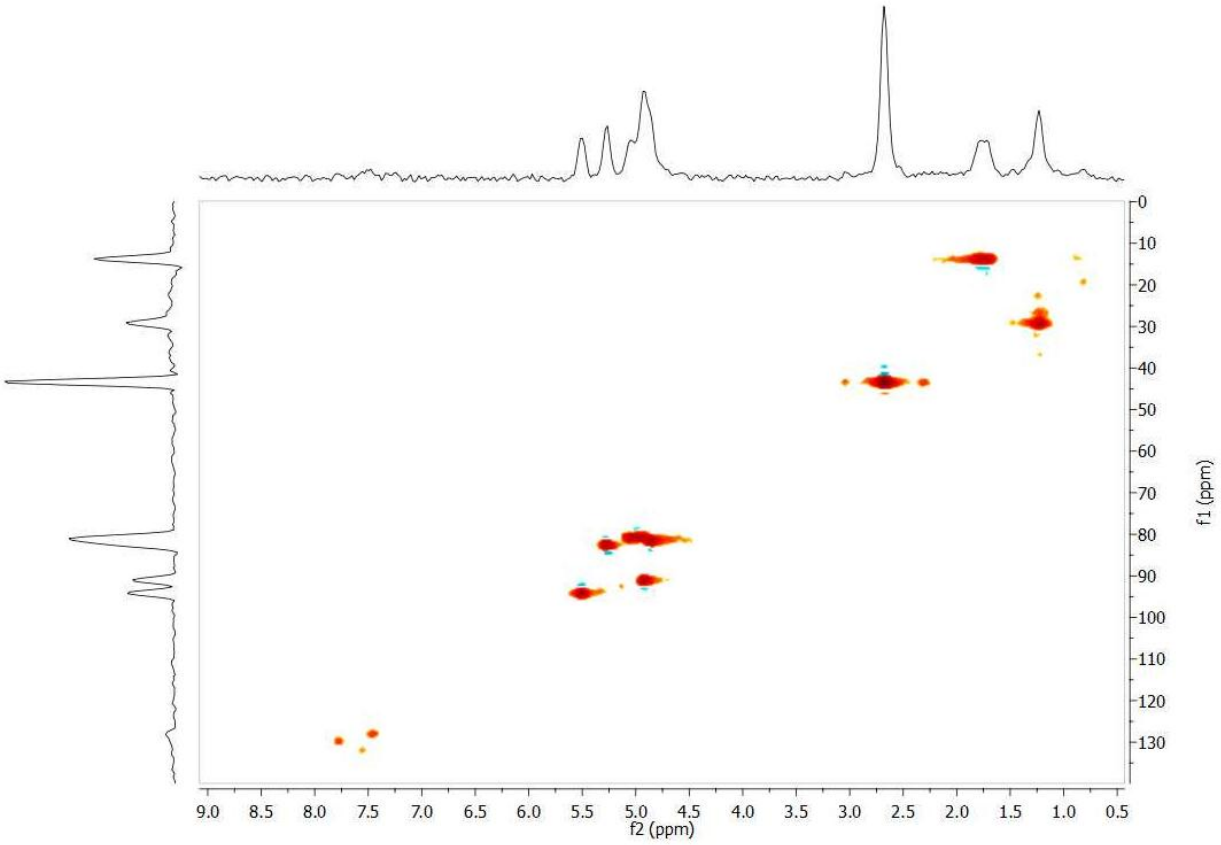

Figure 3.11 HSQC 2D NMR spectrum ($CDCl_3$) of compound **10b** in the π-arene region

Figure 3.11 is a 2D NMR spectrum of the compound in which the uncoordinated compound was clearly visible. These peaks appeared in the region from 7.78 to 7.24 ppm. On coordination to $Cr(CO)_3$ the aromatic ring was no longer aromatic. The chemical shift values expected for the aromatic ring moved upfield towards the olefin chemical shift region which usually lies between 4 and 6 ppm. Another observation to be noted from the proton spectrum was the poor resolution of the peaks. Compounds **10** and **11** have planar chirality. Since the signals of the two enantiomers did not fall precisely over each other, peak broadening of all peaks were observed. This same phenomenon was observed by Meyer[25], for σ,π-bimetallic complexes.

The C^{13} NMR spectrum of **10a** and **10b** showed significant downfield carbene and carbonyl chemical shifts. The expected values for a $Cr(CO)_5$ and $W(CO)_5$-carbene complex are around 310 and 280 ppm respectively, but values of 330 and 320 ppm

© University of Pretoria

were observed for **10a** and **10b** respectively. The carbonyls of the $Cr(CO)_3$ fragment had values of 234 ppm for both **10a** and **10b**. The upfield chemical shifts of the benzene ring carbons further support the loss of aromaticity and localisation of the olefins upon complexation to the $Cr(CO)_3$.

To see the actual effect that the dimethylamine substituent would have on the system was to compare the results with those obtained by Fischer, Gammel and Neugebauer[26]. They synthesised a tungsten and chromium carbene complex with a phenyl ring substituent which was complexed to a $Cr(CO)_3$ fragment to form an arene-carbene complex. The H^1 NMR chemical shift values of the arene ring gave values ranging between 5.72 and 6.45 ppm for both complexes. These values were significantly downfield compared to the values of **10a** and **10b**, whose arene H^1 NMR chemical shifts ranged from 4.86 to 5.58 ppm.

When comparing these values, it seemed that the NMe_2 substituent on the ring, displayed even less aromatic character. The electronic contribution that the amine made to ring stabilisation allowed more electron density from the ring to be donated to the coordinated $Cr(CO)_3$ and carbene substituent. The C^{13} NMR spectrum of $[(\eta^6\text{-}C_6H_5C(OCH_2CH_3)W(CO)_5)Cr(CO)_3]$, synthesized by Fischer[26], listed by the same groups also showed a W-carbene signal with a value of 307.9 ppm, which was also significantly upfield compared to the value of **10b** which was 320.0 ppm. Again, this was proof that greater electron withdrawal from the arene ring occurred in the presence of the NMe_2 substituent, since the carbene carbon was deshielded to a much greater extent. These observations could also be made in the case of **11** and **12**.

Table 3.8 H^1 and C^{13} NMR data ($CDCl_3$) of **11**

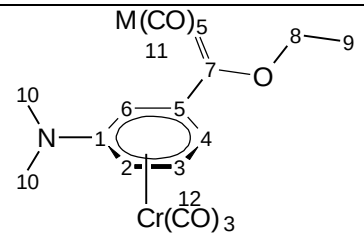

M = Cr**(a)** / W**(b)**

	11a	**11b**

© University of Pretoria

H^1 NMR						
Proton position	δ_h/ppm	*J*/Hz	Integration	δ_h/ppm	*J*/Hz	Integration
2	5.63	d, 6.9	1H	5.04	m	1H
3	5.45	dd, 6.1, -	1H	5.55	dd, 6.8, -	1H
4	5.31	dd, 6.0, -	1H	5.46	dd, 6.8, 0.4	1H
6	5.71	d, 6.5	1H	5.51	s	1H
8	5.16	m	2H	5.06	q, 7.1	2H
9	1.73	t, 7.1	3H	1.68	t, 7.0	3H
10	3.27	s	6H	2.95	s	6H

C^{13} NMR		
	δ_c/ppm	δ_c/ppm
1	104.7	115.0
2	82.9	75.3
3	90.4	93.7
4	91.2	86.0
5	137.3	132.8
6	83.4	79.0
7	330.0	311.0
8	n.o.	80.1
9	15.3	14.8
10	62.1, 55.9	40.0
11	233.6, 230.7	202.2 196.9
12	229.3	234.3

As was the case with compound **10**, compound **11** also displayed planar chirality. In this case, a clear distinction could be made between the two enantiomers in the proton spectra. The proton NMR spectrum also showed J_4-coupling in the arene. This is clearly different from **10** where no coupling could be observed at all because of the poor resolution.

© University of Pretoria

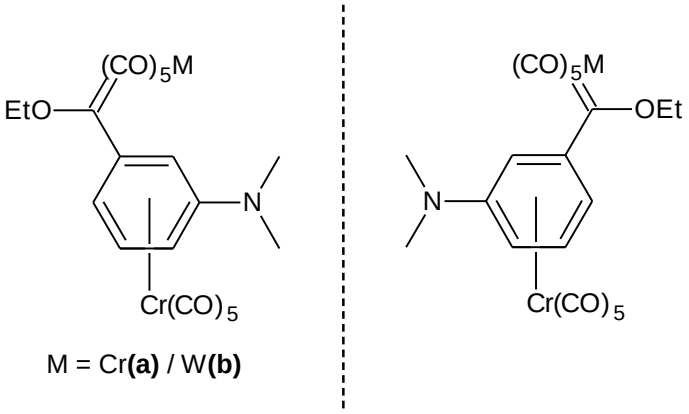

Figure 3.12 Planar chirality of **11**

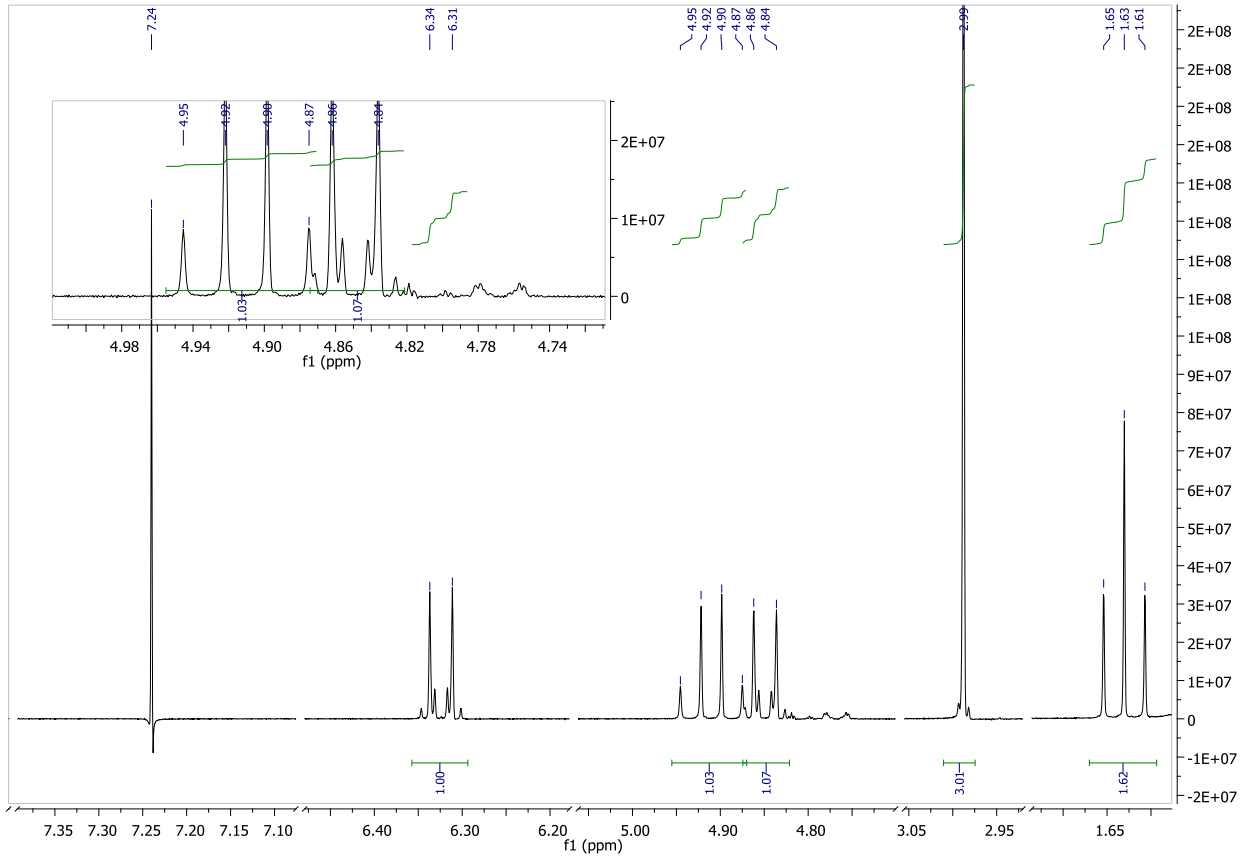

Figure 3.13 H^1 NMR spectrum ($CDCl_3$) of **12b**

Concerning the H^1 NMR spectrum of **12** (Figure 3.13), the two doublets on the aromatic ring were clearly observed. The *ortho*-protons were found more upfield than the methylene signal of the OEt substituent, which showed the significant olefinic character of the ring and the significant electron-withdrawing effects of the carbene carbon.

© University of Pretoria

Table 3.9 H^1 and C^{13} NMR data ($CDCl_3$) of **12**

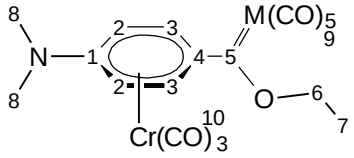

M = Cr (a)/ W (b)

	12a			**12b**		
H^1 NMR						
Proton position	δ_h/ppm	*J*/Hz	Integration	δ_h/ppm	*J*/Hz	Integration
2	4.77	d, 6.4	2H	4.85	d, 7.8	2H
3	5.56	t, 6.3	2H	6.33	d, 7.7	2H
6	4.80	m	2H	4.91	q, 7.1	2H
7	1.66	t, 7.1	3H	1.63	t, 7.1	3H
8	2.85	s	6H	2.99	s	6H

C^{13} NMR		
	δ_c/ppm	δ_c/ppm
1	106.9	105.4
2	74.3	73.0
3	96.9	99.4
4	135.0	136.7
5	331.7	302.8
6	82.9	79.1
7	14.4	14.9
8	39.7	39.8
9	231.8, 216.6	201.9, 197.1
10	234.7	231.7

A comparison between the carbene-arene compounds in the NMR spectra lead to the observation that the doublet of the *ortho*-proton on the aromatic ring (4.86-4.84 ppm) is significantly upfield compared to the doublet of the *meta*-position proton (6.34-6.31 ppm) of compounds **10** and **11** respectively. This was due to the additional electron density that was pushed into the arene ring by the dimethylamine substituent present in the ring. The resonance structures, as discussed previously,

© University of Pretoria

allowed for a greater amount of electron density to be present in the *ortho*- and *para*-positions of the ring. This also played a significant role in the stabilisation of the carbene substituent present at these positions. Further, a clear quartet at 4.95-4.87 ppm was observed for the -CH_2- group of the ethoxy substituent and a triplet 1.65-1.61 ppm for the CH_3 present on the same group in both these compounds.

3.3.4 IR analysis of reaction products

In these novel amines, both an $M(CO)_5$ and $M(CO)_3$ group were present. The $M(CO)_5$ fragment formed part of the Fischer carbene complex, while the $M(CO)_3$ group was π-bonded to the phenyl ring on N,N-dimethyl aniline to form an arene. Please refer to section 2.2.3 for a full discussion on the infrared spectra of the $M(CO)_5$ fragment.

The *fac*-$M(CO)_3$ have two bands for the three terminal carbonyl groups- the A_1 and E- bands. The A_1 band was sharper, found at higher wavenumbers than the E-band and represented the symmetrical stretching movements of the carbonyls. The E-band was broader and represented the unsymmetrical movements of the carbonyls[27]. Figure 3.14 illustrates the symmetrical and unsymmetrical vibration modes of the carbonyl ligands for the two different observed bands. In some cases, it was observed that the degenerate E-mode could split. According to Orgel[28] this phenomenon occurred due to differences in the electron-donor property of the aromatic system in the two mutually perpendicular directions. Small unexplained splitting was also observed in the case when dimethylaniline, aniline and thiophene compounds acted as the aromatic system to which the $M(CO)_3$ was π bonded.

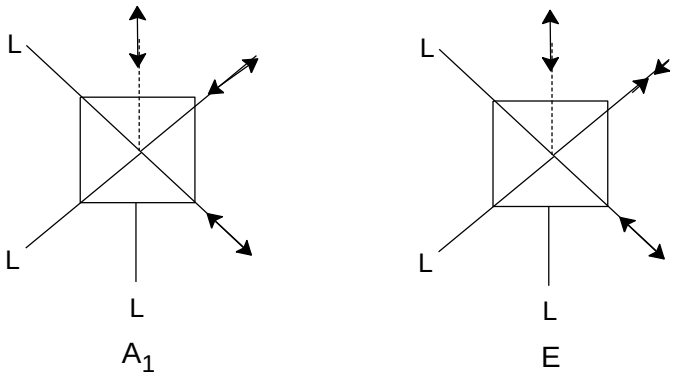

Figure 3.14 IR stretching modes of a *fac*-$M(CO)_3$ fragment

© University of Pretoria

Figure 3.15 shows a typical example where both the $M(CO)_5$ and $M(CO)_3$ groups were observed. Due to signal overlap, some of the bands were not observed in the spectra.

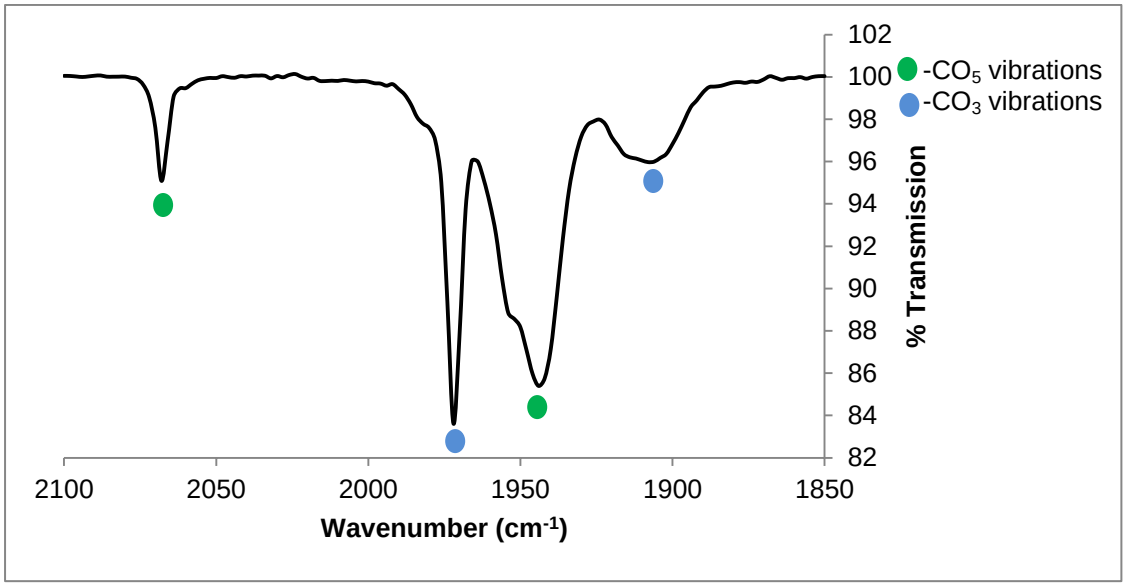

Figure 3.15 The carbonyl region IR spectrum of **12b**

Table 3.10 The carbonyl IR vibration frequencies (hexane) for **10a**, **11a** and **12a**

	IR band positions (cm^{-1})					
	$-CO_3$ vibrations		$-CO_5$ vibrations			
	A_1	E	$A_1^{(1)}$	$A_1^{(2)}$	B_1	E
10a	1988	1908, 1902	2072	1974	1988	1974
11a	1968	1910, 1890	2068	1972	1988	1968
12a	1980	1938, 1928, 1926	2074	1980	-	1980

Table 3.11 The carbonyl IR vibration frequencies (hexane) for **10b**, **11b** and **12b**

	IR band positions (cm^{-1})					
	$-CO_3$ vibrations		$-CO_5$ vibrations			
	A_1	E	$A_1^{(1)}$	$A_1^{(2)}$	B_1	E
10b	1962	1910,	2072	1972	-	1982

© University of Pretoria

		1900				
11b	1952	1914, 1904, 1896	2068	1970	1982	1968
12b	1954	1912	2068	1972	-	1946

When the three compounds were compared, splitting of the E-band in the $M(CO)_3$ carbonyls was observed for **10b** and **11b**. These were the two compounds that had planar chirality (Figure 3.13); as a result, the band splitting could be explained by the differences in electron donor ability of the aromatic ring in the two different perpendicular directions. Orgel[28] further stated that the degenerate mode of the E-band had the lower frequency. When this was taken into consideration in analysis of the E-bands of the different $M(CO)_3$ signals, it was observed that there was little difference in the E-band values with wavenumbers lying between 1910 and 1914 cm^{-1}. When the $M(CO)_5$ substituents are compared, it is important to realise that the $A_1^{(1)}$-bands are not very significant as we are dealing only with carbene ligands when the values are compared. The reason for this phenomenon was discussed in section 2.2.3. When the values of the $A_1^{(1)}$-bands are compared, it is observed that there is no significant difference in the wavenumbers of the three compounds lying between 2068 and 2072 cm^{-1}. There is, nevertheless, quite a large difference in the E-band wavenumbers with values of **10b**, **11b** and **12b** having wavenumbers of 1982, 1968 and 1946 cm^{-1} respectively. It is important to note that, as the stability of the compounds increased, the wavenumbers of the E-band decreased. This is indicative that the stability of the carbene complex is increased at particular positions on the arene ring and correlates with the possible resonance effects present on the arene ring with an electron-donating substituent. The reason for this observed lowering of the E-band wavenumbers was discussed comprehensively in section 2.2.3.

There was an unexpected observation which pertains to **10b**. It had the highest $M(CO)_5$ wavenumbers and also the lowest stability. It was consequently expected that there was significant steric hindrance between the carbene substituent and the methyl groups on the nitrogen. It was, therefore, responsible for the significant instability of **10b**.

© University of Pretoria

3.3.5 X-ray Crystallography

The structures of the π-arene carbene complexes were analysed by single crystal X-ray diffraction. The compounds were crystallised from a dichloromethane:hexane mixture (1:1) layered on top of each other. Initially, it was anticipated that the *ortho*-product of the reaction would possibly not form due to significant steric hindrance, but this assumption proved unfounded. All the complexes did crystallise with significant differences in stability and yield. Stability of the complexes increased in the order **12b** > **11b**, **10b**.

Single crystal X-ray diffraction molecular structures of **10b**, **11b** and **12b** were determined; unfortunately it was not possible to obtain crystal structures for any of the Cr-carbene containing complexes as the latter were less stable than their tungsten analogues.

To initialise the discussion of these single X-Ray crystal structures it is necessary to state that the crystal structures of compounds **10b** and **12b** belongs to a triclinic, P-1 space group while **11b** belongs to a monoclinic, $P2_1/n$ spacegroup. It was noted that **10b** and **11b** were air sensitive (also in the solid state) and could only be obtained in low yields. By contrast **12b** was the major product as well as stable in the solid state.

© University of Pretoria

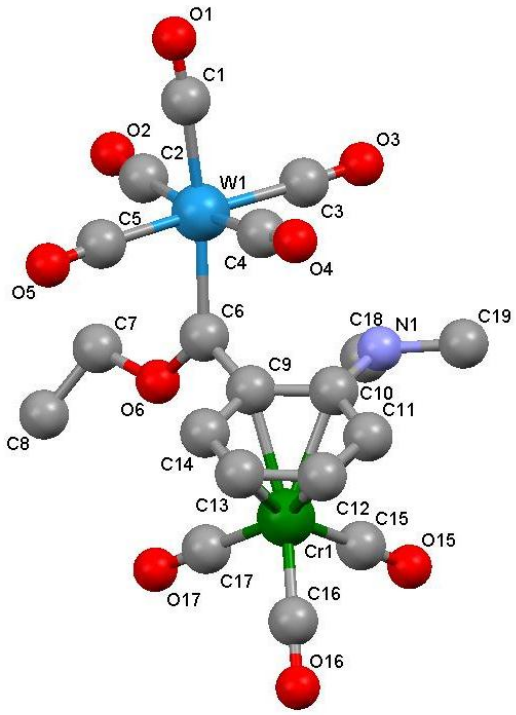

Figure 3.16 Ortep diagram of **10b**.

Table 3:12 Selected bond lengths of **10b**

Atoms	Bond length (Å)	Atoms	Bond length (Å)
W1-C1	2.038(1)	W1-C2	2.045(2)
W1-C6	2.167(1)	W1-C3	
C6-O6	1.315(1)	W1-C4	
C6-C9	1.495(2)	W1-C5	
C9-C10	1.421(2)	C9-Cr1	2.236(1)
C9-C14	1.435(2)	C10-Cr1	
C10-C11	1.430(2)	C11-Cr1	
C11-C12	1.404(2)	C12-Cr1	
C12-C13	1.409(2)	C13-Cr1	
C13-C14	1.401(2)	C14-Cr1	
C10-N1	1.387(2)	Cr1-C15	1.844(1)
N1-C18	1.463(2)	Cr1-C16	
N1-C19		Cr1-C17	

© University of Pretoria

Table 3.13 Selected bond and torsion angles of **10b**

Atoms	Bond angles (°)	Atoms	Torsion angles (°)
W1-C6-O6	131.57(9)	W1-C6-C9-C10	-68.5(1)
W1-C6-C9	119.38(8)	O6-C6-C9-C10	126.6(1)
O6-C6-C9	106.8(1)	O6-C6-C9-C14	-63.9(1)
C10-N1-C18	118.1(1)	C6-C9-C10-N1	-9.8(2)
C10-N1-C19	117.3(1)	C11-C10-N1-C19	-8.9(2)
C18-N1-C19	111.8(1)		

Figure 3.16 shows the crystal structure of **10b** which is crowded because of the *ortho*-substituted carbene ligand being in close proximity with the dimethylamine substituent. It was found that the $Cr(CO)_3$ and $W(CO)_5$ fragments and the are on opposite sides of the arene ring. This is illustrated by Figure 3.17 which shows a plane through the arene ring as well as the amine and carbene substituents.

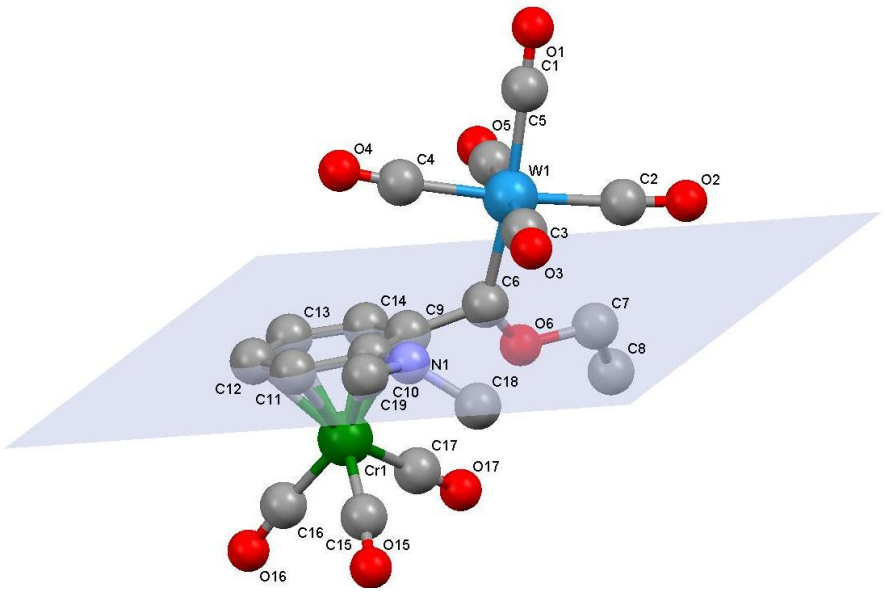

Figure 3.17 View of the geometry of **10b** with a plane through the aromatic ring, amine and carbene substituents

The torsion angle C11-C10-N1-C19 has a value of -8.9°, indicating possible electron delocalisation from the NMe_2 substituent to the arene ring since the torsion angle is

© University of Pretoria

close to 0°. The length of the N-C(arene) bond is 1.387(2) Å (similar to the bond distance of two N^{sp2}-C^{sp2} hybridised atoms[16]), which further supports lone pair delocalisation to the arene ring. Unlike in the structure of **1**, the ethoxy substituent and the $W(CO)_5$ fragment of **10b** are rotated around the C(arene)-C(carbene) bond to take up positions above and below the plane of the ring. The greatest deviation from the plane is found for the $W(CO)_5$ and OEt moieties and is illustrated with the torsion angles of O6-C6-C9-C10 and W1-C6-C9-C10 having a value of 126.6(1)° and -68.5(1)° respectively. The fact that these torsion angles are not close to 0° is an indication that there is very little delocalisation of electron density from the arene ring to the carbene substituent. This is supported with a relatively long C6-C9 bond with a value of 1.495(2) Å compared to an sp^2-sp^2 hybridised carbon distance of 1.470 Å[16].

It seems that the electrophilic carbene carbon finds very little stabilisation from the arene ring and is mostly dependent on the oxygen (OEt) and tungsten ($W(CO)_5$) to fulfil this role. This is ascribed to the involvement of the arene double bonds in the coordination to the $Cr(CO)_3$ fragment which is further supported by the C-C bonds lengths in the arene ring which shows an interesting pattern of alternating long and short distances. The three adjacent C-C bond distances around the ring substituents are longer to compensate three shorter bonds away from the substituents. This is clearly a result of the crowdedness around the substituents and the lengthening of the C-C bonds to alleviate some of the strain.

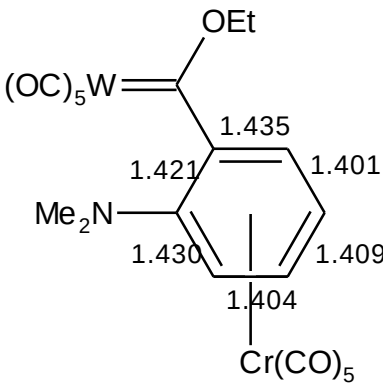

Figure 3.18 The three long and three short bond distances (Å) in the arene ring of **10b**

A final observation from the structure deals with the ability of the nitrogen lone pair to coordinate to another metal centre.

© University of Pretoria

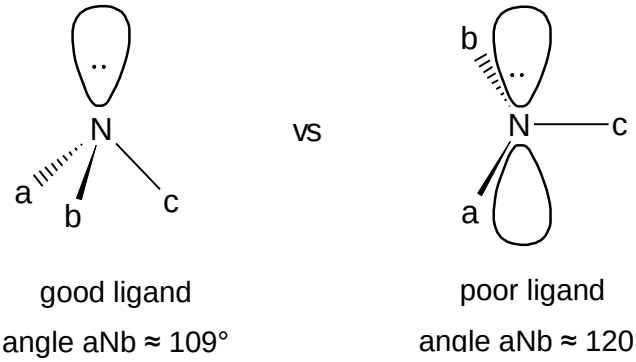

good ligand
angle aNb ≈ 109°

poor ligand
angle aNb ≈ 120°

Figure 3.19 A comparison between the substituent angles of a good and poor amine ligand

The angles C10-N1-C18, C10-N1-C19 and C18-N1-C19 have respective values of 118.1(1), 117.3(1) and 111.8(1)°. These values are closer to 120° than 109°, but there is still slight electron density present on the nitrogen atom. However, the lone pair points towards a carbonyl ligand and occupies an area which is crowded. Based on steric considerations it is very unlikely that **10b** will participate in bonding with another metal fragment. Since the cone angle of the amine is large, with the average angle size closer to 120° than 109°, and due to steric crowdedness the lone pair is not readily available for coordination to large metal fragments.

When the meta-complex (**11b**) was considered, it was predicted that this compound would be the major product, but this was not the case. The *meta*-position on an aromatic ring containing an electron donating substituent will be the activated position for deprotonation to occur. The inclusion of an electrophilic carbene substituent on this position, decreased stabilisation of the substituent is experienced relative to the other positions. This phenomenon was illustrated by Figure 3.8.

© University of Pretoria

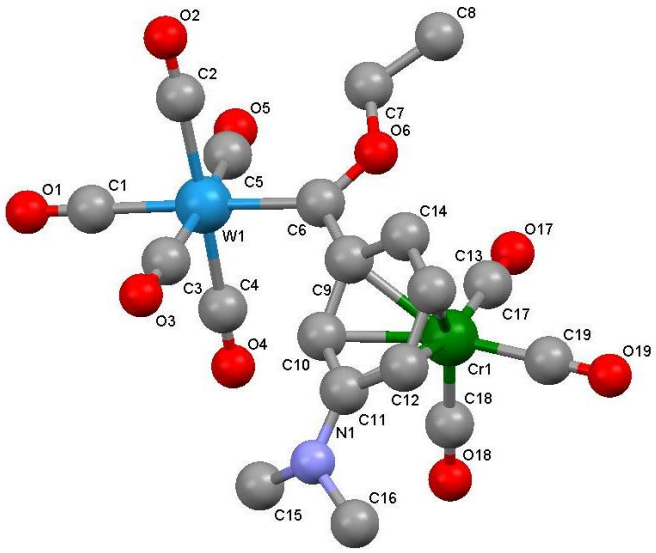

Figure 3.20 Ortep diagram of **11b**.

Table 3.14 Selected bond lengths of **11b**

Atoms	Bond length (Å)	Atoms	Bond length (Å)
W1-C1	2.038(1)	W1-C2	2.045(2)
W1-C6	2.167(1)	W1-C3	
C6-O6	1.315(1)	W1-C4	
C6-C9	1.495(2)	W1-C5	
C9-C10	1.421(2)	C9-Cr1	2.236(1)
C10-C11	1.430(2)	C10-Cr1	
C11-C12	1.404(2)	C11-Cr1	
C12-C13	1.409(2)	C12-Cr1	
C13-C14	1.401(2)	C13-Cr1	
C10-N1	1.387(2)	C14-Cr1	
N1-C18	1.463(2)	Cr1-C15	1.844(1)
N1-C19		Cr1-C16	
		Cr1-C17	

© University of Pretoria

Table 3.15 Selected bond and torsion angles of **11b**

Atoms	Bond angles (°)	Atoms	Torsion angles (°)
W1-C6-O6	130.8(2)	W1-C6-C9-C10	32.2(5)
W1-C6-C9	123.5(2)	O6-C6-C9-C10	-153.6(3)
O6-C6-C9	105.4(3)	O6-C6-C9-C14	26.2(4)
C11-N1-C15	119.3(3)	C12-C11-N1-C15	-170.8(4)
C11-N1-C16	119.1(3)	C12-C11-N1-C16	-18.1(5)
C15-N1-C16	116.1(4)		

Due to the decrease in electron density at the *meta*-position, the carbene substituent on this position shows significant instability. Figure 3.21 depicts a plane through the arene ring, the amine substituent and carbene substituent of **11b**. The torsion angles C12-C11-N1-C15 and C12-C11-N1-C16 have respective values of -170.8(4) and -18.1(5)°. The former value is closer to 0 (180)° which indicates electron delocalisation of the lone pair on the amine towards the arene ring. To further support this observation the angles around the nitrogen atom have values of 119.3(3), 119.1(3) and 116.1(4)°, which are all close to 120°. The trigonal planar geometry of this substituent will hamper its ability to coordinate to another metal centre.

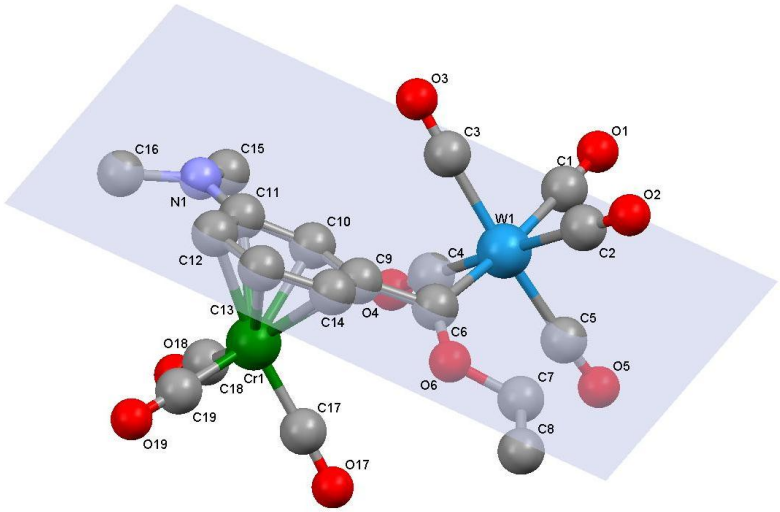

Figure 3.21 View of the geometry of **11b** with a plane through the aromatic ring, amine and carbene substituents.

© University of Pretoria

To investigate the contribution that the arene ring makes to the stabilisation of the carbene substituent in **11b** the torsion angle between the C(arene)-C(carbene) is examined. The torsion angles O6-C6-C9-C14 and W1-C6-C9-C10 have values of 26.2(4) and 32.2(5)° respectively which indicates that there is very little (if any) electron stabilisation that occurs from the arene ring to stabilise the carbene substituent.

The N-C(arene) bond has a length of 1.387(2) Å. The lengths of the N-C(arene) bonds for **10b** and **11b** are the same while the torsion angle for **10b** is smaller around the N-C(arene) bond, indicating a slightly larger increased electron delocalisation from the nitrogen to the arene ring in the case of **10b**. The similar pattern of long and short bonds in the arene ring of **11b** was observed as was the case of **10b**, only the two longer bonds are those between the arene ring substituents while the other four bonds are shorter.

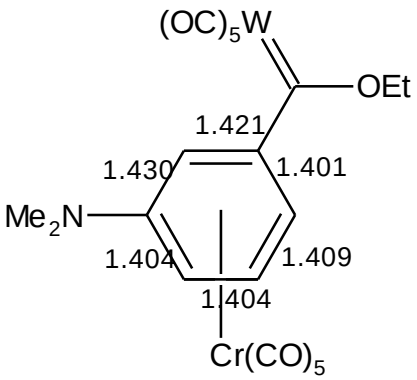

Figure 3.22 The two long and four short bond distances (Å) in the arene ring of **11b**

Figure 3.23 is the single crystal X-Ray structure of the *para*-complex (**12b**), which is by far the most stable product that formed.

© University of Pretoria

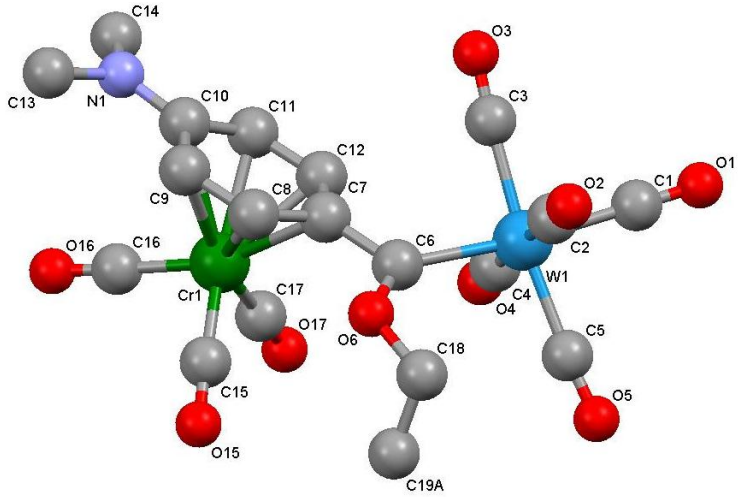

Figure 3.23 Ortep diagram of **12b**.

Table 3.16 Selected bond lengths of **12b**

Atoms	Bond length (Å)	Atoms	Bond length (Å)
W1-C1	2.027(3)	W1-C2	2.038(3)
W1-C6	2.195(2)	W1-C3	
C6-O6	1.328(3)	W1-C4	
C6-C7	1.483(3)	W1-C5	
C7-C8	1.417(3)	C7-Cr1	2.224(2)
C7-C12	1.421(3)	C8-Cr1	
C8-C9	1.399(3)	C9-Cr1	
C9-C10	1.422(3)	C10-Cr1	
C10-C11	1.422(3)	C11-Cr1	
C11-C12	1.400(3)	C12-Cr1	
C10-N1	1.353(3)	Cr1-C15	1.841(2)
N1-C13	1.452(4)	Cr1-C16	
N1-C14		Cr1-C17	

© University of Pretoria

Table 3.17 Selected bond and torsion angles of **12b**

Atoms	Bond angles (°)	Atoms	Torsion angles (°)
W1-C6-O6	129.0(2)	W1-C6-C7-C12	29.1(3)
W1-C6-C7	124.6(1)	O6-C6-C7-C8	14.5(3)
O6-C6-C7	105.6(2)	O6-C6-C7-C12	-160.5(2)
C10-N1-C13	120.4(2)	C9-C10-N1-C14	-169.7(2)
C10-N1-C14	120.6(2)	C11-C10-N1-C13	173.1(2)
C13-N1-C14	117.8(2)		

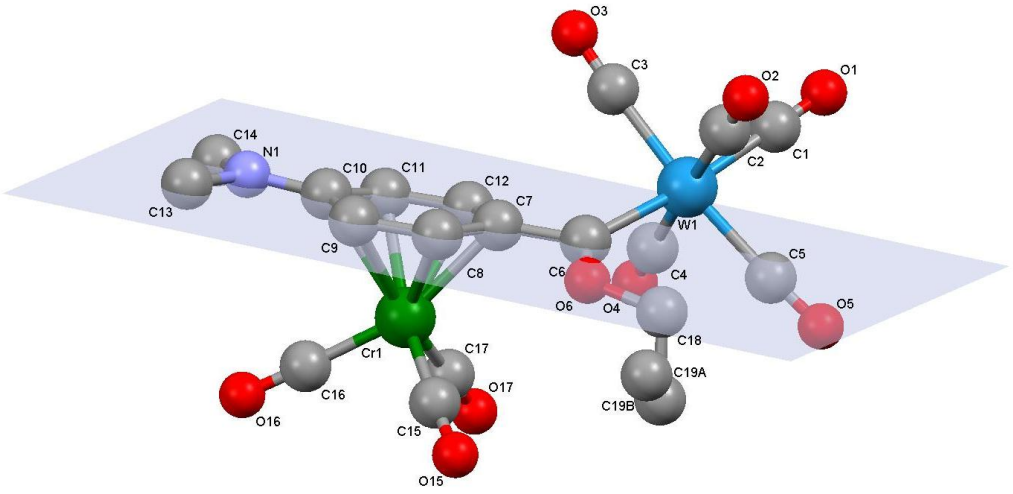

Figure 3.24 View of the geometry of **12b** with a plane through the aromatic ring, amine and carbene substituents.

The angles around the nitrogen have values of 120.4(2), 120.6(2) and 117.8(2)°. These values show the largest delocalisation of the lone pair present on the nitrogen to the arene ring when compared to **10b** and **11b** and will also make **12b** an even poorer ligand. The torsion angle around the C(arene)-C(carbene) (O6-C6-C7-C8) bond have a value of 14.5(3)° and that of C13-N1-C10-C9 a value of 173.1(2)°. It is clear that some delocalisation from the nitrogen via the arene ring to the carbene is present in this structure. This is supported by the significantly shortened N-arene

© University of Pretoria

bond distance of 1.353(3) Å in **12b** compared with 1.387(2) Å in **11b** and 1.387(2) Å in **10b**. Also, by the slightly shorter carbene-arene distance of 1.495(2) Å in **12b** compare to the corresponding distances of 1.495(2) Å for **10b** and **11b**. Final confirmation is found in alternating long and short C-C arene bond distances. This is the only one of the three structures that displays this delocalised feature (Figure 3.25).

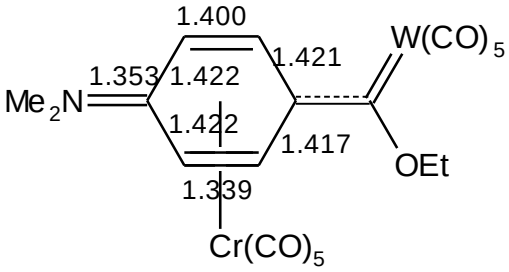

Figure 3.25 The alternating long and short bond distances (Å) in the arene ring of **12b**

A final point to consider about arene complexes is the conformations of the tricarbonyl group relative to the coordinated benzene or benzene derivative. The carbonyls can either be eclipsed or staggered. Albright[29] stated that the staggered conformation was slightly more stable than the eclipsed. According to a review by Muetterties, Bleeke, Wucherer and Albright[30], there are different conformations for disubstituted η^6-arene-ML_3 structures which the ML_3 fragement could adopt relative to a substituted arene ring.

© University of Pretoria

A. *Ortho*-substitution

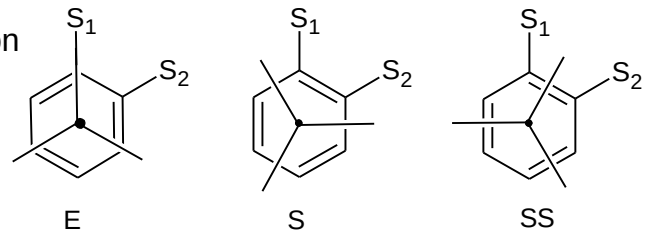

B. *Meta*-substitution

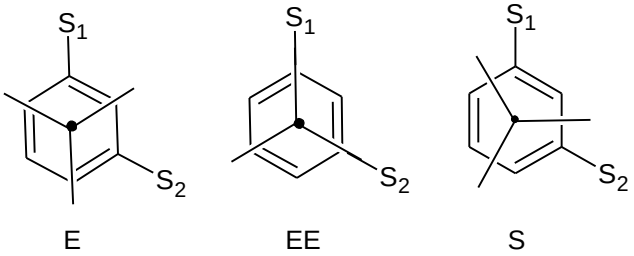

C. *Para*-substitution

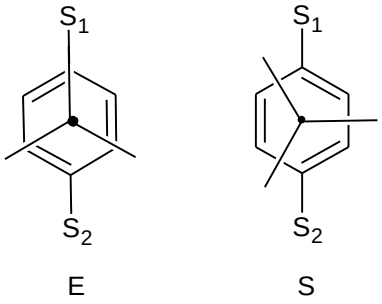

Figure 3.26 Conformational possibilities for η^6-arene-ML_3 complexes

Ortho-structures in Figure 3.26, exhibiting the E orientation will have D (any electron donating substituent) eclipsed while A (electron accepting substituent) is not eclipsed. If S_1 and S_2 have identical or very similar electronic characteristics the S orientation is usually preferred over the SS orientation mainly due to steric interactions. There are few *meta*-structures and in every case the S orientation is observed. In *para*-structures the orientation is usually E especially when S_1 and S_2 is a D and A substituent respectively[30]. In this research the $-NMe_2$ group will represent "D", while the carbene substituent on the arene ring represents "A".

In Figure 3.27 – 3.29 the orientation of the carbonyl tripod with respect to the arene ring is shown for the crystal structures of **10b**, **11b** and **12b** and the final orientation determined.

© University of Pretoria

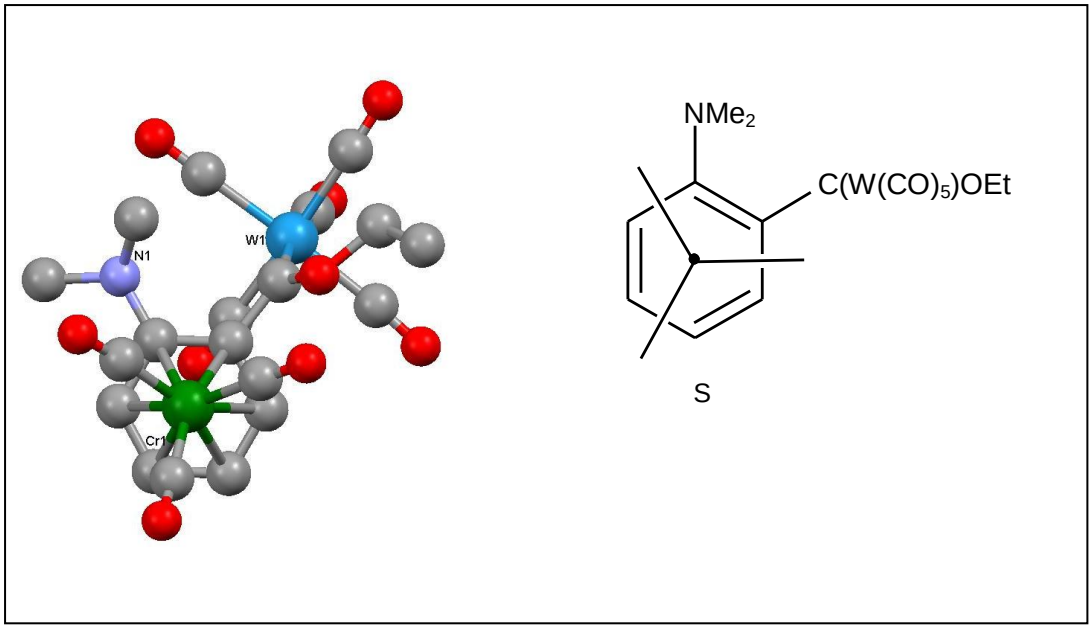

Figure 2.27 The S conformation of **10b**

The carbonyl tripod of **10b** has the two ring substituents between two legs, this indicates that the molecule has an S conformation.

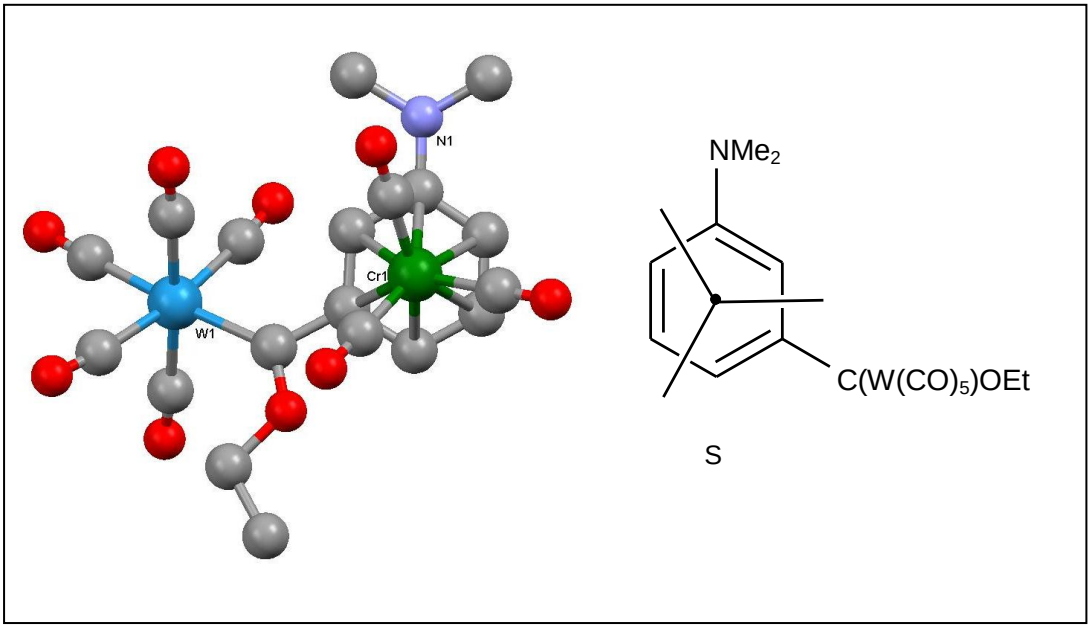

Figure 2.28 The S conformation of **11b**

One leg of the carbonyl tripod does not eclipse either the NMe_2 group or the carbene substituent. One of the tripod legs is found between these two ring substituents, but

© University of Pretoria

in a staggered conformation with respect to the arene carbon atom, thus **11b** has an S configuration.

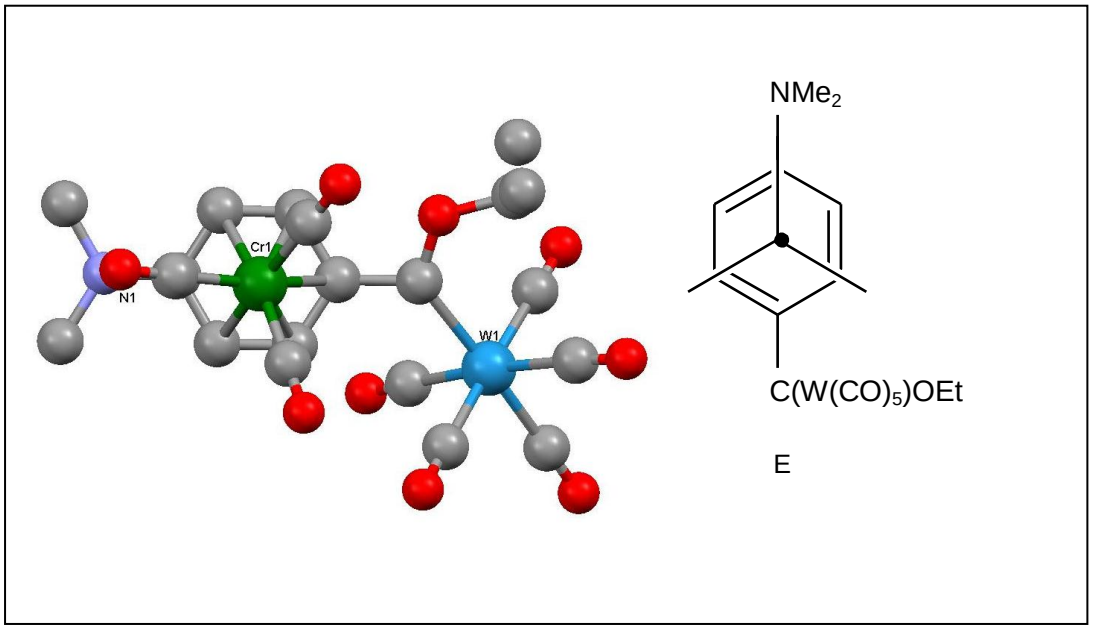

Figure 2.29 The E conformation of **12b**

The orientation of the carbonyl tripod with respect the arene ring is such that the one leg eclipses the carbon bearing the acceptor carbene substituent. This orientation is supported by the electron donating nitrogen substituent not being opposite to a carbonyl ligand and is the favoured and predicted conformation of the $M(CO)_3$-tripod. From these observations it can be concluded that **12b** has an E orientation.

3.4 Conclusion

The multiple carbene ligand synthesis from $N(C_6H_4Br)_3$ formed three products: the mono-, bis- and triscarbene (**7**, **8** and **9** respectively) all of which showed significant stability. The increased stability was assigned to the conjugated system that existed from the nitrogen lone pair to the carbene moiety. The crystal structure of **7a** revealed that the phenyl rings around the nitrogen atom displayed a trigonal planar geometry and the carbene-metal bond was also found in this plane. Since the lone pair on the nitrogen was spread throughout the molecule, synthesised amines were no longer deemed to function as suitable ligands for coordination.

© University of Pretoria

The *ortho*-, *meta*- and *para*-carbene complexes, **10**, **11** and **12** respectively, that were synthesised on η^6-N,N-dimethylaniline-tricarbonylchromium revealed the significant activation of the arene ring on coordination to $Cr(CO)_3$. The synthesized complexes were very sensitive, especially the Cr-carbene complexes. The sensitivity of the compounds was found to be caused by steric strain in the case of the ortho-carbene substituent and no electronic stabilisation received from the ring in the case of the meta-carbene substituent. The crystal structures of tungsten complexes **10b**, **11b** and **12b** revealed that the nitrogen lone pair played a small role in the stabilisation of the respective carbene-substituents, with most of the electron density being drawn towards the π-coordinated $Cr(CO)_3$ substituent. The coordination capability of these ligands was also questioned as the nitrogen substituents closely resembled those of a planar moiety.

© University of Pretoria

3.5 References

1. A. L. Seligson and W. C. Trogler. Cone angles for amine ligands. X-ray crystal structures and equilibrium measurements for ammonia, ethylamine, diethylamine, and triethylamine complexes with the [bis(dimethylphosphino)ethane]-methylpalladium(II) cation. *J. Am. Chem. Soc.* (1991) **113,** 2520–2527.

2. H. Gilman and A. L. Jacoby. Dibenzothiophene: Orientation and Derivatives. *J. Org. Chem.* (1938) **3,** 108–119.

3. H. Gilman and C. E. Arntzen. Halogen—Metal Interconversions with Halides Containing Functional Groups. *J. Am. Chem. Soc.* (1947) **69,** 1537–1538.

4. N. A. van Jaarsveld, D. C. Liles and S. Lotz. Thiophene decorated with Fischer carbene ligands. *Dalton Trans.* (2010) **39,** 5777–5779.

5. E. O. Fischer and A. Maasböl. On the Existence of a Tungsten Carbonyl Carbene Complex. *Angew. Chem. Int. Ed.* (1964) **3,** 580–581.

6. S. Lotz, N. A. van Jaarsveld, D. C. Liles, C. Crause, H. Görls and Y. M. Terblans. Fischer Dinuclear and Mononuclear Bis-Carbene Complexes of Thiophene and Thiophene Derivatives. *Organomet.* (2012) **31,** 5371–5383.

7. L. Eberson, M. P. Hartshorn and J. O. Svensson. Photochemical Nitration by Tetranitromethane. Part XXXVIII. Nitration of Tris(4-bromophenyl)amine, a Compound Corresponding to a Stable Radical Cation. *Acta. Chem. Scand.* (1997) **51,** 279–288.

8. E. Baciocchi and G. Illuminati. Steric Effects of the Nitro Group on the Uncatalyzed Halogenation of Methylbenzenes. *J. Am. Chem. Soc.* (1964) **86,** 2677–2680.

9. C. F. Bernasconi. The Physical Organic Chemistry of Fischer Carbene Complexes. *Adv. Phys. Org. Chem.* (2002) **37,** 137–237.

10. F. A. Cotton and C. S. Kraihanzel. Vibrational Spectra and Bonding in Metal Carbonyls. I. Infrared Spectra of Phosphine-substituted Group VI Carbonyls in the CO Stretching Region. *J. Am. Chem. Soc.* (1962) **84,** 4432–4438.

11. D. I. Bezuidenhout. *Synthesis and Structural Investigations of Manganese Carbene Complexes*. (2006). 24.

12. L. J. Farrugia. ORTEP-3 for Windows - a version of ORTEP-III with a Graphical User Interface (GUI). *J. Appl. Ctrystallogr.* (1997) **30,** 565.

13. POV-Ray. POV-Ray. (2004) at <http://www.povray.org/download/>

© University of Pretoria

14. O. S. Mills and A. D. Redhouse. Carbon compounds of the transition metals. Part XII. Crystal and molecular structure of phenylmethoxycarbenepentacarbonylchromium. *J. Chem. Soc. A* (1968) 642–647. doi:10.1039/J19680000642

15. E. O. Fischer and A. Maasbol. Tungsten carbonyl-carbene complex. *Angew. Chem.* (1964) **76,** 645.

16. F. H. Allen, O. Kennard, D. G. Watson, L. Brammer, A. G. Orpen and R. Taylor. Tables of Bond Lengths determined by X-Ray and Neutron Diffraction. Part I. Bond Lengths in Organic Compounds. *J. Chem. Soc. Perkin Trans. II* (1987) S1–S19.

17. J. T. Carlock. A comparative study of triphenylamine, triphenylphosphine, triphenylarsine, triphenylantimony and triphenylbismuth as ligands in the rhodium-catal yzed hydroformylation of 1-dodecene. *Tetrahedron* (1984) **40,** 185–187.

18. A. R. Katritzky and R. D. Topsom. Distortions of the π-Electron System in Substituted Benzenes. *Angew. Chem. Int. Ed.* (1970) **9,** 87–100.

19. R. J. Card and W. S. Trahanovsky. Arene-metal complexes. 13. Reaction of substituted (benzene)tricarbonylchromium complexes with n-butyllithium. *J. Org. Chem.* (1980) **45,** 2560–2566.

20. M. F. Semmelhack and G. Clark. Meta-substituted aromatics by carbanion attack on .pi.-anisole and .pi.-toluenechromium tricarbonyl. *J. Am. Chem. Soc.* (1977) **99,** 1675–1676.

21. M. F. Semmelhack, J. Bisaha and M. Czarny. Metalation of arenechromium tricarbonyl complexes and electrophilic trapping of the complexed phenyllithium intermediate. *J. Am. Chem. Soc.* (1979) **101,** 768–770.

22. A. R. Lepley, W. A. Khan, A. B. Giumanini and A. G. Giumanini. Metallation of N,N-Dimethylaniline. *J. Org. Chem.* (1966) **31,** 2047–2051.

23. D. G. Carroll and S. P. McGlynn. Semiempirical molecular orbital calculations. V. Electronic structure of arenechromium tricarbonyls and chromium hexacarbonyl. *Inorg. Chem.* (1968) **7,** 1285–1290.

24. D. K. Wells and W. S. Trahanovsky. Arene-metal complexes. II. Thermodynamic stabilities of .alpha.-substituted .alpha.-hydroxybenzyl cations complexed with tricarbonylchromium. The variable cation-stabilizing ability of the tricarbonylchromium moiety. *J. Am. Chem. Soc.* (1969) **91,** 215871–5872.

25. R. Meyer, P. L. Wessels, P. H. van Rooyen and S. Lotz. π-Arene complexes: 11. Site control affected by steric and electronic factors of ring substituents in σ,π-coordinated bimetallic complexes. *Inorg. Chim. Acta* (1999) **284,** 127–132.

© University of Pretoria

26. E. O. Fischer, F. J. Gammel and D. Neugebauer. Übergangsmetall-Carbin-Komplexe, LII. (Tricarbonylchrom)-η;6-phenyl als Substituent in Carben- und Carbinkomplexen der VI. Nebengruppe. *Chem. Ber.* (1980) **113,** 1010–1019.

27. P. S. Braterman. *Metal carbonyl spectra*. (Academic Press Inc., 1975).

28. L. E. Orgel. The Infrared Spectra of Substituted Metal Carbonyls. *Inorg. Chem* (1962) **1,** 25–29.

29. T. A. Albright, P. Hofmann and R. Hoffmann. Conformational preferences and rotational barriers in polyene-ML3 transition metal complexes. *J. Am. Chem. Soc.* (1977) **99,** 7546–7557.

30. E. L. Muetterties, J. R. Bleeke, E. J. Wucherer and T. Albright. Structural, stereochemical, and electronic features of arene-metal complexes. *Chem. Rev.* (1982) **82,** 499–525.

© University of Pretoria

Chapter 4

Piggybacking of a pentacarbonyl carbene substituent into the coordination sphere of group 6 and 7 transition metal carbonyl complexes

4.1 Background

In this section of the project, a carbene containing phosphine ligand was coordinated to a group 6 or 7 metal carbonyl complex through substitution of one of the carbonyl ligands. The substitution of the carbonyl ligand involved replacing a CO group with a solvent that can act as a ligand like THF or $NCCH_3$ either through chemical means or UV irradiation. When a better ligand than the place-holding ligand is added, which in this case is either **1a** or **1b**, the phosphine replaces the place-holding ligand. The phosphorylated transition metal is fully characterised by NMR and IR spectroscopy.

4.2 Group 6 carbonyl complexes

The following section was the only part of the project in which **1a**, the chromium carbene containing phosphine, was coordinated to group six transition metal carbonyl complexes. Both the transition metal to which the particular phosphine was being coordinated, as well as the metal-carbene complex contained a pentacarbonyl group. By using the different transition metals in the carbene complex, it was possible to determine which of the spectroscopic carbonyl signals were particular to which metal group. In the case where the carbene substituent was the same as the metal carbonyl to which the phosphine was being coordinated to, the bonding properties of the phosphine and carbene ligands would be reflected in the IR spectra.

All the carbonyl complexes were synthesised by the same method. The metal hexacarbonyl was dissolved in hexane with a small amount of THF added to the solution. The mixture was UV irradiated during which a carbonyl ligand was

© University of Pretoria

replaced by a THF ligand via an S_N1 mechanism[1]. Addition of the phosphine replaced the place-holding THF molecule to form the desired product.

4.2.1 Tungsten complexes

4.2.1.1 $W(CO)_6$ as acceptor complex for phosphine coordination

The reaction scheme in the synthesis of the desired product is given below. The obtained red-brown product was purified by column chromatography.

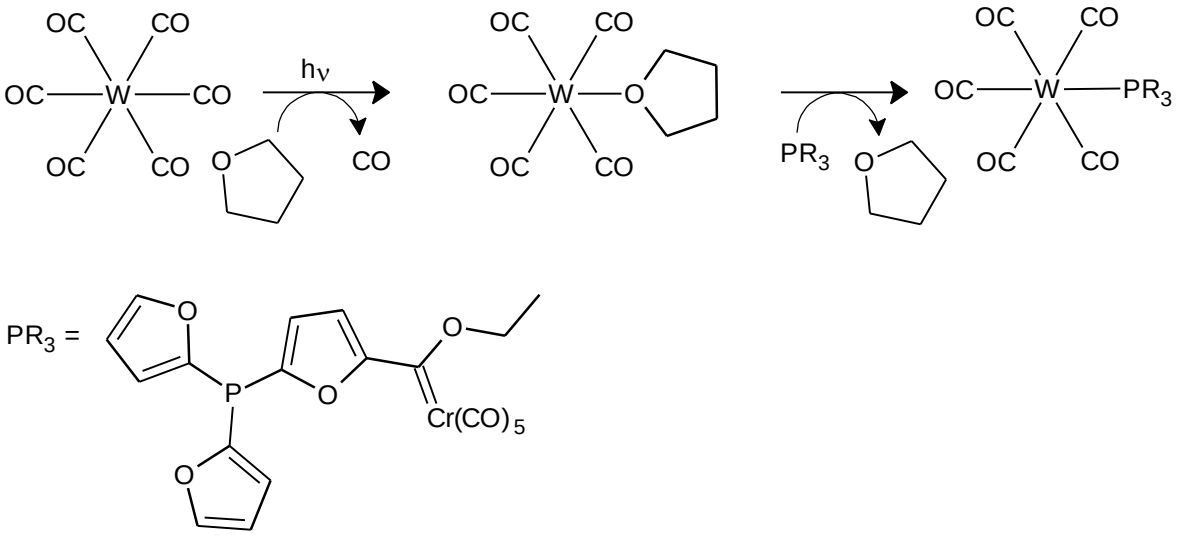

Scheme 4.1 Synthesis of compound **13**

4.2.1.2 Characterisation

The characterisation of **13** involved analysis by ^{1}H, ^{13}C, ^{31}P NMR and IR spectroscopy. The ^{1}H spectrum revealed broadened peaks for the furyl protons which could not be accurately assigned. The ^{1}H NMR spectrum further revealed the presence of large amounts of ester and olefin products that formed and were present in the product solution. These products are indicative of increased reactivity of the Cr-carbene complex on coordination to the $W(CO)_5$ metal centre. The presence of an olefin in the product mixture indicated that a carbene-carbene coupling reaction had occurred.

© University of Pretoria

The ^{13}C NMR spectrum showed the presence of the two different pentacarbonyl groups. Due to the presence of the catalytic products that formed during the isolation and analysis of the product, it was difficult to distinguish clearly between peaks belonging to the actual dimetallic product and those belonging to the organic products in the ^{13}C NMR spectrum. The chromium pentacarbonyl carbene group was clearly visible in the spectrum and comparing the chemical shift values of carbonyl peaks of the $W(CO)_5$ group with those found by Ainscough[2] it was clear that the phosphine coordinated $W(CO)_5$ group had carbonyl chemical shift values between 196.9 and 199.3 ppm.

Grim and his co-workers found that the phosphorous-tungsten coupling constant in a series of tungsten pentacarbonyl-phosphorous compounds was an indication of the π-acceptor ability of the phosphine ligand[3]. The phosphine ligands' coupling constants ranged from 200 to 411 Hz with the bigger coupling constant representing the better π-acceptor. On ^{31}P chemical shift analysis of the product mixture it was found that the signal at -31.3 ppm had a phosphorous-tungsten coupling constant of 332 Hz. In comparing the coupling constant against the series formed by Grim[3], it was found that the π-accepting ability of the carbene containing phosphine (**1a**) was in the same range as those of a $(MeO)_2PhP$ ligand. To establish that coordination had in fact occurred, it was necessary to state that the ^{31}P chemical shift value of the uncoordinated phosphine **1a**, had a value of -73 ppm. The coordination is visible in the fact that a significant downfield shift of the phosphorous atom was observed in addition to the presence of a W-P coupling constant.

© University of Pretoria

Table 4.1 ^{1}H, ^{13}C and ^{31}P NMR data ($CDCl_3$) of **13**

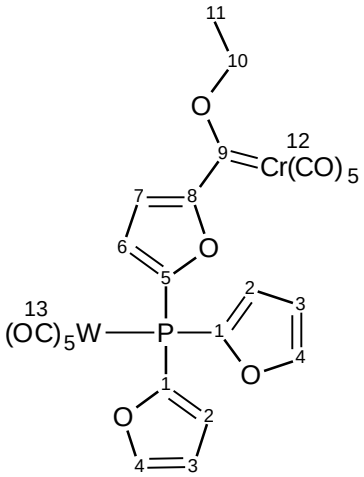

^{1}H NMR

Position	δ_h/ppm	Multiplicity *J*/Hz	Integration
2	7.72 – 6.37	m	8H
3			
4			
6			
7			
10	5.15	br	2H
11	1.58	br	3H

^{13}C NMR

	δ_c/ppm	*J*/Hz
1	111.0 – 147.8	-
2		-
3		-
4		-
5		-
6		-
7		-
8		-
9	311.1	-
10	77.2	-

© University of Pretoria

11	15.4	-
12	224.9, 216.1	-
13	199.3, 195.6	-

^{31}P NMR		
	δ_p/ppm	$J_{W\{P\}}$/Hz
	-31.3	332

The IR spectrum of **13** showed two different pentacarbonyl groups, one belonging to the chromium-carbene substituent and the other belonging to the tungsten metal centre to which the phosphine was coordinated.

Table 4.2 Infrared carbonyl spectrum of **13**

IR carbonyl stretching frequencies (cm^{-1})			
Cr(CO)$_5$ group			
$A_1^{(1)}$	$A_1^{(2)}$	B_1	E
2097	1957	2023	1953
W(CO)$_5$ group			
$A_1^{(1)}$	$A_1^{(2)}$	B_1	E
2075	1924	1995	1924

There are some unusual observations that need to be addressed. The E band of the W(CO)$_5$ group appears at 1925 cm^{-1} which is at much lower wavenumbers than what is expected for a pentacarbonyl group E band. In the article by Grim[3], it was shown that the E band of the tungsten pentacarbonyl could appear at such low wavenumbers when particular phosphine ligands were coordinated to the metal centres. The significantly low wavenumber of the E band can be attributed to the increased electron density donated to the metal centre by the coordinating phosphorous atom. The $A_1^{(2)}$-band of the W(CO)$_5$ group is not visible on the spectrum, but it is believed to lie under the E band of the W(CO)$_5$ group.

Comparing the Cr(CO)$_5$ in **1a** with **13**, a general shift of all the bands to higher wavenumbers is observed on coordination of the phosphine. The Cr(CO)$_5$ IR bands of **1a** appear at 2060, 1990 and 1944 cm^{-1} for the $A_1^{(1)}$, B_1 and E bands respectively,

© University of Pretoria

while those of **13** is found at 2097, 1957, 2023 and 1953 cm^{-1} respectively. The higher wavenumbers are indicative of less electron density on the Cr due to the coordination of the phosphorous ligand. The electron lone-pair present on the phosphorous is no longer able to be used for the stabilisation of the carbene carbon and for this reason the stabilisation of this carbon comes from π-back bonding the metal to which it is coordinated.

4.2.2 Chromium complexes

4.2.1.1 $Cr(CO)_6$ as acceptor complex for phosphine coordination

As in the case of the tungsten carbonyl complexes, a CO group was removed from the $Cr(CO)_6$ complex by UV irradiation. The space left by the CO group is immediately filled by a THF molecule present in the solution, but it also acts as a readily displaceable ligand. On addition of the phosphine **1a** to the reaction mixture, the THF molecule is replaced and the desired complex is formed.

4.2.1.2 Characterisation

The characterisation of compound involved analysis of ^{1}H, ^{13}C and ^{31}P NMR spectra as well as IR spectroscopic analysis.

The ^{1}H NMR spectrum revealed the presence of furyl groups between 7.72 and 6.33 ppm as well as the ethoxy substituent used to stabilise the carbene complex with -CH_2- and -CH_3 signals at 5.10 and 1.60 ppm respectively. The presence of these protons was indicative that the phosphine ligand **1a** was present in the product. It was, however, not necessarily proven that coordination of the phosphine had taken place. Formation of a large amount of ester product was also observed indicated by a prominent signal of the RC(O)O$\underline{CH_2}$R protons at 4.32 ppm. This signal appeared upfield from the carbene ethoxy substituent. The formation of only the ester shows increased reactivity of the chromium carbene complex, but not any significant

© University of Pretoria

catalytic activity of the $Cr(CO)_5$ metal centre to which the phosphine has been coordinated.

The ^{13}C NMR showed one set of carbonyl peaks, depicting the *cis* and *trans*-carbonyl ligand positions on a $Cr(CO)_5$-carbene complex. It has to be noted that no additional ^{13}C NMR signals for the other chromium pentacarbonyl group was observed indicating the insensitivity of the signals for different ligands. It is possible that the carbonyl peaks of the two $Cr(CO)_5$ groups lie exactly over each other. It is further important to note that the carbene carbon at 311.7 ppm was visible, but that the *ipso*-carbons (C1 and C5) on the furyl rings could not be assigned. The ^{13}C NMR data reveals the presence of the ligand, but it still was not enough proof to show definite coordination to the $Cr(CO)_5$ group.

The proof that coordination had occurred was found in the ^{31}P NMR spectrum that showed a peak at -11.7 ppm. The difference between the coordinated and the uncoordinated phosphine ligands is 62.1 ppm. This change in the phosphorous environment clearly indicates that the phosphine is no longer free but coordinated There was no P{M} coupling observed for the compound.

Table 4.3 ^{1}H, ^{13}C and ^{31}P NMR data ($CDCl_3$)of **14**

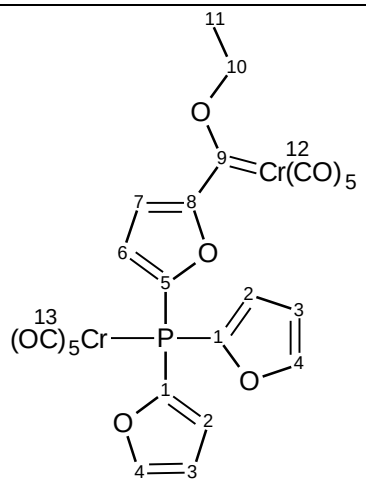

^{1}H NMR			
Position	δ_h/ppm	Multiplicity *J*/Hz	Integration
2	6.54	s	2H

© University of Pretoria

3	6.84 – 6.77	m	2H
4	7.72	s	2H
6	7.14	s	1H
7	6.79	s	1H
10	5.10	q, 7.1	2H
11	1.60	t, 7.1	3H

^{13}C NMR		
	δ_c/ppm	Multiplicity *J*/Hz
1	-	-
2	111.1	d, 9.1
3	110.9	-
4	147.5	d, 2.2
5	-	-
6	120.9	d, 9.9
7	110.8	d, 6.6
8	177.6	-
9	311.7	-
10	77.2	-
11	15.3	-
12	223.8, 216.6	-
13	-	-

^{31}P NMR (δ_p/ppm)
-11.7

A final aspect to consider was the IR spectrum of the compound. The IR spectrum was indicative of two different sets of pentacarbonyl groups, both being $Cr(CO)_5$. The presence of the two different carbonyl groups is indicated by two equally sized $A_1^{(1)}$–and E bands at 2073, 2062, 1960, 1950 cm^{-1} respectively.

© University of Pretoria

Table 4.4 Infrared carbonyl spectrum of **14**

IR carbonyl stretching frequencies (cm^{-1})			
$Cr(CO)_5$ groups			
$A_1^{(1)}$	$A_1^{(2)}$	B_1	E
2073, 2062	1960	1997	1960

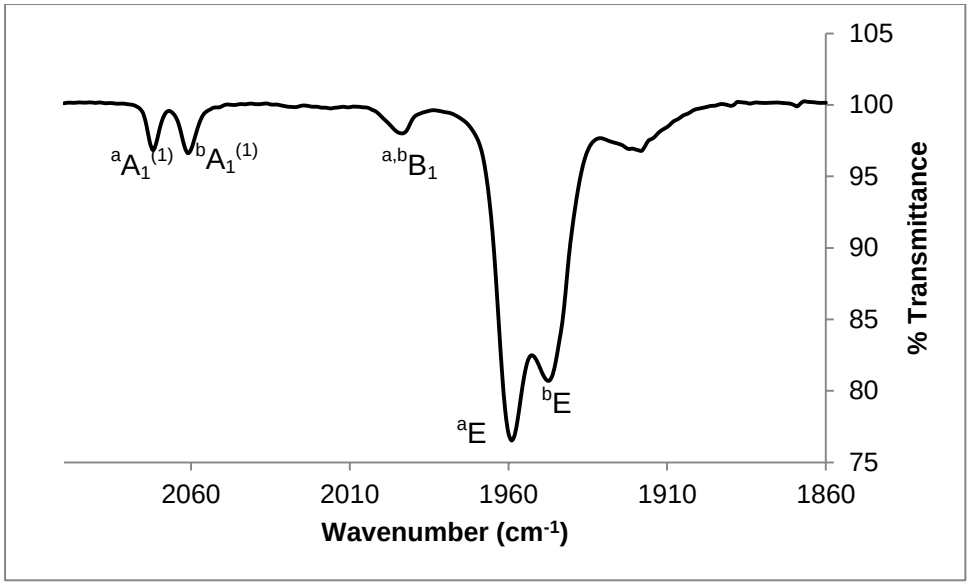

Figure 4.1 Carbonyl IR spectrum (hexane) of **14**

Figure 4.1 represents the IR spectrum of **14**. The differences in bonding properties of the stronger π-acceptor carbene ligand (higher wavenumbers) compared to the weaker π-acceptor properties of the phosphine (lower wavenumbers) are illustrated by the IR spectrum.

4.2.3 Group 6 metals compared

In the case of both **13** and **14**, **1a** was successfully coordinated to the metal centres by replacing a CO ligand. Comparing the ^1H NMR of the two products, it is first necessary to state that for both of these products additional template reactions occurred. In the case of **13,** both ester and olefin formation was observed, indicating that a metathesis reaction was occurring, most likely catalysed by the $W(CO)_5$ metal centre to which the phosphine was coordinated. A large amount of ester formation was also visible in the case of **14**, but it is important to note that no olefin formation

© University of Pretoria

occurred. This is an indication that the $Cr(CO)_5$ metal centre to which **1a** is coordinated, does not have as large a catalytic notion as the $W(CO)_5$ group in **13**. The ^{13}C NMR spectrum also showed little difference between **13** and **14**. In both cases, it was difficult to distinguish any C-P coupling in the spectra, however, the peak values of the two products show very little difference.

A significant difference was found in the ^{31}P NMR spectra of the two compounds. Compound **13** had a peak at -31 ppm, while **14** showed a peak at -11 ppm. The distinct difference between the amounts of electron density on the phosphorous has to do with the amount of electron density present on the metal to which the phosphine was coordinated. The Cr metal centre is found in period three while the W metal centre is found in period five. On coordination of the phosphine to the $W(CO)_5$ metal centre, the metal centre is able to back-donate more electron density into the empty π-orbitals of the phosphorous atom. The increased amount of electron density will shield the phosphorous atom and the signal in the ^{31}P NMR spectrum shifted upfield.

A final aspect to consider is the infrared spectrum of **13** and **14**. Both the spectra revealed the presence of two separate pentacarbonyl patterns. Compound **13** displays the effect of two different metal fragments and shows a clear difference between the two groups since two different metal pentacarbonyls are present in the molecule whereas **14** displays the result of two of the same pentacarbonyl groups with different ligands and properties.

4.3 Group 7 carbonyl complexes

4.3.1 Rhenium complexes

4.3.1.1 $Re_2(CO)_{10}$ as acceptor complex for phosphine coordination

In this reaction, one of the CO ligands present on $Re_2(CO)_{10}$ is removed from the complex with triethylaminoxide and replaced with an acetonitrile ligand. The

© University of Pretoria

acetonitrile acts as a weak coordinating ligand and can easily be replaced by a ligand with stronger bonding properties like the carbene-containing phosphine **1b**.

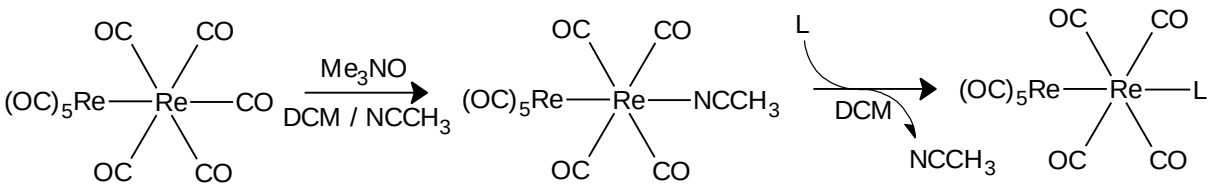

Scheme 4.2 Synthesis of **15**

In the case of a dimetal centre, it is possible for ligand coordination to occur either at an axial or an equatorial position. Based on steric considerations the proposed structure of the final product $Re_2(CO)_9L$, where L represents the coordinated **1b** phosphine, follows:

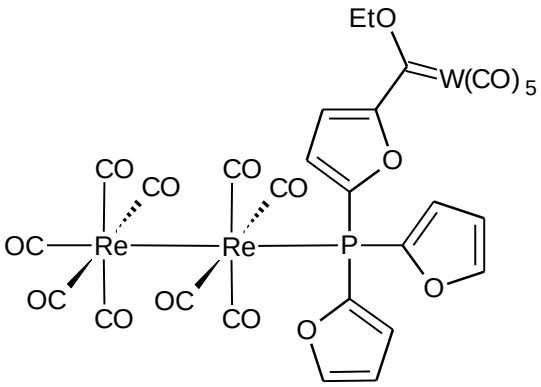

Figure 4.2 Axially coordinated phosphine ligand of **15**

4.3.1.1 Characterisation

Reaction of **1b** with one equivalent $Re_2(CO)_9NCMe$ in DCM gave a brown-orange solid product. The obtained product was free of any contaminants and also showed no sign of catalytic activity as in the case of Pd(II) and Au(I) complexes.

The ^1H NMR spectrum of the single isolated product showed very clear furyl signals between 7.76 and 6.53 ppm. The quartet and triplet at 4.94 and 1.62 ppm was representative of the OEt group with an R group of a tungsten carbonyl carbene group. The ^1H NMR revealed resolution in which the $^1H\{^{31}P\}$ coupling was obvious,

© University of Pretoria

especially in the case of the furyl groups not containing the carbene substituents. In a study by Ghosh[4], PFu_3 was coordinated to $Re_2(CO)_9NCMe$; replacing the NCMe ligand with PFu_3. The same product was isolated, but with the exception of the carbene substituent present on the PFu_3. The ^1H NMR of their product revealed three multiplets at 7.73, 6.73 and 6.53 ppm. The three multiplets can be compared with the furyl groups without the carbene substituent in **15** which have five resonances (Figure 4.3). These three signals appeared as ddd with couplings from each other and the $^1H\{^{31}P\}$ coupling at 7.76, 6.68 and 6.54 ppm. These values are very close to those found by Ghosh and his research group. The furyl group containing the metal carbene substituent will have much more significant differences with a dd coupling pattern observed for both protons as well as more downfield values of 7.27 and 6.76 ppm due to the deshielding effect caused by the carbene ligand.

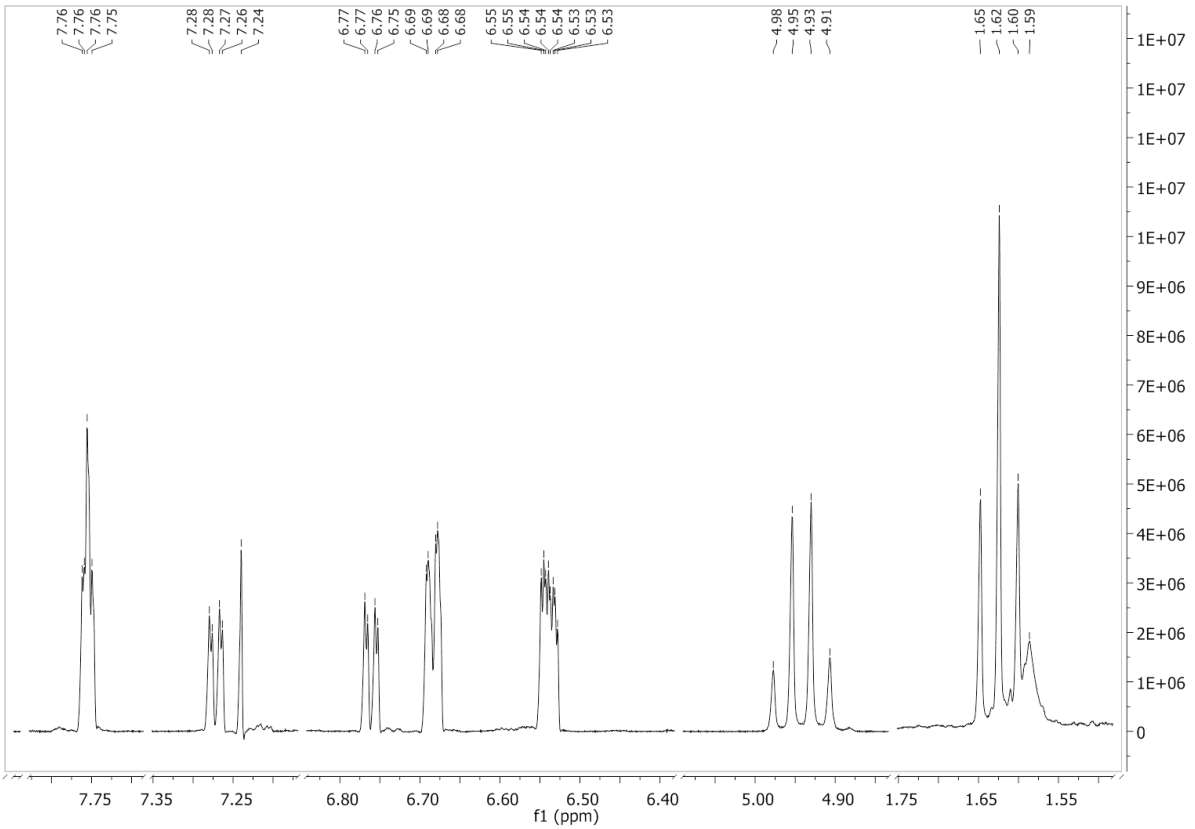

Figure 4.3 ^1H NMR spectrum ($CDCl_3$) of **15**

The ^{13}C NMR spectrum revealed the presence of all the expected furyl, carbene and tungsten-carbonyl peaks in addition to the CO peaks of the $Re(CO)_9$ group.

© University of Pretoria

The final NMR spectrum to consider is the ^{31}P NMR of **15**. A single peak is observed at -41.0 ppm and no additional coupling is observed. The ^{31}P spectrum of Ghosh and his research group revealed an uncoupled ^{31}P peak at -36.9 ppm. The only difference between the molecule synthesised by Ghosh and **15** is the fact that **15** contains a carbene substituent on one of the furyl groups of the PFu_3 ligand. Hence, in comparing the ^{31}P NMR shifts of the two molecules, the effect that the carbene has on the electron density present on the phosphorous atom can be seen in the coordinated complex. The NMR reveals greater electron density on the phosphorous atom in the presence of the carbene substituent than in its absence. The presence of the carbene allows the phosphorous atom to become a better π-accepting ligand, allowing it to accept more back-bonding electron density from the metal than in the case where the carbene substituent was not present.

Table 4.5 ^{1}H, ^{13}C and ^{31}P NMR data ($CDCl_3$) of **15**

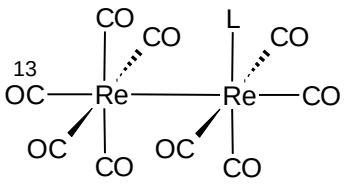

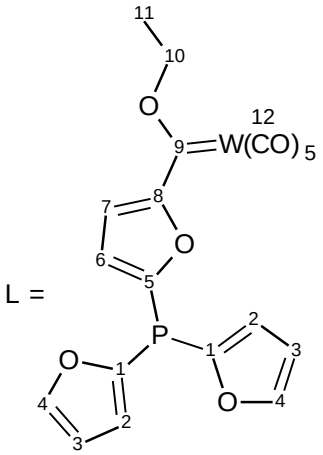

^{1}H NMR

Position	δ_h/ppm	Multiplicity *J*/Hz	Integration
2	6.54	ddd, 3.4, 1.7, 1.0	2H
3	6.68	ddd, 3.5, 1.1, 0.7	2H
4	7.76	ddd, 2.2, 1.8, 0.7	2H
6	7.27	dd, 3.8, 1.1	1H
7	6.76	dd, 3.8, 1.1	1H
10	4.94	q, 7.1	2H
11	1.62	t, 7.1	3H

© University of Pretoria

^{13}C NMR		
	δ_c/ppm	Multiplicity *J*/Hz
1	143.6	d, 80.4
2	122.8	d, 14.8
3	111.7	d, 6.1
4	148.7	d, 6.1
5	153.5	d, 66.0
6	122.9	d, 15.0
7	118.6	d, 5.6
8	169.1	d, 4.1
9	285.0	-
10	78.9	-
11	14.8	-
12	203.1, 196.8	-
13	199.9, 192.9, 185.4	-

^{31}P NMR	
	δ_p/ppm
	-41.0

In comparing the ^{1}H NMR spectrum of **15** with **1b**, there are some significant differences. There is a downfield shift of some of the peaks in the furyl groups without the carbene substituent, i.e. H2, H3 and H4 with values of 6.46, 6.99 and 6.70 ppm respectively. No notable changes are observed in the furyl group containing the carbene substituent. This can be explained when the σ-donating and π-acceptor ability of both the phosphine and the metal centre is brought to question. Since the π-back-donating ability of a Re-metal centre is not as good as in the case of a late transition metal such as Pd or Au, it is expected that downfield values will be observed for the furyl groups. The loss of the electron lone pair on the phosphorous to the σ-bond on coordination to a transition metal will cause a deshielding effect in the furyl groups, especially those that do not contain carbene substituents. This is

© University of Pretoria

not observed for the furyl groups with the carbene substituent as the substituent is already putting electronic strain on the furyl group for its stabilisation.

The ^{13}C NMR spectrum gave a clear indication of ligand coordination. In comparing the free phosphine to the coordinated one, it was found that a very large difference was observed in furyl chemical shift values and no significant changes were observed for the carbene substituent. The C1 and C5 carbons of the free phosphine (**1b**) displayed values of 123.2 and 125.1 ppm respectively while those of **15** had values of 143.6 and 153.5 ppm respectively. This very large difference observed for the two compounds is a clear indication of the effect that the electron lone pair on the phosphorous atom has on the stabilisation of the free phosphine (**1b**). On coordination, this electron density is removed with very little electron density donated to the phosphorous atom from the metal centre. The general trend throughout the ^{13}C NMR is that the carbons present in the furyl groups of **15** are slightly downfield from that of **1b**.

The change in the chemical shift values of the ^{31}P NMR spectrum between the free phosphine and the coordinated one clearly indicates that coordination took place. The value shifted from -72.8 ppm for **1b** to -41.0 ppm for **15**.

The final aspect to consider in analysis of this compound is the IR spectrum. All IR spectral properties of CO groups were fully discussed in Chapter 2 for a $M(CO)_5$ fragment. In this section of the work, both the $M(CO)_5$ as well as a $M_2(CO)_9$ carbonyl fragment has to be considered. In 1965, Ziegler et.al.[5] fully described the IR carbonyl frequencies for a $M_2(CO)_9$ carbonyl group. There are two different classes of $[M_2(CO)_9L]$-complex IR symmetries. The C_s symmetry displays a nine band pattern, six of which include A' bands, three degenerate A" bands and contains the L-ligand in the equatorial position. The IR-active normal modes for eq-$[M_2(CO)_9L]$ are presented in Figure 4.4.

© University of Pretoria

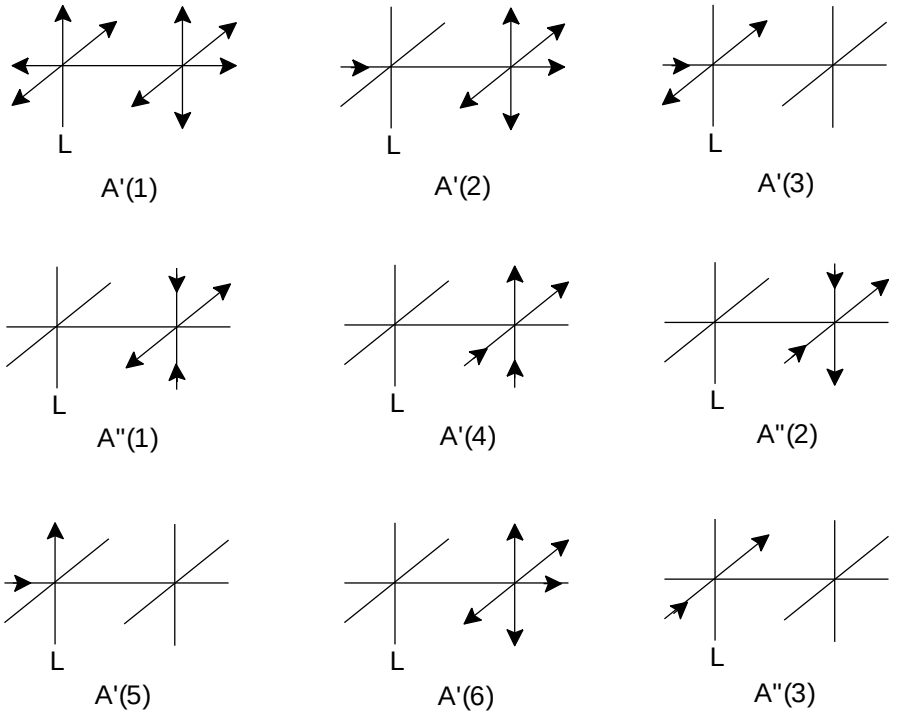

Figure 4.4 Carbonyl vibration modes (9) for the *Cs* symmetry of eq-$[M_2(CO)_9L]$ complexes

By contrast the C_{4V} symmetry has five bands: three A' bands and two E-bands, and the L-ligand is found in the axial position. The IR-active normal modes for ax-$[M_2(CO)_9L]$ are represented by Figure 4.5.

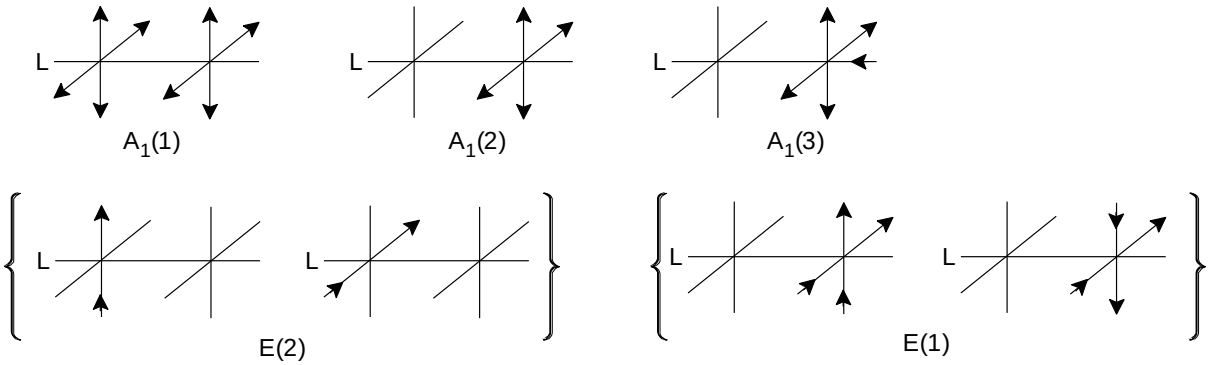

Figure 4.5 Carbonyl vibration modes (5) for the C_{4V} symmetry of ax-$[M_2(CO)_9L]$ complexes

The IR spectrum of **15** revealed eight bands. All eight of these bands represented two different carbonyl groups: The dimetal centre to which the phosphine was coordinated and the pentacarbonyl group coordinated to the carbene. The five bands observed for $[Re_2(CO)_9(PFur_3)]$ by Ghosh[4] had values of 2107, 2042, 1996, 1964 and 1943 cm^{-1}, indicating that the phosphine ligand was found in an axial

© University of Pretoria

position. All observed bands for **15** are listed in Table 4.6. There were seven bands that could be assigned to the $M_2(CO)_9L$ group, indicating that the formed product had the phosphine coordinated in the equatorial position of the metal. Only two bands established the presence of the pentacarbonyl group with all the other bands showing overlap with the $M_2(CO)_9L$ group. The IR spectrum for **15** is shown in Figure 4.6. The bands representing each group are also marked.

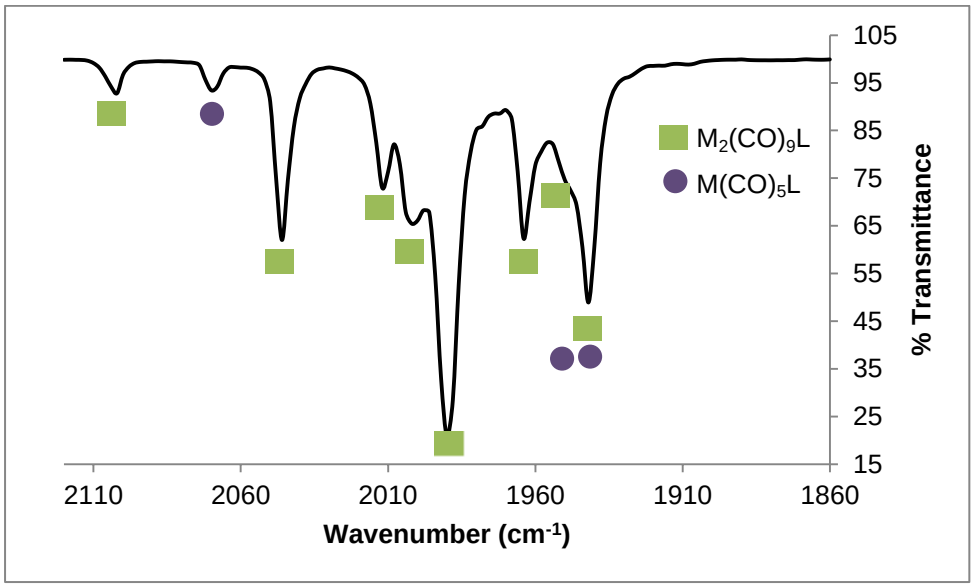

Figure 4.6 Carbonyl IR spectrum (Hexane) of **15**

Table 4.6 Carbonyl infrared spectrum (Hexane) of **15** in wavenumbers (cm^{-1})

$M_2(CO)_9L$ group								
A'(1)	A'(2)	A'(3)	A"(1)	A'(4)	A"(2)	A'(5)	A'(6)	A"(3)
2104 (w)	2046 (m)	2012 (s)	2004 (vs)	1990 (s)	1964 (m)	1950 (m)	1942 (m)	n.o.
$M(CO)_5$ group								
$A_1^{(1)}$		$A_1^{(2)}$		B_1		E		
2072		1942		n.o.		1942		

Comparing the IR spectrum of **15** with those found by Ghosh[4], it was found that the spectra was significantly different. The Ghosh complex showed the PFu_3 phosphine coordinated in the axial plane, while **1b** in **15** coordinated in the equatorial plane.

© University of Pretoria

Another prominent difference is the presence of the additional pentacarbonyl peak in **15**. .

Comparing the pentacarbonyl group of **15** to that of **1b** (carbene-containing phosphine), it was found that the E-band of **15** occurred at higher wavenumbers than those of **1b**. Carbene-containing phosphine **1b** had an E- band value of 1944 cm^{-1} while **15** had a values of 1964 cm^{-1}.

4.3.2 Manganese complexes

4.3.2.1 $Mn_2(CO)_{10}$ as acceptor complex for phosphine coordination

As in the case of $Re_2(CO)_{10,}$ a carbonyl is removed from the complex with triethylaminoxide and replaced with an acetonitrile ligand. The acetonitrile ligand is then replaced with **1b** to afford a dimetal centre containing a carbene-containing phosphine ligand (**16**). This reaction was very much the same as that of the $Re_2(CO)_{10}$ reaction, however, a smaller yield of the product was observed for this reaction.

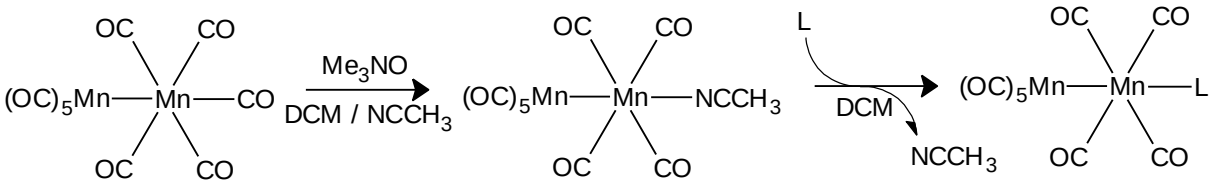

Scheme 4.3 Synthesis of **16**

As in the case with the rhenium dimetal centre, it is possible for ligand coordination to either occur equatorially or axially. Analysis of the IR spectrum could reveal which substitution had occurred in this reaction.

© University of Pretoria

4.3.2.2 Characterisation

Two product fractions were isolated from the reaction. The one fraction was the desired phosphine coordinated product and the other contained traces of secondary products which indicated increased carbene reactivity upon coordination of the phosphine to the dimanganese metal centre. The red and yellow fractions were analysed by NMR and IR spectroscopy. Recently Karmaker[6] reported the coordination of PFu_3 to a $[Mn_2(CO)9(NCMe)]$ complex. Comparing their mono-substituted phosphine complex with the synthesised product, **16**, will determine the effect that the metal-carbene substituent present on the phosphine will have in the reaction.

Poor resolution was observed in the ^{1}H NMR for the first fraction; but it was possible to determine that all the required signals were present for proof that coordination of the carbene containing phosphine was successful to the manganese dimetal centre to form the desired product (**16**).

The ^{13}C NMR spectrum also confirmed that **1b** was successfully coordinated to the dimanganese complex. Both the pentacarbonyl peaks of the carbene-$W(CO)_5$ group and that of the nonacarbonyl group was clearly visible in the isolated product. The ^{31}P NMR spectra revealed a peak at -11.0 ppm. This value was very closely correlated with the ^{31}P value of the $[Mn_2(CO)_9(PFu_3)]$ complex synthesised by Karmaker[6] which occurred at -10.2 ppm. Again, it is necessary to mention the significant downfield shift of the ^{31}P NMR signal before and after coordination of the phosphine. The difference between the coordinated and uncoordinated ^{31}P signals in this case is 61.8 ppm.

© University of Pretoria

Table 4.7 ^{1}H, ^{13}C and ^{31}P NMR data ($CDCl_3$) of **16**

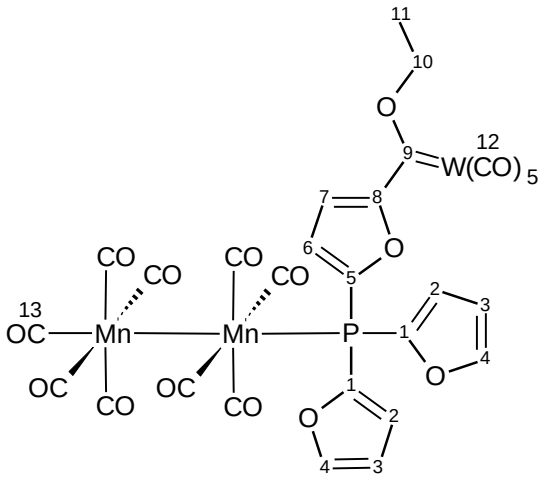

^{1}H NMR

Position	δ_h/ppm	Multiplicity *J*/Hz	Integration
2	6.55	-	2H
3	6.79	-	2H
4	7.76	-	2H
6	7.28	-	1H
7	6.98	-	1H
10	4.94	-	2H
11	1.62	-	3H

^{13}C NMR

	δ_c/ppm	Multiplicity *J*/Hz
1	148.1	d, 33.4
2	111.3	d, 19.5
3	120.1	d, 15.3
4	-	-
5	149.1	d, 42.5
6	121.5	d, 17.2
7	117.3	d, 17.3
8	-	-
9	284.7	-
10	78.6	-

© University of Pretoria

11	14.9	-
12	203.3, 197.0	-
13	224.4, 223.6, 207.0	-

^{31}P NMR (δ_p/ppm)
-11.0

The final aspect to consider is the IR spectrum of the compound. In previous studies by Chan[7], it was found that the different phosphine ligands coordinated in the axial position of the dimanganese nonacarbonyl metal centres. The same was observed for $[Mn_2(CO)_9(PFu_3)]$ synthesised by Karmaker and coworkers[6]. All these complexes showed five IR bands, indicating the C_{4V} symmetry for the compounds. The phosphine ligand in **16** is too bulky to be accommodated in the electronically favoured equatorial position. Due to the significantly shorter Mn-Mn bond distance compared to the Re-Re bond distance in **15**, the $Mn(CO)_5$ fragment is too close to the other $Mn(CO)_4PR_3$ fragment to allow for equatorial coordination. The IR spectrum of **16** was found to contain a total of eight bands all ranging between 2110 and 1910 cm^{-1}. The eight bands was representative of the CO ligands present on the dimetal centres as well as the five CO ligands present in the tungsten carbene complex.

Table 4.8 Carbonyl infrared spectrum (hexane) of **16**

$M_2(CO)_9L$ group				
$A_1(1)$	$A_1(2)$	E(1)	$A_1(3)$	E(2)
2081	2018	1999	1983	1947
$M(CO)_5$ group				
$A_1^{(1)}$	$A_1^{(2)}$	B_1	E	
2069	1958	n.o.	1947	

Unlike for $Re_2(CO)_9PR_3$, the IR spectrum revealed that the phosphine was coordinated in an axial position of the dimanganese metal centres, since only five bands were observed for the nonacarbonyl group. Comparing the IR values with those found by Karmaker's research group, it was found that there is little difference

© University of Pretoria

between the carbonyl bands of the different compounds. When **16** was compared to the free phosphine, **1b**, there was also no significant difference between the carbonyl spectra.

The first fraction was found to contain the desired product **16**, the second isolated fraction revealed the presence of esters that formed during the course of the reaction. The ^{1}H NMR spectrum revealed the major product as an ester with a prominent -O$\underline{CH_2}CH_3$ signal at 4.33 ppm, upfield from the carbene -O$\underline{CH_2}CH_3$ peak. This product formation was an indication of significant increased reactivity of the carbene substituent present on the phosphine ligand. Trace amounts of O_2 present in the solvent oxidizes with the reactive carbene carbon to form the ester product.

4.3.4 Group 7 metals compared

The first difference that has to be noted between compounds **15** and **16** was their synthesis and yield. In the synthesis of **15,** much more prominent colour changes and higher yields were observed than in the case of **16**. The ^{1}H NMR spectrum of the two compounds showed slight differences between the two compounds with the furyl protons of **16** being slightly downfield from those of **15**. Already an indication of electron back-donation from the metal centre to the phosphorous is visible, but still very small. It also has to be noted that the $^{31}P\{^{1}H\}$ coupling of **15** was significantly clearer than the broadened peaks observed in the ^{1}H spectrum of **16**.

The ^{13}C spectra of the two respective metals did not only show a difference in the nonacarbonyl signals, but there was also a clear distinction between the observed $^{13}C\{^{31}P\}$ coupling constants for the two compounds. The coupling constants of **15** were extremely large for the carbons closest to the phosphorous atom with values of 80.4 and 66.0 Hz for the different furyl groups. The coupling constants of **16** were much smaller for the same carbons with values of 33.4 and 42.5 Hz. The ^{13}C signals of the compounds themselves did not show any significant difference between the compounds. The final NMR spectrum to consider is the ^{31}P spectra in which a difference was observed. Compounds **15** and **16** had respective ^{31}P chemical shift values of -41.0 and -11.0 ppm. The amount of electron density present on a metal

© University of Pretoria

centre plays an obvious role in the coordinated phosphine ^{31}P signal position. The Mn metal centre has significantly less electron density to back-donate to the phosphorous atom, causing the large shift downfield in the ^{31}P spectrum due to electron deshielding of the phosphorous atom.

The IR peaks of **15** and **16** are significantly different because of the respective equatorial and axial coordination of **1b** in the complexes. The pentacarbonyl groups coordinated to the carbene carbon showed differences between **15** and **16**, with **15** bands having slightly higher wavenumbers than **16**. The pentacarbonyl group of **15** had wavenumbers of 2072, 1964 and 1964 cm^{-1} for the $A_1^{(1)}$, $A_1^{(2)}$ and E bands respectively, while **16** had respective bands at 2069, 1958 and 1947 cm^{-1}.

© University of Pretoria

4.4 References

1. W. Strohmeier. Photochemical Substitutions on Metal Carbonyls and Their Derivatives. *Angew. Chem. Int. Ed.* (1964) **3,** 730–737.

2. E. W. Ainscough, A. M. Brodie, S. L. Ingham and J. M. Waters. Functionalised phosphine complexes of Group 6 metal carbonyls: structure of pentacarbonyl-(phenyl-2-carbaldehyde diphenylphosphine-κP)tungsten. *Inorg. Chim. Acta* (1995) **234,** 163–167.

3. S. O. Grim, P. R. McAllister and R. M. Singer. Correlation between phosphorus–tungsten coupling constants and carbonyl stretching frequencies in phosphorus-ligand derivatives of tungsten hexacarbonyl. *J. Chem. Soc. D* (1969) 38b–39.

4. S. Ghosh, M. Khatun, D. T. Haworth, S. V. Lindeman, T. A. Siddiquee, D. W. Bennett, G. Hogarth, E. Nordlander and S. E. Kabir. Activation of tri(2-furyl)phosphine at a dirhenium centre: Formation of phosphido-bridged dirhenium complexes. *J. Organomet. Chem.* (2009) **694,** 2941–2948.

5. M. L. Ziegler, H. Haas and R. K. Sheline. Die photochemische Darstellung von Mangancarbonylderivaten. *Chem. Ber.* (1965) **98,** 2454–2459.

6. S. Karmaker, S. Ghosh, S. E. Kabir, D. T. Haworth and S. V. Lindeman. Reactivity of tri(2-furyl)phosphine (PFu_3) with [$Mn_2(CO)_{10}$–n($NCMe)_n$] (n = 0–2): X-ray Structure of mer-[$Mn(CO)_3(\eta^1$-$C_4H_3O)(PFu_3)_2$]. *Inorg. Chim. Acta* (2012) **382,** 199–202.

7. H. S. O. Chan, T. S. A. Hof, K.-L. Tan and L. Ying-Phooi. Substituted metal carbonyls part 19. Synthesis and XPS characterisation of dimanganese(O) carbonyl phosphites. *Inorg. Chim. Acta* (1991) **184,** 23–26.

© University of Pretoria

Chapter 5

Piggybacking a tungsten pentacarbonyl carbene substituent into the coordination sphere of group 10 transition metal complexes

5.1 Background

Platinum and Palladium complexes with phosphine ligands are known for their ease of synthesis and formation of square planar complexes[1]. On coordination of phosphines to these transition metals, the particular combination of ligands will determine whether *cis*- or *trans*- isomers will form and in most cases, there is an equilibrium between isomers. The Ni(0) compounds used in this study are prone to form tetrahedral complexes when coordination occurs[2].

The ligand selected for coordination to the transition metals is a phosphine which contains a Fischer metal-carbene substituent riding on one of its furyl groups (**1b**, fully described in Chapter 2). It is important to realise that, in this chapter, the transition metals to which this ligand will be coordinated are known to have catalytic properties. The effect and further reactions of such phosphine ligand data will be investigated by a comparison of NMR and IR spectroscopy before and after ligand coordination.

To investigate phosphine coordination, the ^{31}P NMR chemical shifts of each compound are closely analysed. In 1961, Meriwether and Leto[3] found that on coordination of the phosphine to a metal centre, the ^{31}P chemical shift values changed dramatically. They either became more positive or negative, depending on the degree of the σ-bonding and π-back bonding character of both the metal and the phosphine. Through the ^{31}P chemical shift values, it is possible to determine whether the phosphine is free or coordinated to the transition metal and will further provide information on the amount of electron density which is present on the phosphorous atom itself.

© University of Pretoria

In this chapter, special interest is given to the group 10 transition metals: in their ability to coordinate ligands, the possible isomers that can form, as well as catalytic or template properties of the transition metal once the particular carbene containing phosphine has been coordinated.

5.2 Platinum complexes

5.2.1 $PtCl_2$(COD) as precursor or receptor complex for phosphine coordination

$PtCl_2$(COD) is a well-known air-stable complex of which the COD ligand can easily be replaced by two choice ligands such as phosphines or amines. In 1952, Chatt and Wilkins first suggested that Pt(II)-phosphine complexes preferred the *cis*-isomer over the *trans*-isomer by measuring the bond strengths between the phosphorous and platinum atoms in $Pt(PEt_3)_2Cl_2$ for both isomers[4]. They also successfully measured the equilibrium constants between the *cis*- and *trans*- isomers of several $Pt(PR_3)_2X_2$ complexes[5]. The study revealed that when chlorine was replaced by iodine and an aromatic group was replaced with an alkyl group, the equilibrium favoured the *trans*-isomer.

The synthesis of the piggybacked complex involved stirring excess phosphine with $Pt(COD)Cl_2$ in dichloromethane for 24 hours. Since the chloro-ligand was coordinated to the metal and an aromatic substituent was present on the coordinated phosphine-ligand, it was expected that the *cis*-product would be the major product of the coordination reaction.

© University of Pretoria

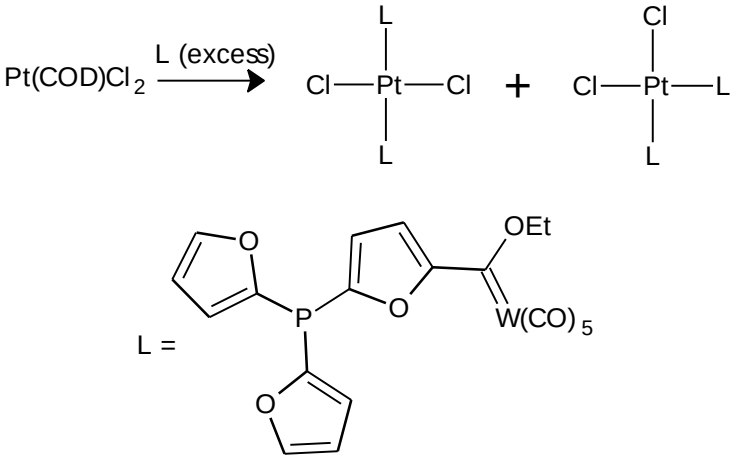

Figure 5.1 The formation of the *cis* and *trans*-coordinated phosphine-Pt(II) complexes

5.2.2 Characterisation

The characterisation of the complexes involved analysis of the ^{1}H, ^{13}C and ^{31}P NMR spectra as well as IR spectra.

Table 5.1 ^{1}H, ^{13}C and ^{31}P NMR spectra data ($CDCl_3$) of compounds **17a** and **17b**

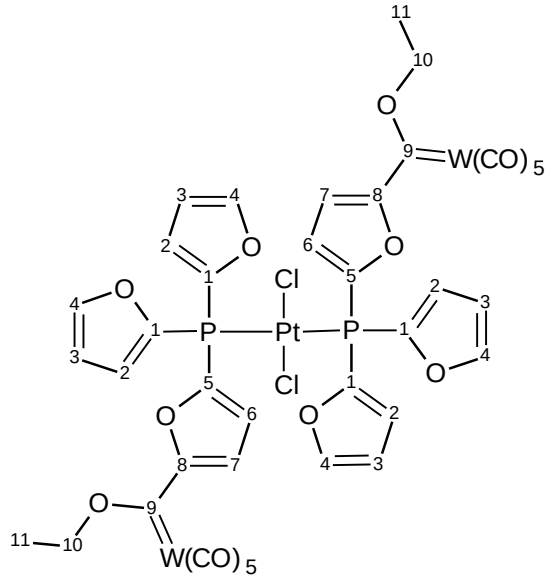

	17a(*trans*)			**17b(*cis*)**		
^{1}H NMR						
Proton position	δ_h/ppm	Multiplicity *J*/Hz	Integration	δ_h/ppm	Multiplicity *J*/Hz	Integration
2	6.40	ddd, 5.2, 2.5, 1.2	4H	6.41	m	4H

© University of Pretoria

3	7.06	m	4H	6.97	ddd	4H
4	7.71	dd, 1.7, 0.6	4H	7.08	m	4H
6	6.96	m	2H	7.53	m	2H
7	6.55	ddd, 4.1, 2.9, 1.3	2H	7.08	m	2H
10	4.88	q, 7.1	4H	4.88	q, 7.1	4H
11	1.58	t, 7.1	6H	1.58	t, 7.1	6H

^{13}C NMR				
	δ_c/ppm	Multiplicity *J*/Hz	δ_c/ppm	*J*/Hz
1	126.8	d, 19.7	126.0	-
2	111.8	d, 9.9	111.6	-
3	111.5	d, 4.2	112.5	-
4	150.2	d, 6.5	149.3	-
5	128.1	d, 28.1	126.4	-
6	137.0	d, 20.6	138.3	-
7	135.4	d, 17.4	137.7	-
8	169.5	d, 5.2	169.3	-
9	286.4	-	285.4	-
10	78.5	-	78.6	-
11	14.9	-	14.9	-
12	203.3, 196.5	-	203.7, 196.7	-

^{31}P NMR				
	δ_p/ppm	^{195}Pt{^{31}P} (*J*)	δ_p/ppm	^{195}Pt{^{31}P} (*J*)
	-33.2	1833	-35.3	1847

It was possible to determine if the phosphine ligands were *cis* or *trans*-coordinated relative to each other from the ^{31}P NMR spectrum. An extensive study was conducted by Grim, Keiter and McFarlane[6] on a range of phosphines coordinated in the *cis* and *trans*-fashion to Pt(II), which showed that the *cis*-coordinated phosphines

© University of Pretoria

had a larger $^{195}Pt\{^{31}P\}$ coupling constant and also appeared more upfield in the ^{31}P NMR spectrum compared to the *trans*-coordinated phosphines.

Two brown-orange products were isolated during separation by column chromatography. On analysis of the NMR spectra of the synthesized compounds the ^{13}C and ^{1}H chemical shift values were found to be relatively the same for the two compounds with slight differences in the furyl group chemical shifts and the ^{13}C NMR carbene and carbonyl shift values. The small differences of the carbene and carbonyl signals could be contributed to the increased amount of electron density present on the phosphorous atom in the case of the *cis*-isomer. The reason for this was investigated by Grim and his research team and is discussed in more detail below. The increased electron density on the phosphorous allowed for increased carbene stabilisation through the conjugated system from the phosphine to the carbene substituent present on the furyl group. It was expected that compound **17b** would have a slightly upfield carbene carbon ^{13}C NMR chemical shift, since it was expected to be slightly more stable. This was observed with values of 286.4 and 285.4 ppm for **17a** and **17b** respectively.

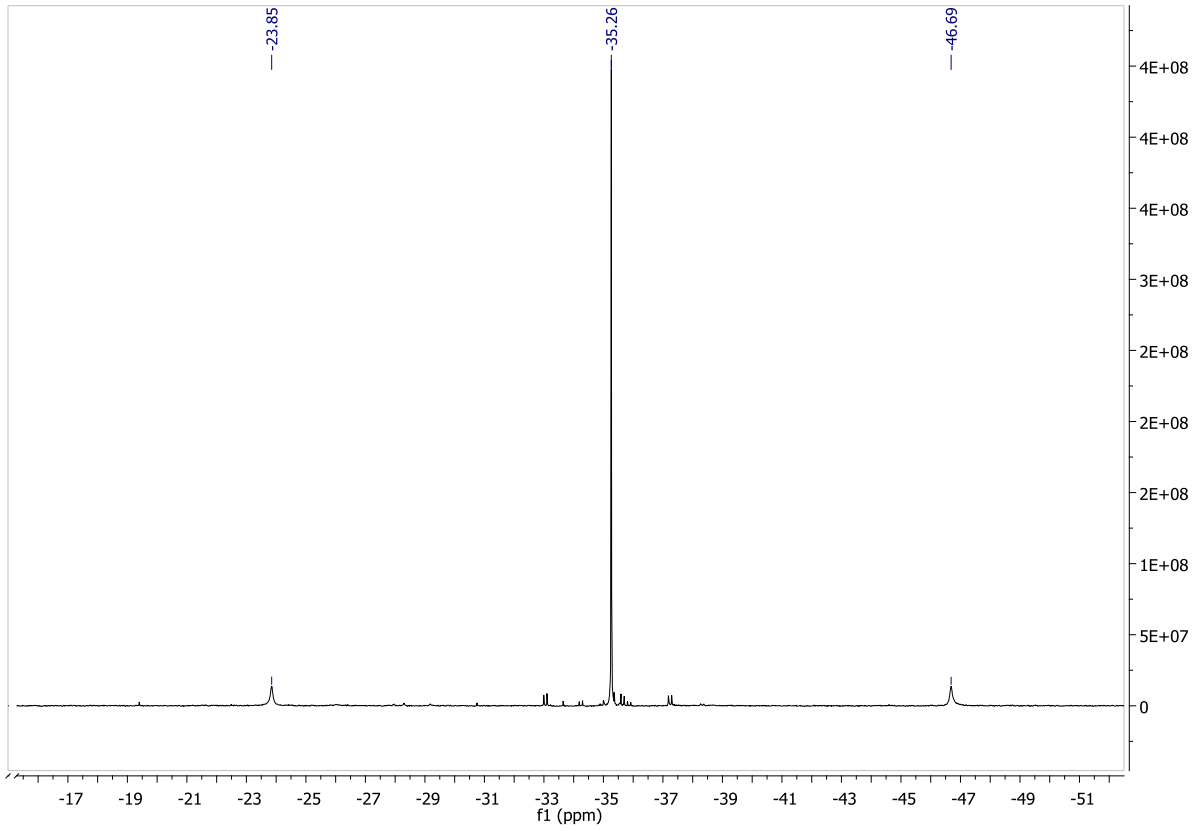

Figure 5.2 ^{31}P NMR spectrum ($CDCl_3$) of compound **17b**

© University of Pretoria

Grim[6] noted that the greater coupling constant of the *cis*-isomer was due to increased π-bonding between the phosphorous and platinum. The *cis*- isomer the platinum can use both the d_{yz} and the d_{xz} orbitals for bonding, as opposed to the *trans*-isomer where only the d_{xz} orbital can be used when the x-axis is defined in the P-Pt-P direction. If this statement was correct, it would be expected that the *cis*-isomer would have greater electron density present on the phosphine than the *trans*-isomer due to increased back donation by electrons in the Platinum d-orbitals. Comparing the ^{13}C NMR carbene chemical shift values of the synthesised compounds, it was found that the *cis*-complex had a slightly more upfield value compared to the *trans*-complex with values of 285.4 and 286.4 ppm respectively. This indicated that there was a slight increase in the electron density on the carbene carbons in the case of the *cis*-complex.

It is important to note that no other products were isolated in the synthesis of the Pt-phosphine compounds. The ^{1}H NMR spectra of the isolated compounds further revealed that there was no activity that could be ascribed to catalysis during analysis of the reaction products.

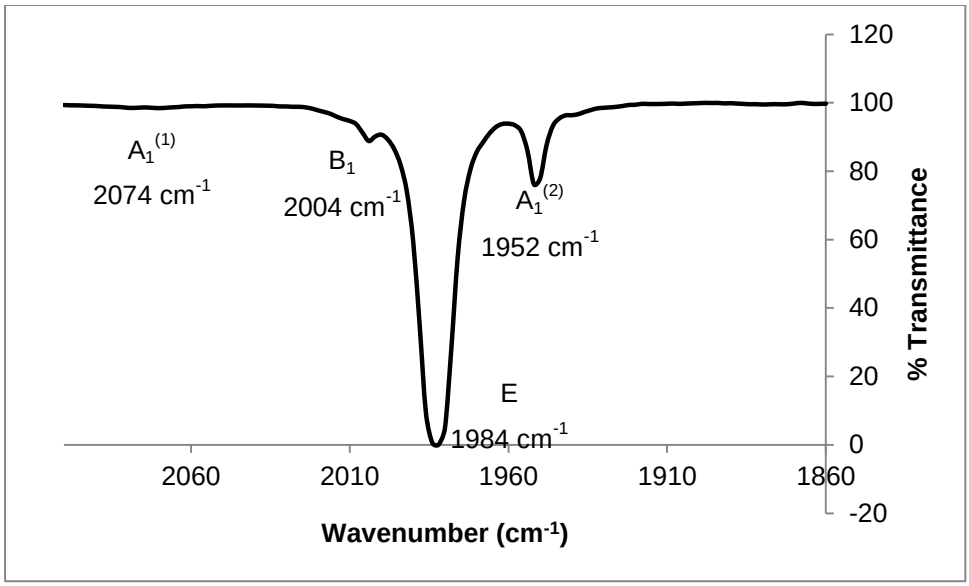

Figure 5.3 Carbonyl IR spectrum (DCM) of **17a**

© University of Pretoria

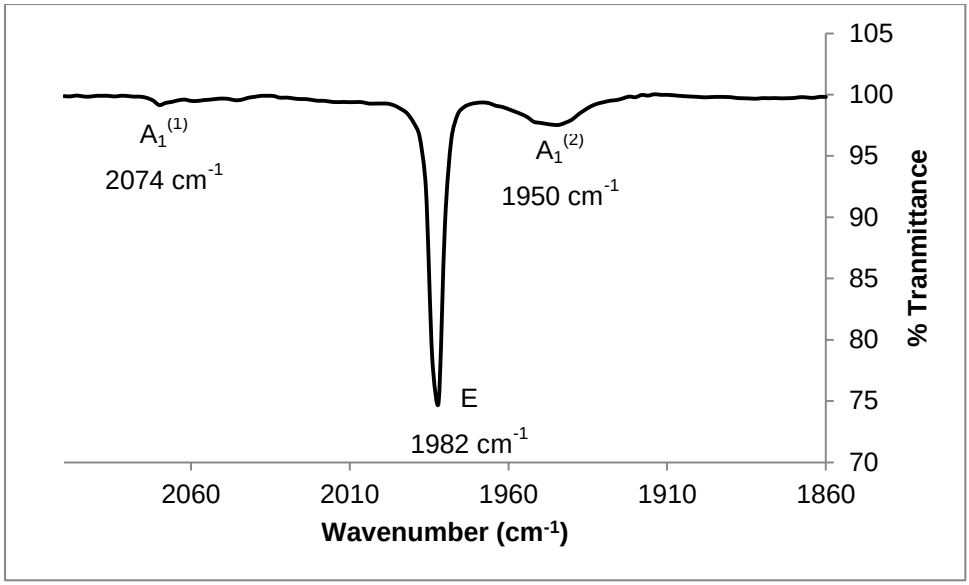

Figure 5.4 Carbonyl IR spectrum (DCM) of **17b**

In comparing the uncoordinated phosphine with the newly coordinated phosphine compounds, it was observed that in the case of compound **17a**, the B_1-band could be distinguished, but this was not the case for **17b**. The patterns and intensities of the bands differed greatly whereas the $A_1^{(2)}$ band was a shoulder of the E band for the phosphine ligand. $A_1^{(2)}$ was now found on the other side of the E-band in the coordination complex. The $A_1^{(2)}$-band of **17b** was also very insignificant and appeared as a flat, broad signal compared to the $A_1^{(2)}$-band of **17a**. The E- and $A_1^{(2)}$-band values for the uncoordinated carbene containing phosphine had values of 1944 and 1957 cm^{-1} respectively. The most significant difference was the large shift of the E-band from 1944 to 1982 and 1984 cm^{-1} for the *cis*- and *trans*-compounds respectively. Upon coordination of the phosphine there is a significant increase in the wavenumber of the carbonyl vibration frequencies in the equatorial plane of $W(CO)_5$, the *cis*-position relative to the ligand. The higher wavenumber at which the signal is observed, is indicative of increased energy required for carbonyl vibration. This observation indicated that, on coordination of the phosphorous atom to a transition metal, the amount of electron density from the metal back-donated to the carbonyl ligands are significantly decreased. Consequently, the CO bond is shortened and it requires more energy for their respective vibrations. It is believed that upon coordination of the phosphine, the electron lone pair on the phosphorous atom is used for bonding to the transition metal. It is no longer able to effectively stabilise the carbene-carbon substituent through the conjugated π-system.

© University of Pretoria

5.2.3 Conclusion

Successful coordination of the carbene containing phosphine was achieved in order to form *cis*- and *trans*-coordinated Pt(II) complexes. The ease of synthesis of these compounds is phenomenal with extremely high product yields. Further, it was determined that the major product of the reaction was compound **17b.** This was expected from literature[5].

Even though the Pt(II) complexes did not show any significant catalytic activity at the carbene carbon, these complexes would be a key feature in creating macro-molecular and nano-structures. Examples of these kinds of networks were investigated in more recent years[7,8]. The fact that these novel, synthesised Pt(II) centres do not undergo any inter- or intra-molecular template reactions, will enable the centres to act as corners or linkers between parts of a larger organometallic framework system.

5.3 Palladium complexes

5.3.1 $PdCl_2$ as receptor transition metal for phosphine coordination

Palladium complexes are of the best known catalysts for carbon-carbon coupling reactions. The Pd-complexes are able to accommodate a range of ligands easily and these ligands are very labile. Amatore[9] did a comparative study on Pd-complexes containing furyl and phenyl substituents on phosphine ligands. They found that, in THF specifically, the catalytic reaction is enhanced when using PFu_3 instead of PPh_3. The PFu_3 ligand is less electron-rich than PPh_3, making the PPh_3 ligand more labile in solution. When the reactivity of the two ligands were compared, it was found that the active $Pd(PFu_3)_2$ species was present in solution at a higher concentration than in the case when PPh_3 acted as the ligand in question.

It is known that the existence of isomers in an equilibrium can be influenced by the solvent or the amount of phosphine that is present during the reaction. Redfield and

© University of Pretoria

Nelson[10], however, found that isomerisation of the Pd(II)-phosphine complexes occurred at a greater rate than the isomerisation of the Pt(II)-phosphine complexes. The increased rate of isomerisation and the fact that the Pd(II) complexes required no catalyst (excess phosphine) for isomerisation to occur lead to the conclusion that the ligands in Pd complexes had increased lability. The increased lability of the phosphines on the Pd(II) complexes created an interesting problem: since the Fischer furyl-carbene substituent on the phosphine was quite electrophilic, combined with its double bond character, it was susceptible to catalytic reactions by the Pd(II) atom itself. The intermolecular reactions between the carbene substituent and another Pd(II)-phosphine complex was also possible. Since these reactions took place whenever the synthesized compound was in solution, it was never possible to obtain a pure sample of one of the products.

5.3.2 Characterisation

The coordination of the phosphines on palladium, relative to each other, was earlier believed to be most stable in the *trans*-configuration with very few compounds that were isolated in the *cis*-fashion[10]. The isomerisation between the *cis* and *trans*-configuration also made assignment of particular configurations difficult due to the increased lability of the ligands in palladium compounds. Grim and Keiter[11] did an extensive study on the ^{31}P NMR spectra of *cis*- and *trans*-tertiary phosphine complexes and found that the *cis*-conformer always had a ^{31}P NMR chemical shift downfield from the *trans*-conformer. This observation was found to be opposite from that of Pt-phosphine complexes in which the *cis*-isomer had a ^{31}P resonating value upfield from the *trans*-isomer.

On analysis of the reaction mixture, it was found that there were five compounds consistently present in the product solution. The products from this reaction consisted out of the desired $PdCl_2(phosphine)_2$ complex, an ester compound, a mixture of E- and Z- olefins and excess phosphine-carbene (**1b**). The formation of the ester and olefins is described by Scheme 5.1.

© University of Pretoria

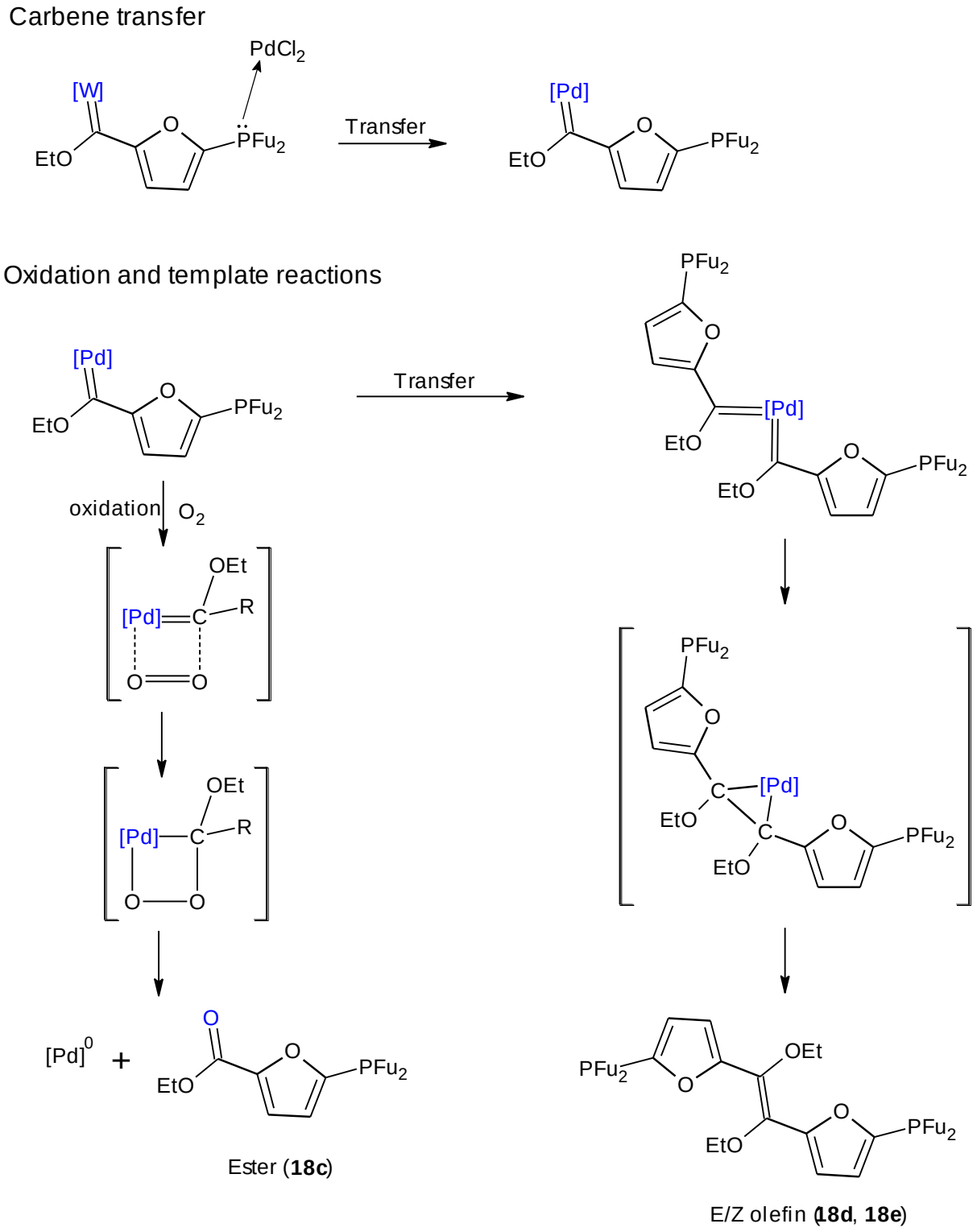

Scheme 5.1 Formation of ester and olefins from carbene transfer, oxidation and template reactions

Once coordinated to the Pd the reactivity of the carbene moiety was greatly increased. The carbene complex can either be oxidised to a metal-free ester or participate in a carbene-carbene coupling reaction on a Pd metal centre after

© University of Pretoria

carbene transfer from the W to the Pd occurred. Scheme 5.2 represents the formation of the olefin complexes as described by Sierra and his coworkers[12] to form the very interesting carbene-carbene coupled bisphosphine compounds **18d** and **18e**.

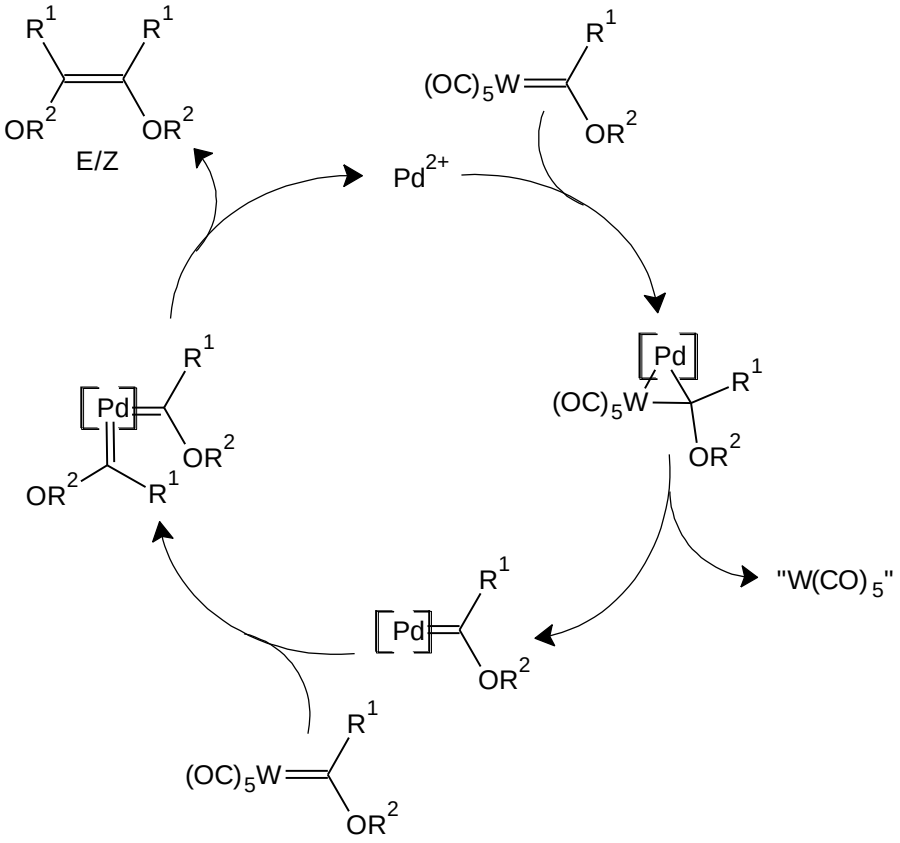

Scheme 5.2 The catalytic cycle of carbene-carbene coupling reaction via a Pd(II)-catalyst[12]

Many factors may influence the E/Z ratio during a reaction, of which the kind of Pd-catalyst, the amount of catalyst as well as the solvent in which the reaction is taking place my play a role[15]. In this research project, the $PdCl_2$ was added to excess ligand to ensure coordination of most of the Pd. However, following this approach, a significant amount of Pd(II) was available to catalyse the carbene-carbene coupling reaction. It is expected that the bulkiness of the furyl-phosphine will cause the isomeric ratio to lie greatly in favour of the E isomer.

© University of Pretoria

It was not possible to obtain a completely pure sample for analysis since the catalytic reaction always occurred once the complexes were in solution.

Table 5.2 contains the NMR data of the *trans* (**18a**) and *cis* (**18b**)-$PdCl_2(phosphine)_2$ complexes. The two isomers could not be distinguished in the ^{1}H and ^{13}C NMR spectra, but was visible in the ^{31}P spectrum.

Table 5.2 ^{1}H, ^{13}C and ^{31}P NMR spectra data ($CDCl_3$) of compound **18a** and **18b**

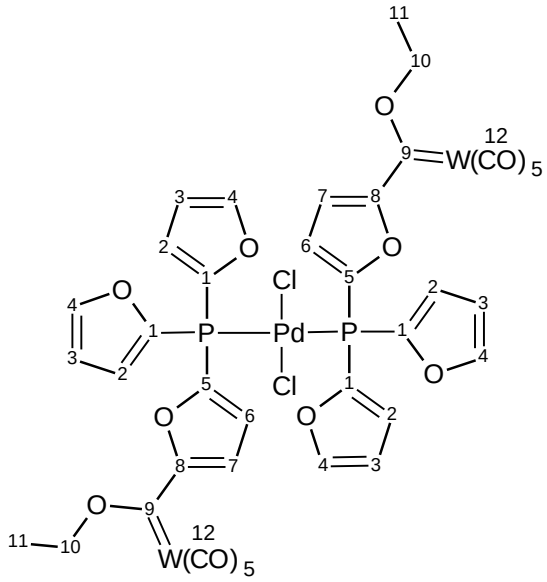

^{1}H NMR

Proton position	δ_h/ppm	Multiplicity *J*/Hz	Integration
2	7.76-6.38	m	16H
3			
4			
6			
7			
10	4.89	q, 6.9	4H
11	1.58	t, 6.9	6H

^{13}C NMR

	δ_c/ppm
1	128.4
2	111.6

© University of Pretoria

3	111.3
4	148.8
5	127.9
6	125.8
7	138.4
8	169.6
9	286.3
10	78.4
11	15.4
12	201.9. 196.7

^{31}P NMR (δ_p/ppm)
-21.2 (cis) , -27.8 (trans)

Assuming that the properties of the novel phosphine was close enough to the phosphines used in the study of Grim and Keiter[11], the *trans*-isomer was the major product, as determined from the peak intensity of ^{31}P NMR signals of the respective compounds. The ^{31}P NMR signal at -27.8 ppm represented the major product as well as the *trans*-isomer (**18a**). The *cis*-isomer (**18b**) was portrayed by the signal at -21.2 ppm in the ^{31}P NMR spectrum.

On further analysis of this reaction mixture, the only factor that indicated the presence of the ester and the olefins were the –$\underline{CH_2}CH_3$ signals of the respective compounds, since the furyl substituents present on the phosphine did not have any identifiable differences unique to each of the compounds.

Sierra[12] did an extensive study on carbene-carbene coupling reactions in the presence of various palladium catalysts. They observed an intermediate containing two carbene ligands and dimerisation occurring at the carbene sites. These olefins formed in the case of various Pd-catalysts and they were also observed when the products of this study were analysed. The formation of olefins and esters were noted in the ^{1}H NMR chemical shift values of the methylene protons of the ethoxy substituent having chemical shift values of 4.32 ppm for the esters and 3.75 and 3.69

© University of Pretoria

ppm for the E- and Z- olefins. Again, the furyl groups of these compounds had such similar ^{1}H and ^{13}C NMR chemical shift values that there were not any other significant identifiable peaks specific to each compound.

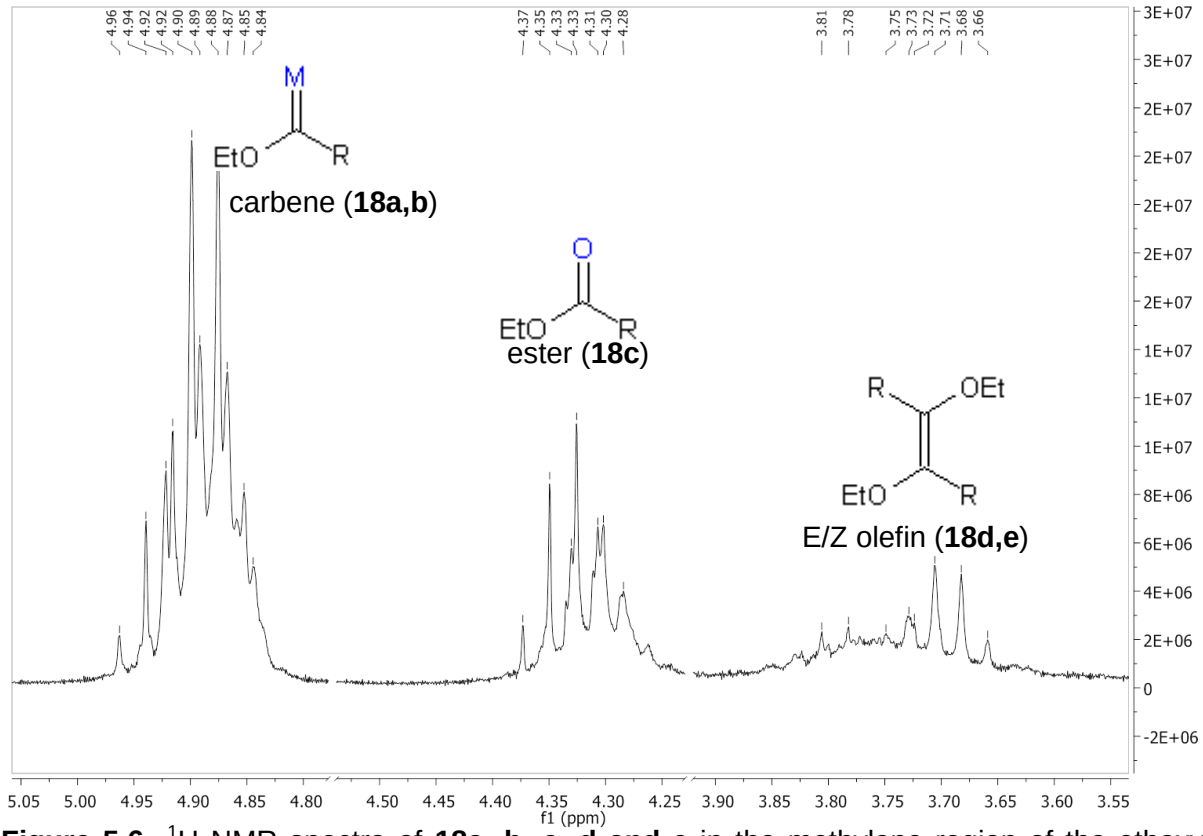

Figure 5.6 ^{1}H NMR spectra of **18a, b, c**, **d and e** in the methylene region of the ethoxy substituent

As seen from Figure 5.6, there was always more than a single product present on analysis of the sample. The reason why and how an ester compound is formed during the reactions is still unclear. It clearly represents an oxidation of the carbene ligand which is catalysed by a Pd metal centre. This reaction is in competition with a carbene-carbene coupling reaction. In research by both Sierra[13] and Espinet[14], the formation of an ester compound in the presence of particular Pd catalysts is mentioned.

In Figure 5.7 the two olefins that form are shown. The Z-olefin (**18e**) has an -O$\underline{CH_2}$R signal that appears slightly downfield from that of the E-olefin. It also appears as a

© University of Pretoria

multiplet where the E-olefin (**18d**) signals can be clearly distinguished as a quartet with a J-coupling value of 7.1 Hz.

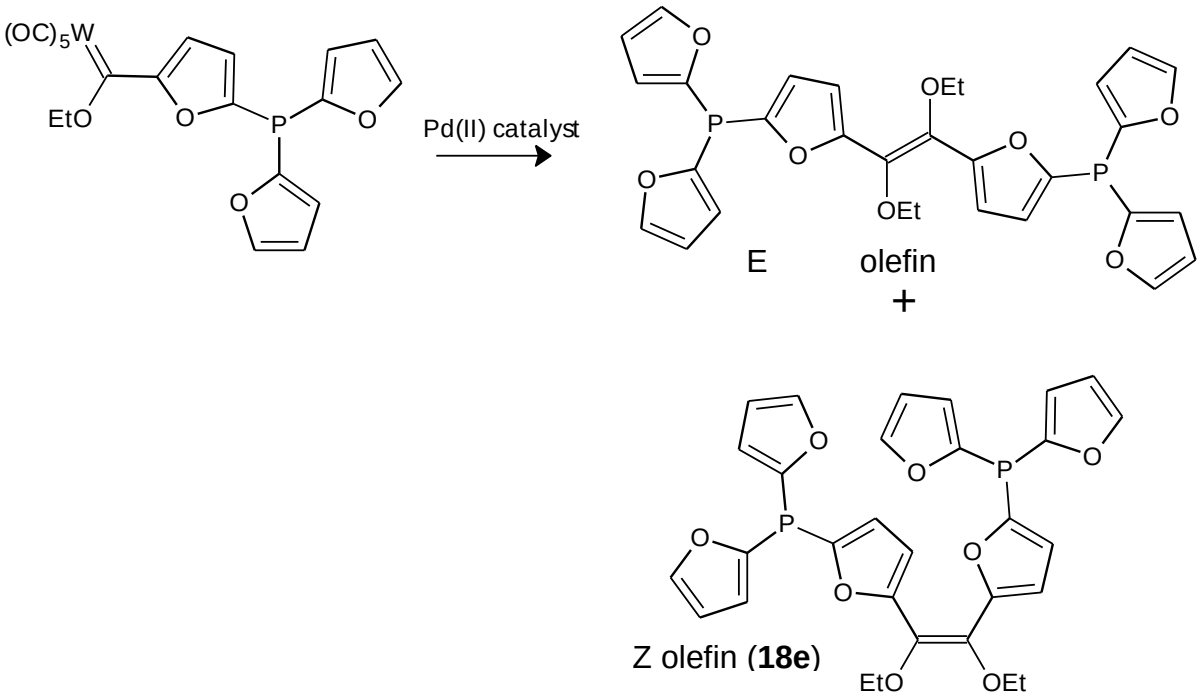

Figure 5.7 Isomers of the catalytic products **18d** and **18e**

Analysis of the compound by IR spectroscopy provided the necessary proof to establish the presence of a pentacarbonyl fragment within the compound. The full IR spectrum in the carbonyl region of a typical pentacarbonyl system is discussed in section 2.2.3. Usually the $M(CO)_5$ unit affords four peaks, two (the E and $A_1^{(2)}$ bands) which are very prominent and may overlap.

© University of Pretoria

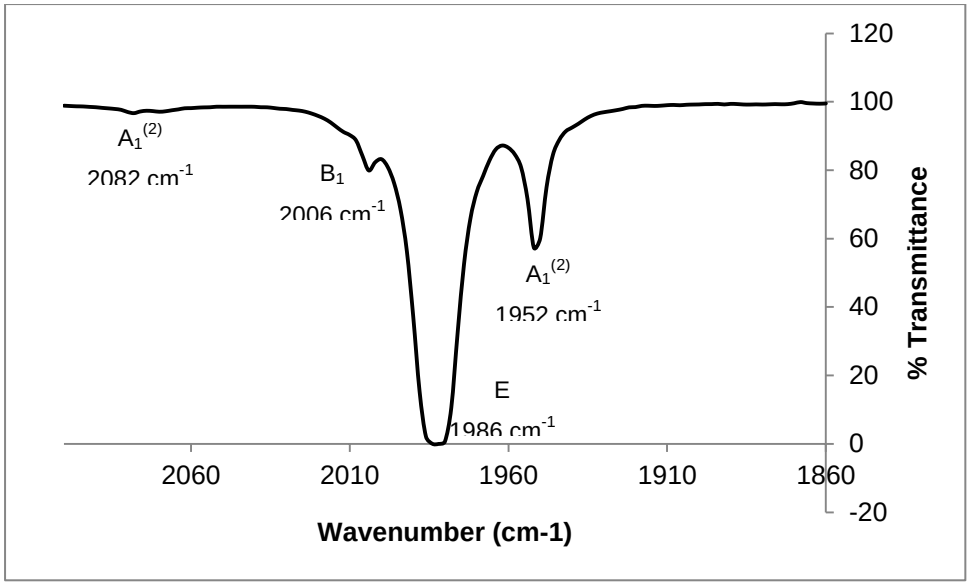

Figure 5.8 Pentacarbonyl IR spectrum of compound **18a** and **18b**

In the uncoordinated phosphine, the carbene carbonyl IR spectrum exhibited three observed peaks, the $A_1^{(1)}$, $A_1^{(2)}$ and E-bands with wavenumbers of 2069, 1957 and 1944 cm^{-1} respectively. The Pd(II)-phosphine complex alternately showed $A_1^{(1)}$ vibrations as a very flat, broad band and the B_1-band was visible at 2006 cm^{-1}. Again, the significant shift in the E-band is observed as was the case of the Pt-products **17a** and **17b**.

5.3.3 Conclusion

The tungsten Fischer carbene containing phosphine was successfully coordinated to the $PdCl_2$ complex in a *cis*- and *trans*-fashion as was expected for the square planar complex. It was not possible, however, to separate the *cis*- and *trans*-isomers. When the two complexes were present in solution, intermolecular template and catalytic reactions occurred in which an ester, as well as E- and Z-olefins formed. It can be concluded that the $PdCl_2$ complexes have the potential to act as a catalyst in the presence of the carbene phosphine and is also the active unit in these systems.

© University of Pretoria

5.4 Nickel complexes

5.4.1 $Ni(COD)_2$ as receptor transition metal for phosphine coordination

There are many examples where Ni(0) is known as catalyst with a lot of emphasis on oligomerisation reactions of olefins[16]. In the case of Ni(0) and other transition metals which act as catalysts, the ligands present on the metal may influence the properties of the specific catalyst. In this study, $Ni(COD)_2$ was the transition-metal complex to which the novel carbene containing phosphine was coordinated. A single COD molecule normally coordinates in a η^4-fashion to the nickel and is replaced stepwise by two phosphine ligands. Scheme 5.3 below clearly shows the mechanism in which COD in the $Ni(COD)_2$ complex is systematically replaced by a phosphine.

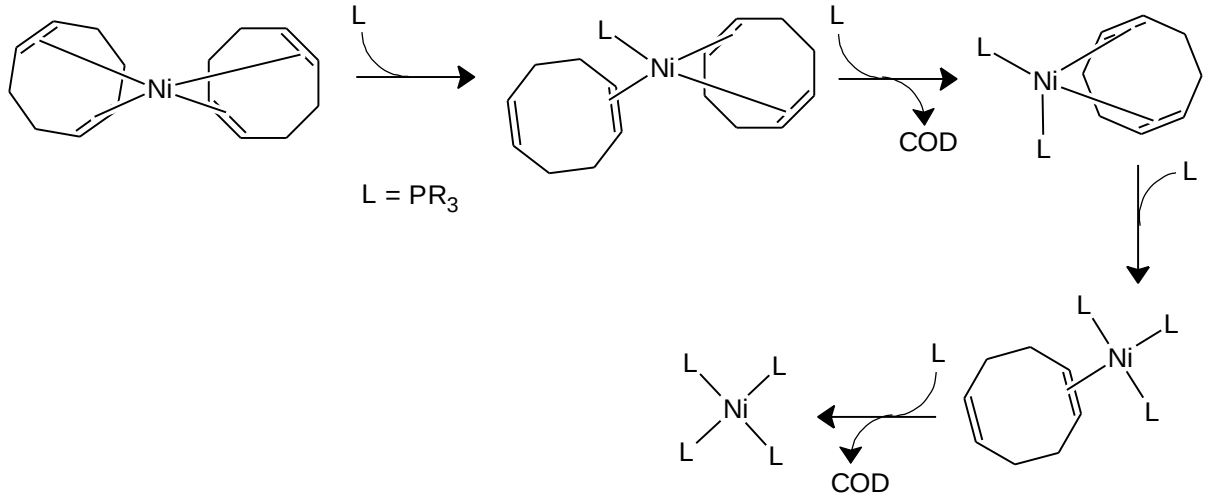

Scheme 5.3 Systematic phosphorylation of the $Ni(COD)_2$ complex

In research by Tolman, Reutter and Seidal[17], the extent of phosphorylation with different phosphine ligands of $Ni(COD)_2$ was investigated. They found that the phosphines that contained large steric substituents like phenyl groups did not fully replace COD ligands in the Ni-complex. Consequently, compounds like $Ni(COD)_2$-PPh_3 or $Ni(COD)$-$(PPh_3)_2$ formed. By investigating the ratios in which the furyl groups present on the phosphine occurred against COD ligands in each product, it was possible to determine the extent to which the replacement of the COD molecules had taken place.

© University of Pretoria

5.4.2 Characterisation

In this reaction $Ni(COD)_2$ was allowed to stir in the presence of excess **1b** for 18 hours after which a single characterised product was isolated. The product contained two 1b ligands coordinated to the Ni-centre with a signle COD molecule coordinated in a η^4-fashion (**19**). The Ni complex that was synthesized was the only group 10 complex that was analysed in deuterated benzene since the possibility existed that the Ni(0) metal centre could be oxidised in the chlorinated environment of $CDCl_3$

Table 5.3 ^{1}H, ^{13}C and ^{31}P NMR spectra (C_6D_6) of **19**

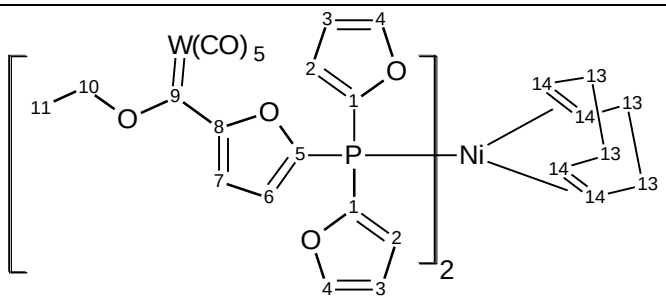

^{1}H NMR

Proton position	δ_h/ppm	Multiplicity J/Hz	Integration
2	6.88	m	4H
3	6.75	ddd, 3.2, 2.4, 0.7	4H
4	7.19	d, 1.8	4H
6	6.63	dd, 3.7, 1.2	2H
7	6.40	d, 3.7	2H
10	4.47	q, 7.1	4H
11	1.56	m	6H
13	2.13	s	8H
14	4.26	s	4H

^{13}C NMR

	δ_c/ppm
1	123.3
2	111.3

© University of Pretoria

3	121.5
4	148.4
5	123.6
6	111.2
7	121.4
8	-
9	284.0
10	78.2
11	14.3
12	203.9, 197.6
13	31.9
14	90.1

^{31}P NMR (δ_p/ppm)
-23.7

The integration ratios of the furyl protons against the COD protons were the determining factor that established to what extent the Ni-compounds were phosphorylated. Compound **19** was found to contain a single COD ligand and two coordinated phosphines. The carbene carbon appeared at 284 ppm in the ^{13}C NMR spectrum while the furyl rings were found between 6.40 and 7.20 ppm in the ^{1}H NMR spectrum. The ^{31}P NMR spectra of the compound showed a value of -23.7 ppm for **19**.

Infrared spectroscopy

Table 5.4 IR spectra of the pentacarbonyl region for **19**

Compound	**IR carbonyl stretching frequencies (cm^{-1})**			
	$A_1^{(1)}$	$A_1^{(2)}$	B_1	E
19	2080	1957	1996	1957

In the analysis of the IR spectra, it is important to realise the spectrum being analysed is that of a carbonyl system that is not directly bonded to the Ni(0) atom but is rather present as a substituent on the phosphine coordinated to the Ni.

© University of Pretoria

Comparing the IR pentacarbonyl values of **19** with those of **1b**, it was found that on coordination of **1b**, the $A_1^{(1)}$ and the E band moved to higher wavenumbers (2069 to 2080 cm^{-1} and 1944 to 1957 2069cm^{-1}, respectively). Again a significant electronic effect within the carbene moiety is observed upon coordination of the phosphine ligand.

5.4.3 Conclusion

1b was successfully coordinated to the Ni(0) complex, although complete replacement of all COD ligands did not take place. Using the integration of the ^1H NMR spectra, it was possible to determine the degree of phosphorylation that had taken place. An important fact to note is that no catalytic activity took place during the synthesis of the Ni-compounds which was the case of the Pd complex.

5.5 Comparing the Group 10 complexes

When comparing the different compounds, it is important to realise that the differences can only be analysed in terms of the environmental properties that the ligands experience once coordinated to the metal. In this case, the only ligands that can be analysed are **1b** and COD which were coordinated to the different group 10 metals. To clearly show the changes that occur upon coordination of the carbene-containing phosphine, the free phosphine is shown in Figure 5.10 with all the NMR shifts of the susceptible atoms.

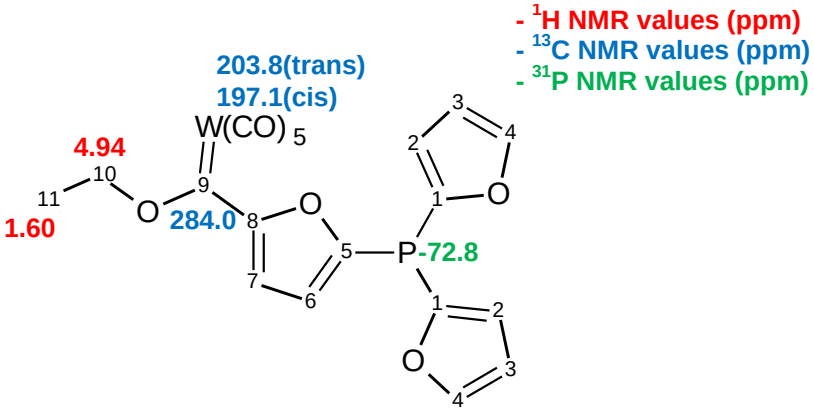

Figure 5.10 ^1H, ^{13}C and ^{31}P NMR chemical shifts (ppm) of selected atoms of W-carbene containing phosphines

© University of Pretoria

Unfortunately the NMR spectra of the Ni complex had to be recorded in C_6D_6 and will not form part of this comparison. The ^{1}H NMR spectra of the Pt and Pd complexes did not disclose any differences between the complexes, let alone to the uncoordinated **1b**. The –OEt groups of all the complexes had ^{1}H NMR chemical shifts of 4.88 and 1.58 ppm. The ^{13}C NMR spectra revealed that carbene complexes present in the coordinated complexes did experience slightly different environments on coordination of the phosphine to the different metal centres. The *cis*(**17b**)- and *trans*(**17a**)- complexes of platinum had carbene carbon chemical shift values of 285.4 and 286.4 ppm, while the Pd complexes had carbene chemical shift values of 286.3 ppm.

The most important factor determining whether the novel phosphine was coordinated to the particular metal was the ^{31}P NMR spectra. The free phosphine had a ^{31}P NMR chemical shift value of -72.8 ppm. The *cis*- and *trans*-Pt(II) complexes displayed chemical shift values of -35.2 and -33.2 ppm respectively while the two unseparated Pd(II) compounds had shifts of -21.2 and -27.8 ppm. The Ni(0) compound, **19**, had ^{31}P NMR signal at -23.7 ppm. Upon coordination of the phosphine, the phosphorous atom is significantly deshielded, moving from a very high upfield value to between -23 and -33 ppm. The significant deshielding occurs when the lone pair present on the phosphorous atom is used to form a covalent σ-bond with the particular transition metal; however, some back bonding from the metal to the phosphorous atom occurs. As a result, the negative chemical shift values are still observed and not more prominent positive ^{31}P NMR resonances.

The final aspect to consider is the IR data of the pentacarbonyl fragments. The information that was provided by the IR gave a clear indication what the effect of the bonding of the phosphine had on the electrophilicity of the carbene carbon. Since it was observed in most cases a drastic shift in the E-band to higher wavenumbers occurred upon coordination, it can be concluded that a large electronic change had occurred on the carbene-metal complex. The major change in the pentacarbonyl vibration frequencies was observed for the carbonyl groups *cis* to the carbene ligand, indicating that electron density from the $W(CO)_5$ was donated to the stabilisation of the carbene carbon. This occurred because electron density from the phosphorous

© University of Pretoria

atom was used for covalent bonding. As mentioned in chapter two, it was clear that some electron density of the uncoordinated phosphorous atom contributed to the stabilisation of the carbene carbon through the conjugated system of the furyl ring to the carbene substituent.

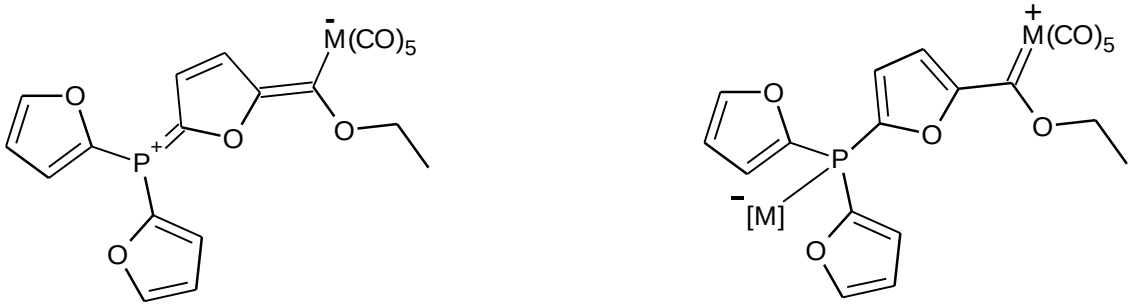

a) Free ligand:
Lower wavenumbers for CO vibrations are observed

b) Coordinated ligand:
Higher wavenumbers for CO vibrations are observed

Figure 5.11 Extreme resonance effects for a coordinating and an uncoordinated carbene-containing phosphine

However, the electron density that is no longer supplied by the phosphorous atom for the stabilisation of the carbene carbon is now used in bonding to the second metal. This implies that the electrophilic carbene carbon needs to be stabilized by back bonding from the metal-carbonyl group and the ethoxy substituent. Not only does the coordination of the phosphorous atom remove electron density from the carbene carbon, but now the carbene complex is also significantly more reactive than when the phosphine is uncoordinated.

© University of Pretoria

5.6 References

1. G. K. Anderson and R. J. Cross. Isomerisation mechanisms of square-planar complexes. *Chem. Soc. Rev.* (1980). **9,** 185–215

2. H. G. M. Edwards. The synthesis and vibrational spectra of tetrakistrimethylphosphinenickel(O) and -platinum(O), $Ni(PMe_3)_4$ and $Pt(PMe_3)_4$. *Spectrochim. Acta* (1986). **42,** 1401–1404

3. L. S. Meriwether and J. R. Leto. Bonding in Ni(0) Complexes. II. The ^{31}P Nuclear Magnetic Resonance Spectra of Some Nickel-Carbonyl-Phosphine Complexes. *J. Am. Chem. Soc.* (1961). **83,** 3192–3196

4. J. Chatt and R. G. Wilkins. The nature of the co-ordinate link. Part VI. A comparison of equilibria between cis- and trans-$(MEt_3)_2PtCl_2$, where M = P, As, and Sb. *J. Chem. Soc.* (1952). 4300–6

5. J. Chatt and R. G. Wilkins. Equilibria between cis- and trans-$[(MR_3)_2PtX_2]$ (where M = P, As, and Sb; X = halogen). *J. Chem. Soc.* (1956). 525–9

6. S. O. Grim, R. L. Keiter and W. McFarlane. A phosphorus-31 nuclear magnetic resonance study of tertiary phosphine complexes of platinum (II). *Inorg. Chem.* (1967). **6,** 5–9

7. L. Pirondini, F. Bertolini, B. Cantadori, F. Ugozzoli, C. Massera and E. Dalcanale. Design and self-assembly of wide and robust coordination cages. *P. Natl. Acad. Sci. USA* (2002). **99,** 4911– 4915

8. S. ALQaisi, K. Galat, C. Minghui and D. Ray. Synthesis of neutral tetranuclear and octanuclear macrocyclic platinum-butadiyne heterocyclynes. *J. Am. Chem. Soc.* (1998). **120,** 12149–12150

9. C. Amatore, A. Jutand, G. Meyer, H. Atmani, F. Khalil and F. O. Chahdi. Comparative Reactivity of Palladium(0) Complexes Generated in Situ in Mixtures of Triphenylphosphine or Tri-2-furylphosphine and $Pd(dba)_2$. *Organometallics.* (1998). **17,** 2958–2964

10. D. A. Redfield and J. H. Nelson. Equilibrium energetics of cis-trans isomerization for two square-planar palladium(II)-phosphine complexes. *Inorg. Chem.* (1973). **12,** 15–19

11. S. O. Grim and R. L. Keiter. A phosphorus-31 magnetic resonance study of tertiary phosphine palladium(II) compounds. *Inorg. Chim. Acta* (1970). **4,** 56–60

12. M. A. Sierra, J. C. del Amo, M. J. Mancheño and M. Gómez-Gallego. Pd-Catalyzed Inter- and Intramolecular Carbene Transfer from Group 6 Metal−Carbene Complexes. *J. Am. Chem. Soc.* (2001). **123,** 851–861

© University of Pretoria

13. M. P. López-Alberca, M. J. Mancheño, I. Fernández, M. Gómez-Gallego, M. A. Sierra and R. Torres. Divergent Pathways in the Reaction of Fischer Carbenes and Palladium. *Org. Lett.* (2007). **9,** 1757–1759

14. I. Meana, A. Toledo, A. C. Albeniz and P. Espinet. Detection and Reactivity of a Palladium Alkoxycarbene. *Chem. Eur. J.* (2012). **18,** 7658 – 7661

15. G. M. Chu, I. Fernández and M. A. Sierra. Control over the E/Z Selectivity of the Catalytic Dimerization of Group 6 (Fischer) Metal Carbene Complexes. *J. Org. Chem.* (2013). **78,** 865–871

16. F. Speiser, P. Braunstein and L. Saussine. Catalytic Ethylene Dimerization and Oligomerization: Recent Developments with Nickel Complexes Containing P,N-Chelating Ligands. *Acc. Chem. Res.* (2005). **38,** 784–793

17. C. A. Tolman, D. W. Reutter and W. C. Seidel. A Calometric study of steric effects in the reactions of phosphorus ligands with $Ni(COD)_2$. *J. Organomet.. Chem.* (1976). **117,** C30–C33

© University of Pretoria

Chapter 6

Piggybacking of a tungsten pentacarbonyl carbene substituent into the coordination sphere of group 11 transition metal complexes

6.1 Background

In this part of the research, a phosphine containing a tungsten carbene complex was coordinated to different halogenated group 11 transition metals. Group 11 transition metals have an extremely wide functional window. Gold complexes, for example, have recently found application in drugs and catalysis[1,2]. Gold complexes play a catalytic role in the reduction of nitrogen oxides, epoxidation of propene as well as low temperature oxidation of CO[3], to name a few of many examples. The properties of silver and copper are just as diverse if not more. Recently it has been shown that the group 11 transition metals are also able to accept a carbene from group 6 metals[4].

Throughout this chapter, the coordination of the phosphine to the transition metal will be discussed. The different products from the reactions were analysed in order to determine whether any additional organic products were found or whether any new carbene complexes were formed after completion of the coordination reactions.

6.2 Gold complexes

6.2.1 Au(THT)Cl as acceptor complex for phosphine coordination

The coordination of the carbene containing phosphine to AuCl involved replacement of tetrahydrothiophene (THT) by the excess phosphine present in the solution. The high yield reaction did not only deliver the wanted red-brown linear product, but also underwent catalytic reactions which formed aldehydes, esters and, olefins. These

© University of Pretoria

additional products were an indication of the catalytic activity of the newly synthesised complex.

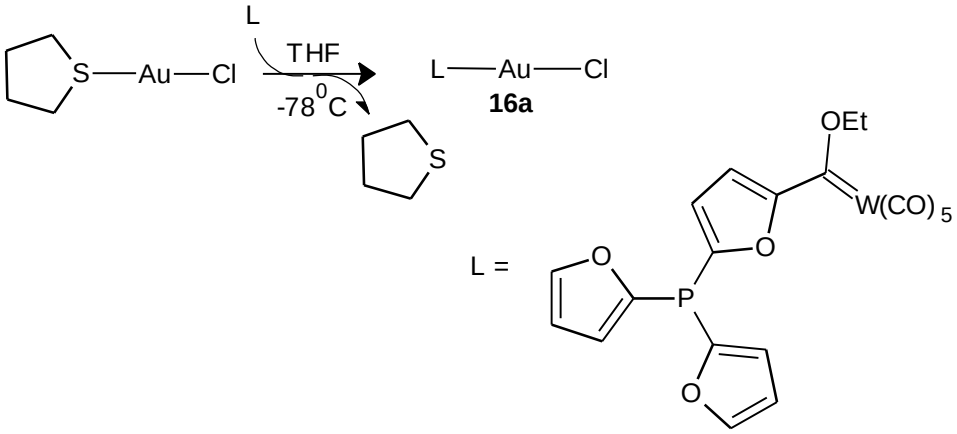

Scheme 6.1 Complexation of **1b** to AuCl (**20a**)

6.2.2 Characterisation

In a quantum theoretical study by Schwerdtfeger, Hermann and Schmidbaur[5], they reported that AuCl(PR_3) complexes are linear in geometry and will seldom have a coordination number larger than two, consequently indicating that only a single phosphine is expected to coordinate to the gold complex. From the NMR spectra, it was not possible to determine whether a single phosphine or multiple phosphines coordinated to the gold. However, coordination was observed as discussed below.

Table 6.1 ^{1}H, ^{13}C and ^{31}P NMR data ($CDCl_3$) of **20a**

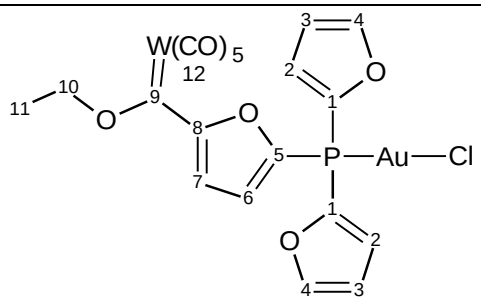

^{1}H NMR			
Position	δ_H/ppm	Multiplicity *J*/Hz	Integration
2	6.55	ddd, 3.2, 1.5, 1.0	2H
3	6.98 – 6.96	m	2H
4	7.75	dd, 2.5, 1.7	2H

© University of Pretoria

6	7.16	dd, 3.8, 1.2	1H
7	6.81	dd, 3.7, 1.1	1H
10	4.92	q, 7.1	2H
11	1.61	t, 7.1	3H

^{13}C NMR		
	δ_c/ppm	Multiplicity *J*/Hz
1	145.4	d, 72.2
2	122.7	d, 18.9
3	111.6	d, 6.9
4	148.8	d, 6.0
5	156.1	d, 60.5
6	121.7	d, 16.3
7	115.5	d, 5.5
8	169.2	d, 4.7
9	285.3	-
10	78.6	-
11	14.9	-
12	203.2 (trans), 196.9 (cis)	-

^{31}P NMR (δ_p/ppm)
-30.7

The ^{31}P NMR of the coordinated phosphine-gold(I) complex is shown in Figure 6.1. This NMR spectrum clearly indicated coordination of the phosphine because the signal shifted downfield from -72.8 ppm for the free phosphine to -30.7 ppm. Further, extensive P-Au coupling was observed with J-coupling values of 305.1 and 125.6 Hz from the large central peak. Since it is possible for Fischer carbene transfer reactions to occur with Au(I) complexes[4], it was considered to be possible with the phosphine ligand bearing the carbene substituent. The presence of the carbonyl peaks in the ^{13}C NMR spectrum indicated that no carbene transfer had occurred, but rather that successful coordination of the phosphine with the carbene-

© University of Pretoria

tungsten complex as substituent was found. Furthermore, the carbene carbon signal appeared at 285.3 ppm, which would be expected for a $W(CO)_5$-carbene complex. This value was slightly downfield from the free phosphine carbene carbon ^{13}C NMR chemical shift value of 284.0 ppm.

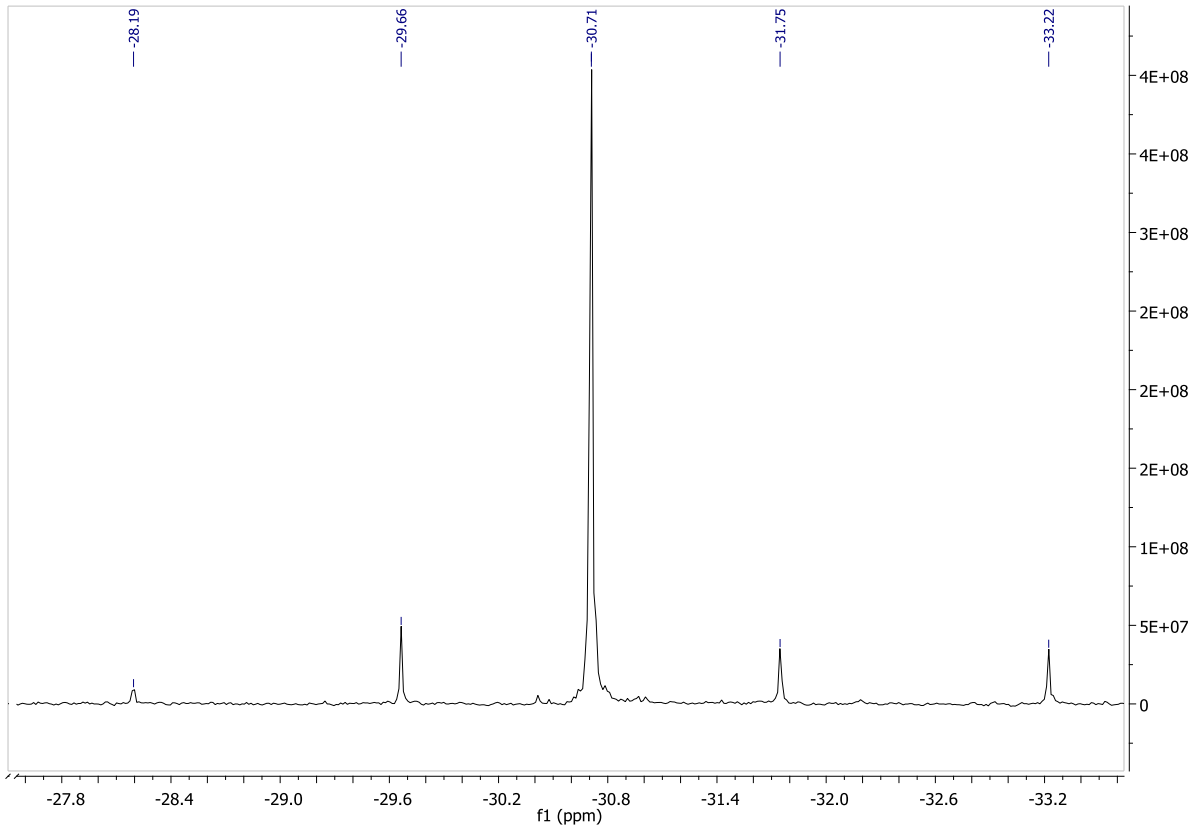

Figure 6.1 ^{31}P NMR spectrum ($CDCl_3$) of **20a**

The pentacarbonyl fragment had IR spectral peaks at wavenumbers of 2070, 1994, 1958 and 1954 cm^{-1} for the $A_1^{(1)}$, B_1, $A_1^{(2)}$ and E-bands respectively. When compared to the uncoordinated phosphine, the only significant difference was observed in the case of the E-band, which moved from 1944 to 1954 cm^{-1} once coordination took place. The shift towards higher wavenumbers is indicative of a higher positive charge on the metal which is reflected in less back bonding to the carbonyl ligands with a larger CO bond order. As was the case in Chapter 5, it is most probable that the electron density on the phosphorous atom, which partially stabilised the Fischer carbene complex, was no longer available once the phosphine coordinated to the transition metal. This shortfall of electron density is made up by π-donation from the tungsten and ethoxy substituents of the carbene ligand.

© University of Pretoria

A second product mixture was isolated after completion of the reaction. This mixture was isolated and contained no traces of the coordinated carbene containing phosphine, but rather showed clear traces of olefin, ester and small amounts of aldehyde which formed during the reaction.

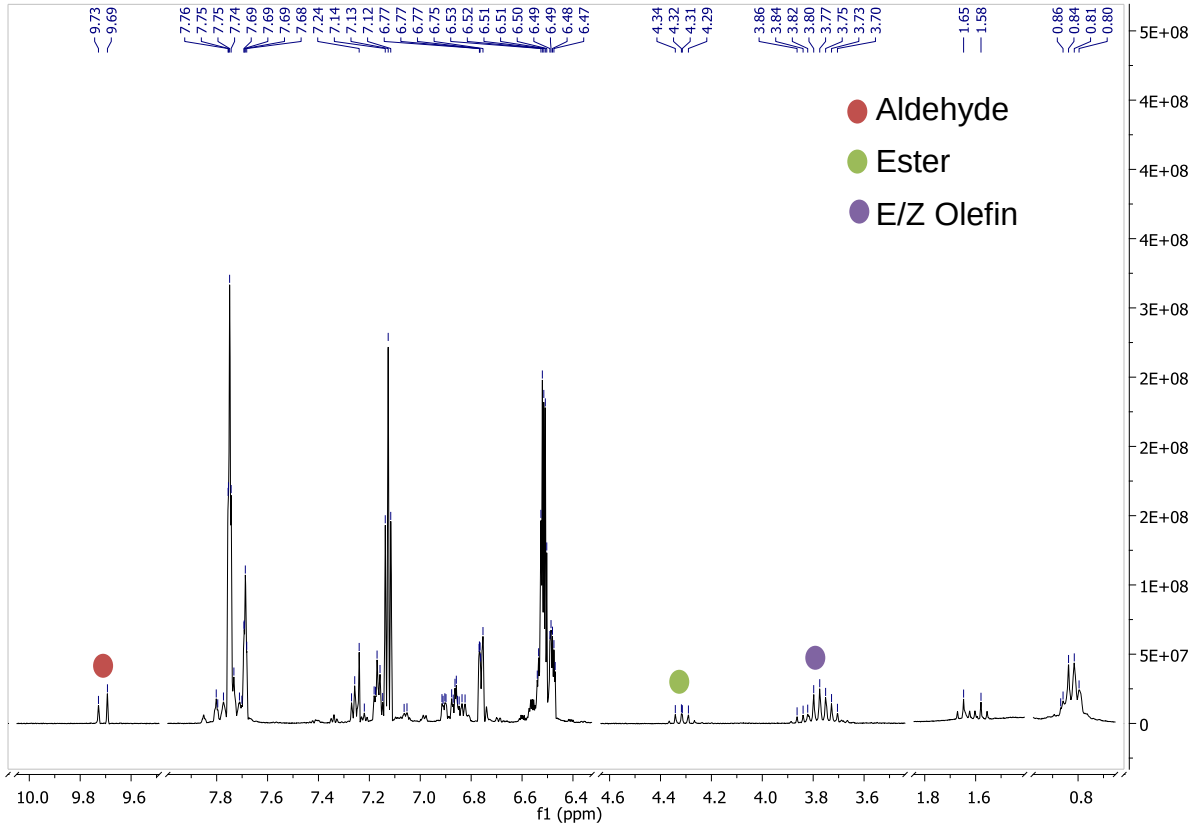

Figure 6.2 ^{1}H NMR spectrum ($CDCl_3$) of the ester (**20b**), aldehyde (**20c**) and E/Z olefin (**20d, e**) by products from the coordination reaction of **1b** to AuCl(THT)

Figure 6.2 revealed the formation of products produced by catalytic reactions involving the Au(I)Cl-Phosphine complex. The major product was the E/Z-olefin (**20d**, **20e**) which had pronounced ^{1}H NMR –$\underline{CH_2}$Me peaks between 3.86 and 3.70 ppm. These products formed in a ratio of 1:3 in favour of the E-olefin[6]. Small amounts of aldehyde (**20c**) also formed with the –CO(H) chemical shift values visible at 9.73 and 9.69 ppm. The cause of the two different aldehyde chemical shifts is the presence of the phosphine isomers that could not be separated from each other, as explained in Chapter 2. One final product that was observed was the ester product (**20b**) that displayed a –O$\underline{CH_2}$Me chemical shift value between 4.34 and 4.29 ppm in

© University of Pretoria

the ^{1}H NMR spectrum. Figure 6.3 illustrates the structures of **20b** and **20c**. **20d** and **20e** were shown in Section 5.3.2 as **22d** and **22e**.

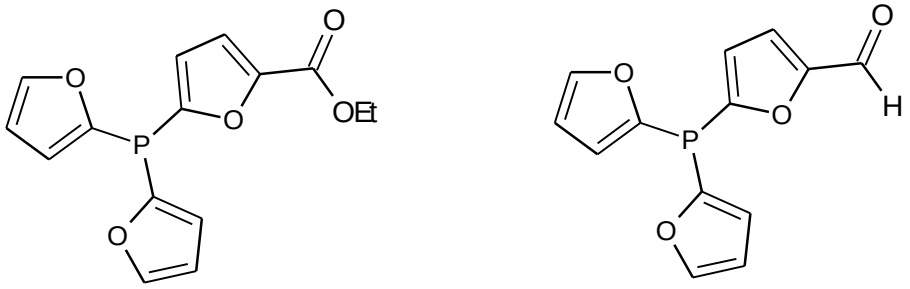

20b **20c**

Figure 6.3 Structures of **20b** and **20c**

These three additional products are a clear indication of the effect coordination of the carbene containing phosphine has on the metal-carbene group itself. There are two possibilities to consider in view of the three observed species, especially the formed esters and aldehyde products. It is known that the olefins form via the catalytic carbene-carbene coupling reaction by the Au(I) metal centre. The ester and aldehyde are known to form via a catalytic reaction in the presence of either O_2 or H_2O present in trace amounts in the solvent. The carbene centre reactivity is significantly increased due to the removal of the stabilisation effect on coordination of the phosphorous atom to the AuCl fragment. Proof that the AuCl remained coordinated during the conversion is evident from the ^{31}P NMR chemical shifts that indicate coordination to gold.

6.2.3 Conclusion

The analysed data revealed four different products that were formed during the coordination reaction. Compound **20a** revealed a coordinated carbene containing phosphine on an AuCl complex. Other catalytic products such as E- and Z- olefins were formed during the reaction, where **20d**,**e** coupled two carbene substituents. The products were aldehydes and ester compounds that formed due to the presence of H_2O and O_2 present in the solvent. These products may give an indication of increased reactivity of the carbene substituent when the phosphine is coordinated to gold.

© University of Pretoria

6.3 Silver complexes

6.3.1 AgBr as acceptor complex for phosphine coordination

This section describes the synthesis of a Ag(I) complexes by coordination of the novel phosphine described in Chapter 2 (**1b**) to the complex. There are many examples where silver phosphine complexes are examined for their interesting crystal structures that form as well as the amount of phosphines that can be coordinated to a single metal centre[7–9]. Silver-halogen complexes are able to accommodate up to three L-type ligands before forming AgL_4^+ species[8] (L = **1b**).

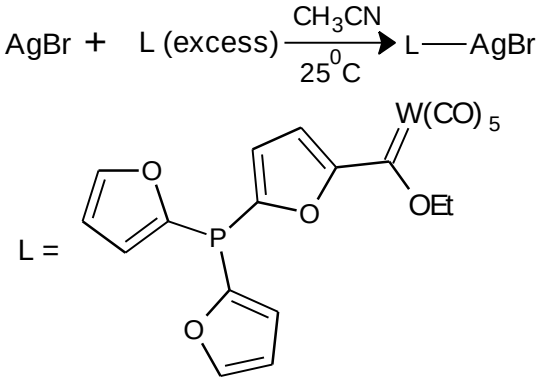

Scheme 6.2 The coordination of **1b** to AgBr

The coordination of **1b** to silver revealed interesting facts about carbene chemistry.

6.3.2 Characterisation

Difficulty was experienced in the characterisation of the products from the reaction because two fractions were isolated after the synthesis of the compounds, but it was obvious that there were more than a single product in each of the fractions collected. The yellow products were all very closely related as will be shown in the ^{1}H NMR spectrum of the first fraction (Figure 6.4).

© University of Pretoria

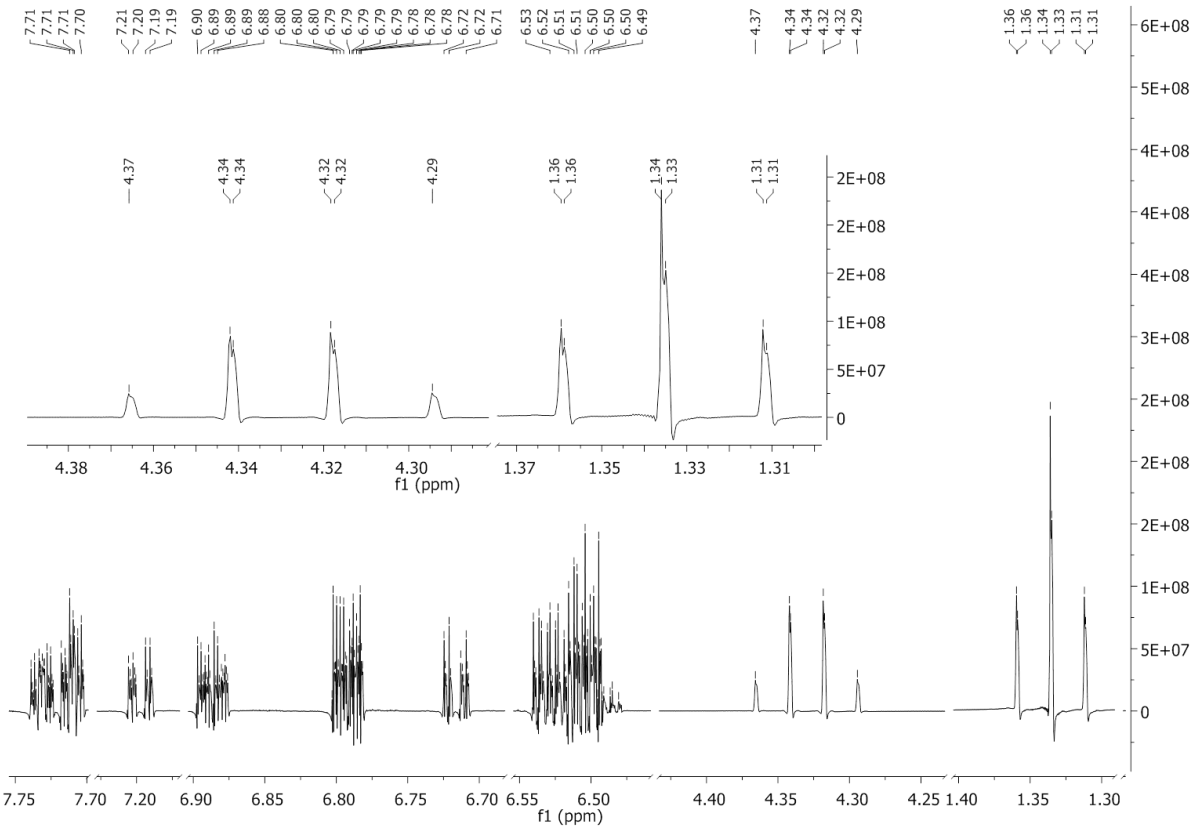

Figure 6.4 ^{1}H NMR spectrum ($CDCl_3$) of the first fraction

The ^{1}H NMR spectrum in Figure 6.4 shows a duplication of the furyl groups and it is possible to distinguish between the two formed products. The –OEt groups present in the products revealed the presence of the two slightly different products on closer examination, but also gave an indication of how similar the two products were. Even though the splitting of the quartet is very small, these signals are not nearly as complex as the furyl resonances. From the spectrum the furyl group $^{31}P\{^{1}H\}$ couplings are clearly visible, forming multiplets for the furyl protons within the molecules. The extensive multiplet formation observed in the spectrum could also be further representative of more than a single carbene containing phosphine ligand coordinated to the AgBr complex.

The ^{1}H NMR spectrum of the second fraction showed three different compounds as shown in Figure 6.5.

© University of Pretoria

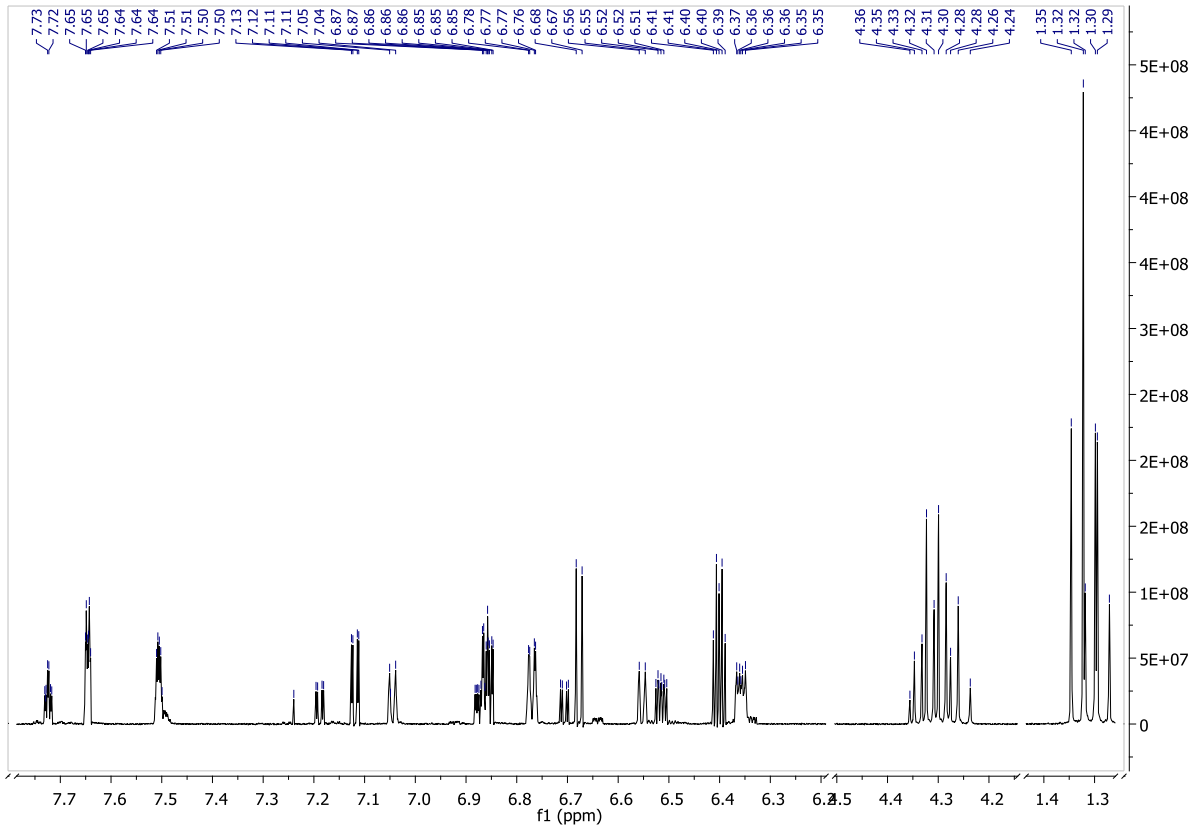

Figure 6.5 ^{1}H NMR spectrum ($CDCl_3$) of the second fraction after the coordination of **1b** AgBr

The ^{1}H NMR spectra revealed very little except a significant upfield shift of the –OEt group protons from 4.94 and 1.60 ppm for **1b** to a value around 4.30 and 1.31 ppm for the new compounds. As a result, the ^{31}P NMR spectra of the two fractions were very closely examined.

The ^{31}P NMR spectrum in Figure 6.6 is a superimposed spectrum of the first and second collected fractions, representing all the phosphorous containing species in the two fractions. In fraction 1, two signals are observed at -31.5 and -33.4 ppm, both having P{Ag} coupling constants of 126.5 Hz. The second fraction contained three major products at chemical shift values of -28.6, -31.5 and -75.3 ppm (the product appearing at -31.5 ppm was present in the first and second fraction), again a Ag{P} coupling constant for the two downfield peaks is observed at a value of 126.5 Hz. The highest upfield peak has no coupling and in total there are four unique compounds observed.

© University of Pretoria

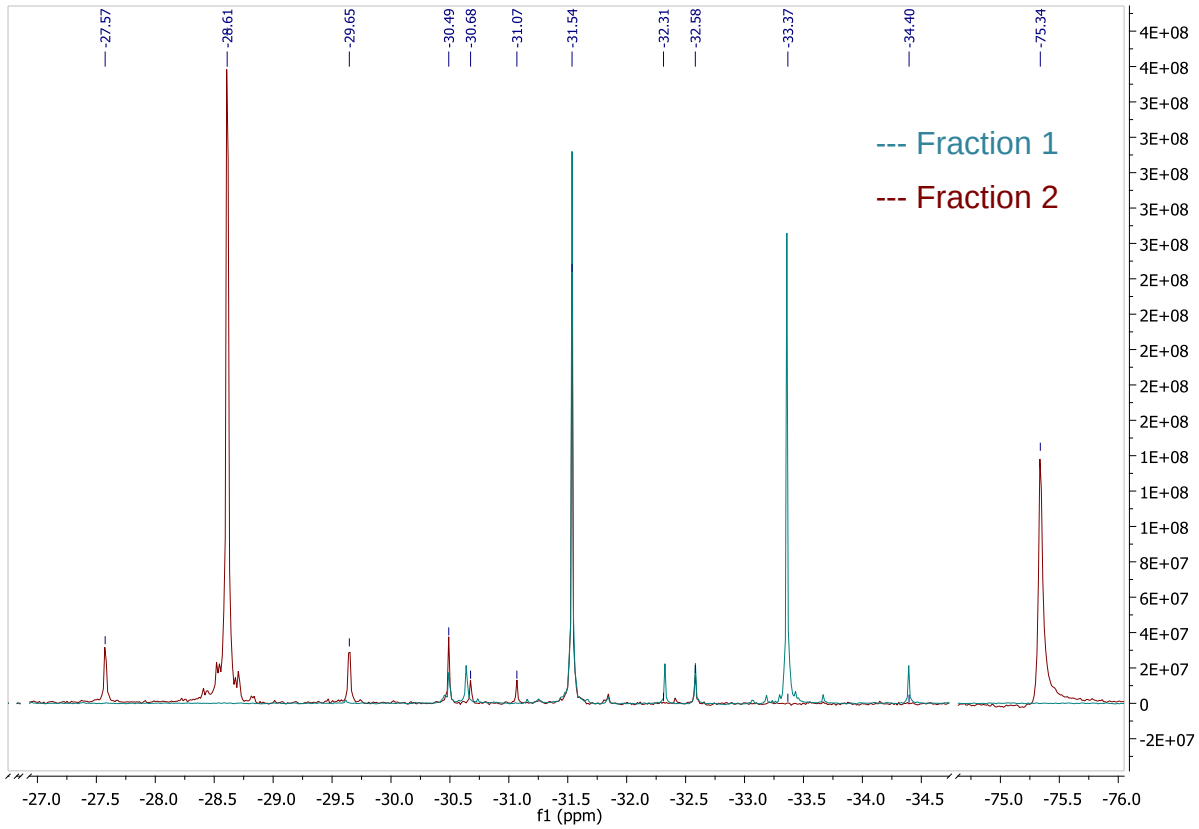

Figure 6.6 ^{31}P NMR superimposed spectrum ($CDCl_3$) of the first and second collected fractions

The first isolated fraction contained the *mono*- and *bis*-coordinated Ag(I)-phosphine complexes. The *mono*-phosphorylated complex has a ^{31}P NMR signal at -33.4 ppm and the *bis*-phosphorylated complex has a signal at -31.5 ppm. Examples of other *mono*- and *bis*-phosphorilated Ag(I) complexes were obtained in crystal form by Baker[9] and Bowmaker[10]. The second isolated product mixture could initially have been a particular Ag(I) complex in the form of $[AgBr(PR_3)_3]$. According to Muetterties and Alegranti[7], there exists an equilibrium between the $[AgBr(PR_3)_3]$ complex and the $[AgBr(PR_3)_2]$ complex, as depicted in Figure 6.7 below.

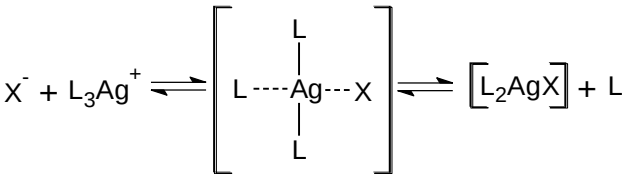

Figure 6.7 An equilibrium that exists between AgBrL complexes[7]

© University of Pretoria

The ^{31}P NMR spectrum in Figure 6.6 shows three products in the second isolated fraction, each of the three neutral products in the equilibrium mentioned above are represented. The product that occurs at -31.5 ppm was present in large quantities in both of the fractions and is the major product of the reaction. The $[AgBr(PR_3)_3]$ complex appears to have the highest downfield chemical shift of -28.6 ppm, followed by the $[AgBr(PR_3)_2]$ complex at -31.5 ppm and lastly the free phosphine at a value of -75.3 ppm. Alyea[11] did a study where one to four PPh_3 ligands were coordinated to an Ag(I) complex. It was found that as the amount of phosphine ligands in complex increased, the ^{31}P NMR signal of the compound moved upfield. The ^{31}P NMR values obtained for these $[AgL_n]^+$ (where L=PPh_3 and n=1-4) were 15.8, 15.3, 11.5 and 5.6 ppm respectively. The $^{31}P\{^{107}Ag\}$ coupling also decreased as the amount of phosphine ligands in the molecule increased. This is not the observed pattern for the synthesised complexes found in Figure 6.5, as their coupling constants are all the same at a value of 125.09 Hz. It will not be possible to compare the chemical shift values determined by Alyea with those of the synthesized complexes because the electronic differences in the phosphine ligands are too big.

When the new phosphorylated compounds are compared on the ^{31}P NMR spectrum, it is clear that the amount of electron density on the phosphine becomes less each time another phosphine ligand is added to the complex. All the phosphorous atoms present in a single complex experience the same environment, thus a single signal is observed with coupling. The downfield position of the signals representing the compounds with the most phosphines was due to the decreased back bonding that occurs from the Ag(I)-atom to the phosphorous. The was because the electron density present on the Ag(I) atom had to be shared by three coordinated phosphorous atoms. As the number of phosphine ligands present in the complex decreases, electron shielding around in the phosphorous atom increases, causing the ^{31}P NMR signals to move downfield.

As stated earlier in this section, when the proton spectra was analysed, it was found that the methylene protons of the carbene –OEt groups had unexpected upfield chemical shift values compared to those of the uncoordinated phosphine. Extensive amount of ester formation was considered with the prominent upfield shift in the ^1H NMR spectrum of the OEt-group. The new complexes had values of 4.30 and 1.31

© University of Pretoria

ppm compared to the value of 4.94 and 1.60 ppm of the $–OCH_2CH_3$ of the uncoordinated carbene containing phosphine. In recent research by Sierra[12], the oxidation of a carbene complex in the presence of a Pd catalyst to form an ester compound also created an upfield shift of the OEt group to values of 4.22 and 1.32 ppm. The recorded ^{1}H NMR values of the OEt groups of all the products that formed during the reaction of silver and **1b** had OEt values very close to these "ester proton" values. There is a slight difference between the values of the different OEt groups, but the difference is not large enough to ignore the possibility of ester formation during the reaction. Analysis of the ^{13}C NMR spectra of the two isolated fractions revealed that each of these products did not have any carbonyl representing peaks and the carbene signals had significantly upfield values lying between 202.5 and 195.1 ppm all having dd multiplicities for all the formed products, compared to a ^{13}C NMR chemical shift value of 285 ppm for a $W(CO)_5$-carbene complex.

Sierra and his research group[12] recorded an ester (–RC(O)OR) ^{13}C NMR signal at 170.1 ppm, which is further upfield than the recorded carbene signals for the Ag-phosphine complexes. Arduengo and his fellow researchers[13] synthesised an NHC carbene, two which were coordinated to a single Ag^+ atom[14]. The uncoordinated ^{13}C carbene signal appeared at a value of 219.7 ppm while the coordinated carbene signals appeared at a chemical shift value of 183.6 ppm with a dd multiplicity and coupling constants of 208.57 and 187.95 Hz, indicating an upfield shift on coordination of the carbene to the silver.

Returning to the products obtained during the coordination of **1b** to a Ag^+ atom, the significant shift of the carbene carbon can either be attributed to complete ester formation throughout all products or rather a carbene transfer from the $W(CO)_5$ group to the AgBr complex. Since the ester (RC(O)OR) ^{13}C NMR chemical shift value occurs slightly higher upfield than those of the recorded compounds and the fact that there are no remains of the $W(CO)_5$ fragment, it can only be concluded that a carbene transfer reaction had occurred from $W(CO)_5$ to AgBr during the synthesis of these compounds. Wang and Lin[15] synthesized a complex where two NHC carbenes were coordinated to a Ag(I) metal centre. The recorded carbene ^{13}C NMR chemical shift value was 188 ppm. This value is upfield, but still in the range of the

© University of Pretoria

^{13}C NMR carbene shifts recorded for the two fractions collected during from our reaction.

Further evidence for a carbene transfer reaction is revealed in the ^{31}P NMR spectrum. The free phosphine containing the Ag-carbene as a substituent was assigned a chemical shift value of -75.3 ppm. This value differed slightly from that of **1b**, which had a value of -72.8 ppm. This corresponds to a more electron rich metal coordinating the carbene carbon, since the phosphine atom becomes more shielded once the carbene transfer from the $W(CO)_5$ group to the AgBr group occurs. In a review by Liu and Reddy[16], it is stated that in some cases there is an equilibrium that is observed between the two metal-carbene complexes once the carbene transfer has been started, however, this is not the case for Ag(I) complexes. Once the carbene was transferred to the Ag(I) from the group 6 metal, no return carbene transfer reactions occurred.

To summarise the above observations, the complexes in the two fractions are shown in Figure 6.8.

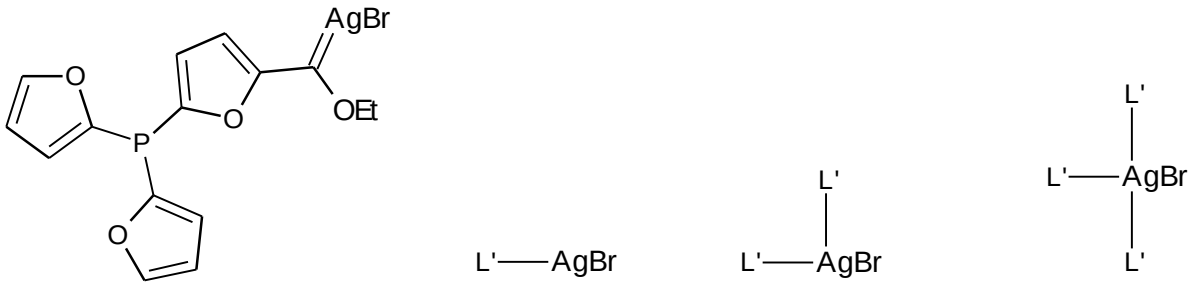

21a **21b** **21c** **21d**

Figure 6.8 The complexes formed during coordination of **1b** to AgBr

Table 6.2 ^{1}H, ^{13}C and ^{31}P NMR data ($CDCl_3$) of **21a**

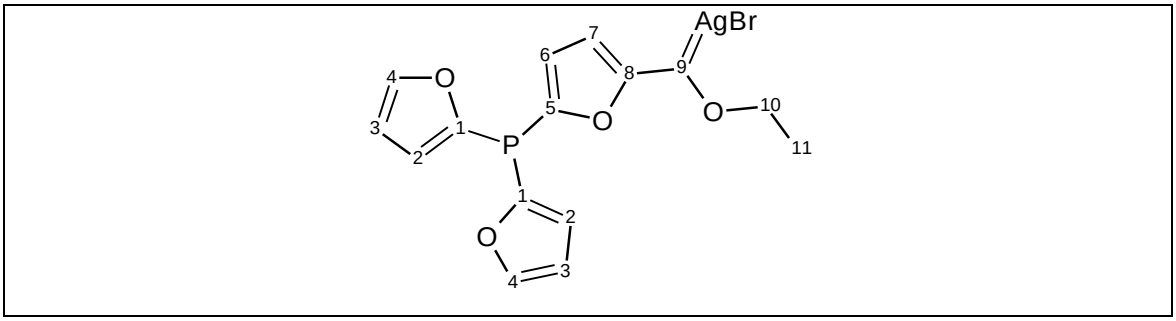

© University of Pretoria

^{1}H NMR			
Position	δ_H/ppm	Multiplicity *J*/Hz	Integration
2	6.51	ddd, 3.4, 1.7, 1.2	2H
3	6.86	ddd, 1.7, 0.7, 0.2	2H
4	7.72	ddd, 1.1, 0.9, 0.3	2H
6	7.19	dd, 3.6, 0.9	1H
7	6.88	dd, 1.5, 0.7	1H
10	4.32	q, 7.1	2H
11	1.29	t, 7.1	3H

^{13}C NMR		
	δ_c/ppm	Multiplicity *J*/Hz
1	121.8	d, 17.8
2	110.9	d, 7.1
3	117.9	d, 5.3
4	148.5	d, 4.9
5	122.4	d, 27.8
6	111.5	d, 6.7
7	118.3	d, 1.7
8	158.5	-
9	202.4	dd, 10.8, 0.6
10	61.3	-
11	14.1	-

^{31}P NMR (δ_p/ppm)
-75.3

Mass spectral analysis of the two fractions were acquired and listed in Table 6.3

© University of Pretoria

Table 6.3 Mass spectral analysis of **21a**, **21b** and **21c**

Complex	m/z	Intensity (%)	Fragment ion
21a	476	7	$[L]^+$
21b	664	21	$[L + AgBr]^+$
21c	1140	5	$[2L + AgBr]^+$

* No assignable fragment ions were observed for **21d**

The mass spectral analysis of **21a**, **21b** and **21c** confirmed previous postulations made in regards to these complexes, were true. The m/z values for these compounds showed no traces of tungsten carbonyl fragments indicating that the carbene transfer reaction was successful.

6.3.3 Conclusion

In this study it was found that a carbene transfer reaction had occurred from tungsten to silver.to yield a phosphine that displayed a more electron-rich character. The silver carbene-containing phosphine (**21a**) was also successfully coordinated to the Ag(I) metal centre to form three different isomers with one, two or three coordinated phosphines (**21b**, **c** and **d**). The free silver carbene-containing phosphine (**21a**) was found to have a ^{31}P NMR chemical shift of -75.3 ppm while the coordinated complexes had ^{31}P NMR shifts more upfield relative to **21a**.

6.4 Copper complexes

This section of the project involves coordination of **1b**, to Cu(I) and Cu(II)-halogen complexes.

6.4.1 Cu(I) and Cu(II) as acceptor complexes for phosphine coordination

There have been a great amount of research in the 1970s and 1980s concerning the equilibrium products that exist within solution between ratios of L and CuX where L represents a tertiary phosphine and X a halogen[17–19]. Detailed crystal structures of

© University of Pretoria

these compounds have been recorded, however, the structural integrity of the complexes are not necessarily retained in solution. Attempts have been made to determine the identity and concentrations of the different isomers once in solution, but have not been successful until 1970. In 1970, Muetterties and Alegranti[20] were successful in isolating and determining the concentrations of species with tri-*p*-tolylphosphine as L at -100°C and slightly higher temperatures in 50% v/v dichloromethane-toluene solution. The structures that were identified are shown in Figure 6.9.

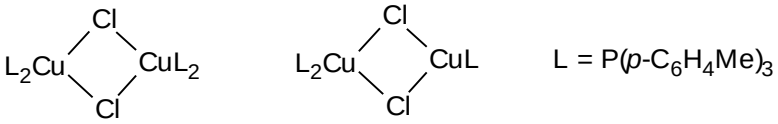

Figure 6.9 Two CuX_nL_n species isolated at -100°C by Muetterties and Alegranti[20]

It was found that at a temperature of -100°C, the saturated dimer **A** was the major species present, while at higher temperatures i.e. -70 to -80°C, dimer **B** was the additional species present. The bromide complex underwent similar dissociation; however, *monomeric* (single units) L_2CuBr was present in higher concentrations upon dissociation. Lippard and Mayerle[17] reported that there could be as many as six distinct types of complexes: L_3CuX, $(L_2CuX)_2$, $L_3Cu_2X_2$, $(LCuX)_4$ and $(LCuX)_2$ in solution. The number of intermediates that form during this reaction poses an obvious problem when it comes to characterisation of a particular complex. Each study delivers a different set of results and the results all determined by different methods. It can be concluded that the composition of intermediate ligands are dependent on the physical properties of L, the solvent as well as the temperature.

The coordination of the phosphines to Cu(II)-halogen complexes without stabilisation is not supported by literature. It should not be mistaken that the synthesis of these compounds have never been tried, but actual Cu(II)-halogen complexes do not phosphorylate. Instead, the Cu(II)-halogen complex is reduced by the tertiary phosphine and forms Cu(I)-phosphine complexes[21]. Two decades ago, Lobana and Bhatia[22] isolated Cu(II)-tertiary phosphine complexes stabilised by 1-hydroxypyridine-2-thione.

© University of Pretoria

6.4.2 Characterisation

The characterisation of the Cu-phosphine compounds was difficult, given that a mixture of products was always observed. As mentioned above, there is a constant, equilibrium between all the isomers present in the solution, where some of the isomers also undergo halogen bridging when a tertiary phosphine should dissociate from the complex. Due to the many isomeric species that may possibly exist in the solution, it was not possible to determine which of the isomers were the major product of the reaction.

6.4.2.1 Cu(I)Br ligand coordination

The experiment involved stirring **1b** with CuBr for 24 hours and isolating the red-brown product by chromatography. No separation of isomers was observed during the chromatography, but some intermediates were observed on characterisation of the compound by NMR spectroscopy. In research conducted earlier, it was found that $Cu(PPh)_3Br$ was synthesised as a major product by adding the correct ratio of reactants, i.e. 1:3 CuBr to phosphine[23].

Table 6.3 ^{1}H, ^{13}C and ^{31}P NMR data ($CDCl_3$) of **22a**

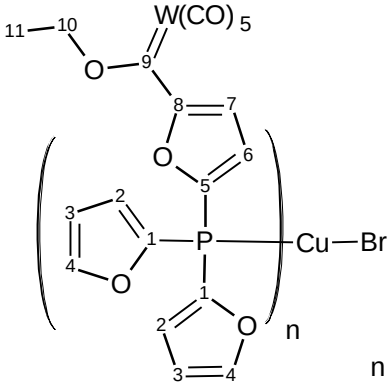

^{1}H NMR

Position	δ_H/ppm	Multiplicity *J*/Hz	Integration
2	6.37	d, 1.4	2H
3	7.29	s	2H
4	7.58	s	2H

© University of Pretoria

6	7.34	d, 1.8	1H
7	6.89	d, 1.9	1H
10	4.92	q, 7.0	2H
11	1.60	t, 7.0	3H

^{13}C NMR		
	δ_c/ppm	Multiplicity *J*/Hz
1	142.6	d, 49.0
2	124.7	d, 25.2
3	111.2	d, 8.7
4	148.6	-
5	144.6	d, 49.6
6	123.5	d, 26.5
7	113.7	d, 6.1
8	169.4	-
9	285.3	-
10	78.4	-
11	15.0	-
12	203.8 (trans), 196.9 (cis)	-

^{31}P NMR (δ_p/ppm)
-66.1 and -11.6

Figure 6.10 shows the ^{1}H NMR spectrum of the phosphorylated Cu(I) products of the reaction of **1b** with CuBr. It shows the broadening of furyl peaks, which could mean that closely related isomers were present.

It is important to note that coordination of the phosphine did occur and the broadened ^{1}H NMR peaks indicated that more than one phosphine was coordinated.

© University of Pretoria

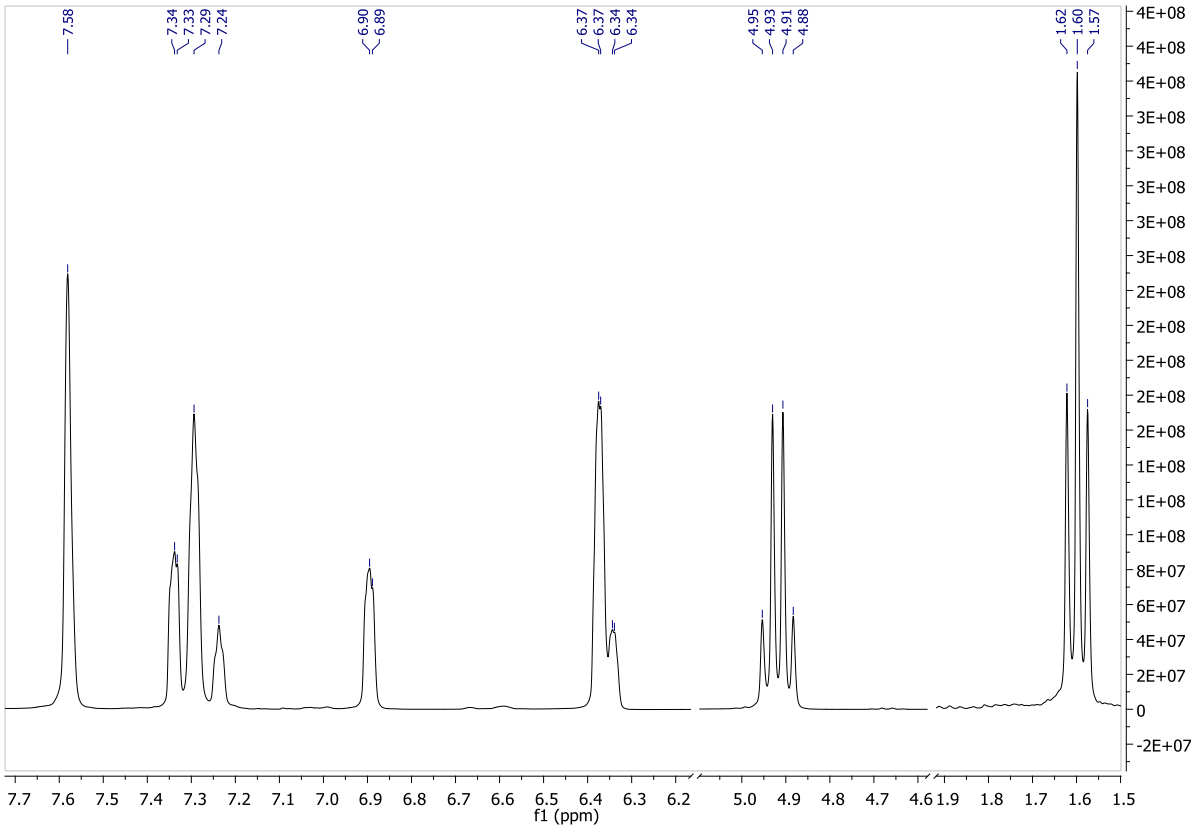

Figure 6.10 ^{1}H NMR spectrum ($CDCl_3$) of the phosphorylated Cu(I) products

Two products were observed in the ^{31}P NMR in Figure 6.11 with chemical shift values of -11.6 ppm for the minor product and a broadened peak at -66.1 ppm for the major product. The latter value was close to the ^{31}P NMR value of the uncoordinated phosphine which had a chemical shift of -72.8 ppm. The small difference between the uncoordinated phosphine and that of the major product revealed that a significant amount of electron density was present on the phosphorous atom.

Since the ratio of ligand to Cu(I) was 3:1 in the synthesis of these compounds, the expected product was $Cu(PR_3)_3Br$. Fife, Moore and Morse[19] stated that, in a reaction with a ratio of CuCl to PPh_3 of 1:3, they observed in addition to the expected $Cu(PPh_3)_3Cl$-complex, a small amount of $Cu(PPh_3)_2Cl$ in the reaction mixture. The ligand dissociation constant of the $Cu(PPh_3)_3Cl$-complex is quite large ($K_3 = 2 \times 10^{-2}$), consequently, it would be expected that some of the $Cu(PPh_3)_2Cl$ complex would form. A very relevant question now has to be asked: Will the carbene containing phosphine (**1b**) have a significantly different K_3 value compared to PPh_3?

© University of Pretoria

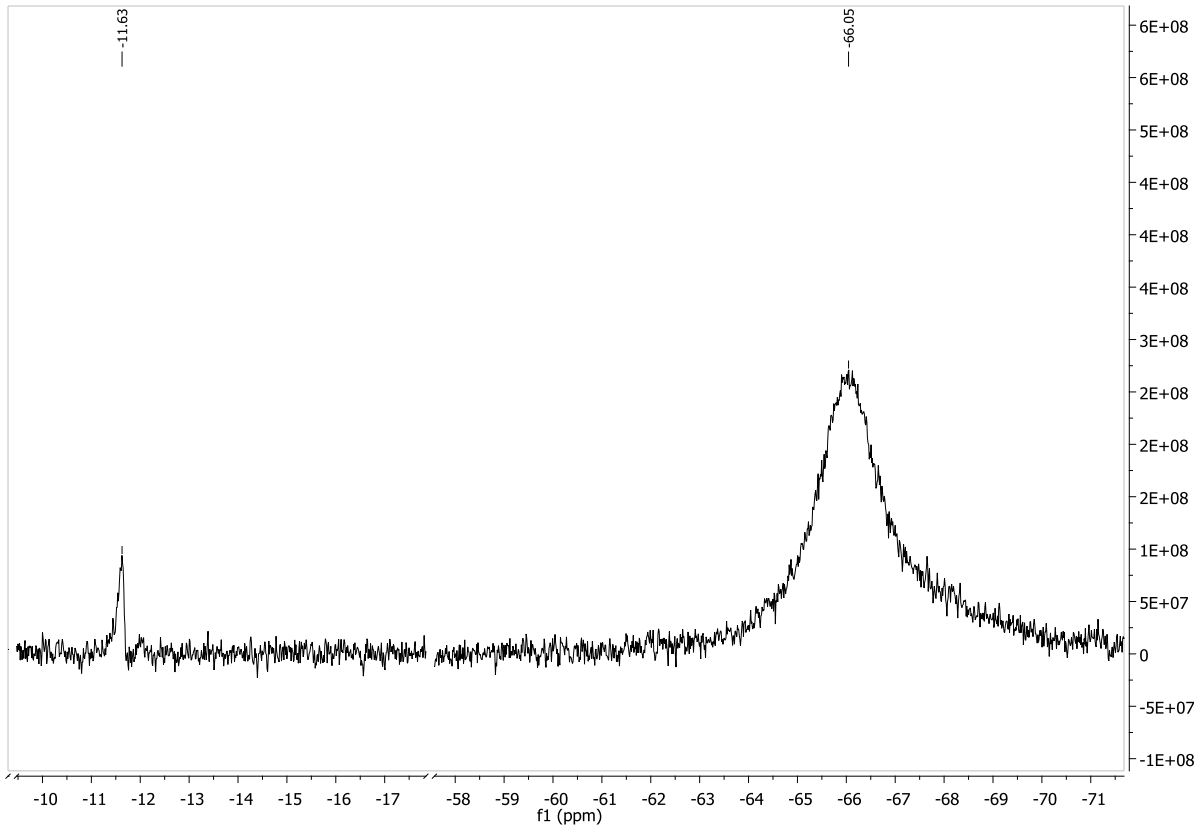

Figure 6.11 ^{31}P NMR spectrum ($CDCl_3$) of the phosphorylated Cu(I) products

Chapter 2 indicated that a PFu_3 is much more electron-withdrawing than PPh_3 and the additional carbene substituent present on **1b** will have an even greater overall electron-withdrawing effect when compared to the PPh_3. It is more likely that the newly coordinated phosphine of **22a** will have a significantly greater K_3 value than that of $Cu(PPh_3)_3Br$. This is supported by the fact that **1b** has a much greater withdrawing character, ensuring more dissociation or poorer coordination of the phosphine from or to the CuBr centre.

It is obvious from the high upfield ^{31}P chemical shift value that there is still a significant amount of electron density present on the phosphorous atom, suggesting that a carbene transfer reaction had occurred during the synthesis of the compound. This is not the case when the ^{13}C NMR spectrum of the compound is analysed (Figure 6.12). The $W(CO)_5$-carbene substituent is still visible on the spectrum at 285.3, 203.8 and 196.9 ppm, eliminating the possibility of a carbene transfer reaction.

© University of Pretoria

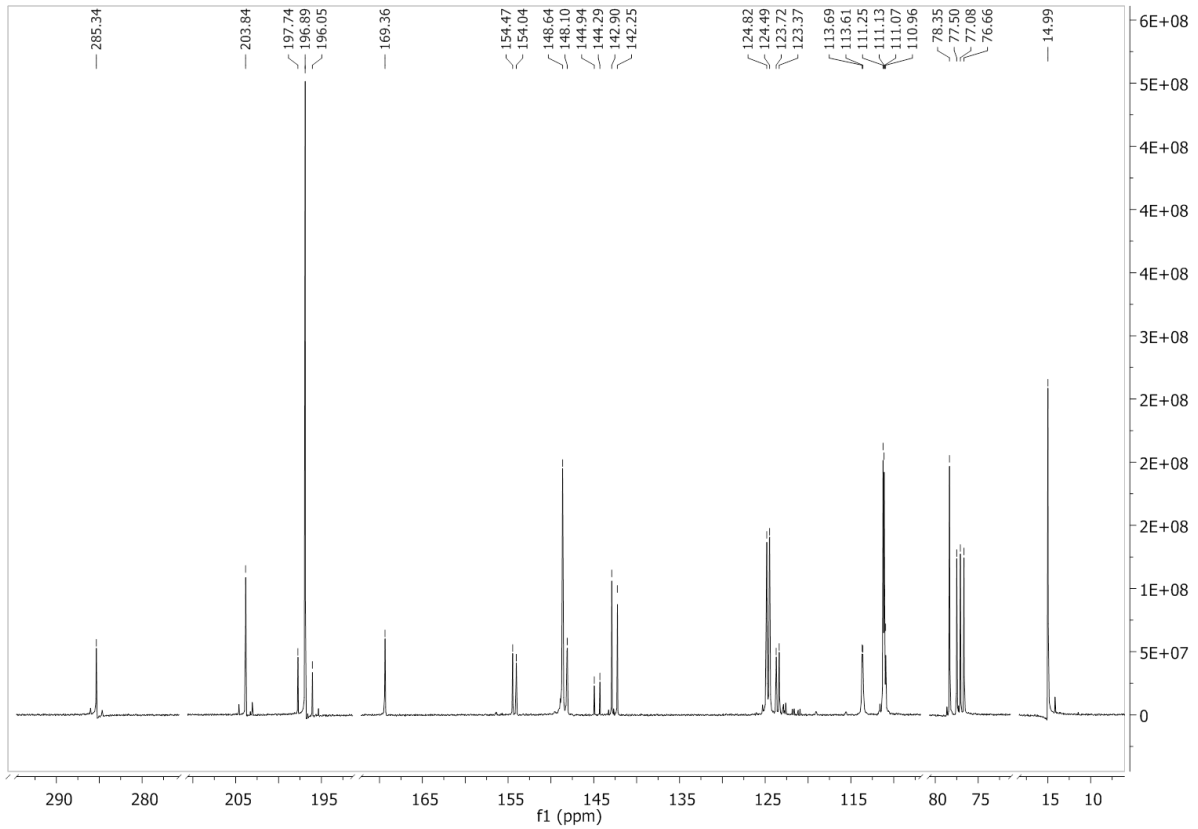

Figure 6.12 ^{13}C NMR ($CDCl_3$) spectrum of the phosphorylated Cu(I) products

Further support of the presence of the pentacarbonyl fragment was found in the IR spectrum which displayed $A_1^{(1)}$, B_1 and an E-bands at 2069, 1994 and 1945 cm^{-1} respectively. These values are very close to those of the uncoordinated phosphine and are corroborated by a ^{31}P NMR signal at -66.05 ppm.

Research by Barron, Dyason and Healy[18] showed by ^{31}P solid state NMR that several complexes of the form $CuX(PR_3)_3$ showed two symmetric quartets with extremely large coupling constants. The ^{31}P NMR chemical shift values for $CuBr(PPh_3)_3$ ranged between 10 and -20 ppm. With the ^{31}P NMR chemical shift value of PPh_3 as -6 ppm, comparing this value with that of the coordinated PPh_3 in the complexes prepared by Barron, Dyason and Healy, will reveal the effect coordination has on the phosphine.

Since it was still unclear which isomer was present as the major product in the isolated product mixture, the mass to charge ratio was measured for the fragments. The mass spectral analysis revealed a fragment of [(CuBr+**1b**) + Na]$^+$ as well as

© University of Pretoria

large amounts of [**1b**]$^+$. These two fragments were indicative of [CuBr(**1b**)], but could not exclude the possibility that more than one **1b** ligand was coordinated. Thus, in further reference to the products of this reaction, [CuBr(**1b**)$_n$] where n = 1-3 will be used to describe the composition of the product.

6.4.2.2 $CuCl_2$ ligand coordination

The synthesis of the coordination compound entailed a 10 minute reaction in which **1b** was stirred at room temperature with $CuCl_2$. Unlike for Cu(I) a very high yield of product was obtained after the isolation of the product on a silica column. As mentioned in the introduction to this section, phosphorylation of Cu(II)-halogen complexes lead to the reduction of the Cu(II)-metal centre by the phosphines as well as further coordination. [CuCl(**1b**)$_3$] would be the major expected product.

On analysis of the products, it was found that there were some similarities in the ^{1}H and ^{13}C NMR spectra of the Cu(I) and Cu(II) products. The ^{31}P NMR spectrum revealed the presence of three different products within the reaction mixture, two of which occurred at chemical shift values of -66.9 and -11.7 ppm. Analogous products were also obtained in the case of CuBr phosphorylation. The third product, which had a ^{31}P NMR shift of -30.8 ppm was unique. Further analysis revealed only small differences between the CuBr and $CuCl_2$ phosphorylation reactions ascribed to the use of Cl instead of Br.

Table 6.4 ^{1}H, ^{13}C and ^{31}P NMR data ($CDCl_3$) of **22b**

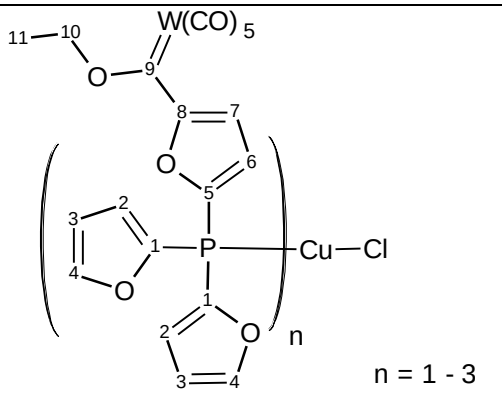

^{1}H NMR

Position	δ_H/ppm	Multiplicity	Integration

© University of Pretoria

		J/Hz	
2	6.37	-	2H
3	7.31	-	2H
4	7.65	-	2H
6	7.40	-	1H
7	6.90	-	1H
10	4.89	q, 7.0	2H
11	1.57	t, 7.0	3H

^{13}C NMR		
	δ_c/ppm	Multiplicity *J*/Hz
1	142.5	53.4
2	123.8	d, 30.1
3	110.9	d, 9.5
4	149.0	d, 3.8
5	144.7	d, 53.0
6	125.1	d, 30.4
7	111.1	d, 9.6
8	169.6	d, 2.2
9	285.8	-
10	78.3	-
11	14.9	-
12	209.0 (trans), 196.8 (cis)	-

^{31}P NMR (δ_p/ppm)
-66.9, -30.8, -11.7

The IR spectrum showed a pentacarbonyl fragment which was the same as that recorded for the products synthesised from coordination of the novel phosphine to CuBr. Both the $A_1^{(2)}$ and the E-bands were resolved which was not the case with the CuBr complex.

© University of Pretoria

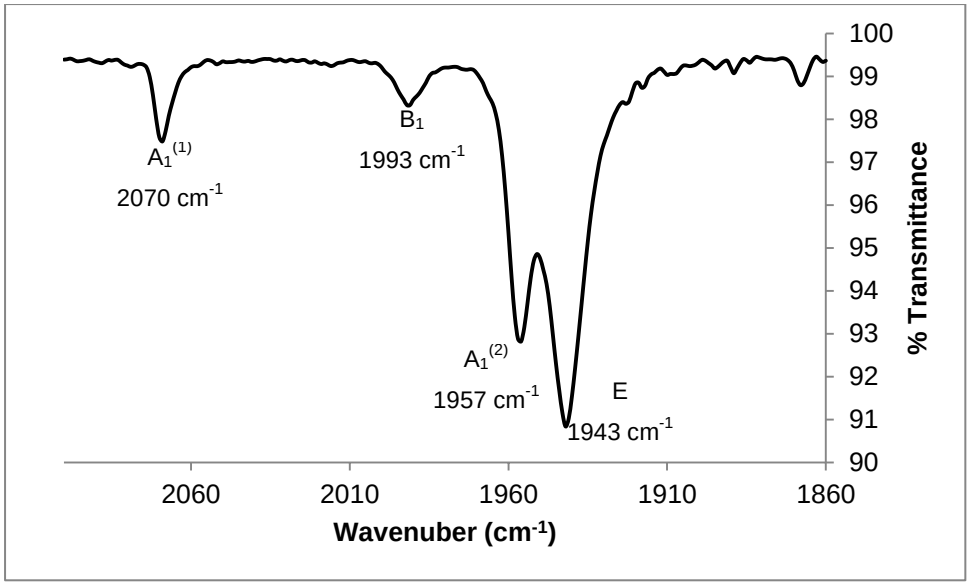

Figure 6.13 IR of pentacarbonyl group present in **22b**

The sample was also analysed with mass spectral analysis, but the mixture revealed the presence of [(CuCl+**1b**) + Na]$^+$ and [**1b**]$^+$ fragments, again not giving an indication of what the major product could have been. With the results obtained it was possible to state that phosphorylation did occur, though it was not possible to determine to what extent.

6.4.3 Conclusion

Two different copper starting materials were used to synthesise the same Cu(I) phosphine complexes, the only difference between the products being the halogen coordinated to the Cu(I) metal centre. The phosphorylation of both compounds was successful with no carbene transfer reactions observed for either of the methods in the synthesis. There were not any indications of catalytic or metathesis reactions that occurred during the synthesis of the compounds, showing that the Cu(I)-metal centre is not prone to react with the Fischer carbene substituents present on the phosphines. Further experimentation and analysis of this reaction is required to fully state whether these compounds will have a significant ability to act as potential catalysts or not.

© University of Pretoria

6.6 References

1. D. J. Gorin and F. D. Toste. Relativistic effects in homogeneous gold catalysis. *Nature* (2007) **446,** 395–403.

2. I. Ott. On the medicinal chemistry of gold complexes as anticancer drugs. *Coord. Chem. Rev.* (2009) **253,** 1670–1681.

3. A. Wolf and F. Schüth. A systematic study of the synthesis conditions for the preparation of highly active gold catalysts. *Appl. Catal. A* (2002) **226,** 1–13.

4. M. Fañanás-Mastral and F. Aznar. Carbene Transfer Reactions from Chromium(0) to Gold(I): Synthesis and Reactivity of New Fischer-Type Gold(I) Alkenyl Carbene Complexes. *Organometallics.* (2009) **28,** 666–668.

5. P. Schwerdtfeger, H. L. Hermann and H. Schmidbaur. Stability of the Gold(I)−Phosphine Bond. A Comparison with Other Group 11 Elements. *Inorg. Chem.* (2003) **42,** 1334–1342.

6. M. A. Sierra, J. C. del Amo, M. J. Mancheño and M. Gómez-Gallego. Pd-Catalyzed Inter- and Intramolecular Carbene Transfer from Group 6 Metal−Carbene Complexes. *J. Am. Chem. Soc.* (2001) **123,** 851–861.

7. E. L. Muetterties and C. W. Alegranti. Solution structure and kinetic study of metal-phosphine and-phosphite complexes. I. Silver (I) system. *J. Am. Chem. Soc.* (1972) **94,** 6386–6391.

8. R. Meijboom, R. J. Bowen and S. J. Berners-Price. Coordination complexes of silver(I) with tertiary phosphine and related ligands. *Coord. Chem. Rev* (2009) **253,** 325–342.

9. L. J. Baker, G. A. Bowmaker, D. Camp, P. C. Healy, H. Schmidbaur, O. Steigelmann and A. H. White. Structural, far-IR and phosphorus-31 NMR studies of two-coordinate complexes of tris(2,4,6-trimethoxyphenyl)phosphine with silver(I) halides. *Inorg. Chem.* (1992) **31,** 3656–3662.

10. G. A. Bowmaker, Effendy, J. V. Hanna, P. C. Healy, B. W. Skelton and A. H. White. Crystal structures and spectroscopic studies of the mononuclear complex $[AgBr(PPh_3)_2]$ and binuclear $[Ag_2X_2(PPh_3)_4]\cdot 2CHCl_3$(X = Cl or Br). *J. Chem. Soc., Dalton Trans.* (1993) 1387–1397.

11. E. C. Alyea, J. Malito and J. H. Nelson. Identification by stopped-exchange solution phosphorus-31 NMR spectroscopy of the stepwise formation of $[AgL_n]PF_6$ (n = 1-4). Comparison of metal-phosphorus coupling constants for triphenylphosphine and 5-phenyldibenzophosphole. *Inorg. Chem.* (1987) **26,** 4294–4296.

© University of Pretoria

12. M. P. López-Alberca, M. J. Mancheño, I. Fernández, M. Gómez-Gallego, M. A. Sierra and R. Torres. Divergent Pathways in the Reaction of Fischer Carbenes and Palladium. *Org. Lett.* (2007) **9,** 1757–1759.

13. A. J. Arduengo, H. V. R. Dias, R. L. Harlow and M. Kline. Electronic stabilization of nucleophilic carbenes. *J. Am. Chem. Soc.* (1992) **114,** 5530–5534.

14. A. J. Arduengo, H. V. R. Dias, J. C. Calabrese and F. Davidson. Homoleptic carbene-silver(I) and carbene-copper(I) complexes. *Organometallics* (1993) **12,** 3405–3409.

15. H. M. J. Wang and I. J. B. Lin. Facile Synthesis of Silver(I)−Carbene Complexes. Useful Carbene Transfer Agents. *Organometallics* (1998) **17,** 972–975.

16. S.-T. Liu and K. R. Reddy. Carbene transfer reactions between transition-metal ions. *Chem. Soc. Rev.* (1999) **28,** 315–322.

17. S. J. Lippard and J. J. Mayerle. Behavior of tertiary phosphine and arsine complexes of copper(I) in chloroform solution. *Inorg. Chem.* (1972) **11,** 753–759.

18. P. F. Barron, J. C. Dyason, P. C. Healy, L. M. Engelhardt, C. Pakawatchai, V. A. Patrick and A. H. White. Lewis-base adducts of Group 11 metal(I) compounds. Part 28. Solid-state phosphorus-31 cross-polarization magic-angle spinning nuclear magnetic resonance and structural studies on the mononuclear 3: 1 adducts of triphenylphosphine with copper(I) halides. *J. Chem. Soc., Dalton Trans.* (1987) 1099–1106.

19. D. J. Fife, W. M. Moore and K. W. Morse. Solution equilibria of tertiary phosphine complexes of copper(I) halides. *Inorg. Chem.* (1984) **23,** 1684–1691.

20. E. L. Muetterties and C. W. Alegranti. Solution structure of coinage metal-phosphine complexes. *J. Am. Chem. Soc.* (1970) **92,** 4114–4115.

21. F. H. Jardine, L. Rule and A. G. Vohra. The Chemistry of Copper(I) Complexes. Part 1. Halogeno-complexes. *J. Chem. Soc. A* (1970) 238.

22. T. S. Lobana and P. K. Bhatia. Chemistry of mercaptopyridines and related ligands. Part 3. Novel examples of copper(II)–tertiary phosphine complexes stabilized by 1-hydroxypyridine-2-thione. *J. Chem. Soc., Dalton Trans.* (1992) 1407–1410.

23. W. Reichie. Preparation, physical properties and reactions of copper (I)-triphenyl-m complexes (M= P, As, Sb). *Inorg. Chim. Acta* (1971) 325–332.

© University of Pretoria

Chapter 7

Experimental

7.1 Standard Operating Procedure

Using Schlenk techniques, all experimental procedures were carried out under an inert atmosphere of either argon or nitrogen gas and the solvents were dried under an atmosphere of nitrogen. Dichloromethane (DCM) and acetonitrile were distilled from phosphorous pentoxide while hexane, benzene, diethyl ether, butyl ether and tetrahydrofuran (THF) were distilled from sodium metal and a benzophenone indicator for the ethers. Kieselgel 60 (particle size 0.0063 – 0.200 mm) or neutral aluminium oxide 90 were used as resins for all separations in column chromatography.

7.2 Characterisation Techniques

7.2.1 Nuclear Magnetic Resonance Spectroscopy

A Bruker ARX-300 and AVANCE 500 spectrometer were used to record the NMR data. The ^{1}H NMR spectra were recorded at 300.135 and 500.139 MHz while the ^{13}C NMR spectra were recorded at 75.469 and 125.75 MHz and the ^{31}P NMR spectra at 121.496 and 161.923 MHz for the respective instruments.

The chemical shift values (δ) were reported in parts per million (ppm), using deuterated solvent signals as internal references. For $CDCl_3$ the ^{1}H NMR spectra the reference peak was calibrated at a δ_H value of 7.2400 and the ^{13}C NMR reference peak at a value of δ_C = 77.000 ppm. For C_6D_6 the ^{1}H reference peak was calibrated to δ_H = 7.1600 ppm and the ^{13}C NMR reference peak to a value of 128.39

© University of Pretoria

ppm. The ^{31}P NMR spectra were referenced to the deuterated lock solvent, and had been referenced to 85% H_3PO_4.

7.2.2 Infrared Spectroscopy

A Perkin-Elmer Spectrum RXI FT-IR spectrophotometer with a NaCl cell was used to record the IR spectra. Hexane and DCM were used as solvents to record the vibrational stretching bands in the carbonyl region lying between 1500 and 2200 cm^{-1}.

7.2.3 X-Ray Crystallography

The X-Ray crystal structures were collected at 20°C on a Siemens P4 diffractometer fitted with a Bruker 1 K CCD detector using graphite-monochromated, Mo-Kα radiation by means of a combination of phi and omega scans. The data reductions were performed using SAINT+ and the intensities corrected for absorption with SADABS. The structures were solved using SHELXTS by direct method and the refined by full-matrix least squares using SHELXTL and SHELXL-97. All hydrogen atoms were included in the structure refinements in their calculated positions and treated as riding on the atom to which they are attached. Isotropic displacement parameters for hydrogen atoms were calculated as X x U_{eq} of the atom to which they were attached with X = 1.5 for methyl hydrogen and 1.2 for all other hydrogen. Anisotropic displacement parameters were used to refine the non-hydrogen atoms with the exception of minor occupied sites of disordered atoms.

© University of Pretoria

7.2.4 Mass spectral analysis

The mass spectral analysis was measured on a Synapt G2 HDMS by direct infusion at 5 µl/min with positive electron spray ionisation as ionisation technique. The m/z range was measured from 400 – 1500 with acetonitrile as solvent.

7.2.5 Photochemical reactions

A Phillips G 313 6E medium pressure mercury lamp was used as UV-source in a special 200 ml Pyrex container that was able to be water cooled. During the irradiation reactions nitrogen was passed through the system.

7.3 Preparation of Starting Materials

7.3.1. Purchased chemicals

All chemicals were purchased from Sigma Aldrich, Merck Chemicals and Strem Chemicals, Inc. The chemicals were used without prior purification, unless it is stated otherwise.

7.3.2 Triethyl oxonium tetralfluoroborate[1]

Epichlorohydrin (140.0 g, 199 ml, 1.51 mol) was added dropwise to a solution of sodium-dried ether (500 ml) and freshly distilled boron fluoride etherate (284.0 g, 252 ml, 2.00 mol) at a rate sufficient to maintain vigorous boiling for about an hour. The mixture was refluxed and allowed to stand at room temperature overnight. The supernatant ether was withdrawn from the crystalline mass of triethyloxonium tetrafluoroborate under an inert atmosphere. Crystals were washed with dry ether and stored under dry ether. Yield: 244 – 272 g (85 – 95%).

© University of Pretoria

7.3.3 Preparation of $PtCl_2COD$[2]

1.02 g (2.5 mmol) $K_2[PtCl_4]$ was dissolved in 18 ml distilled H_2O. 12.5 ml *n*propanol was added to the solution followed by 2.0 ml COD and 0.0176 g $SnCl_2.2H_2O$. The mixture was stirred for 48 hours during which a white precipitate formed. The precipitate was isolated by suction filtration and washed with 15 ml distilled H_2O, 15 ml ethanol and air dried. Yield: 81%

7.4 Synthesis of organometallic complexes

All data analysis (NMR and IR) is discussed throughout this project and will not be listed for complexes with the experimental procedures. The crystal structures for the amines were discussed in Chapter 3. Unfortunately it was not possible to obtain crystal structures for any phosphine containing complex as most of them had an oily consistency as pure substance.

7.4.1 Phosphine reactions and complexes

7.4.1.1 Synthesis of $[P(C_4H_3O)_2(C_4H_2O\text{-}C(M(CO)_5)OCH_2CH_3)]$ (1), $[C_4H_3O\text{-}C(M(CO)_5)OCH_2CH_3]$ (2) and $[P(C_4H_3O)(C_4H_2O\text{-}C(M(CO)_5)OCH_2CH_3)(C_4H_9)]$ (3). M = Cr(a) / W(b)

1.16 g (5.0 mmol) PFu_3 was dissolved in 40 ml dry THF to yield a clear solution. The solution was placed in a prepared -80°C cold bath and lithiated with 3.75 ml (1.6 M) *n*BuLi. After lithiation the yellow solution was removed from the cold bath after 10 minutes and allowed to stir at RT for 40 minutes. The reaction mixture was returned to the cold bath (-70°C) and 5 mmol $M(CO)_6$ was added (M = Cr / W) to the cold solution and allowed to stir at RT till all the metal carbonyl was dissolved. The solvent was removed *in vacuo* and the remaining dark-red residue was redissolved in DCM and the mixture placed in the cold bath (-40°C). A solution of 0.95 g (5 mmol) oxonium salt (Et_3OBF_4) dissolved in DCM was cooled and added to the

© University of Pretoria

aforementioned mixture. Products were separated on a silica gel gradient column with hexane and DCM as solvents. Three products were isolated in the order of complex **2**, **1** then **3**.

Table 7.1 Product mass and yield of **1a**, **2a** and **3a** (Cr carbene complexes)

Complex	Colour	Molar mass (g/mol)	mass (g)	mmol	Yield (%)
1	dark red	480.30	1.73	3.60	72
2	orange	316.20	0.14	0.45	9
3	dark red	439.39	0.11	0.25	5

Table 7.2 Product mass and yield of **1b**, **2b** and **3b** (W carbene complexes)

Complex	Colour	Molar mass (g/mol)	mass (g)	mmol	Yield (%)
1	dark red	612.15	2.48	4.10	81
2	orange	448.05	0.25	0.55	11
3	dark red	571.24	0.17	0.30	6

7.4.1.2 Synthesis of $[P(C_4H_3O)_2(C_4H_2O\text{-}C(M(CO)_5)OCH_2CH_3)]$ (1), $[C_4H_3O\text{-}(C(M(CO)_5)\ OCH_2CH_3)]$ (2), $[P(C_4H_3O)(C_4H_2O\text{-}C(M(CO)_5)OCH_2CH_3)(C_4H_9)]$ (3), $[P(C_4H_3O)(C_4H_2O\text{-}C(M(CO)_5)OCH_2CH_3)_2]$ (4), $[C_4H_2O\text{-}(C(M(CO)_5)OCH_2CH_3)_2]$ (5) and $[P(C_4H_2O\text{-}C(M(CO)_5)OCH_2CH_3)_3]$ (6). M = Cr(a) / W(b)

1.16 g (5 mmol) PFu_3 was dissolved in 40 ml dry THF and placed in a prepared cold bath at -78°C. The dissolved starting material was lithiated with 3.75 ml (1.6 M) *n*BuLi and allowed to stir in the cold bath for 10 minutes. The reaction mixture was removed from the cold bath and allowed to stir at room temperature for 40 minutes. The yellow solution was returned to the cold bath (-65°C), followed by addition of 5

© University of Pretoria

mmol of $M(CO)_6$ (M = Cr/W). The solution was allowed to stir for 20 minutes in the cold bath and was removed to stir at room temperature until all metal carbonyl was dissolved. The lithiation and metallation steps were repeated twice more. After the third metallation was completed the solvent was removed *in vacuo*, the remaining residue dissolved in DCM and placed in the cold bath (-40°C). A solution of 2.85 g (15 mmol) oxonium salt (Et_3OBF_4) was dissolved in DCM, cooled and was added to the aforementioned mixture. Products were separated on a silica gel gradient column with hexane and DCM as solvents. Six products were isolated and characterised from the reaction.

Table 7.3 Product mass and yield of **1a**, **2a**, **3a**, **4a**, **5a** and **6a** (Cr carbene complexes)

Complex	Colour	Molar mass (g/mol)	mass (g)	mmol	Yield (%)
1	dark red	480.30	0.36	0.75	15
2	orange	316.20	0.14	0.45	9
3	dark red	439.39	0.07	0.15	3
4	dark red	728.41	0.84	1.15	23
5	purple	564.32	0.11	0.20	4
6	dark red	976.54	0.73	0.75	15

Table 7.4 Product mass and yield of **1b**, **2b**, **3b**, **4b**, **5b** and **6b** (W carbene complexes)

Complex	Colour	Molar mass (g/mol)	mass (g)	mmol	Yield (%)
1	dark red	612.15	0.58	0.95	19
2	orange	448.05	0.25	0.55	11
3	dark red	571.24	0.20	0.35	7
4	dark red	992.12	1.54	1.55	31
5	purple	828.02	0.25	0.30	6
6	dark red	1372.09	1.23	0.90	18

© University of Pretoria

7.4.2 Amine reactions and complexes

7.4.2.1 Synthesis of $[N(C_6H_5)_2(C_6H_4\text{-}C(M(CO)_5)OCH_2CH_3)]$ (7), $[N(C_6H_5)(C_6H_4\text{-}C(M(CO)_5)OCH_2CH_3)_2]$ (8) and $[N(C_6H_4\text{-}C(M(CO)_5)OCH_2CH_3)_3]$ (9). M = Cr(a) / W(b)

0.49 g (1.00 mmol) tris(4-bromophenyl)amine was dissolved in 20 ml dry THF, placed in a cold bath at -80°C and lithiated with 0.8 ml (1.5 M) *n*BuLi. 5 minutes after lithiation $M(CO)_6$ (1 mmol, M = Cr or W) was added to the lithiated solution. The reaction mixture was removed from the cold bath after 20 minutes and allowed to stir at room temperature until all metalcarbonyl was dissolved. The lithiation and metallation steps were repeated another two times before the solvent was removed *in vacuo*. The remaining residue was dissolved in DCM and placed in the cold bath (-40°C). The solution was alkylated with a cold solution of 0.57 g (3 mmol) Et_3OBF_4. Three bright orange products were isolated on a silica gel gradient column using hexane and DCM as solvents and separated in the order **7, 8** then **9**.

Table 7.5 Product mass and yield of **7a**, **8a** and **9a** (Cr carbene complexes)

Complex	Colour	Molar mass (g/mol)	mass (g)	mmol	Yield (%)
7	red	493.46	0.03	0.07	7
8	red	741.58	0.13	0.18	18
9	orange	989.70	0.67	0.68	68

Table 7.6 Product mass and yield of **7b**, **8b** and **9b** (W carbene complexes)

Complex	Colour	Molar mass (g/mol)	mass (g)	mmol	Yield (%)
7	red	625.31	0.06	0.09	9
8	red	1005.28	0.20	0.20	20
9	orange	1385.25	0.97	0.70	70

© University of Pretoria

7.4.2.2 Synthesis of o, m and p-[{η^6-(CH$_3$)$_2$N(C$_6$H$_5$)OCH$_2$CH$_3$}Cr(CO)$_3$] 10, 11 and 12. M = Cr (a) or W (b)

Coordination of N(CH$_3$)$_2$C$_6$H$_5$ to Cr(CO)$_6$

Chromium hexacarbonyl (4.00 g, 18.00 mmol), 25 ml N,N-dimethylaniline, 60.00 ml dibuthylether and 5.00 ml THF was placed in a round-bottom flask equipped with a gas-inlet and cooler. The reaction mixture was refluxed for 24 hours after which the yellow solution was allowed to cool and the products isolated on a silica gel column. Yield: 85%

Fischer carbene synthesis on [{η^6-(CH$_3$)$_2$N(C$_6$H$_5$)OCH$_2$CH$_3$}Cr(CO)$_3$]

The synthesised [N(CH$_3$)$_2$(C$_6$H$_5$)-η^6-Cr(CO)$_3$] (1.8 g, 7.00 mmol) was dissolved in dry THF and cooled to -50°C. *n*BuLi (1.6 M, 4.4 ml) was added to the solution while stirring. The solution turned an intense dark colour. After ten minutes Cr(CO)$_6$ (1.1 g, 5 mmol) was gradually added to the solution and allowed to stir in the cold bath for 10 minutes. The reaction mixture was removed from the cold bath and allowed to stir until all the M(CO)$_6$ (M = Cr/W) was dissolved (30 minutes). The solvent was removed *in vacuo* and the remaining residue dissolved in DCM. The reaction mixture was cooled and alkylated with Et$_3$OBF$_4$ (0.95 g, 5 mmol) dissolved in DCM. Three products, **10**, **11** and **12**, were isolated on a gradient hexane/DCM silica gel column in the order **10**, **11** and **12**.

Table 7.7 Product mass and yield of **10a**, **11a** and **12a** (Cr carbene complexes)

Complex	Colour	Molar mass (g/mol)	mass (g)	mmol	Yield (%)
10a	purple-red	505.35	0.28	0.55	11
11a	pink	505.35	0.45	0.90	18
12a	dark pink	505.35	1.06	2.10	42

© University of Pretoria

Table 7.8 Product mass and yield of **10b**, **11b** and **12b** (W carbene complexes)

Complex	Colour	Molar mass (g/mol)	mass (g)	mmol	Yield (%)
10b	purple-red	637.20	0.41	0.65	13
11b	pink	637.20	0.70	1.10	22
12b	dark pink	637.20	1.69	2.65	53

7.4.3 Piggybacking of a Tungsten-pentacarbonyl Carbene Substituent on Group 6 and 7 Transition Metal Complexes

7.4.3.1 Synthesis of [W(CO)$_5$(P(C$_4$H$_3$O)$_2$(C$_4$H$_2$O-C(Cr(CO)$_5$)OCH$_2$CH$_3$))], 13

$W(CO)_6$ (0.135 g, 0.38 mmol) was dissolved in 30 ml hexane and 1 ml dry THF was added. The solution was irradiated by UV light for 120 minutes to yield a green-brown solution. A solution of **1a** (0.18 g, 0.38 mmol) dissolved in hexane was immediately added to the reaction mixture and the solvent removed *in vacuo*. The products were isolated by gradient column with hexane and DCM as solvent. Unreacted starting materials were removed from the column before the product was isolated.

Table 7.9 Product mass and yield of **13**

Complex	Colour	Molar mass (g/mol)	mass (g)	mmol	Yield (%)
13	brown	804.20	0.13	0.16	43

7.4.3.2 Synthesis of [Cr(CO)$_5$(P(C$_4$H$_3$O)$_2$(C$_4$H$_2$O-C(Cr(CO)$_5$)OCH$_2$CH$_3$))], 14

The same method was used as in 7.4.5.1. $Cr(CO)_6$ (0.178 g, 0.38 mmol) was used instead of $W(CO)_6$ for coordination.

© University of Pretoria

Table 7.10 Product mass and yield of **14**

Complex	Colour	Molar mass (g/mol)	mass (g)	mmol	Yield (%)
14	brown	672.35	0.10	0.15	39

7.4.3.3 Synthesis of $[Re_2(CO)_9(P(C_4H_3O)_2(C_4H_2O\text{-}C(W(CO)_5)OCH_2CH_3))]$, 15

To make $Re_2(CO)_{10}$ more reactive towards the phosphine, $Re_2(CO)_9(NCMe)$ was synthesized according to the method by Koelle[8].

$Re_2(CO)_{10}$ (0.52 g, 0.8 mmol) was dissolved in 20 ml DCM and a small amount (2 ml) dried acetonitrile was added to the solution. On addition of triemethylaminoxide (0.08 g, 0.96 mmol) to the pale yellow solution, the solution immediately coloured bright yellow. The solution was left to stir at RT for three hours. The reaction mixture was passed through an Al_2O_3 filter and the solvent removed *in vacuo*. The remaining product was used for reactions without further purification.

The method was followed according to the one proposed by Karmaker[9]. The $Re_2(CO)_9(NCMe)$ was dissolved in 20 ml DCM and a solution of **1b**, dissolved in DCM was added. The reaction mixture was allowed to stir at RT for 24 hours after which the solvent was removed *in vacuo*. A gradient silica gel column was used for product isolation with hexane and DCM as solvents. Unreacted reactants were isolated before the product was removed from the column.

Table 7.11 Product mass and yield of **15**

Complex	Colour	Molar mass (g/mol)	mass (g)	mmol	Yield (%)
15	red brown	1236.65	0.52	0.42	53

© University of Pretoria

7.4.3.4 Synthesis of $[Mn_2(CO)_9(P(C_4H_3O)_2(C_4H_2O\text{-}C(W(CO)_5)OCH_2CH_3))]$, 16

The same method was followed as in the synthesis of $[Re_2(CO)_9(P(C_4H_3O)_2\text{-}(C_4H_2O\text{-}C(W(CO)_5)OCH_2CH_3))]$. 0.90 g (1.5 mmol) **1b** was coordinated to 0.40 g (1.0 mmol) $[Mn_2(CO)_9(NCMe)]$.

Table 7.12 Product mass and yield of **16**

Complex	Colour	Molar mass (g/mol)	mass (g)	mmol	Yield (%)
16	red brown	974.11	0.38	0.39	39

7.4.4 Piggybacking of a tungsten-pentacarbonyl carbene substituent on group 10 transition metal complexes

7.4.4.1 Synthesis of $[PtCl_2(P(C_4H_3O)_2(C_4H_2O\text{-}C(W(CO)_5)OCH_2CH_3))_2]$ 17a, 17b.

$PtCl_2COD$ (0.24 g, 0.64 mmol) was dissolved in 20 ml DCM and added to a solution of **1b** (0.78 g, 1.3 mmol) dissolved in 10 ml DCM. The reaction mixture was allowed to stir for 18 hours at RT. Two products were isolated from silica gel column chromatography: the first with DCM (**17a**) and the second (**17b**) with dried, cold diethyl ether. Quantitative yields were obtained between the two products, forming 2:3 *trans* (**17a**) to *cis*- (**17b**) isomers of **17**.

Table 7.13 Product mass and yield of **17a** and **17b**

Complex		Colour	Molar mass (g/mol)	mass (g)	mmol	Yield (%)
17	**a**	brown-red	1490.28	0.57	0.38	60
	b	brown-red	1490.28	0.38	0.26	40

© University of Pretoria

7.4.4.2 Synthesis of [$PdCl_2(P(C_4H_3O)_2(C_4H_2O\text{-}C(W(CO)_5)OCH_2CH_3))_2$] 18a, 18b.

$PdCl_2$ (0.09 g, 0.5 mmol) was partially dissolved in 15 ml DCM and added to **1b** (1.14 g, 1.9 mmol) dissolved in 10 ml DCM and was allowed to stir for 4 hours. The products were separated on a gradient column with hexane and DCM as solvents. **18a** and **18b** was separated in a single fraction, followed by a fraction containing **18c**, **18d** and **18e**. These were all observed as separate products on analysis.

Table 7.14 Product mass and yield of **18a-e**

Complex		Colour	Molar mass (g/mol)	mass (g)	mmol	Yield (%)
18	a	brown-red	1401.62	0.43	0.31	62
	b					
	c	yellow	304.25	0.06	0.21	11
	d	yellow	576.50	0.03	0.06	3
	e					

7.4.4.3 Synthesis of [$Ni(\eta^2\text{-}COD)(P(C_4H_3O)_2(C_4H_2O\text{-}C(M(CO)_5)OCH_2CH_3))_2$] 19.

The method of synthesis was adapted from literature[3].

1b (0.47 g, 0.78 mmol) was dissolved in 25 ml DCM and added to a Schlenk containing $Ni(COD)_2$ (0.05 g, 0.20 mmol). The reaction mixture was allowed to stir for 18 hours. The dark brown product was isolated on a silica gel gradient column using hexane and DCM as solvents.

© University of Pretoria

Table 7.15 Product mass and yield of **19**

Complex	Colour	Molar mass (g/mol)	mass (g)	mmol	Yield (%)
19	orange	1391.19	0.10	0.07	35

7.4.5 Piggybacking of a tungsten-pentacarbonyl carbene substituent on group 11 transition metal complexes

7.4.5.1 Synthesis of [AuCl(P(C_4H_3O)$_2$(C_4H_2O-C(W(CO)$_5$)OCH_2CH_3))], 20a

Au(tht)Cl was prepared according to a literature procedure[4] and the reaction procedure was adapted from the reaction by Monkowius[5].

Au(tht)Cl (0.20 g, 0.63 mmol) was dissolved in 15 ml dry THF and placed in a cold bath at -78°C. **1b** (0.57 g, 0.95 mmol) dissolved in 10 ml THF was added to the cold solution and allowed to stir for two hours. The products were isolated on a gradient column (silica gel) with hexane and DCM as solvents. **20a** was removed from the column first, followed by a fraction containing **20b**, **c**, **d** and **e**. Yields in this fraction were determined from the integration of ^{1}H NMR spectrum.

Table 7.16 Product mass and yield of **20a-e**

Complex		Colour	Molar mass (g/mol)	mass (g)	mmol	Yield (%)
20	**a**	red-brown	844.57	0.36	0.43	68
	b	yellow	304.25	0.01	0.03	3
	c	yellow	260.19	0.01	0.04	4
	d	yellow	576.50	0.05	0.10	10
	e					

© University of Pretoria

7.4.5.2 Synthesis of [P(C$_4$H$_3$O)$_2$(C$_4$H$_2$O-C(AgBr)OCH$_2$CH$_3$)] (21a) and [AgCl(P(C$_4$H$_3$O)$_2$(C$_4$H$_2$O-C(AgBr)OCH$_2$CH$_3$))$_n$], 21 n = 1(b), 2(c), 3(d)

A adapted synthesis method by Cassel was followed[6].

$AgNO_3$ and $N(CH_3)_4Br$ was dried and partially dissolved in warm acetonitrile. **1b** dissolved in acetonitrile was added to the solution and allowed to stir until the Ag(0) started forming on the sides of the Schlenk. The reaction mixture was filtered through silica gel to give a red-orange filtrate. The products were separated on a dark silica gel column with DCM as eluent. Two fractions containing a mixture of the products were isolated; however it was possible to determine the ratios of the products in the reaction mixture from peak intensities from the ^{31}P NMR spectra.

Table 7.17 Product mass and yield of **21a-d**

Complex		Colour	Molar mass (g/mol)	mass (g)	mmol	Yield (%)
21	**a**	bright yellow	476.02	0.03	0.07	18
	b	bright yellow	663.77	0.06	0.08	21
	c	bright yellow	1139.81	0.14	0.12	31
	d	bright yellow	1615.83	0.18	0.11	28

7.4.5.3 Synthesis of [CuBr(P(C$_4$H$_3$O)$_2$(C$_4$H$_2$O-C(W(CO)$_5$)OCH$_2$CH$_3$))$_n$], 22a n=1-3

A literature procedure was followed[7].

1b (0.54 g, 0.90 mmol) was dissolved in hexane and added to a solution of CuBr (0.043 g, 0.300 mmol) dissolved in 20 ml DCM. The solution was refluxed for four hours and stirred for another 12 hours. The products were isolated as a mixture on a gradient column (silica gel) with hexane and DCM as solvents. Yield: 48%

© University of Pretoria

Synthesis of [CuCl(P(C_4H_3O)$_2$(C_4H_2O-C(W(CO)$_5$)OCH_2CH_3))$_n$], 22b n=1-3

Blue $CuCl_2.2H_2O$ (0.13 g, 0.75 mmol) was dried *in vacuo* while applying heat to form a brown powder. The powder was dissolved in 80 ml DCM and **1b** (0.40 g, 0.67 mmol), dissolved in DCM was added to the solution. The reaction mixture was refluxed for 30 minutes. The products were separated on a gradient silica gel column with hexane and DCM as solvents. Quantitative product yield was obtained.

7.5 Mass spectral data

Complex	m/z	Intensity (%)	Fragment ion
1b	651	68	[M + K]+
7b	597	50	[M - CO]+
8b	1005	5	[M]+
9b	1388	1	[M+H]+
10b	660	2	[M+Na]+
11b	637	3	[M]+
11c	637	4	[M]+
15	1236	4	[M]+
16	997	6	[M + Na]+
17a	1490	5	[M - Cl]+
18a	1401	15	[M]+
19	1282	3	[M - COD]+
20a	845	8	[M]+
21a	476	7	[M + Na]+
21b	664	21	[M + Na]+
21c	1140	5	[M + Na]+

© University of Pretoria

7.6 References

1. H. Meerwein. TRIETHYLOXONIUM FLUOBORATE. *Org. Synth.* (1966) **46,** 113.

2. H. C. Clark and L. E. Manzer. Reactions of (π-1,5-cyclooctadiene) organoplatinum(II) compounds and the synthesis of perfluoroalkylplatinum complexes. *J. Organomet. Chem.* (1973) **59,** 411–428.

3. R. J. Angelici. *Inorganic Syntheses, Volume 28, Reagents for Transition Metal Complex and Organometallic Syntheses*. (1991) 102.

4. E. Matoušová, A. Růžička, Jiří Kuneš, Jarmila Králová and Milan Pour. TFP as a ligand in Au(I)-catalyzed dihydropyran synthesis. Unprecedented rearrangement of dihydropyrans into cyclopentenones. *Chem. Commun.* (2011) **47,** 9390–9392.

5. U. Monkowius, S. Nogai and H. Schmidbaur. Ligand Properties of Tri(2-thienyl)- and Tri(2-furyl)phosphine and -arsine $(2\text{-}C_4H_3E)_3$ P/As (E = O, S) in Gold(I) Complexes. *Z. Naturforsch.* (2003) **58b,** 751 – 758.

6. A. Cassel. Chlorotris(triphenylphosphine)silver. *Acta. Crystallogr., Sect B* (1981) **37,** 229–231.

7. P. F. Barron, J. C. Dyason, P. C. Healy, L. M. Engelhardt, C. Pakawatchai, V. A. Patrick and A. H. White. Lewis-base adducts of Group 11 metal(I) compounds. Part 28. Solid-state phosphorus-31 cross-polarization magic-angle spinning nuclear magnetic resonance and structural studies on the mononuclear 3: 1 adducts of triphenylphosphine with copper(I) halides. *J. Chem. Soc., Dalton Trans.* (1987) 1099–1106.

8. U. Koelle. Aminoxidinduzierte ligandensubstitution anübergangsmetallcarbonylen. II. *J. Organomet. Chem.* (1978) **155,** 53–62.

9. S. Karmaker, S. Ghosh, S. E. Kabir, D. T. Haworth and S. V. Lindeman. Reactivity of tri(2-furyl)phosphine (PFu_3) with $[Mn_2(CO)_{10}–n(NCMe)_n]$ (n = 0–2): X-ray Structure of mer-$[Mn(CO)_3(\eta^1\text{-}C_4H_3O)(PFu_3)_2]$. *Inorg. Chim. Acta* (2012) **382,** 199–202.

© University of Pretoria

Appendix A

Crystallographic data of complex 1b

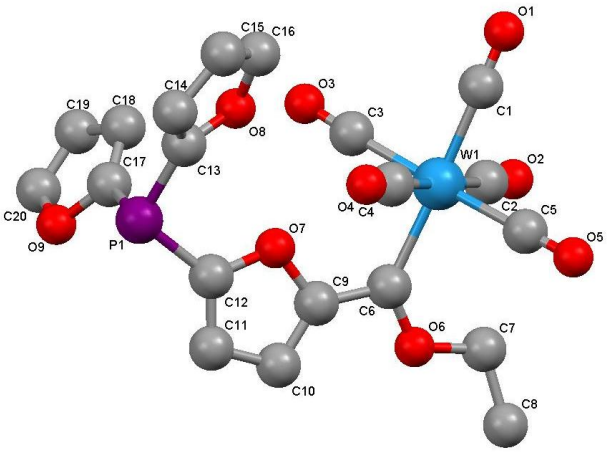

Table A.1 Crystal data and structure refinement

Emperical formula	$C_{20}H_{14}O_9PW$		
Formula weight	613.13 g/mol		
Temperature	150(2) K		
Wavelength	0.71073		
Crystal system	monoclinic		
Space group	C2/c		
Unit cell dimensions	**a** 40.3819(18) Å	**α** 90°	
	b 7.6045(3) Å	**β** 93.651(3)°	
	c 13.7313(6) Å	**γ** 90°	
Volume	4208.1(3) $Å^3$		
Z	8		
Density (calculated)	1.936 Mg/m^3		
Absorption coefficient	5.616 mm^{-1}		
F(000)	2360		
Crystal size	0.264 x 0.088 x 0.071 mm^3		
Theta range for data collection	2.725 to 37.517		
Index ranges	-67 ≤ h ≤ 67	-12 ≤ k ≤ 12	-22 ≤ l ≤ 22
Reflections collected	10217		
Independent reflections	9118 [R(int) = 0.0445]		
Completeness to theta = 25.00°	100%		

© University of Pretoria

Refinement method	Full-matrix least squares on F^2
Data / restraints / parameters	10217 / 0 / 336
Goodness of fit on F2	1.112
Final R indices [I>2sigma(I)]	R1 = 0.0363
R indices (all data)	R1 = 0.0274 wR2 = 0.0541
Largest diff. peak and hole	2.348 and -0.474 e.Å^{-3}

Table A.2 Atomic coordinates (x10^4) and equivalent isotropic displacement paramenters (Å^2 x 10^3)
U_{eq} is difined as one third of the trace of the orthogonalized U^{ij} tensor

Atom	x	y	z	Ueq
W1	673(2)	365(2)	9927(2)	17(1)
C1	393(5)	-1546(3)	9251(1)	25(1)
O1	237(4)	-2620(2)	8860(1)	41(1)
C2	330(4)	2196(3)	9435(1)	24(1)
O2	134(4)	3178(2)	9145(1)	35(1)
C3	913(5)	667(3)	8666(1)	25(1)
O3	1038(4)	811(3)	7950(1)	41(1)
C4	1013(4)	-1491(3)	10412(1)	23(1)
O4	1199(4)	-2530(2)	10690(1)	36(1)
C5	434(5)	-27(3)	11177(1)	23(1)
O5	304(4)	-293(2)	11879(1)	37(1)
C6	996(4)	2308(2)	10652(1)	20(1)
O6	932(3)	3653(1)	11227(1)	30(1)
C7	593(5)	4219(4)	11344(2)	41(1)
C8	595(6)	5387(3)	12210(1)	34(1)
P1	2103(2)	-52(7)	9429(1)	22(1)
O7	1493(3)	1067(1)	10025(1)	20(1)
C9	1357(4)	2269(2)	10634(1)	19(1)
C10	1606(4)	3179(3)	11130(1)	23(1)
C11	1909(4)	2497(3)	10832(1)	24(1)
C12	1830(4)	1219(2)	10157(1)	19(1)
O8	1543(3)	-1835(1)	8699(1)	27(1)
C13	1863(5)	-1963(2)	9101(1)	23(1)
C14	1949(6)	-3690(3)	9177(1)	29(1)

© University of Pretoria

C15	1671(7)	-4683(3)	8810(1)	32(1)
C16	1435(6)	-3524(3)	8534(1)	30(1)
O9	2296(4)	2489(2)	8245(1)	36(1)
C17	2062(4)	1178(2)	8297(1)	22(1)
C18	1866(6)	1150(3)	7458(1)	29(1)
C19	1982(6)	2504(3)	6849(1)	35(1)
C20	2236(6)	3261(4)	7347(1)	41(1)

Table A.3 Bond lengths [Å] and angles [°]

W1-C1	2.031(2)	W1-C3-O3	177.9(2)
W1-C2	2.050(2)	W1-C4-O4	179.1(2)
W1-C3	2.051(2)	W1-C5-O5	178.0(2)
W1-C4	2.050(2)	W1-C6-O6	131.5(1)
W1-C5	2.045(2)	W1-C6-C9	123.4(1)
W1-C6	2.171(2)	O6-C6-C9	105.0(1)
C1-O1	1.143(3)	C6-O6-C7	121.0(2)
C2-O2	1.140(2)	O6-C7-H7A	105(2)
C3-O3	1.139(3)	O6-C7-H7B	107(2)
C4-O4	1.139(2)	O6-C7-C8	108.0(2)
C5-O5	1.144(3)	H7A-C7-H7B	108(3)
C6-O6	1.327(2)	H7A-C7-C8	109(2)
C6-C9	1.460(2)	H7B-C7-C8	118(2)
O6-C7	1.455(3)	C7-C8-H8A	108(2)
C7-H7A	0.91(4)	C7-C8-H8B	111(2)
C7-H7B	0.95(4)	C7-C8-H8C	109(2)
C7-C8	1.484(4)	H8A-C8-H8B	100(3)
C8-H8A	0.92(4)	H8A-C8-H8C	112(3)
C8-H8B	0.99(3)	H8B-C8-H8C	116(3)
C8-H8C	0.91(4)	H1-P1-C12	119.7(9)
P1-H1	1.30(2)	H1-P1-C13	119.6(9)
P1-C12	1.812(2)	H1-P1-C17	110.1(9)
P1-C13	1.789(2)	C12-P1-C13	103.54(8)
P1-C17	1.812(2)	C12-P1-C17	99.99(8)
O7-C9	1.376(2)	C13-P1-C17	100.68(8)
O7-C12	1.366(2)	C9-O7-C12	107.2(1)
C9-C10	1.366(2)	C6-C9-O7	117.5(1)

© University of Pretoria

C10-H10	0.89(3)	C6-C9-C10	133.2(2)
C10-C11	1.412(2)	O7-C9-C10	109.2(1)
C11-H11	0.90(2)	C9-C10-H10	125(2)
C11-C12	1.366(3)	C9-C10-C11	107.0(2)
O8-C13	1.376(2)	H10-C10-C11	128(2)
O8-C16	1.371(3)	C10-C11-H11	129(1)
C13-C14	1.361(3)	C10-C11-C12	106.9(2)
C14-H14	0.92(3)	H11-C11-C12	124(1)
C14-C15	1.419(3)	P1-C12-O7	121.1(1)
C15-H15	0.91(3)	P1-C12-C11	129.1(1)
C15-C16	1.335(3)	O7-C12-C11	109.6(1)
C16-H16	0.95(3)	C13-O8-C16	106.3(1)
O9-C17	1.379(2)	P1-C13-O8	121.6(1)
O9-C20	1.372(3)	P1-C13-C14	129.2(2)
C17-C18	1.355(3)	O8-C13-C14	109.2(2)
C18-H18	0.85(3)	C13-C14-H14	127(2)
C18-C19	1.424(3)	C13-C14-C15	107.0(2)
C19-H19	0.88(3)	H14-C14-C15	126(2)
C19-C20	1.330(3)	C14-C15-H15	129(2)
C20-H20	0.85(3)	C14-C15-C16	106.5(2)
		H15-C15-C16	124(2)
C1-W1-C2	89.37(8)	O8-C16-C15	111.0(2)
C1-W1-C3	88.51(8)	O8-C16-H16	118(2)
C1-W1-C4	89.93(8)	C15-C16-H16	131(2)
C1-W1-C5	89.99(8)	C17-O9-C20	105.9(2)
C1-W1-C6	176.84(8)	P1-C17-O9	113.1(1)
C2-W1-C3	89.53(8)	P1-C17-C18	137.4(1)
C2-W1-C4	179.30(8)	O9-C17-C18	109.4(2)
C2-W1-C5	91.68(8)	C17-C18-H18	127(2)
C2-W1-C6	93.61(7)	C17-C18-C19	107.0(2)
C3-W1-C4	90.52(8)	H18-C18-C19	126(2)
C3-W1-C5	178.06(9)	C18-C19-H19	129(2)
C3-W1-C6	90.48(7)	C18-C19-C20	106.4(2)
C4-W1-C5	88.25(8)	H19-C19-C20	125(2)
C4-W1-C6	87.09(7)	O9-C20-C19	111.3(2)
C5-W1-C6	90.95(7)	O9-C20-H20	118(2)

© University of Pretoria

W1-C1-O1	179.1(2)	C19-C20-H20	131(2)
W1-C2-O2	178.0(2)		

Table A.4 Anisotropic displacement parameters ($Å^2 \times 10^3$)
The anisotropic displacement factor exponent takes the form: $-2p^2[h^2a^{*2}U^{11} + \ldots + 2hka^*b^*U^{12}]$

Atom	U11	U22	U33	U23	U13	U12
W1	13(1)	19(1)	21(1)	-2(1)	2(1)	(1)
C1	21(1)	25(1)	30(1)	-4(1)	2(1)	-1(1)
O1	36(1)	34(1)	53(1)	-16(1)	1(1)	-9(1)
C2	18(1)	25(1)	29(1)	0(1)	2(1)	-2(1)
O2	28(1)	32(1)	44(1)	6(1)	-2(1)	6(1)
C3	19(1)	29(1)	26(1)	4(1)	1(1)	4(1)
O3	31(1)	65(1)	29(1)	14(1)	8(1)	14(1)
C4	19(1)	25(1)	26(1)	0(1)	6(1)	-1(1)
O4	33(1)	33(1)	44(1)	12(1)	9(1)	10(1)
C5	17(1)	25(1)	26(1)	-2(1)	2(1)	1(1)
O5	32(1)	49(1)	30(1)	3(1)	11(1)	3(1)
C6	17(1)	20(1)	25(1)	-4(1)	3(1)	0(1)
O6	18(1)	29(1)	45(1)	-18(1)	7(1)	0(1)
C7	20(1)	41(1)	62(1)	-28(1)	6(1)	5(1)
C8	33(1)	36(1)	33(1)	-7(1)	9(1)	7(1)
P1	16(1)	25(1)	24(1)	0(1)	4(1)	3(1)
O7	14(1)	22(1)	24(1)	-6(1)	3(1)	0(1)
C9	16(1)	19(1)	21(1)	-3(1)	4(1)	0(1)
C10	21(1)	25(1)	23(1)	-6(1)	4(1)	-4(1)
C11	16(1)	30(1)	25(1)	-4(1)	1(1)	-4(1)
C12	14(1)	23(1)	20(1)	1(1)	1(1)	(1)
O8	24(1)	23(1)	33(1)	-1(1)	(1)	1(1)
C13	23(1)	24(1)	21(1)	1(1)	4(1)	4(1)
C14	35(1)	24(1)	27(1)	1(1)	1(1)	9(1)
C15	50(1)	21(1)	27(1)	-2(1)	6(1)	1(1)
C16	33(1)	27(1)	30(1)	-5(1)	5(1)	-6(1)
O9	23(1)	42(1)	43(1)	11(1)	4(1)	-9(1)
C17	19(1)	22(1)	26(1)	1(1)	9(1)	1(1)
C18	37(1)	25(1)	24(1)	-2(1)	2(1)	-3(1)

© University of Pretoria

C19	49(1)	33(1)	24(1)	4(1)	12(1)	5(1)
C20	37(1)	41(1)	46(1)	16(1)	17(1)	-4(1)

Table A.5 Hydrogen coordinates (x 10^4) and isotropic displacement paramenters (Å^2 x 10^3)

Atom	x	y	z	Ueq
H7A	479(8)	3220(5)	11470(2)	15718(1)
H7B	508(10)	4670(5)	10730(3)	14704(1)
H8A	636(8)	4710(4)	12760(3)	17486(1)
H8B	367(8)	5810(4)	12320(2)	16883(1)
H8C	751(8)	6240(5)	12150(2)	16650(1)
H10	1576(6)	4000(4)	11574(18)	15860(1)
H11	2119(6)	2740(3)	11060(16)	15156(1)
H14	2151(7)	-4140(4)	9390(2)	12868(1)
H15	1641(7)	-5870(4)	8810(2)	12073(1)
H16	1215(7)	-3700(4)	8266(19)	11327(1)
H18	1699(9)	480(4)	7330(2)	10045(1)
H19	1909(6)	2790(4)	6249(19)	8563(1)
H20	2365(8)	4080(4)	7190(2)	9853(1)

Table A.6 Torsion angles [°]

C2-W1-C1-O1	95(12)	H1-P1-C13-C14	6(1)
C3-W1-C1-O1	5(12)	C12-P1-C13-O8	50.6(2)
C4-W1-C1-O1	-85(12)	C12-P1-C13-C14	-130.2(2)
C5-W1-C1-O1	-173(12)	C17-P1-C13-O8	-52.6(2)
C6-W1-C1-O1	-66(13)	C17-P1-C13-C14	126.7(2)
C1-W1-C2-O2	-8(5)	H1-P1-C17-O9	-36(1)
C3-W1-C2-O2	80(5)	H1-P1-C17-C18	142(1)
C4-W1-C2-O2	-13(10)	C12-P1-C17-O9	91.1(1)
C5-W1-C2-O2	-98(5)	C12-P1-C17-C18	-90.7(2)
C6-W1-C2-O2	171(5)	C13-P1-C17-O9	-162.9(1)
C1-W1-C3-O3	21(5)	C13-P1-C17-C18	15.3(2)
C2-W1-C3-O3	-69(5)	C12-O7-C9-C6	-177.6(1)
C4-W1-C3-O3	111(5)	C12-O7-C9-C10	0.8(2)
C5-W1-C3-O3	60(6)	C9-O7-C12-P1	-176.1(1)

© University of Pretoria

C6-W1-C3-O3	-162(5)	C9-O7-C12-C11	-0.3(2)
C1-W1-C4-O4	-72(11)	C6-C9-C10-H10	-0(2)
C2-W1-C4-O4	-67(14)	C6-C9-C10-C11	177.1(2)
C3-W1-C4-O4	-160(11)	O7-C9-C10-H10	-178(2)
C5-W1-C4-O4	18(11)	O7-C9-C10-C11	-1.0(2)
C6-W1-C4-O4	109(11)	C9-C10-C11-H11	-174(2)
C1-W1-C5-O5	67(5)	C9-C10-C11-C12	0.8(2)
C2-W1-C5-O5	157(5)	H10-C10-C11-H11	3(3)
C3-W1-C5-O5	28(7)	H10-C10-C11-C12	178(2)
C4-W1-C5-O5	-23(5)	C10-C11-C12-P1	175.0(1)
C6-W1-C5-O5	-110(5)	C10-C11-C12-O7	-0.3(2)
C1-W1-C6-O6	-154(1)	H11-C11-C12-P1	-10(2)
C1-W1-C6-C9	22(1)	H11-C11-C12-O7	175(2)
C2-W1-C6-O6	45.6(2)	C16-O8-C13-P1	179.7(1)
C2-W1-C6-C9	-139.0(1)	C16-O8-C13-C14	0.2(2)
C3-W1-C6-O6	135.2(2)	C13-O8-C16-C15	-0.2(2)
C3-W1-C6-C9	-49.5(1)	C13-O8-C16-H16	179(2)
C4-W1-C6-O6	-134.3(2)	P1-C13-C14-H14	-3(2)
C4-W1-C6-C9	41.0(1)	P1-C13-C14-C15	-179.6(2)
C5-W1-C6-O6	-46.1(2)	O8-C13-C14-H14	177(2)
C5-W1-C6-C9	129.2(1)	O8-C13-C14-C15	-0.2(2)
W1-C6-O6-C7	-10.3(3)	C13-C14-C15-H15	-174(2)
C9-C6-O6-C7	173.7(2)	C13-C14-C15-C16	0.1(3)
W1-C6-C9-O7	8.4(2)	H14-C14-C15-H15	9(3)
W1-C6-C9-C10	-169.6(2)	H14-C14-C15-C16	-177(2)
O6-C6-C9-O7	-175.2(1)	C14-C15-C16-O8	0.0(3)
O6-C6-C9-C10	6.8(3)	C14-C15-C16-H16	-179(2)
C6-O6-C7-H7A	49(2)	H15-C15-C16-O8	174(2)
C6-O6-C7-H7B	-66(3)	H15-C15-C16-H16	-5(3)
C6-O6-C7-C8	164.9(2)	C20-O9-C17-P1	178.8(1)
O6-C7-C8-H8A	-71(2)	C20-O9-C17-C18	0.1(2)
O6-C7-C8-H8B	180(2)	C17-O9-C20-C19	-0.1(3)
O6-C7-C8-H8C	52(2)	C17-O9-C20-H20	-178(2)
H7A-C7-C8-H8A	43(3)	P1-C17-C18-H18	4(3)
H7A-C7-C8-H8B	-66(3)	P1-C17-C18-C19	-178.3(2)
H7A-C7-C8-H8C	165(3)	O9-C17-C18-H18	-177(3)

© University of Pretoria

H7B-C7-C8-H8A	167(4)	O9-C17-C18-C19	-0.0(2)
H7B-C7-C8-H8B	58(3)	C17-C18-C19-H19	178(2)
H7B-C7-C8-H8C	-71(3)	C17-C18-C19-C20	-0.1(3)
H1-P1-C12-O7	-163(1)	H18-C18-C19-H19	-5(3)
H1-P1-C12-C11	22(1)	H18-C18-C19-C20	177(3)
C13-P1-C12-O7	-27.0(2)	C18-C19-C20-O9	0.1(3)
C13-P1-C12-C11	158.1(2)	C18-C19-C20-H20	177(3)
C17-P1-C12-O7	76.7(1)	H19-C19-C20-O9	-178(2)
C17-P1-C12-C11	-98.2(2)	H19-C19-C20-H20	-0(3)
H1-P1-C13-O8	-173(1)		

© University of Pretoria

Appendix B

Crystallographic data of complex 7a

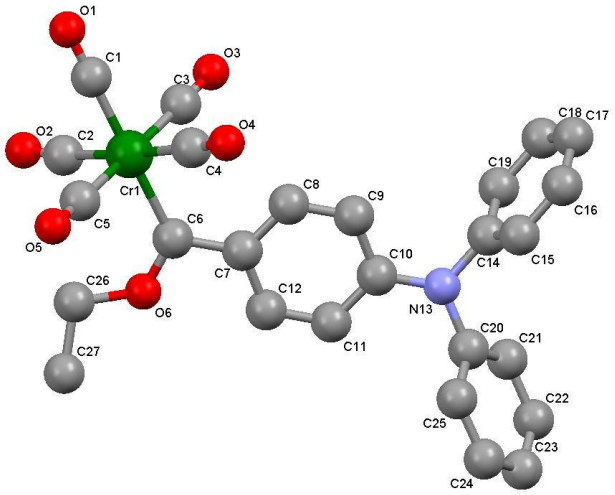

Table B.1 Crystal data and structure refinement

Emperical formula	$C_{26}H_{19}CrNO_6$		
Formula weight	493.42 g/mol		
Temperature	100(2) K		
Wavelength	0.71073		
Crystal system	triclinic		
Space group	P - 1		
Unit cell dimensions	**a** 9.2423(6) Å	**α** 82.9800(10)°	
	b 9.7790(7) Å	**β** 71.6530(10)°	
	c 13.6276(9) Å	**γ** 82.6000(10)°	
Volume	1154.95(14) $Å^3$		
Z	2		
Density (calculated)	1.419 Mg/m^3		
Absorption coefficient	0.538 mm^{-1}		
F(000)	508		
Crystal size	0.36 x 0.26 x 0.18 mm^3		
Theta range for data collection	2.77 to 28.34		
Index ranges	$-12 \leq h \leq 12$	$-12 \leq k \leq 12$	$-18 \leq l \leq 17$
Reflections collected	5513		
Independent reflections	4656 [R(int) = 0.0445]		

© University of Pretoria

Completeness to theta = 25.00°	91.7%
Refinement method	Full-matrix least squares on F^2
Data / restraints / parameters	5513 / 0 / 308
Goodness of fit on F2	1.053
Final R indices [I>2sigma(I)]	R1 = 0.0369
R indices (all data)	R1 = 0.0457 wR2 = 0.0929
Largest diff. peak and hole	0.353 and -0.379 e.Å^{-3}

Table B.2 Atomic coordinates (x10^4) and equivalent isotropic displacement paramenters (Å^2 x 10^3) U_{eq} is difined as one third of the trace of the orthogonalized U^{ij} tensor

Label	x	y	z	Ueq
Cr1	2004(3)	2128(3)	859(2)	17(1)
C1	226(2)	1670(1)	643(1)	21(1)
O1	-875(1)	1435(1)	502(1)	28(1)
C2	1930(1)	3644(1)	-152(1)	21(1)
O2	1754(1)	4541(1)	-737(1)	28(1)
C3	725(2)	3243(1)	1899(1)	21(1)
O3	-95(1)	3897(1)	2525(1)	31(1)
C4	1958(2)	552(2)	1835(1)	26(1)
O4	1910(2)	-426(1)	2392(1)	43(1)
C5	3213(2)	892(1)	-134(1)	22(1)
O5	3886(1)	77(1)	-682(1)	31(1)
C6	3940(1)	2725(1)	1122(1)	17(1)
O6	5166(1)	3192(1)	412(1)	20(1)
C7	4210(1)	2737(1)	2135(1)	16(1)
C8	3138(1)	2306(1)	3071(1)	18(1)
C9	3397(1)	2255(1)	4016(1)	18(1)
C10	4769(1)	2658(1)	4085(1)	17(1)
C11	5851(1)	3116(1)	3156(1)	18(1)
C12	5578(1)	3144(1)	2217(1)	18(1)
N13	5014(1)	2619(1)	5035(1)	19(1)
C14	3825(1)	2259(1)	5981(1)	18(1)
C15	3910(2)	936(1)	6464(1)	24(1)
C16	2759(2)	561(2)	7359(1)	26(1)

© University of Pretoria

C17	1538(2)	1512(2)	7766(1)	23(1)
C18	1469(2)	2838(1)	7289(1)	22(1)
C19	2616(2)	3221(1)	6390(1)	20(1)
C20	6487(1)	2741(1)	5138(1)	18(1)
C21	6636(2)	3787(1)	5692(1)	22(1)
C22	8048(2)	3915(2)	5807(1)	26(1)
C23	9297(2)	3004(2)	5379(1)	28(1)
C24	9143(2)	1949(2)	4841(1)	26(1)
C25	7735(2)	1812(1)	4714(1)	22(1)
C26	5430(2)	3289(2)	-701(1)	24(1)
C27	7103(2)	3464(2)	-1198(1)	26(1)

Table B.3 Bond lengths [Å] and angles [°]

Cr1-C1	1.875(2)	Cr1-C5-O5	175.1(2)
Cr1-C2	1.906(2)	Cr1-C6-O6	126.9(1)
Cr1-C3	1.893(2)	Cr1-C6-C7	127.2(1)
Cr1-C4	1.904(2)	O6-C6-C7	105.9(1)
Cr1-C5	1.908(2)	C6-O6-C26	124.9(1)
Cr1-C6	2.096(2)	C6-C7-C8	121.8(2)
C1-O1	1.149(3)	C6-C7-C12	122.2(2)
C2-O2	1.143(2)	C8-C7-C12	116.0(2)
C3-O3	1.146(2)	C7-C8-H8	118.7(2)
C4-O4	1.142(2)	C7-C8-C9	122.6(2)
C5-O5	1.143(2)	H8-C8-C9	118.7(2)
C6-O6	1.328(2)	C8-C9-H9	119.6(2)
C6-C7	1.480(3)	C8-C9-C10	120.7(2)
O6-C26	1.452(2)	H9-C9-C10	119.7(2)
C7-C8	1.402(2)	C9-C10-C11	117.6(2)
C7-C12	1.413(3)	C9-C10-N13	120.4(2)
C8-H8	0.950(2)	C11-C10-N13	121.9(2)
C8-C9	1.377(3)	C10-C11-H11	119.6(2)
C9-H9	0.950(1)	C10-C11-C12	120.7(2)
C9-C10	1.408(3)	H11-C11-C12	119.6(2)
C10-C11	1.408(2)	C7-C12-C11	122.3(2)
C10-N13	1.378(3)	C7-C12-H12	118.9(2)
C11-H11	0.950(2)	C11-C12-H12	118.8(2)

© University of Pretoria

C11-C12	1.377(3)	C10-N13-C14	120.5(1)
C12-H12	0.950(1)	C10-N13-C20	122.6(1)
N13-C14	1.446(2)	C14-N13-C20	116.3(1)
N13-C20	1.434(3)	N13-C14-C15	119.0(2)
C14-C15	1.382(2)	N13-C14-C19	120.4(2)
C14-C19	1.382(2)	C15-C14-C19	120.6(2)
C15-H15	0.950(2)	C14-C15-H15	120.1(2)
C15-C16	1.389(2)	C14-C15-C16	119.8(2)
C16-H16	0.951(2)	H15-C15-C16	120.1(2)
C16-C17	1.381(2)	C15-C16-H16	120.1(2)
C17-H17	0.950(2)	C15-C16-C17	119.9(2)
C17-C18	1.381(3)	H16-C16-C17	120.0(2)
C18-H18	0.950(2)	C16-C17-H17	120.0(2)
C18-C19	1.392(2)	C16-C17-C18	120.1(2)
C19-H19	0.950(2)	H17-C17-C18	119.9(2)
C20-C21	1.387(3)	C17-C18-H18	119.8(2)
C20-C25	1.388(2)	C17-C18-C19	120.4(2)
C21-H21	0.950(2)	H18-C18-C19	119.8(2)
C21-C22	1.386(3)	C14-C19-C18	119.2(2)
C22-H22	0.950(2)	C14-C19-H19	120.4(2)
C22-C23	1.380(2)	C18-C19-H19	120.4(2)
C23-H23	0.950(2)	N13-C20-C21	118.7(2)
C23-C24	1.382(3)	N13-C20-C25	120.8(2)
C24-H24	0.950(2)	C21-C20-C25	120.5(2)
C24-C25	1.391(3)	C20-C21-H21	120.2(2)
C25-H25	0.950(2)	C20-C21-C22	119.6(2)
C26-H26A	0.990(2)	H21-C21-C22	120.2(2)
C26-H26B	0.990(2)	C21-C22-H22	119.8(2)
C26-C27	1.503(2)	C21-C22-C23	120.2(2)
C27-H27A	0.979(2)	H22-C22-C23	119.9(2)
C27-H27B	0.980(2)	C22-C23-H23	119.9(2)
C27-H27C	0.981(2)	C22-C23-C24	120.2(2)
		H23-C23-C24	119.9(2)
C1-Cr1-C2	85.39(8)	C23-C24-H24	119.9(2)
C1-Cr1-C3	87.81(8)	C23-C24-C25	120.2(2)

© University of Pretoria

C1-Cr1-C4	90.07(8)	H24-C24-C25	119.9(2)
C1-Cr1-C5	89.85(8)	C20-C25-C24	119.3(2)
C1-Cr1-C6	177.43(7)	C20-C25-H25	120.4(2)
C2-Cr1-C3	88.95(8)	C24-C25-H25	120.3(2)
C2-Cr1-C4	175.34(8)	O6-C26-H26A	110.5(2)
C2-Cr1-C5	94.36(8)	O6-C26-H26B	110.5(2)
C2-Cr1-C6	93.33(7)	O6-C26-C27	106.4(1)
C3-Cr1-C4	91.92(8)	H26A-C26-H26B	108.7(2)
C3-Cr1-C5	175.79(8)	H26A-C26-C27	110.4(2)
C3-Cr1-C6	89.94(7)	H26B-C26-C27	110.4(2)
C4-Cr1-C5	84.57(8)	C26-C27-H27A	109.5(2)
C4-Cr1-C6	91.25(8)	C26-C27-H27B	109.5(2)
C5-Cr1-C6	92.47(8)	C26-C27-H27C	109.5(2)
Cr1-C1-O1	177.8(2)	H27A-C27-H27B	109.5(2)
Cr1-C2-O2	174.1(2)	H27A-C27-H27C	109.5(2)
Cr1-C3-O3	177.5(2)	H27B-C27-H27C	109.4(2)
Cr1-C4-O4	176.9(2)		

Table B.4 Anisotropic displacement parameters ($Å^2$ x 10^3). The anisotropic displacement factor exponent takes the form: $-2p^2[h^2a^{*2}U^{11} + \ldots + 2hka^*b^*U^{12}]$

Atom	U11	U22	U33	U23	U13	U12
Cr1	18(1)	19(1)	16(1)	1(1)	-7(1)	-4(1)
C1	25(1)	22(1)	16(1)	3(1)	-5(1)	-4(1)
O1	22(1)	39(1)	28(1)	4(1)	-11(1)	-12(1)
C2	17(1)	26(1)	20(1)	-3(1)	-6(1)	-4(1)
O2	28(1)	31(1)	26(1)	8(1)	-11(1)	-4(1)
C3	22(1)	22(1)	20(1)	5(1)	-8(1)	-4(1)
O3	31(1)	32(1)	24(1)	-1(1)	-4(1)	4(1)
C4	32(1)	25(1)	25(1)	-2(1)	-13(1)	-7(1)
O4	72(1)	28(1)	36(1)	10(1)	-28(1)	-15(1)
C5	20(1)	25(1)	26(1)	-1(1)	-13(1)	-4(1)
O5	28(1)	33(1)	36(1)	-13(1)	-14(1)	3(1)
C6	18(1)	14(1)	16(1)	(1)	-4(1)	-1(1)
O6	20(1)	27(1)	12(1)	1(1)	-4(1)	-8(1)

© University of Pretoria

C7	17(1)	17(1)	15(1)	-1(1)	-6(1)	-1(1)
C8	15(1)	22(1)	17(1)	-1(1)	-5(1)	-5(1)
C9	16(1)	24(1)	14(1)	(1)	-3(1)	-5(1)
C10	16(1)	19(1)	15(1)	-3(1)	-5(1)	1(1)
C11	14(1)	23(1)	17(1)	(1)	-5(1)	-4(1)
C12	17(1)	19(1)	15(1)	(1)	-2(1)	-4(1)
N13	13(1)	32(1)	13(1)	-1(1)	-3(1)	-5(1)
C14	17(1)	26(1)	12(1)	-1(1)	-6(1)	-5(1)
C15	24(1)	24(1)	22(1)	-4(1)	-5(1)	2(1)
C16	34(1)	21(1)	22(1)	3(1)	-8(1)	-4(1)
C17	25(1)	30(1)	14(1)	(1)	-3(1)	-8(1)
C18	19(1)	27(1)	18(1)	-3(1)	-3(1)	-1(1)
C19	19(1)	22(1)	19(1)	2(1)	-6(1)	-3(1)
C20	17(1)	24(1)	14(1)	3(1)	-6(1)	-6(1)
C21	24(1)	24(1)	18(1)	1(1)	-7(1)	-4(1)
C22	31(1)	32(1)	19(1)	(1)	-10(1)	-13(1)
C23	22(1)	43(1)	23(1)	6(1)	-11(1)	-12(1)
C24	17(1)	35(1)	23(1)	2(1)	-5(1)	-1(1)
C25	21(1)	25(1)	19(1)	-1(1)	-6(1)	-4(1)
C26	25(1)	36(1)	12(1)	1(1)	-5(1)	-10(1)
C27	24(1)	34(1)	17(1)	-1(1)	-2(1)	-6(1)

Table B.5 Hydrogen coordinates (x 10^4) and isotropic displacement paramenters (Å^2 x 10^3)

Label	x	y	z	Ueq
H8	2196(1)	2039(1)	3051(1)	3932(1)
H9	2642(1)	1944(1)	4629(1)	5965(1)
H11	6781(1)	3408(1)	3178(1)	4095(1)
H12	6334(1)	3449(1)	1603(1)	2066(1)
H15	4754(1)	285(1)	6184(1)	7969(1)
H16	2811(1)	-349(1)	7692(1)	9912(1)
H17	745(1)	1254(1)	8374(1)	10791(1)
H18	634(1)	3493(1)	7576(1)	9763(1)
H19	2568(1)	4133(1)	6062(1)	7812(1)
H21	5775(1)	4411(1)	5990(1)	7719(1)
H22	8156(1)	4633(1)	6183(1)	7967(1)
H23	10265(1)	3103(1)	5454(1)	7028(1)

© University of Pretoria

H24	10002(1)	1315(1)	4557(1)	5872(1)
H25	7629(1)	1091(1)	4341(1)	5594(1)
H26A	4795(1)	4092(1)	-916(1)	-1180(1)
H26B	5168(1)	2438(1)	-906(1)	-1167(1)
H27A	7335(1)	4331(1)	-1015(1)	-1308(1)
H27B	7350(1)	3488(1)	-1954(1)	-2518(1)
H27C	7716(1)	2685(1)	-950(1)	-1224(1)

Table B.6 Torsion angles [°]

C2-Cr1-C1-O1	-28(4)	C10-C11-C12-H12	-179.3(2)
C3-Cr1-C1-O1	62(4)	H11-C11-C12-C7	-179.3(2)
C4-Cr1-C1-O1	154(4)	H11-C11-C12-H12	0.7(3)
C5-Cr1-C1-O1	-122(4)	C10-N13-C14-C15	101.3(2)
C6-Cr1-C1-O1	33(5)	C10-N13-C14-C19	-78.1(2)
C1-Cr1-C2-O2	23(2)	C20-N13-C14-C15	-70.5(2)
C3-Cr1-C2-O2	-65(2)	C20-N13-C14-C19	110.1(2)
C4-Cr1-C2-O2	36(2)	C10-N13-C20-C21	123.1(2)
C5-Cr1-C2-O2	112(2)	C10-N13-C20-C25	-58.4(2)
C6-Cr1-C2-O2	-155(2)	C14-N13-C20-C21	-65.2(2)
C1-Cr1-C3-O3	10(4)	C14-N13-C20-C25	113.2(2)
C2-Cr1-C3-O3	95(4)	N13-C14-C15-H15	1.6(3)
C4-Cr1-C3-O3	-80(4)	N13-C14-C15-C16	-178.4(2)
C5-Cr1-C3-O3	-47(4)	C19-C14-C15-H15	-178.9(2)
C6-Cr1-C3-O3	-172(4)	C19-C14-C15-C16	1.0(3)
C1-Cr1-C4-O4	39(3)	N13-C14-C19-C18	178.6(2)
C2-Cr1-C4-O4	26(4)	N13-C14-C19-H19	-1.4(3)
C3-Cr1-C4-O4	127(3)	C15-C14-C19-C18	-0.9(3)
C5-Cr1-C4-O4	-50(3)	C15-C14-C19-H19	179.1(2)
C6-Cr1-C4-O4	-143(3)	C14-C15-C16-H16	179.7(2)
C1-Cr1-C5-O5	-64(2)	C14-C15-C16-C17	-0.2(3)
C2-Cr1-C5-O5	-149(2)	H15-C15-C16-H16	-0.3(3)
C3-Cr1-C5-O5	-7(3)	H15-C15-C16-C17	179.7(2)
C4-Cr1-C5-O5	26(2)	C15-C16-C17-H17	179.3(2)
C6-Cr1-C5-O5	117(2)	C15-C16-C17-C18	-0.7(3)
C1-Cr1-C6-O6	-102(2)	H16-C16-C17-H17	-0.6(3)
C1-Cr1-C6-C7	77(2)	H16-C16-C17-C18	179.4(2)

© University of Pretoria

C2-Cr1-C6-O6	-41.7(2)	C16-C17-C18-H18	-179.2(2)
C2-Cr1-C6-C7	137.2(2)	C16-C17-C18-C19	0.8(3)
C3-Cr1-C6-O6	-130.6(2)	H17-C17-C18-H18	0.8(3)
C3-Cr1-C6-C7	48.2(2)	H17-C17-C18-C19	-179.2(2)
C4-Cr1-C6-O6	137.5(2)	C17-C18-C19-C14	-0.1(3)
C4-Cr1-C6-C7	-43.7(2)	C17-C18-C19-H19	180.0(2)
C5-Cr1-C6-O6	52.8(2)	H18-C18-C19-C14	180.0(2)
C5-Cr1-C6-C7	-128.3(2)	H18-C18-C19-H19	-0.0(3)
Cr1-C6-O6-C26	-4.3(2)	N13-C20-C21-H21	-0.5(3)
C7-C6-O6-C26	176.7(1)	N13-C20-C21-C22	179.5(2)
Cr1-C6-C7-C8	0.9(2)	C25-C20-C21-H21	-179.0(2)
Cr1-C6-C7-C12	179.1(1)	C25-C20-C21-C22	1.0(3)
O6-C6-C7-C8	179.9(2)	N13-C20-C25-C24	-179.1(2)
O6-C6-C7-C12	-1.9(2)	N13-C20-C25-H25	0.9(3)
C6-O6-C26-H26A	76.2(2)	C21-C20-C25-C24	-0.6(3)
C6-O6-C26-H26B	-44.1(2)	C21-C20-C25-H25	179.4(2)
C6-O6-C26-C27	-163.9(2)	C20-C21-C22-H22	179.7(2)
C6-C7-C8-H8	-2.8(3)	C20-C21-C22-C23	-0.3(3)
C6-C7-C8-C9	177.2(2)	H21-C21-C22-H22	-0.3(3)
C12-C7-C8-H8	178.9(2)	H21-C21-C22-C23	179.6(2)
C12-C7-C8-C9	-1.1(3)	C21-C22-C23-H23	179.3(2)
C6-C7-C12-C11	-178.0(2)	C21-C22-C23-C24	-0.7(3)
C6-C7-C12-H12	2.1(3)	H22-C22-C23-H23	-0.7(3)
C8-C7-C12-C11	0.3(3)	H22-C22-C23-C24	179.3(2)
C8-C7-C12-H12	-179.6(2)	C22-C23-C24-H24	-179.0(2)
C7-C8-C9-H9	-179.2(2)	C22-C23-C24-C25	1.0(3)
C7-C8-C9-C10	0.8(3)	H23-C23-C24-H24	1.1(3)
H8-C8-C9-H9	0.8(3)	H23-C23-C24-C25	-178.9(2)
H8-C8-C9-C10	-179.2(2)	C23-C24-C25-C20	-0.4(3)
C8-C9-C10-C11	0.2(3)	C23-C24-C25-H25	179.6(2)
C8-C9-C10-N13	179.3(2)	H24-C24-C25-C20	179.7(2)
H9-C9-C10-C11	-179.8(2)	H24-C24-C25-H25	-0.3(3)
H9-C9-C10-N13	-0.7(3)	O6-C26-C27-H27A	-62.8(2)
C9-C10-C11-H11	179.1(2)	O6-C26-C27-H27B	177.2(2)
C9-C10-C11-C12	-0.9(3)	O6-C26-C27-H27C	57.2(2)

© University of Pretoria

N13-C10-C11-H11	0.0(3)	H26A-C26-C27-H27A	57.1(2)
N13-C10-C11-C12	-180.0(2)	H26A-C26-C27-H27B	-62.9(2)
C9-C10-N13-C14	-4.4(2)	H26A-C26-C27-H27C	177.1(2)
C9-C10-N13-C20	166.9(2)	H26B-C26-C27-H27A	177.3(2)
C11-C10-N13-C14	174.6(2)	H26B-C26-C27-H27B	57.3(2)
C11-C10-N13-C20	-14.1(3)	H26B-C26-C27-H27C	-62.6(2)
C10-C11-C12-C7	0.7(3)		

© University of Pretoria

Appendix C

Crystallographic data of complex 10b

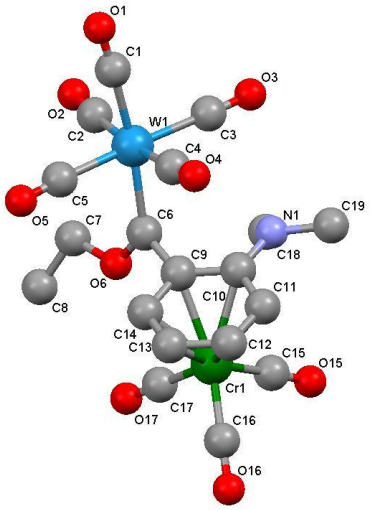

Table C.1 Crystal data and structure refinement

Emperical formula	$C_{19}H_{15}CrNO_9W$		
Formula weight	637.17 g/mol		
Temperature	150(2) K		
Wavelength	0.71073 Å		
Crystal system	triclinic		
Space group	P - 1		
Unit cell dimensions	**a** 6.8755(2) Å	**α** 100.8285(11)°	
	b 8.5877(3) Å	**β** 92.1596(10)°	
	c 18.8128(6) Å	**γ** 106.1381(11)°	
Volume	1043.25(5) $Å^3$		
Z	2		
Density (calculated)	2.028 Mg/m^3		
Absorption coefficient	6.081 mm^{-1}		
F(000)	612		
Crystal size	0.240 x 0.209 x 0.101 mm^3		
Theta range for data collection	2.994 to 46.969°		
Index ranges	$-14 \leq h \leq 14$	$-17 \leq k \leq 17$	$-38 \leq l \leq 38$
Reflections collected	77230		
Independent reflections	18900 [R(int) = 0.0445]		

© University of Pretoria

Completeness to theta = 25.00°	98.7%
Refinement method	Full-matrix least squares on F2
Data / restraints / parameters	18900 / 0 / 283
Goodness of fit on F2	1.106
Final R indices [I>2sigma(I)]	R1 = 0.0281 wR2 = 0.0551
R indices (all data)	R1 = 0.0380 wR2 = 0.0573
Largest diff. peak and hole	3.159 and -1.823 e.Å^{-3}

Table C.2 Atomic coordinates (x10^4) and equivalent isotropic displacement paramenters (Å^2 x 10^3)
U_{eq} is difined as one third of the trace of the orthogonalized U^{ij} tensor

Atom	x	y	z	Ueq
W1	4417(1)	6737(1)	8720(1)	13(1)
C1	6188(3)	8418(1)	9574(1)	24(1)
O1	7185(3)	9308(2)	10066(1)	41(1)
C2	2022(2)	6700(1)	9338(1)	22(1)
O2	762(2)	6778(1)	9711(1)	36(1)
C3	3730(2)	8592(1)	8301(1)	21(1)
O3	3393(3)	9647(1)	8080(1)	36(1)
C4	6944(2)	7043(1)	8169(1)	23(1)
O4	8418(2)	7278(2)	7893(1)	44(1)
C5	5187(3)	4901(1)	9101(1)	23(1)
O5	5653(3)	3842(2)	9274(1)	41(1)
C6	2835(1)	4687(1)	7846(1)	13(1)
O6	1270(1)	3384(1)	7834(1)	20(1)
C7	67(3)	3242(1)	8453(1)	28(1)
C8	-1239(3)	1472(1)	8332(1)	34(1)
C9	3869(1)	4314(1)	7177(1)	12(1)
C10	4335(1)	5332(1)	6655(1)	12(1)
C11	5602(1)	4914(1)	6109(1)	15(1)
C12	6464(1)	3614(1)	6103(1)	18(1)
C13	6047(2)	2632(1)	6631(1)	18(1)
C14	4714(2)	2954(1)	7146(1)	15(1)
Cr1	3128(3)	2578(1)	6073(1)	11(1)
C15	1433(2)	3107(1)	5437(1)	16(1)

© University of Pretoria

O15	433(2)	3395(1)	5001(1)	27(1)
C16	3044(1)	875(1)	5306(1)	15(1)
O16	2853(1)	-209(1)	4817(1)	23(1)
C17	944(2)	1106(1)	6369(1)	17(1)
O17	-381(1)	158(1)	6554(1)	28(1)
N1	3578(1)	6677(1)	6674(1)	14(1)
C18	1394(2)	6414(1)	6726(1)	19(1)
C19	4363(3)	7791(1)	6186(1)	24(1)

Table C.3 Bond lengths [Å] and angles [°]

W1-C1	2.038(1)	C6-C9-C14	114.6(1)
W1-C2	2.047(1)	C6-C9-Cr1	138.44(8)
W1-C3	2.061(2)	C10-C9-C14	119.3(1)
W1-C4	2.036(1)	C10-C9-Cr1	73.79(6)
W1-C5	2.034(2)	C14-C9-Cr1	68.09(6)
W1-C6	2.167(1)	C9-C10-C11	117.7(1)
C1-O1	1.143(2)	C9-C10-Cr1	70.04(6)
C2-O2	1.144(2)	C9-C10-N1	121.1(1)
C3-O3	1.139(2)	C11-C10-Cr1	68.59(7)
C4-O4	1.142(2)	C11-C10-N1	121.2(1)
C5-O5	1.141(3)	Cr1-C10-N1	132.82(8)
C6-O6	1.315(1)	C10-C11-H11	119.0(1)
C6-C9	1.495(2)	C10-C11-C12	121.9(1)
O6-C7	1.458(2)	C10-C11-Cr1	74.79(7)
C7-H7A	0.990(2)	H11-C11-C12	119.1(1)
C7-H7B	0.990(2)	H11-C11-Cr1	127.5(1)
C7-C8	1.505(2)	C12-C11-Cr1	70.81(7)
C8-H8A	0.980(2)	C11-C12-H12	119.9(1)
C8-H8B	0.980(2)	C11-C12-C13	120.4(1)
C8-H8C	0.980(2)	C11-C12-Cr1	72.34(8)
C9-C10	1.421(2)	H12-C12-C13	119.8(1)
C9-C14	1.435(2)	H12-C12-Cr1	128.6(1)
C9-Cr1	2.2640(9)	C13-C12-Cr1	71.54(8)
C10-C11	1.430(2)	C12-C13-H13	120.7(1)
C10-Cr1	2.313(1)	C12-C13-C14	118.7(1)
C10-N1	1.387(2)	C12-C13-Cr1	71.35(8)

© University of Pretoria

C11-H11	0.950(1)	H13-C13-C14	120.7(1)
C11-C12	1.404(2)	H13-C13-Cr1	130.2(1)
C11-Cr1	2.232(1)	C14-C13-Cr1	70.17(7)
C12-H12	0.950(1)	C9-C14-C13	121.9(1)
C12-C13	1.409(2)	C9-C14-H14	119.0(1)
C12-Cr1	2.212(1)	C9-C14-Cr1	74.30(7)
C13-H13	0.949(2)	C13-C14-H14	119.1(1)
C13-C14	1.401(2)	C13-C14-Cr1	72.68(8)
C13-Cr1	2.214(1)	H14-C14-Cr1	125.8(1)
C14-H14	0.951(1)	C9-Cr1-C10	36.16(4)
C14-Cr1	2.182(1)	C9-Cr1-C11	65.75(4)
Cr1-C15	1.841(2)	C9-Cr1-C12	78.59(4)
Cr1-C16	1.838(1)	C9-Cr1-C13	67.20(4)
Cr1-C17	1.853(1)	C9-Cr1-C14	37.61(4)
C15-O15	1.156(2)	C9-Cr1-C15	114.21(5)
C16-O16	1.154(2)	C9-Cr1-C16	162.43(5)
C17-O17	1.154(2)	C9-Cr1-C17	93.39(5)
N1-C18	1.465(2)	C10-Cr1-C11	36.62(4)
N1-C19	1.461(2)	C10-Cr1-C12	66.35(5)
C18-H18A	0.980(1)	C10-Cr1-C13	78.71(5)
C18-H18B	0.980(2)	C10-Cr1-C14	66.46(4)
C18-H18C	0.980(2)	C10-Cr1-C15	90.24(5)
C19-H19A	0.980(2)	C10-Cr1-C16	151.12(5)
C19-H19B	0.980(2)	C10-Cr1-C17	122.30(5)
C19-H19C	0.979(2)	C11-Cr1-C12	36.85(5)
		C11-Cr1-C13	66.59(5)
C1-W1-C2	86.86(6)	C11-Cr1-C14	78.42(5)
C1-W1-C3	91.26(6)	C11-Cr1-C15	92.60(5)
C1-W1-C4	87.39(6)	C11-Cr1-C16	115.34(5)
C1-W1-C5	89.21(7)	C11-Cr1-C17	158.50(5)
C1-W1-C6	170.55(6)	C12-Cr1-C13	37.11(5)
C2-W1-C3	87.89(6)	C12-Cr1-C14	66.72(5)
C2-W1-C4	173.46(6)	C12-Cr1-C15	119.99(6)
C2-W1-C5	94.63(6)	C12-Cr1-C16	92.63(5)
C2-W1-C6	97.25(5)	C12-Cr1-C17	148.23(6)
C3-W1-C4	89.13(6)	C13-Cr1-C14	37.15(5)

© University of Pretoria

C3-W1-C5	177.45(6)	C13-Cr1-C15	157.08(6)
C3-W1-C6	97.38(5)	C13-Cr1-C16	96.62(5)
C4-W1-C5	88.39(6)	C13-Cr1-C17	111.46(6)
C4-W1-C6	88.91(5)	C14-Cr1-C15	151.62(5)
C5-W1-C6	81.99(6)	C14-Cr1-C16	124.87(5)
W1-C1-O1	177.2(2)	C14-Cr1-C17	88.11(5)
W1-C2-O2	175.4(1)	C15-Cr1-C16	83.36(6)
W1-C3-O3	178.2(1)	C15-Cr1-C17	91.43(6)
W1-C4-O4	176.3(1)	C16-Cr1-C17	86.11(6)
W1-C5-O5	175.9(2)	Cr1-C15-O15	175.5(1)
W1-C6-O6	131.57(9)	Cr1-C16-O16	175.4(1)
W1-C6-C9	119.38(8)	Cr1-C17-O17	178.0(1)
O6-C6-C9	106.8(1)	C10-N1-C18	118.1(1)
C6-O6-C7	121.3(1)	C10-N1-C19	117.3(1)
O6-C7-H7A	110.3(2)	C18-N1-C19	111.8(1)
O6-C7-H7B	110.3(2)	N1-C18-H18A	109.5(1)
O6-C7-C8	107.1(1)	N1-C18-H18B	109.5(1)
H7A-C7-H7B	108.6(2)	N1-C18-H18C	109.5(1)
H7A-C7-C8	110.3(2)	H18A-C18-H18B	109.5(1)
H7B-C7-C8	110.3(2)	H18A-C18-H18C	109.4(1)
C7-C8-H8A	109.5(2)	H18B-C18-H18C	109.5(1)
C7-C8-H8B	109.5(2)	N1-C19-H19A	109.5(1)
C7-C8-H8C	109.5(2)	N1-C19-H19B	109.5(1)
H8A-C8-H8B	109.6(2)	N1-C19-H19C	109.5(1)
H8A-C8-H8C	109.5(2)	H19A-C19-H19B	109.5(2)
H8B-C8-H8C	109.4(2)	H19A-C19-H19C	109.4(2)
C6-C9-C10	125.3(1)	H19B-C19-H19C	109.5(2)

Table C.4 Anisotropic displacement parameters ($Å^2$ x 10^3)
The anisotropic displacement factor exponent takes the form: $-2p^2[h^2a^{*2}U^{11} + \ldots + 2hka^*b^*U^{12}]$

Atom	U11	U22	U33	U23	U13	U12
W1	17(1)	13(1)	9(1)	1(1)	3(1)	3(1)
C1	29(1)	21(1)	18(1)	-3(1)	1(1)	4(1)
O1	45(1)	35(1)	29(1)	-11(1)	-10(1)	2(1)
C2	28(1)	19(1)	18(1)	1(1)	10(1)	5(1)

© University of Pretoria

O2	38(1)	33(1)	34(1)	1(1)	24(1)	8(1)
C3	25(1)	17(1)	22(1)	6(1)	4(1)	5(1)
O3	47(1)	23(1)	41(1)	14(1)	2(1)	12(1)
C4	20(1)	22(1)	22(1)	-3(1)	7(1)	2(1)
O4	29(1)	43(1)	48(1)	-7(1)	22(1)	0(1)
C5	34(1)	24(1)	13(1)	4(1)	2(1)	13(1)
O5	69(1)	43(1)	28(1)	15(1)	7(1)	36(1)
C6	15(1)	12(1)	11(1)	3(1)	3(1)	3(1)
O6	22(1)	16(1)	16(1)	2(1)	9(1)	-2(1)
C7	33(1)	20(1)	23(1)	3(1)	17(1)	-3(1)
C8	37(1)	24(1)	30(1)	6(1)	13(1)	-8(1)
C9	14(1)	11(1)	10(1)	2(1)	2(1)	4(1)
C10	12(1)	12(1)	10(1)	2(1)	3(1)	2(1)
C11	14(1)	16(1)	12(1)	1(1)	5(1)	2(1)
C12	12(1)	21(1)	18(1)	-3(1)	3(1)	5(1)
C13	16(1)	18(1)	18(1)	-2(1)	-2(1)	9(1)
C14	18(1)	14(1)	14(1)	2(1)	-1(1)	7(1)
Cr1	10(1)	11(1)	10(1)	1(1)	1(1)	3(1)
C15	16(1)	17(1)	16(1)	3(1)	1(1)	5(1)
O15	27(1)	34(1)	24(1)	11(1)	-3(1)	13(1)
C16	14(1)	16(1)	15(1)	0(1)	0(1)	5(1)
O16	24(1)	21(1)	20(1)	-8(1)	-1(1)	8(1)
C17	16(1)	18(1)	16(1)	3(1)	0(1)	3(1)
O17	22(1)	30(1)	26(1)	10(1)	4(1)	-4(1)
N1	17(1)	12(1)	15(1)	5(1)	3(1)	5(1)
C18	19(1)	22(1)	20(1)	6(1)	4(1)	11(1)
C19	28(1)	19(1)	28(1)	14(1)	5(1)	5(1)

Table C.5 Hydrogen coordinates (x 10^4) and isotropic displacement paramenters (Å^2 x 10^3)

Atom	x	y	z	Ueq
H7A	-795	4000	8486	15609
H7B	969	3533	891	16389
H8A	-2086	1187	7869	14474
H8B	-2112	1337	873	16058
H8C	-368	739	832	15304
H11	5868	5546	5739	10556

© University of Pretoria

H12	7333	3393	5741	10560
H13	6657	1769	6638	12210
H14	4359	2252	7485	13768
H18A	65	5848	6251	11498
H18B	1128	7486	6876	12648
H18C	942	5731	7085	13032
H19A	5851	8075	6222	11445
H19B	3915	8803	6322	11629
H19C	3815	7242	5685	10457

Table C.6 Torsion angles [°]

C2-W1-C1-O1	82(3)	C10-C11-Cr1-C13	-103.00(8)
C3-W1-C1-O1	170(3)	C10-C11-Cr1-C14	-65.93(7)
C4-W1-C1-O1	-101(3)	C10-C11-Cr1-C15	86.90(8)
C5-W1-C1-O1	-13(3)	C10-C11-Cr1-C16	170.79(7)
C6-W1-C1-O1	-34(3)	C10-C11-Cr1-C17	-13.7(2)
C1-W1-C2-O2	18(2)	H11-C11-Cr1-C9	-143.7(1)
C3-W1-C2-O2	-73(2)	H11-C11-Cr1-C10	-115.2(1)
C4-W1-C2-O2	-10(2)	H11-C11-Cr1-C12	112.4(2)
C5-W1-C2-O2	107(2)	H11-C11-Cr1-C13	141.8(1)
C6-W1-C2-O2	-170(2)	H11-C11-Cr1-C14	178.9(1)
C1-W1-C3-O3	19(5)	H11-C11-Cr1-C15	-28.3(1)
C2-W1-C3-O3	105(5)	H11-C11-Cr1-C16	55.6(1)
C4-W1-C3-O3	-69(5)	H11-C11-Cr1-C17	-128.8(1)
C5-W1-C3-O3	-82(5)	C12-C11-Cr1-C9	103.84(8)
C6-W1-C3-O3	-158(5)	C12-C11-Cr1-C10	132.4(1)
C1-W1-C4-O4	-2(2)	C12-C11-Cr1-C13	29.39(8)
C2-W1-C4-O4	27(3)	C12-C11-Cr1-C14	66.45(8)
C3-W1-C4-O4	90(2)	C12-C11-Cr1-C15	-140.71(8)
C5-W1-C4-O4	-91(2)	C12-C11-Cr1-C16	-56.83(9)
C6-W1-C4-O4	-173(2)	C12-C11-Cr1-C17	118.7(1)
C1-W1-C5-O5	-127(2)	C11-C12-C13-H13	-178.2(1)
C2-W1-C5-O5	146(2)	C11-C12-C13-C14	1.8(2)
C3-W1-C5-O5	-26(3)	C11-C12-C13-Cr1	55.5(1)

© University of Pretoria

C4-W1-C5-O5	-40(2)	H12-C12-C13-H13	1.8(2)
C6-W1-C5-O5	49(2)	H12-C12-C13-C14	-178.2(1)
C1-W1-C6-O6	87.9(4)	H12-C12-C13-Cr1	-124.5(1)
C1-W1-C6-C9	-72.6(4)	Cr1-C12-C13-H13	126.3(1)
C2-W1-C6-O6	-27.4(1)	Cr1-C12-C13-C14	-53.7(1)
C2-W1-C6-C9	172.08(9)	C11-C12-Cr1-C9	-64.58(7)
C3-W1-C6-O6	-116.2(1)	C11-C12-Cr1-C10	-28.75(7)
C3-W1-C6-C9	83.28(9)	C11-C12-Cr1-C13	-131.7(1)
C4-W1-C6-O6	154.8(1)	C11-C12-Cr1-C14	-102.12(8)
C4-W1-C6-C9	-5.70(9)	C11-C12-Cr1-C15	46.9(1)
C5-W1-C6-O6	66.3(1)	C11-C12-Cr1-C16	130.77(8)
C5-W1-C6-C9	-94.2(1)	C11-C12-Cr1-C17	-142.4(1)
W1-C6-O6-C7	10.0(2)	H12-C12-Cr1-C9	-179.1(1)
C9-C6-O6-C7	172.3(1)	H12-C12-Cr1-C10	-143.2(1)
W1-C6-C9-C10	-68.5(1)	H12-C12-Cr1-C11	-114.5(2)
W1-C6-C9-C14	101.0(1)	H12-C12-Cr1-C13	113.8(2)
W1-C6-C9-Cr1	-174.96(7)	H12-C12-Cr1-C14	143.4(1)
O6-C6-C9-C10	126.6(1)	H12-C12-Cr1-C15	-67.6(2)
O6-C6-C9-C14	-63.9(1)	H12-C12-Cr1-C16	16.3(1)
O6-C6-C9-Cr1	20.2(2)	H12-C12-Cr1-C17	103.2(2)
C6-O6-C7-H7A	73.4(2)	C13-C12-Cr1-C9	67.15(8)
C6-O6-C7-H7B	-46.6(2)	C13-C12-Cr1-C10	102.98(8)
C6-O6-C7-C8	-166.6(1)	C13-C12-Cr1-C11	131.7(1)
O6-C7-C8-H8A	-57.7(2)	C13-C12-Cr1-C14	29.61(8)
O6-C7-C8-H8B	-177.8(1)	C13-C12-Cr1-C15	178.65(8)
O6-C7-C8-H8C	62.2(2)	C13-C12-Cr1-C16	-97.50(8)
H7A-C7-C8-H8A	62.2(2)	C13-C12-Cr1-C17	-10.6(1)
H7A-C7-C8-H8B	-57.9(2)	C12-C13-C14-C9	-3.9(2)
H7A-C7-C8-H8C	-177.8(2)	C12-C13-C14-H14	176.1(1)
H7B-C7-C8-H8A	-177.8(2)	C12-C13-C14-Cr1	54.2(1)
H7B-C7-C8-H8B	62.1(2)	H13-C13-C14-C9	176.1(1)
H7B-C7-C8-H8C	-57.8(2)	H13-C13-C14-H14	-3.9(2)
C6-C9-C10-C11	170.5(1)	H13-C13-C14-Cr1	-125.8(1)
C6-C9-C10-Cr1	-138.5(1)	Cr1-C13-C14-C9	-58.2(1)
C6-C9-C10-N1	-9.8(2)	Cr1-C13-C14-H14	121.9(1)
C14-C9-C10-C11	1.5(2)	C12-C13-Cr1-C9	-101.53(8)

© University of Pretoria

C14-C9-C10-Cr1	52.47(9)	C12-C13-Cr1-C10	-65.54(8)
C14-C9-C10-N1	-178.8(1)	C12-C13-Cr1-C11	-29.19(8)
Cr1-C9-C10-C11	-50.97(9)	C12-C13-Cr1-C14	-131.3(1)
Cr1-C9-C10-N1	128.7(1)	C12-C13-Cr1-C15	-3.0(2)
C6-C9-C14-C13	-167.9(1)	C12-C13-Cr1-C16	85.60(8)
C6-C9-C14-H14	12.1(2)	C12-C13-Cr1-C17	174.00(8)
C6-C9-C14-Cr1	134.66(9)	H13-C13-Cr1-C9	143.7(2)
C10-C9-C14-C13	2.2(2)	H13-C13-Cr1-C10	179.6(1)
C10-C9-C14-H14	-177.8(1)	H13-C13-Cr1-C11	-144.0(2)
C10-C9-C14-Cr1	-55.2(1)	H13-C13-Cr1-C12	-114.8(2)
Cr1-C9-C14-C13	57.4(1)	H13-C13-Cr1-C14	113.9(2)
Cr1-C9-C14-H14	-122.6(1)	H13-C13-Cr1-C15	-117.8(2)
C6-C9-Cr1-C10	125.4(1)	H13-C13-Cr1-C16	-29.2(1)
C6-C9-Cr1-C11	154.3(1)	H13-C13-Cr1-C17	59.2(2)
C6-C9-Cr1-C12	-169.3(1)	C14-C13-Cr1-C9	29.75(7)
C6-C9-Cr1-C13	-132.2(1)	C14-C13-Cr1-C10	65.74(8)
C6-C9-Cr1-C14	-102.8(1)	C14-C13-Cr1-C11	102.09(8)
C6-C9-Cr1-C15	72.8(1)	C14-C13-Cr1-C12	131.3(1)
C6-C9-Cr1-C16	-108.1(2)	C14-C13-Cr1-C15	128.3(1)
C6-C9-Cr1-C17	-20.3(1)	C14-C13-Cr1-C16	-143.12(8)
C10-C9-Cr1-C11	28.89(6)	C14-C13-Cr1-C17	-54.72(9)
C10-C9-Cr1-C12	65.33(7)	C9-C14-Cr1-C10	28.66(6)
C10-C9-Cr1-C13	102.42(7)	C9-C14-Cr1-C11	65.10(7)
C10-C9-Cr1-C14	131.8(1)	C9-C14-Cr1-C12	101.86(8)
C10-C9-Cr1-C15	-52.60(8)	C9-C14-Cr1-C13	131.4(1)
C10-C9-Cr1-C16	126.5(2)	C9-C14-Cr1-C15	-8.5(1)
C10-C9-Cr1-C17	-145.70(7)	C9-C14-Cr1-C16	178.04(7)
C14-C9-Cr1-C10	-131.8(1)	C9-C14-Cr1-C17	-98.03(7)
C14-C9-Cr1-C11	-102.94(7)	C13-C14-Cr1-C9	-131.4(1)
C14-C9-Cr1-C12	-66.50(7)	C13-C14-Cr1-C10	-102.79(8)
C14-C9-Cr1-C13	-29.41(7)	C13-C14-Cr1-C11	-66.34(8)
C14-C9-Cr1-C15	175.57(7)	C13-C14-Cr1-C12	-29.58(8)
C14-C9-Cr1-C16	-5.3(2)	C13-C14-Cr1-C15	-140.0(1)
C14-C9-Cr1-C17	82.47(8)	C13-C14-Cr1-C16	46.6(1)
C9-C10-C11-H11	176.5(1)	C13-C14-Cr1-C17	130.52(8)
C9-C10-C11-C12	-3.6(2)	H14-C14-Cr1-C9	114.8(1)

© University of Pretoria

C9-C10-C11-Cr1	51.66(9)	H14-C14-Cr1-C10	143.4(1)
Cr1-C10-C11-H11	124.8(1)	H14-C14-Cr1-C11	179.9(1)
Cr1-C10-C11-C12	-55.2(1)	H14-C14-Cr1-C12	-143.4(1)
N1-C10-C11-H11	-3.2(2)	H14-C14-Cr1-C13	-113.8(1)
N1-C10-C11-C12	176.7(1)	H14-C14-Cr1-C15	106.2(1)
N1-C10-C11-Cr1	-128.0(1)	H14-C14-Cr1-C16	-67.2(1)
C9-C10-Cr1-C11	-132.4(1)	H14-C14-Cr1-C17	16.7(1)
C9-C10-Cr1-C12	-103.48(7)	C9-Cr1-C15-O15	149(2)
C9-C10-Cr1-C13	-66.64(7)	C10-Cr1-C15-O15	121(2)
C9-C10-Cr1-C14	-29.74(6)	C11-Cr1-C15-O15	85(2)
C9-C10-Cr1-C15	133.57(7)	C12-Cr1-C15-O15	59(2)
C9-C10-Cr1-C16	-149.8(1)	C13-Cr1-C15-O15	61(2)
C9-C10-Cr1-C17	41.72(9)	C14-Cr1-C15-O15	155(2)
C11-C10-Cr1-C9	132.4(1)	C16-Cr1-C15-O15	-30(2)
C11-C10-Cr1-C12	28.92(7)	C17-Cr1-C15-O15	-116(2)
C11-C10-Cr1-C13	65.76(7)	C9-Cr1-C16-O16	138(1)
C11-C10-Cr1-C14	102.66(8)	C10-Cr1-C16-O16	-121(1)
C11-C10-Cr1-C15	-94.03(8)	C11-Cr1-C16-O16	-132(1)
C11-C10-Cr1-C16	-17.4(1)	C12-Cr1-C16-O16	-162(1)
C11-C10-Cr1-C17	174.12(8)	C13-Cr1-C16-O16	161(1)
N1-C10-Cr1-C9	-114.3(1)	C14-Cr1-C16-O16	134(1)
N1-C10-Cr1-C11	113.3(1)	C15-Cr1-C16-O16	-42(1)
N1-C10-Cr1-C12	142.2(1)	C17-Cr1-C16-O16	50(1)
N1-C10-Cr1-C13	179.0(1)	C9-Cr1-C17-O17	-105(4)
N1-C10-Cr1-C14	-144.1(1)	C10-Cr1-C17-O17	-128(4)
N1-C10-Cr1-C15	19.2(1)	C11-Cr1-C17-O17	-119(4)
N1-C10-Cr1-C16	95.8(1)	C12-Cr1-C17-O17	-31(4)
N1-C10-Cr1-C17	-72.6(1)	C13-Cr1-C17-O17	-38(4)
C9-C10-N1-C18	-50.0(2)	C14-Cr1-C17-O17	-68(4)
C9-C10-N1-C19	171.5(1)	C15-Cr1-C17-O17	141(4)
C11-C10-N1-C18	129.6(1)	C16-Cr1-C17-O17	57(4)
C11-C10-N1-C19	-8.9(2)	C10-N1-C18-H18A	-76.4(2)
Cr1-C10-N1-C18	40.8(2)	C10-N1-C18-H18B	163.7(1)
Cr1-C10-N1-C19	-97.7(1)	C10-N1-C18-H18C	43.6(2)
C10-C11-C12-H12	-178.0(1)	C19-N1-C18-H18A	64.3(2)
C10-C11-C12-C13	1.9(2)	C19-N1-C18-H18B	-55.7(2)

© University of Pretoria

C10-C11-C12-Cr1	57.1(1)	C19-N1-C18-H18C	-175.8(1)
H11-C11-C12-H12	1.9(2)	C10-N1-C19-H19A	-47.7(2)
H11-C11-C12-C13	-178.1(1)	C10-N1-C19-H19B	-167.7(1)
H11-C11-C12-Cr1	-123.0(1)	C10-N1-C19-H19C	72.2(2)
Cr1-C11-C12-H12	124.9(1)	C18-N1-C19-H19A	171.3(1)
Cr1-C11-C12-C13	-55.1(1)	C18-N1-C19-H19B	51.3(2)
C10-C11-Cr1-C9	-28.55(6)	C18-N1-C19-H19C	-68.8(2)
C10-C11-Cr1-C12	-132.4(1)		

© University of Pretoria

Appendix D

Crystallographic data of complex 11b

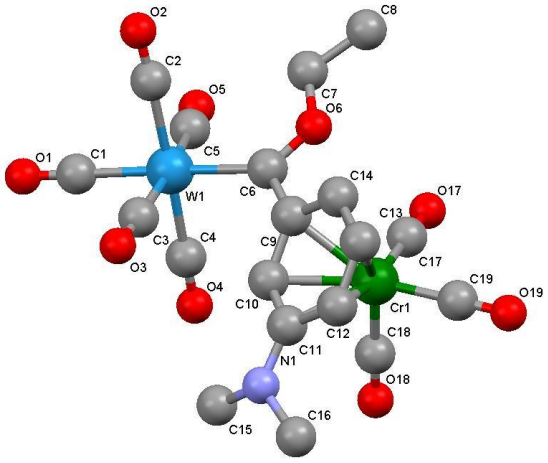

Table D.1 Crystal data and structure refinement

Emperical formula	$C_{19}H_{15}CrNO_9W$		
Formula weight	637.17 g/mol		
Temperature	150(2) K		
Wavelength	0.71073		
Crystal system	monoclinic		
Space group	$P2_1/n$		
Unit cell dimensions	**a** 12.5295(6) Å	**α** 90.00°	
	b 15.9703(7) Å	**β** 103.166(2)°	
	c 22.0120(11) Å	**γ** 90.00°	
Volume	4288.4(4) $Å^3$		
Z	8		
Density (calculated)	1.974 Mg/m^3		
Absorption coefficient	5.917 mm^{-1}		
F(000)	2448		
Crystal size	0.333 x 0.095 x 0.035 mm^3		
Theta range for data collection	2.457 to 28.320		
Index ranges	-16 ≤ h ≤ 16	-21 ≤ k ≤ 21	-29 ≤ l ≤ 29
Reflections collected	10740		
Independent reflections	9539 [R(int) = 0.0445]		

© University of Pretoria

Completeness to theta = 25.00°	99.5%
Refinement method	Full-matrix least squares on F^2
Data / restraints / parameters	10740 / 0 / 565
Goodness of fit on F2	1.178
Final R indices [I>2sigma(I)]	R1 = 0.0249
R indices (all data)	R1 = 0.0315 wR2 = 0.0669
Largest diff. peak and hole	1.821 and -0.622 e.Å^{-3}

Table D.2 Atomic coordinates (x10^4) and equivalent isotropic displacement paramenters (Å^2 x 10^3)
U_{eq} is difined as one third of the trace of the orthogonalized U^{ij} tensor

Atom	x	y	z	Ueq
W1	5658(1)	8782(8)	1299(6)	15(1)
C1	5140(1)	9882(2)	872(1)	25(1)
O1	4881(3)	10517(2)	642(1)	39(1)
C2	6722(3)	8695(2)	715(1)	20(1)
O2	7276(2)	8662(1)	372(1)	30(1)
C3	6713(3)	9517(2)	1933(1)	20(1)
O3	7228(2)	9972(1)	2276(1)	30(1)
C4	4518(3)	8890(2)	1825(1)	21(1)
O4	3874(2)	8950(2)	2112(1)	33(1)
C5	4490(1)	8203(3)	646(1)	23(1)
O5	3785(2)	7939(2)	272(1)	35(1)
C6	6367(3)	7667(2)	1812(1)	17(1)
O6	6501(2)	6911(1)	1619(1)	22(1)
C7	6113(3)	6666(2)	972(1)	24(1)
C8	6550(1)	5796(3)	913(2)	37(1)
C9	6933(3)	7675(2)	2491(1)	16(1)
C10	6606(3)	8232(2)	2912(1)	17(1)
C11	7160(1)	8292(2)	3552(1)	18(1)
C12	7974(3)	7681(2)	3776(1)	19(1)
C13	8322(3)	7121(2)	3358(1)	22(1)
C14	7819(3)	7111(2)	2725(1)	19(1)
N1	6866(3)	8874(2)	3934(1)	24(1)
C15	5914(4)	9402(3)	3696(2)	33(1)
C16	7141(5)	8733(3)	4604(2)	46(1)

© University of Pretoria

Cr1	6537(5)	6934(3)	3258(3)	16(1)
C17	5653(1)	6225(2)	2701(1)	25(1)
O17	5081(3)	5780(2)	2362(1)	38(1)
C18	5350(1)	7158(2)	3584(1)	26(1)
O18	4603(3)	7295(2)	3796(1)	46(1)
C19	6914(3)	6063(2)	3819(1)	25(1)
O19	7163(3)	5534(2)	4176(1)	44(1)

Table D.3 Bond lengths [Å] and angles [°]

W1-C1	2.028(3)	C6-C9-C14	120.3(3)
W1-C2	2.057(4)	C6-C9-Cr1	128.3(2)
W1-C3	2.057(3)	C10-C9-C14	118.5(3)
W1-C4	2.041(4)	C10-C9-Cr1	71.7(2)
W1-C5	2.026(4)	C14-C9-Cr1	71.2(2)
W1-C6	2.187(3)	C9-C10-H10	118.5(3)
C1-O1	1.147(5)	C9-C10-C11	122.9(3)
C2-O2	1.137(5)	C9-C10-Cr1	71.1(2)
C3-O3	1.137(4)	H10-C10-C11	118.6(3)
C4-O4	1.136(5)	H10-C10-Cr1	125.3(3)
C5-O5	1.142(4)	C11-C10-Cr1	76.8(2)
C6-O6	1.304(4)	C10-C11-C12	116.6(3)
C6-C9	1.502(5)	C10-C11-N1	121.2(3)
O6-C7	1.449(4)	C10-C11-Cr1	67.0(2)
C7-H7A	0.990(4)	C12-C11-N1	122.1(3)
C7-H7B	0.990(4)	C12-C11-Cr1	68.1(2)
C7-C8	1.510(6)	N1-C11-Cr1	133.1(3)
C8-H8A	0.979(5)	C11-C12-H12	119.6(3)
C8-H8B	0.980(4)	C11-C12-C13	120.8(3)
C8-H8C	0.981(5)	C11-C12-Cr1	76.0(2)
C9-C10	1.411(5)	H12-C12-C13	119.6(3)
C9-C14	1.431(5)	H12-C12-Cr1	125.7(3)
C9-Cr1	2.209(4)	C13-C12-Cr1	70.5(2)
C10-H10	0.950(3)	C12-C13-H13	119.4(3)
C10-C11	1.425(5)	C12-C13-C14	121.3(3)
C10-Cr1	2.216(3)	C12-C13-Cr1	72.4(2)
C11-C12	1.416(5)	H13-C13-C14	119.3(4)

© University of Pretoria

C11-N1	1.359(5)	H13-C13-Cr1	129.3(3)
C11-Cr1	2.345(3)	C14-C13-Cr1	71.5(2)
C12-H12	0.950(3)	C9-C14-C13	119.4(3)
C12-C13	1.421(5)	C9-C14-H14	120.4(3)
C12-Cr1	2.242(3)	C9-C14-Cr1	71.0(2)
C13-H13	0.949(3)	C13-C14-H14	120.3(3)
C13-C14	1.392(5)	C13-C14-Cr1	71.9(2)
C13-Cr1	2.217(4)	H14-C14-Cr1	129.1(3)
C14-H14	0.949(4)	C11-N1-C15	119.3(3)
C14-Cr1	2.212(4)	C11-N1-C16	119.1(3)
N1-C15	1.457(6)	C15-N1-C16	116.1(4)
N1-C16	1.454(5)	N1-C15-H15A	109.4(4)
C15-H15A	0.982(5)	N1-C15-H15B	109.5(4)
C15-H15B	0.979(5)	N1-C15-H15C	109.5(4)
C15-H15C	0.980(5)	H15A-C15-H15B	109.4(5)
C16-H16A	0.980(5)	H15A-C15-H15C	109.4(5)
C16-H16B	0.981(5)	H15B-C15-H15C	109.6(5)
C16-H16C	0.981(6)	N1-C16-H16A	109.5(4)
Cr1-C17	1.844(3)	N1-C16-H16B	109.5(4)
Cr1-C18	1.828(4)	N1-C16-H16C	109.5(4)
Cr1-C19	1.849(4)	H16A-C16-H16B	109.5(5)
C17-O17	1.153(5)	H16A-C16-H16C	109.4(5)
C18-O18	1.157(6)	H16B-C16-H16C	109.4(5)
C19-O19	1.147(5)	C9-Cr1-C10	37.2(1)
		C9-Cr1-C11	66.3(1)
C1-W1-C2	87.3(1)	C9-Cr1-C12	79.0(1)
C1-W1-C3	84.8(1)	C9-Cr1-C13	66.8(1)
C1-W1-C4	89.9(1)	C9-Cr1-C14	37.8(1)
C1-W1-C5	87.9(2)	C9-Cr1-C17	91.5(1)
C1-W1-C6	174.0(1)	C9-Cr1-C18	122.7(2)
C2-W1-C3	93.2(1)	C9-Cr1-C19	147.8(1)
C2-W1-C4	176.0(1)	C10-Cr1-C11	36.3(1)
C2-W1-C5	89.6(2)	C10-Cr1-C12	65.7(1)
C2-W1-C6	91.3(1)	C10-Cr1-C13	77.9(1)
C3-W1-C4	89.5(1)	C10-Cr1-C14	67.0(1)
C3-W1-C5	172.1(2)	C10-Cr1-C17	114.2(1)

© University of Pretoria

C3-W1-C6	89.5(1)	C10-Cr1-C18	92.9(1)
C4-W1-C5	87.4(2)	C10-Cr1-C19	155.4(1)
C4-W1-C6	91.7(1)	C11-Cr1-C12	35.9(1)
C5-W1-C6	97.9(1)	C11-Cr1-C13	65.4(1)
W1-C1-O1	177.5(3)	C11-Cr1-C14	78.0(1)
W1-C2-O2	177.0(3)	C11-Cr1-C17	149.7(1)
W1-C3-O3	174.3(3)	C11-Cr1-C18	87.7(1)
W1-C4-O4	179.2(3)	C11-Cr1-C19	119.6(1)
W1-C5-O5	174.2(4)	C12-Cr1-C13	37.2(1)
W1-C6-O6	130.8(2)	C12-Cr1-C14	66.8(1)
W1-C6-C9	123.5(2)	C12-Cr1-C17	163.0(2)
O6-C6-C9	105.4(3)	C12-Cr1-C18	109.1(2)
C6-O6-C7	122.0(3)	C12-Cr1-C19	90.4(1)
O6-C7-H7A	110.4(3)	C13-Cr1-C14	36.6(1)
O6-C7-H7B	110.4(3)	C13-Cr1-C17	126.0(2)
O6-C7-C8	106.6(3)	C13-Cr1-C18	145.9(2)
H7A-C7-H7B	108.6(3)	C13-Cr1-C19	86.4(2)
H7A-C7-C8	110.4(3)	C14-Cr1-C17	97.1(1)
H7B-C7-C8	110.4(3)	C14-Cr1-C18	159.6(2)
C7-C8-H8A	109.4(4)	C14-Cr1-C19	110.2(2)
C7-C8-H8B	109.4(4)	C17-Cr1-C18	87.8(2)
C7-C8-H8C	109.4(4)	C17-Cr1-C19	90.3(2)
H8A-C8-H8B	109.5(5)	C18-Cr1-C19	89.5(2)
H8A-C8-H8C	109.5(5)	Cr1-C17-O17	178.2(3)
H8B-C8-H8C	109.5(5)	Cr1-C18-O18	179.3(4)
C6-C9-C10	121.1(3)	Cr1-C19-O19	178.5(3)

Table D.4 Anisotropic displacement parameters ($Å^2$ x 10^3)
The anisotropic displacement factor exponent takes the form: $-2p^2[h^2a^{*2}U^{11} + \ldots + 2hka^*b^*U^{12}]$

Atom	U11	U22	U33	U23	U13	U12
W1	15(1)	16(1)	13(1)	0(1)	2(1)	1(1)
C1	27(1)	27(1)	20(1)	1(1)	4(1)	4(1)
O1	51(1)	32(1)	35(1)	14(1)	9(1)	19(1)
C2	22(1)	20(1)	18(1)	1(1)	2(1)	-1(1)
O2	31(1)	35(1)	27(1)	0(1)	13(1)	-1(1)

© University of Pretoria

C3	22(1)	17(1)	19(1)	5(1)	3(1)	0(1)
O3	32(1)	23(1)	32(1)	-2(1)	0(1)	-5(1)
C4	20(1)	18(1)	23(1)	-4(1)	2(1)	-1(1)
O4	26(1)	37(1)	39(1)	-10(1)	17(1)	-4(1)
C5	19(1)	33(1)	18(1)	-4(1)	6(1)	1(1)
O5	22(1)	60(1)	24(1)	-16(1)	3(1)	-5(1)
C6	17(1)	16(1)	18(1)	-2(1)	8(1)	-2(1)
O6	31(1)	16(1)	17(1)	-4(1)	4(1)	1(1)
C7	32(1)	21(1)	19(1)	-8(1)	4(1)	2(1)
C8	43(1)	30(1)	40(1)	-17(1)	11(1)	0(1)
C9	19(1)	15(1)	16(1)	1(1)	6(1)	-1(1)
C10	21(1)	15(1)	14(1)	1(1)	2(1)	-1(1)
C11	19(1)	19(1)	14(1)	2(1)	0(1)	-5(1)
C12	19(1)	22(1)	15(1)	3(1)	-1(1)	-3(1)
C13	17(1)	21(1)	25(1)	5(1)	2(1)	-2(1)
C14	18(1)	17(1)	21(1)	1(1)	7(1)	1(1)
N1	35(1)	21(1)	16(1)	-1(1)	6(1)	2(1)
C15	41(1)	28(1)	27(1)	-7(1)	4(1)	12(1)
C16	66(1)	52(1)	16(1)	-5(1)	-1(1)	19(1)
Cr1	16(1)	15(1)	17(1)	2(1)	4(1)	1(1)
C17	25(1)	22(1)	30(1)	3(1)	9(1)	-3(1)
O17	34(1)	32(1)	45(1)	-13(1)	3(1)	-11(1)
C18	22(1)	26(1)	30(1)	-3(1)	6(1)	-3(1)
O18	30(1)	54(1)	61(1)	-8(1)	27(1)	-3(1)
C19	24(1)	25(1)	29(1)	5(1)	10(1)	0(1)
O19	45(1)	36(1)	50(1)	26(1)	12(1)	7(1)

Table D.5 Hydrogen coordinates (x 10^4) and isotropic displacement paramenters (Å^2 x 10^3)

Atom	x	y	z	Ueq
H7A	6386(1)	7060(1)	695(1)	1490(1)
H7B	5302(1)	6666(1)	856(1)	1835(1)
H8A	7352(1)	5813(1)	1002(1)	2148(1)
H8B	6265(1)	5589(1)	488(1)	1046(1)
H8C	6315(1)	5422(1)	1211(1)	2596(1)
H10	5989(1)	8582(1)	2762(1)	5920(1)
H12	8292(1)	7646(1)	4210(1)	9023(1)

© University of Pretoria

H13	8910(1)	6747(1)	3513(1)	7530(1)
H14	8061(1)	6733(1)	2452(1)	5255(1)
H15A	6025(1)	9716(1)	3332(1)	7142(1)
H15B	5820(1)	9795(1)	4021(1)	8618(1)
H15C	5259(1)	9051(1)	3573(1)	7658(1)
H16A	6768(1)	8228(1)	4701(1)	10076(1)
H16B	6905(1)	9216(1)	4816(1)	10322(1)
H16C	7936(1)	8661(1)	4748(1)	10177(1)

Table C.6 Torsion angles [°]

C2-W1-C1-O1	-76(8)	C10-C11-Cr1-C13	103.6(2)
C3-W1-C1-O1	18(8)	C10-C11-Cr1-C14	67.2(2)
C4-W1-C1-O1	107(8)	C10-C11-Cr1-C17	-16.3(4)
C5-W1-C1-O1	-165(8)	C10-C11-Cr1-C18	-98.1(2)
C6-W1-C1-O1	2(9)	C10-C11-Cr1-C19	173.8(2)
C1-W1-C2-O2	-36(6)	C12-C11-Cr1-C9	-104.7(2)
C3-W1-C2-O2	-121(6)	C12-C11-Cr1-C10	-134.0(3)
C4-W1-C2-O2	11(7)	C12-C11-Cr1-C13	-30.4(2)
C5-W1-C2-O2	52(6)	C12-C11-Cr1-C14	-66.8(2)
C6-W1-C2-O2	150(6)	C12-C11-Cr1-C17	-150.3(3)
C1-W1-C3-O3	36(3)	C12-C11-Cr1-C18	127.9(2)
C2-W1-C3-O3	123(3)	C12-C11-Cr1-C19	39.8(3)
C4-W1-C3-O3	-54(3)	N1-C11-Cr1-C9	141.2(4)
C5-W1-C3-O3	13(4)	N1-C11-Cr1-C10	111.9(4)
C6-W1-C3-O3	-146(3)	N1-C11-Cr1-C12	-114.1(4)
C1-W1-C4-O4	60(23)	N1-C11-Cr1-C13	-144.5(4)
C2-W1-C4-O4	13(25)	N1-C11-Cr1-C14	179.1(4)
C3-W1-C4-O4	145(23)	N1-C11-Cr1-C17	95.5(4)
C5-W1-C4-O4	-28(23)	N1-C11-Cr1-C18	13.8(4)
C6-W1-C4-O4	-126(23)	N1-C11-Cr1-C19	-74.4(4)
C1-W1-C5-O5	-24(4)	C11-C12-C13-H13	174.9(3)
C2-W1-C5-O5	-112(4)	C11-C12-C13-C14	-5.0(5)
C3-W1-C5-O5	-2(4)	C11-C12-C13-Cr1	-59.4(3)
C4-W1-C5-O5	66(4)	H12-C12-C13-H13	-5.0(6)
C6-W1-C5-O5	157(3)	H12-C12-C13-C14	175.1(3)
C1-W1-C6-O6	-132(1)	H12-C12-C13-Cr1	120.8(4)

© University of Pretoria

C1-W1-C6-C9	41(1)	Cr1-C12-C13-H13	-125.7(4)
C2-W1-C6-O6	-55.2(3)	Cr1-C12-C13-C14	54.4(3)
C2-W1-C6-C9	117.4(3)	C11-C12-Cr1-C9	64.4(2)
C3-W1-C6-O6	-148.4(3)	C11-C12-Cr1-C10	27.8(2)
C3-W1-C6-C9	24.3(3)	C11-C12-Cr1-C13	130.4(3)
C4-W1-C6-O6	122.1(3)	C11-C12-Cr1-C14	102.0(2)
C4-W1-C6-C9	-65.2(3)	C11-C12-Cr1-C17	121.3(5)
C5-W1-C6-O6	34.5(3)	C11-C12-Cr1-C18	-56.6(2)
C5-W1-C6-C9	-152.9(3)	C11-C12-Cr1-C19	-146.2(2)
W1-C6-O6-C7	-3.2(5)	H12-C12-Cr1-C9	-179.0(4)
C9-C6-O6-C7	-176.8(3)	H12-C12-Cr1-C10	144.5(4)
W1-C6-C9-C10	32.2(5)	H12-C12-Cr1-C11	116.6(4)
W1-C6-C9-C14	-148.0(3)	H12-C12-Cr1-C13	-113.0(4)
W1-C6-C9-Cr1	122.7(3)	H12-C12-Cr1-C14	-141.4(4)
O6-C6-C9-C10	-153.6(3)	H12-C12-Cr1-C17	-122.1(5)
O6-C6-C9-C14	26.2(4)	H12-C12-Cr1-C18	60.1(4)
O6-C6-C9-Cr1	-63.0(4)	H12-C12-Cr1-C19	-29.6(4)
C6-O6-C7-H7A	52.4(4)	C13-C12-Cr1-C9	-66.0(2)
C6-O6-C7-H7B	-67.7(4)	C13-C12-Cr1-C10	-102.5(2)
C6-O6-C7-C8	172.3(3)	C13-C12-Cr1-C11	-130.4(3)
O6-C7-C8-H8A	-63.8(5)	C13-C12-Cr1-C14	-28.4(2)
O6-C7-C8-H8B	176.1(4)	C13-C12-Cr1-C17	-9.1(6)
O6-C7-C8-H8C	56.2(5)	C13-C12-Cr1-C18	173.1(2)
H7A-C7-C8-H8A	56.1(5)	C13-C12-Cr1-C19	83.4(2)
H7A-C7-C8-H8B	-63.9(5)	C12-C13-C14-C9	-0.1(5)
H7A-C7-C8-H8C	176.1(4)	C12-C13-C14-H14	180.0(3)
H7B-C7-C8-H8A	176.2(4)	C12-C13-C14-Cr1	-54.8(3)
H7B-C7-C8-H8B	56.1(5)	H13-C13-C14-C9	-180.0(3)
H7B-C7-C8-H8C	-63.8(5)	H13-C13-C14-H14	0.1(6)
C6-C9-C10-H10	3.7(5)	H13-C13-C14-Cr1	125.3(4)
C6-C9-C10-C11	-176.4(3)	Cr1-C13-C14-C9	54.7(3)
C6-C9-C10-Cr1	124.2(3)	Cr1-C13-C14-H14	-125.2(4)
C14-C9-C10-H10	-176.1(3)	C12-C13-Cr1-C9	102.8(2)
C14-C9-C10-C11	3.8(5)	C12-C13-Cr1-C10	65.4(2)
C14-C9-C10-Cr1	-55.6(3)	C12-C13-Cr1-C11	29.4(2)
Cr1-C9-C10-H10	-120.6(3)	C12-C13-Cr1-C14	132.9(3)

© University of Pretoria

Cr1-C9-C10-C11	59.4(3)	C12-C13-Cr1-C17	176.7(2)
C6-C9-C14-C13	-179.1(3)	C12-C13-Cr1-C18	-11.7(4)
C6-C9-C14-H14	0.8(5)	C12-C13-Cr1-C19	-95.5(2)
C6-C9-C14-Cr1	-124.0(3)	H13-C13-Cr1-C9	-143.3(4)
C10-C9-C14-C13	0.7(5)	H13-C13-Cr1-C10	179.4(4)
C10-C9-C14-H14	-179.4(3)	H13-C13-Cr1-C11	143.3(4)
C10-C9-C14-Cr1	55.8(3)	H13-C13-Cr1-C12	113.9(5)
Cr1-C9-C14-C13	-55.1(3)	H13-C13-Cr1-C14	-113.2(5)
Cr1-C9-C14-H14	124.8(4)	H13-C13-Cr1-C17	-69.4(4)
C6-C9-Cr1-C10	-115.7(4)	H13-C13-Cr1-C18	102.2(4)
C6-C9-Cr1-C11	-144.3(3)	H13-C13-Cr1-C19	18.4(4)
C6-C9-Cr1-C12	-179.6(3)	C14-C13-Cr1-C9	-30.1(2)
C6-C9-Cr1-C13	143.5(3)	C14-C13-Cr1-C10	-67.5(2)
C6-C9-Cr1-C14	114.3(4)	C14-C13-Cr1-C11	-103.5(2)
C6-C9-Cr1-C17	14.5(3)	C14-C13-Cr1-C12	-132.9(3)
C6-C9-Cr1-C18	-73.8(3)	C14-C13-Cr1-C17	43.8(3)
C6-C9-Cr1-C19	107.4(4)	C14-C13-Cr1-C18	-144.6(3)
C10-C9-Cr1-C11	-28.7(2)	C14-C13-Cr1-C19	131.6(2)
C10-C9-Cr1-C12	-64.0(2)	C9-C14-Cr1-C10	-30.2(2)
C10-C9-Cr1-C13	-100.8(2)	C9-C14-Cr1-C11	-66.5(2)
C10-C9-Cr1-C14	-130.1(3)	C9-C14-Cr1-C12	-102.4(2)
C10-C9-Cr1-C17	130.2(2)	C9-C14-Cr1-C13	-131.2(3)
C10-C9-Cr1-C18	41.8(3)	C9-C14-Cr1-C17	83.2(2)
C10-C9-Cr1-C19	-136.9(3)	C9-C14-Cr1-C18	-19.9(5)
C14-C9-Cr1-C10	130.1(3)	C9-C14-Cr1-C19	176.1(2)
C14-C9-Cr1-C11	101.4(2)	C13-C14-Cr1-C9	131.2(3)
C14-C9-Cr1-C12	66.1(2)	C13-C14-Cr1-C10	101.0(2)
C14-C9-Cr1-C13	29.2(2)	C13-C14-Cr1-C11	64.7(2)
C14-C9-Cr1-C17	-99.8(2)	C13-C14-Cr1-C12	28.8(2)
C14-C9-Cr1-C18	171.9(2)	C13-C14-Cr1-C17	-145.6(2)
C14-C9-Cr1-C19	-6.9(4)	C13-C14-Cr1-C18	111.3(4)
C9-C10-C11-C12	-8.5(5)	C13-C14-Cr1-C19	-52.7(2)
C9-C10-C11-N1	175.6(3)	H14-C14-Cr1-C9	-114.1(4)
C9-C10-C11-Cr1	-56.8(3)	H14-C14-Cr1-C10	-144.3(4)
H10-C10-C11-C12	171.4(3)	H14-C14-Cr1-C11	179.3(4)
H10-C10-C11-N1	-4.4(5)	H14-C14-Cr1-C12	143.5(4)

© University of Pretoria

H10-C10-C11-Cr1	123.2(4)	H14-C14-Cr1-C13	114.7(4)
Cr1-C10-C11-C12	48.2(3)	H14-C14-Cr1-C17	-31.0(4)
Cr1-C10-C11-N1	-127.6(3)	H14-C14-Cr1-C18	-134.0(4)
C9-C10-Cr1-C11	132.1(3)	H14-C14-Cr1-C19	62.0(4)
C9-C10-Cr1-C12	104.5(2)	C11-N1-C15-H15A	-58.8(5)
C9-C10-Cr1-C13	67.4(2)	C11-N1-C15-H15B	-178.7(4)
C9-C10-Cr1-C14	30.6(2)	C11-N1-C15-H15C	61.1(5)
C9-C10-Cr1-C17	-56.9(2)	C16-N1-C15-H15A	147.7(4)
C9-C10-Cr1-C18	-145.8(2)	C16-N1-C15-H15B	27.9(6)
C9-C10-Cr1-C19	118.9(4)	C16-N1-C15-H15C	-92.4(5)
H10-C10-Cr1-C9	112.1(4)	C11-N1-C16-H16A	-62.5(6)
H10-C10-Cr1-C11	-115.8(4)	C11-N1-C16-H16B	177.5(4)
H10-C10-Cr1-C12	-143.4(4)	C11-N1-C16-H16C	57.6(6)
H10-C10-Cr1-C13	179.5(4)	C15-N1-C16-H16A	91.1(5)
H10-C10-Cr1-C14	142.7(4)	C15-N1-C16-H16B	-28.9(6)
H10-C10-Cr1-C17	55.2(4)	C15-N1-C16-H16C	-148.9(4)
H10-C10-Cr1-C18	-33.7(3)	C9-Cr1-C17-O17	-143(11)
H10-C10-Cr1-C19	-129.0(4)	C10-Cr1-C17-O17	-113(11)
C11-C10-Cr1-C9	-132.1(3)	C11-Cr1-C17-O17	-102(11)
C11-C10-Cr1-C12	-27.6(2)	C12-Cr1-C17-O17	162(11)
C11-C10-Cr1-C13	-64.6(2)	C13-Cr1-C17-O17	155(11)
C11-C10-Cr1-C14	-101.4(2)	C14-Cr1-C17-O17	179(11)
C11-C10-Cr1-C17	171.1(2)	C18-Cr1-C17-O17	-21(11)
C11-C10-Cr1-C18	82.1(2)	C19-Cr1-C17-O17	69(11)
C11-C10-Cr1-C19	-13.1(5)	C9-Cr1-C18-O18	-161(29)
C10-C11-C12-H12	-171.2(3)	C10-Cr1-C18-O18	-138(29)
C10-C11-C12-C13	9.0(5)	C11-Cr1-C18-O18	-102(29)
C10-C11-C12-Cr1	-47.7(3)	C12-Cr1-C18-O18	-72(29)
N1-C11-C12-H12	4.6(6)	C13-Cr1-C18-O18	-65(29)
N1-C11-C12-C13	-175.2(3)	C14-Cr1-C18-O18	-147(29)
N1-C11-C12-Cr1	128.1(3)	C17-Cr1-C18-O18	108(29)
Cr1-C11-C12-H12	-123.4(4)	C19-Cr1-C18-O18	18(29)
Cr1-C11-C12-C13	56.7(3)	C9-Cr1-C19-O19	84(13)
C10-C11-N1-C15	4.8(5)	C10-Cr1-C19-O19	1(13)
C10-C11-N1-C16	157.5(4)	C11-Cr1-C19-O19	-8(13)
C12-C11-N1-C15	-170.8(4)	C12-Cr1-C19-O19	14(13)

© University of Pretoria

C12-C11-N1-C16	-18.1(5)	C13-Cr1-C19-O19	51(13)
Cr1-C11-N1-C15	-81.7(5)	C14-Cr1-C19-O19	80(13)
Cr1-C11-N1-C16	70.9(5)	C17-Cr1-C19-O19	177(13)
C10-C11-Cr1-C9	29.4(2)	C18-Cr1-C19-O19	-95(13)
C10-C11-Cr1-C12	134.0(3)		

© University of Pretoria

Appendix E

Crystallographic data of complex 12b

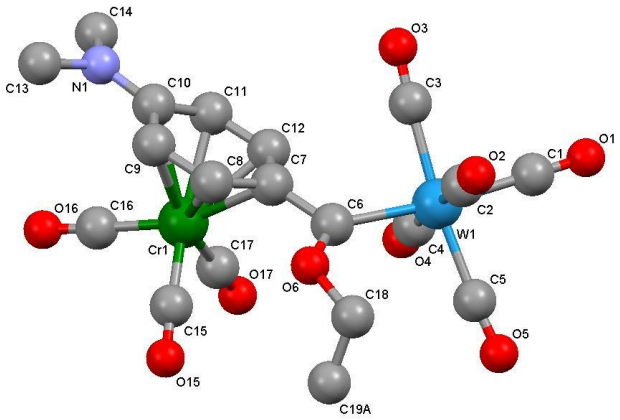

Table E.1 Crystal data and structure refinement

Emperical formula	$C_{19}H_{15}CrNO_9W$		
Formula weight	637.17 g/mol		
Temperature	296(2)		
Wavelength	0.71073		
Crystal system	triclinic		
Space group	P - 1		
Unit cell dimensions	**a** 6.9470(2) Å	**α** 85.6900(9)°	
	b 12.4222(3) Å	**β** 84.1773(8)°	
	c 12.8729(3) Å	**γ** 86.7838(8)°	
Volume	1100.72(5) Å3		
Z	2		
Density (calculated)	1.922 Mg/m^3		
Absorption coefficient	5.763 mm^{-1}		
F(000)	612		
Crystal size	0.300 x 0.191 x 0.152 mm^3		
Theta range for data collection	2.21 to 33.66		
Index ranges	-10 ≤ h ≤ 10	-19 ≤ k ≤ 19	-20 ≤ l ≤ 20
Reflections collected	8701		
Independent reflections	7715 [R(int) = 0.0445]		
Completeness to theta = 25.00°	99.5%		

© University of Pretoria

Refinement method	Full-matrix least squares on F^2
Data / restraints / parameters	8701 / 0 / 294
Goodness of fit on F2	1.051
Final R indices [I>2sigma(I)]	R1 = 0.0248
R indices (all data)	R1 = 0.0302 wR2 = 0.0627
Largest diff. peak and hole	2.284 and -0.353 e.Å^{-3}

Table E.2 Atomic coordinates (x10^4) and equivalent isotropic displacement paramenters (Å^2 x 10^3)
U_{eq} is difined as one third of the trace of the orthogonalized U^{ij} tensor

Atom	x	y	z	Ueq
W1	1900(1)	3578(1)	-1881(1)	45(1)
C1	2384(5)	4714(2)	-899(3)	69(1)
O1	2661(6)	5346(2)	-342(3)	108(1)
C2	3306(5)	4462(2)	-3081(3)	70(1)
O2	4097(6)	4955(3)	-3759(3)	111(1)
C3	4503(4)	2864(2)	-1544(2)	55(1)
O3	5959(4)	2506(2)	-1343(3)	88(1)
C4	382(4)	2721(2)	-671(2)	51(1)
O4	-480(4)	2263(2)	-10.6(19)	77(1)
C5	-627(5)	4420(2)	-2127(3)	66(1)
O5	-2022(4)	4933(2)	-2231(3)	100(1)
C6	1688(3)	2300(1)	-2946(1)	45(1)
O6	1063(4)	2376(1)	-3892(1)	75(1)
C7	2578(3)	1192(1)	-2812(1)	37(1)
C8	3034(3)	547(1)	-3675(1)	39(1)
C9	3857(3)	-504(1)	-3556(1)	39(1)
C10	4345(3)	-963(1)	-2566(1)	37(1)
C11	3693(3)	-368(15)	-1685(1)	37(1)
C12	2884(3)	686(1)	-1811(1)	37(1)
N1	5281(3)	-1943(1)	-2459(1)	47(1)
C13	5736(5)	-2582(2)	-3353(3)	70(1)
C14	5478(4)	-2474(2)	-1423(2)	62(1)
Cr1	1033(1)	-328(1)	-2565(1)	35(1)
C15	-804(3)	-39(3)	-3488(1)	54(1)
O15	-1948(3)	168(3)	-4067(1)	88(1)
C16	567(4)	-1777(2)	-2492(2)	56(1)

© University of Pretoria

O16	329(4)	-2686(1)	-2461(3)	93(1)
C17	-885(3)	-146(1)	-1478(1)	44(1)
O17	-2088(3)	-58(2)	-805(1)	67(1)
C18	-13(8)	3315(3)	-4305(3)	104(1)
C19A	-1966(16)	3030(9)	-4350(18)	127(1)
C19B	-1120(5)	3057(15)	-5040(2)	126(1)

Table E.3 Bond lengths [Å] and angles [°]

W1-C1	2.027(3)	C8-C9-C10	121.4(2)
W1-C2	2.026(3)	C8-C9-Cr1	68.6(1)
W1-C3	2.042(3)	H9-C9-C10	119.3(2)
W1-C4	2.053(2)	H9-C9-Cr1	125.7(2)
W1-C5	2.032(3)	C10-C9-Cr1	78.0(1)
W1-C6	2.195(2)	C9-C10-C11	116.5(2)
C1-O1	1.139(5)	C9-C10-N1	121.8(2)
C2-O2	1.140(5)	C9-C10-Cr1	66.4(1)
C3-O3	1.128(4)	C11-C10-N1	121.6(2)
C4-O4	1.126(3)	C11-C10-Cr1	67.3(1)
C5-O5	1.143(4)	N1-C10-Cr1	135.2(2)
C6-O6	1.328(3)	C10-C11-H11	119.5(2)
C6-C7	1.483(3)	C10-C11-C12	121.0(2)
O6-C18	1.446(5)	C10-C11-Cr1	77.3(1)
C7-C8	1.417(3)	H11-C11-C12	119.5(2)
C7-C12	1.421(3)	H11-C11-Cr1	125.9(2)
C7-Cr1	2.210(2)	C12-C11-Cr1	69.0(1)
C8-H8	0.931(2)	C7-C12-C11	122.2(2)
C8-C9	1.399(3)	C7-C12-H12	118.9(2)
C8-Cr1	2.165(2)	C7-C12-Cr1	71.9(1)
C9-H9	0.930(2)	C11-C12-H12	118.9(2)
C9-C10	1.422(3)	C11-C12-Cr1	74.4(1)
C9-Cr1	2.239(2)	H12-C12-Cr1	126.9(2)
C10-C11	1.422(3)	C10-N1-C13	120.4(2)
C10-N1	1.353(3)	C10-N1-C14	120.6(2)
C10-Cr1	2.390(2)	C13-N1-C14	117.8(2)
C11-H11	0.930(2)	N1-C13-H13A	109.4(3)
C11-C12	1.400(3)	N1-C13-H13B	109.5(3)

© University of Pretoria

C11-Cr1	2.260(2)	N1-C13-H13C	109.5(3)
C12-H12	0.930(2)	H13A-C13-H13B	109.5(3)
C12-Cr1	2.191(2)	H13A-C13-H13C	109.5(3)
N1-C13	1.446(4)	H13B-C13-H13C	109.5(3)
N1-C14	1.458(3)	N1-C14-H14A	109.5(2)
C13-H13A	0.960(4)	N1-C14-H14B	109.5(2)
C13-H13B	0.960(3)	N1-C14-H14C	109.5(2)
C13-H13C	0.959(3)	H14A-C14-H14B	109.4(3)
C14-H14A	0.961(3)	H14A-C14-H14C	109.4(3)
C14-H14B	0.960(3)	H14B-C14-H14C	109.5(3)
C14-H14C	0.960(3)	C7-Cr1-C8	37.78(7)
Cr1-C15	1.834(2)	C7-Cr1-C9	67.20(7)
Cr1-C16	1.841(3)	C7-Cr1-C10	77.73(7)
Cr1-C17	1.848(2)	C7-Cr1-C11	67.06(7)
C15-O15	1.149(3)	C7-Cr1-C12	37.68(7)
C16-O16	1.148(3)	C7-Cr1-C15	99.8(1)
C17-O17	1.148(3)	C7-Cr1-C16	160.8(1)
C18-H18A	0.971(4)	C7-Cr1-C17	106.94(9)
C18-H18B	0.970(4)	C8-Cr1-C9	36.99(7)
C18-C19A	1.43(1)	C8-Cr1-C10	65.15(7)
C19A-H19A	0.96(2)	C8-Cr1-C11	78.26(7)
C19A-H19B	0.96(2)	C8-Cr1-C12	67.15(7)
C19A-H19C	0.96(2)	C8-Cr1-C15	87.9(1)
		C8-Cr1-C16	127.7(1)
C1-W1-C2	89.5(1)	C8-Cr1-C17	142.82(9)
C1-W1-C3	86.7(1)	C9-Cr1-C10	35.58(7)
C1-W1-C4	90.1(1)	C9-Cr1-C11	65.03(7)
C1-W1-C5	87.3(1)	C9-Cr1-C12	77.95(7)
C1-W1-C6	174.2(1)	C9-Cr1-C15	105.5(1)
C2-W1-C3	88.8(1)	C9-Cr1-C16	94.5(1)
C2-W1-C4	177.8(1)	C9-Cr1-C17	165.18(9)
C2-W1-C5	90.5(1)	C10-Cr1-C11	35.47(7)
C2-W1-C6	88.8(1)	C10-Cr1-C12	64.68(7)
C3-W1-C4	93.3(1)	C10-Cr1-C15	139.3(1)
C3-W1-C5	173.9(1)	C10-Cr1-C16	83.8(1)
C3-W1-C6	87.74(9)	C10-Cr1-C17	131.27(9)

© University of Pretoria

C4-W1-C5	87.4(1)	C11-Cr1-C12	36.63(7)
C4-W1-C6	91.78(9)	C11-Cr1-C15	165.7(1)
C5-W1-C6	98.3(1)	C11-Cr1-C16	100.5(1)
W1-C1-O1	179.5(3)	C11-Cr1-C17	100.20(9)
W1-C2-O2	179.7(3)	C12-Cr1-C15	133.7(1)
W1-C3-O3	177.3(3)	C12-Cr1-C16	135.7(1)
W1-C4-O4	178.7(2)	C12-Cr1-C17	89.31(9)
W1-C5-O5	176.3(3)	C15-Cr1-C16	90.5(1)
W1-C6-O6	129.0(2)	C15-Cr1-C17	88.8(1)
W1-C6-C7	124.6(1)	C16-Cr1-C17	89.3(1)
O6-C6-C7	105.6(2)	Cr1-C15-O15	178.4(3)
C6-O6-C18	123.3(3)	Cr1-C16-O16	178.0(3)
C6-C7-C8	121.4(2)	Cr1-C17-O17	178.4(2)
C6-C7-C12	122.2(2)	O6-C18-H18A	110.1(4)
C6-C7-Cr1	126.6(1)	O6-C18-H18B	110.1(4)
C8-C7-C12	116.2(2)	O6-C18-C19A	108.2(7)
C8-C7-Cr1	69.4(1)	H18A-C18-H18B	108.4(4)
C12-C7-Cr1	70.4(1)	H18A-C18-C19A	110.0(7)
C7-C8-H8	119.0(2)	H18B-C18-C19A	110.1(7)
C7-C8-C9	121.9(2)	C18-C19A-H19A	109(1)
C7-C8-Cr1	72.8(1)	C18-C19A-H19B	110(1)
H8-C8-C9	119.0(2)	C18-C19A-H19C	109(1)
H8-C8-Cr1	125.6(2)	H19A-C19A-H19B	109(1)
C9-C8-Cr1	74.4(1)	H19A-C19A-H19C	110(1)
C8-C9-H9	119.3(2)	H19B-C19A-H19C	109(1)

Table E.4 Anisotropic displacement parameters ($Å^2$ x 10^3)
The anisotropic displacement factor exponent takes the form: $-2p^2[h^2a^{*2}U^{11} + \ldots + 2hka^*b^*U^{12}]$

Atom	U11	U22	U33	U23	U13	U12
W1	51(1)	32(1)	53(1)	-1(1)	-6(1)	1(1)
C1	84(1)	47(1)	77(1)	-13(1)	(1)	-8(1)
O1	142(1)	75(1)	114(1)	-48(1)	-4(1)	-20(1)
C2	87(1)	50(1)	71(1)	9(1)	-7(1)	-7(1)
O2	140(1)	92(1)	93(1)	33(1)	7(1)	-30(1)
C3	53(1)	50(1)	65(1)	-2(1)	-13(1)	-8(1)
O3	58(1)	86(1)	123(1)	2(1)	-35(1)	-1(1)

© University of Pretoria

C4	54(1)	43(1)	54(1)	-2(1)	-5(1)	8(1)
O4	81(1)	75(1)	67(1)	16(1)	12(1)	7(1)
C5	73(1)	44(1)	81(1)	1(1)	-10(1)	12(1)
O5	91(1)	76(1)	129(1)	4(1)	-20(1)	40(1)
C6	49(1)	39(1)	47(1)	3(1)	-16(1)	4(1)
O6	109(1)	57(1)	63(1)	-3(1)	-47(1)	25(1)
C7	37(1)	33(1)	40(1)	1(1)	-10(1)	-1(1)
C8	37(1)	43(1)	35(1)	2(1)	-4(1)	-4(1)
C9	35(1)	45(1)	38(1)	-5(1)	3(1)	-2(1)
C10	30(1)	35(1)	46(1)	-2(1)	-3(1)	-1(1)
C11	37(1)	35(1)	38(1)	(1)	-9(1)	(1)
C12	39(1)	36(1)	37(1)	-4(1)	-11(1)	1(1)
N1	46(1)	37(1)	57(1)	-3(1)	-2(1)	7(1)
C13	80(1)	51(1)	80(1)	-21(1)	-9(1)	19(1)
C14	65(1)	44(1)	72(1)	11(1)	-2(1)	12(1)
Cr1	31(1)	42(1)	33(1)	-5(1)	-3(1)	-4(1)
C15	39(1)	85(1)	40(1)	-4(1)	-4(1)	-15(1)
O15	49(1)	160(1)	57(1)	8(1)	-22(1)	-20(1)
C16	47(1)	52(1)	71(1)	-13(1)	2(1)	-12(1)
O16	90(1)	54(1)	137(1)	-21(1)	(1)	-23(1)
C17	40(1)	53(1)	40(1)	-4(1)	-4(1)	-4(1)
O17	50(1)	92(1)	55(1)	-14(1)	12(1)	-3(1)
C18	153(1)	73(1)	92(1)	1(1)	-71(1)	44(1)
C19A	114(1)	127(1)	143(1)	-12(1)	-61(1)	57(1)
C19B	166(1)	138(1)	83(1)	-29(1)	-81(1)	77(1)

Table E.5 Hydrogen coordinates (x 10^4) and isotropic displacement paramenters (Å^2 x 10^3)

Atom	x	y	z	Ueq
H8	2778	830	-4339	-5543
H9	4089	-911	-4137	-5285
H11	3804	-684	-1014	-1295
H12	2537	1068	-1221	-1560
H13A	4559	-2817	-3575	-4567
H13B	6550	-3201	-3163	-4041
H13C	6400	-2153	-3914	-5000
H14A	6101	-2007	-1013	-1294

© University of Pretoria

H14B	6245	-3137	-1490	-1903
H14C	4219	-2627	-1083	-1384
H18A	559	3545	-5000	-6388
H18B	17	3907	-3857	-4927
H19A	-1969	2367	-4688	-5989
H19B	-2644	3594	-4739	-6054
H19C	-2597	2938	-3652	-4665
H19D	-308	2823	-5641	-7206
H19E	-1914	3679	-5253	-6711
H19F	-1941	2485	-4764	-6086

Table C.6 Torsion angles [°]

Atoms	Torsion	Atoms	Torsion
C2-W1-C1-O1	-132(34)	C10-C9-Cr1-C11	26.7(1)
C3-W1-C1-O1	-43(34)	C10-C9-Cr1-C12	63.0(1)
C4-W1-C1-O1	50(34)	C10-C9-Cr1-C15	-164.6(1)
C5-W1-C1-O1	137(34)	C10-C9-Cr1-C16	-72.8(1)
C6-W1-C1-O1	-60(35)	C10-C9-Cr1-C17	31.7(4)
C1-W1-C2-O2	170(57)	C9-C10-C11-H11	170.3(2)
C3-W1-C2-O2	84(57)	C9-C10-C11-C12	-9.6(3)
C4-W1-C2-O2	-109(56)	C9-C10-C11-Cr1	46.0(2)
C5-W1-C2-O2	-102(57)	N1-C10-C11-H11	-5.9(3)
C6-W1-C2-O2	-4(57)	N1-C10-C11-C12	174.2(2)
C1-W1-C3-O3	-17(5)	N1-C10-C11-Cr1	-130.2(2)
C2-W1-C3-O3	73(5)	Cr1-C10-C11-H11	124.3(2)
C4-W1-C3-O3	-107(5)	Cr1-C10-C11-C12	-55.6(2)
C5-W1-C3-O3	-11(6)	C9-C10-N1-C13	-3.0(3)
C6-W1-C3-O3	162(5)	C9-C10-N1-C14	-169.7(2)
C1-W1-C4-O4	83(11)	C11-C10-N1-C13	173.1(2)
C2-W1-C4-O4	3(13)	C11-C10-N1-C14	6.3(3)
C3-W1-C4-O4	170(11)	Cr1-C10-N1-C13	84.5(3)
C5-W1-C4-O4	-4(11)	Cr1-C10-N1-C14	-82.3(3)
C6-W1-C4-O4	-102(11)	C9-C10-Cr1-C7	-67.8(1)
C1-W1-C5-O5	2(5)	C9-C10-Cr1-C8	-30.1(1)
C2-W1-C5-O5	-87(5)	C9-C10-Cr1-C11	-135.4(2)
C3-W1-C5-O5	-4(5)	C9-C10-Cr1-C12	-105.3(1)

© University of Pretoria

C4-W1-C5-O5	92(5)	C9-C10-Cr1-C15	23.0(2)
C6-W1-C5-O5	-176(5)	C9-C10-Cr1-C16	106.7(1)
C1-W1-C6-O6	-123(1)	C9-C10-Cr1-C17	-169.7(1)
C1-W1-C6-C7	45(1)	C11-C10-Cr1-C7	67.5(1)
C2-W1-C6-O6	-50.2(2)	C11-C10-Cr1-C8	105.3(1)
C2-W1-C6-C7	117.8(2)	C11-C10-Cr1-C9	135.4(2)
C3-W1-C6-O6	-139.1(2)	C11-C10-Cr1-C12	30.0(1)
C3-W1-C6-C7	28.9(2)	C11-C10-Cr1-C15	158.4(2)
C4-W1-C6-O6	127.7(2)	C11-C10-Cr1-C16	-118.0(1)
C4-W1-C6-C7	-64.3(2)	C11-C10-Cr1-C17	-34.3(2)
C5-W1-C6-O6	40.1(2)	N1-C10-Cr1-C7	-179.9(2)
C5-W1-C6-C7	-151.9(2)	N1-C10-Cr1-C8	-142.1(2)
W1-C6-O6-C18	-14.3(4)	N1-C10-Cr1-C9	-112.1(3)
C7-C6-O6-C18	175.9(3)	N1-C10-Cr1-C11	112.6(3)
W1-C6-C7-C8	-155.8(2)	N1-C10-Cr1-C12	142.6(2)
W1-C6-C7-C12	29.1(3)	N1-C10-Cr1-C15	-89.0(3)
W1-C6-C7-Cr1	117.7(2)	N1-C10-Cr1-C16	-5.4(2)
O6-C6-C7-C8	14.5(3)	N1-C10-Cr1-C17	78.3(2)
O6-C6-C7-C12	-160.5(2)	C10-C11-C12-C7	3.4(3)
O6-C6-C7-Cr1	-72.0(2)	C10-C11-C12-H12	-176.5(2)
C6-O6-C18-H18A	130.2(3)	C10-C11-C12-Cr1	59.6(2)
C6-O6-C18-H18B	10.8(5)	H11-C11-C12-C7	-176.5(2)
C6-O6-C18-C19A	-109.5(7)	H11-C11-C12-H12	3.6(3)
C6-C7-C8-H8	0.6(3)	H11-C11-C12-Cr1	-120.3(2)
C6-C7-C8-C9	-179.4(2)	Cr1-C11-C12-C7	-56.2(2)
C6-C7-C8-Cr1	-121.1(2)	Cr1-C11-C12-H12	123.9(2)
C12-C7-C8-H8	175.9(2)	C10-C11-Cr1-C7	-101.3(1)
C12-C7-C8-C9	-4.1(3)	C10-C11-Cr1-C8	-63.4(1)
C12-C7-C8-Cr1	54.3(2)	C10-C11-Cr1-C9	-26.8(1)
Cr1-C7-C8-H8	121.6(2)	C10-C11-Cr1-C12	-130.7(2)
Cr1-C7-C8-C9	-58.3(2)	C10-C11-Cr1-C15	-77.2(4)
C6-C7-C12-C11	178.8(2)	C10-C11-Cr1-C16	63.3(1)
C6-C7-C12-H12	-1.2(3)	C10-C11-Cr1-C17	154.5(1)
C6-C7-C12-Cr1	121.5(2)	H11-C11-Cr1-C7	141.3(2)
C8-C7-C12-C11	3.5(3)	H11-C11-Cr1-C8	179.2(2)
C8-C7-C12-H12	-176.5(2)	H11-C11-Cr1-C9	-144.2(2)

© University of Pretoria

C8-C7-C12-Cr1	-53.8(2)	H11-C11-Cr1-C10	-117.4(2)
Cr1-C7-C12-C11	57.3(2)	H11-C11-Cr1-C12	111.9(2)
Cr1-C7-C12-H12	-122.8(2)	H11-C11-Cr1-C15	165.4(4)
C6-C7-Cr1-C8	114.5(2)	H11-C11-Cr1-C16	-54.1(2)
C6-C7-Cr1-C9	143.8(2)	H11-C11-Cr1-C17	37.1(2)
C6-C7-Cr1-C10	179.6(2)	C12-C11-Cr1-C7	29.4(1)
C6-C7-Cr1-C11	-144.8(2)	C12-C11-Cr1-C8	67.3(1)
C6-C7-Cr1-C12	-116.2(2)	C12-C11-Cr1-C9	103.9(1)
C6-C7-Cr1-C15	41.1(2)	C12-C11-Cr1-C10	130.7(2)
C6-C7-Cr1-C16	162.7(3)	C12-C11-Cr1-C15	53.5(4)
C6-C7-Cr1-C17	-50.7(2)	C12-C11-Cr1-C16	-166.0(1)
C8-C7-Cr1-C9	29.3(1)	C12-C11-Cr1-C17	-74.8(1)
C8-C7-Cr1-C10	65.1(1)	C7-C12-Cr1-C8	30.9(1)
C8-C7-Cr1-C11	100.7(1)	C7-C12-Cr1-C9	68.2(1)
C8-C7-Cr1-C12	129.3(2)	C7-C12-Cr1-C10	103.2(1)
C8-C7-Cr1-C15	-73.5(1)	C7-C12-Cr1-C11	132.3(2)
C8-C7-Cr1-C16	48.2(3)	C7-C12-Cr1-C15	-31.8(2)
C8-C7-Cr1-C17	-165.2(1)	C7-C12-Cr1-C16	152.2(1)
C12-C7-Cr1-C8	-129.3(2)	C7-C12-Cr1-C17	-119.5(1)
C12-C7-Cr1-C9	-100.0(1)	C11-C12-Cr1-C7	-132.3(2)
C12-C7-Cr1-C10	-64.2(1)	C11-C12-Cr1-C8	-101.3(1)
C12-C7-Cr1-C11	-28.6(1)	C11-C12-Cr1-C9	-64.1(1)
C12-C7-Cr1-C15	157.2(1)	C11-C12-Cr1-C10	-29.1(1)
C12-C7-Cr1-C16	-81.1(3)	C11-C12-Cr1-C15	-164.1(1)
C12-C7-Cr1-C17	65.5(1)	C11-C12-Cr1-C16	19.9(2)
C7-C8-C9-H9	177.6(2)	C11-C12-Cr1-C17	108.2(1)
C7-C8-C9-C10	-2.4(3)	H12-C12-Cr1-C7	113.0(2)
C7-C8-C9-Cr1	57.6(2)	H12-C12-Cr1-C8	143.9(2)
H8-C8-C9-H9	-2.4(3)	H12-C12-Cr1-C9	-178.8(2)
H8-C8-C9-C10	177.6(2)	H12-C12-Cr1-C10	-143.8(2)
H8-C8-C9-Cr1	-122.4(2)	H12-C12-Cr1-C11	-114.7(2)
Cr1-C8-C9-H9	119.9(2)	H12-C12-Cr1-C15	81.2(2)
Cr1-C8-C9-C10	-60.0(2)	H12-C12-Cr1-C16	-94.8(2)
C7-C8-Cr1-C9	-131.4(2)	H12-C12-Cr1-C17	-6.5(2)
C7-C8-Cr1-C10	-102.4(1)	C10-N1-C13-H13A	-68.0(3)
C7-C8-Cr1-C11	-67.6(1)	C10-N1-C13-H13B	172.0(2)

© University of Pretoria

C7-C8-Cr1-C12	-30.9(1)	C10-N1-C13-H13C	52.0(4)
C7-C8-Cr1-C15	109.1(1)	C14-N1-C13-H13A	99.1(3)
C7-C8-Cr1-C16	-161.9(1)	C14-N1-C13-H13B	-20.9(4)
C7-C8-Cr1-C17	23.9(2)	C14-N1-C13-H13C	-140.9(3)
H8-C8-Cr1-C7	-113.8(2)	C10-N1-C14-H14A	-56.5(3)
H8-C8-Cr1-C9	114.8(2)	C10-N1-C14-H14B	-176.5(2)
H8-C8-Cr1-C10	143.8(2)	C10-N1-C14-H14C	63.5(3)
H8-C8-Cr1-C11	178.7(2)	C13-N1-C14-H14A	136.5(2)
H8-C8-Cr1-C12	-144.6(2)	C13-N1-C14-H14B	16.5(3)
H8-C8-Cr1-C15	-4.7(2)	C13-N1-C14-H14C	-103.6(3)
H8-C8-Cr1-C16	84.3(2)	C7-Cr1-C15-O15	-20(9)
H8-C8-Cr1-C17	-89.9(2)	C8-Cr1-C15-O15	-56(9)
C9-C8-Cr1-C7	131.4(2)	C9-Cr1-C15-O15	-89(9)
C9-C8-Cr1-C10	29.0(1)	C10-Cr1-C15-O15	-102(9)
C9-C8-Cr1-C11	63.8(1)	C11-Cr1-C15-O15	-42(9)
C9-C8-Cr1-C12	100.5(1)	C12-Cr1-C15-O15	-1(9)
C9-C8-Cr1-C15	-119.5(1)	C16-Cr1-C15-O15	177(9)
C9-C8-Cr1-C16	-30.5(2)	C17-Cr1-C15-O15	87(9)
C9-C8-Cr1-C17	155.3(1)	C7-Cr1-C16-O16	-10(8)
C8-C9-C10-C11	9.1(3)	C8-Cr1-C16-O16	25(8)
C8-C9-C10-N1	-174.6(2)	C9-Cr1-C16-O16	7(8)
C8-C9-C10-Cr1	55.5(2)	C10-Cr1-C16-O16	-27(8)
H9-C9-C10-C11	-170.8(2)	C11-Cr1-C16-O16	-58(8)
H9-C9-C10-N1	5.4(3)	C12-Cr1-C16-O16	-70(8)
H9-C9-C10-Cr1	-124.4(2)	C15-Cr1-C16-O16	113(8)
Cr1-C9-C10-C11	-46.4(2)	C17-Cr1-C16-O16	-159(8)
Cr1-C9-C10-N1	129.8(2)	C7-Cr1-C17-O17	-178(8)
C8-C9-Cr1-C7	-29.9(1)	C8-Cr1-C17-O17	167(7)
C8-C9-Cr1-C10	-130.9(2)	C9-Cr1-C17-O17	-113(7)
C8-C9-Cr1-C11	-104.2(1)	C10-Cr1-C17-O17	-89(8)
C8-C9-Cr1-C12	-67.9(1)	C11-Cr1-C17-O17	-109(8)
C8-C9-Cr1-C15	64.4(1)	C12-Cr1-C17-O17	-144(8)
C8-C9-Cr1-C16	156.2(1)	C15-Cr1-C17-O17	82(8)
C8-C9-Cr1-C17	-99.2(4)	C16-Cr1-C17-O17	-8(8)
H9-C9-Cr1-C7	-141.4(2)	O6-C18-C19A-H19A	-49(1)
H9-C9-Cr1-C8	-111.5(2)	O6-C18-C19A-H19B	-169(1)

© University of Pretoria

H9-C9-Cr1-C10	117.6(2)	O6-C18-C19A-H19C	71(1)
H9-C9-Cr1-C11	144.3(2)	H18A-C18-C19A-H19A	71(1)
H9-C9-Cr1-C12	-179.4(2)	H18A-C18-C19A-H19B	-49(1)
H9-C9-Cr1-C15	-47.0(2)	H18A-C18-C19A-H19C	-169(1)
H9-C9-Cr1-C16	44.8(2)	H18B-C18-C19A-H19A	-170(1)
H9-C9-Cr1-C17	149.3(3)	H18B-C18-C19A-H19B	70(1)
C10-C9-Cr1-C7	101.0(1)	H18B-C18-C19A-H19C	-50(1)
C10-C9-Cr1-C8	130.9(2)		

© University of Pretoria